# SIMULATING TREE GROWTH RESPONSE TO CLIMATE CHANGE IN STRUCTURALLY-COMPLEX OAK AND BEECH STANDS ACROSS EUROPE

*DOCTORAL DISSERTATION PRESENTED BY*

Louis de Wergifosse

*IN FULFILLMENT OF THE REQUIREMENTS*
*FOR THE DEGREE OF DOCTOR IN BIOENGINEERING*

---

THESIS COMMITTEE

| | |
|---|---|
| Prof. Mathieu JONARD (supervisor) | Université catholique de Louvain |
| Prof. Hugues GOOSSE (supervisor) | Université catholique de Louvain |
| Dr. Nicolas DELPIERRE | Université Paris Saclay |
| Prof. Thierry FICHEFET | Université catholique de Louvain |
| Prof. Quentin PONETTE | Université catholique de Louvain |
| Dr. Christopher REYER | Potsdam-Institut für Klimafolgenforschung |
| Prof. Emmanuel HANERT (chair) | Université catholique de Louvain |

LOUVAIN-LA-NEUVE
APRIL 2021

# ACKNOWLEDGEMENTS

Je voudrais adresser mes remerciements, en français, le message n'en sera que plus sincère, à toutes les personnes qui m'ont permis de mener à bien ce projet.

Tout d'abord je tiens à remercier Mathieu pour avoir vécu et survécu avec moi à ce projet qui aura su nous faire passer par toutes les émotions. Merci pour la confiance que tu m'as accordée même si nous n'avions pas la même méthode de travail. Merci pour les nombreux enseignements, la découverte du monde de la forêt et de la modélisation, l'apprentissage de la rigueur scientifique et rédactionnelle. Merci aussi pour les discussions, les conférences, les séjours post-conférence et tout le reste. Et bien entendu, un tout grand merci pour ton aide dont je n'oserais même pas estimer le nombre d'heures. J'espère, pour ma part, avoir pu t'offrir une première expérience d'encadrement de doctorat enrichissante et fait progresser HETEROFOR qui, je n'en doute pas, est promis à un bel avenir. Profite bien d'un peu de repos à présent !

Hugues, je suis ressorti avec de nouvelles idées et perspectives de chacune de nos rencontres et discussions. Ton expérience de la recherche et ton pragmatisme auront été extrêmement précieux durant ce projet, merci pour cela. Merci également pour les Noëls d'équipe, qu'ils aient lieu en hiver ou au printemps, qu'importe, ce furent toujours des moments mémorables. Merci de m'avoir fait confiance et d'avoir mis sur pied le projet. J'espère que cette première collaboration avec le monde de la forêt ne sera pas la dernière, il reste encore beaucoup à explorer.

Merci aux autres membres de mon jury de thèse. Christopher et Nicolas, votre expérience en modélisation de la forêt a apporté un véritable plus dans la discussion lors de la défense privée qui aura été un moment d'une grande intensité intellectuelle, j'en garderai un très bon souvenir. Thierry et Quentin, votre vision plus holistique de la forêt et du climat m'auront aidé à fixer un cadre à ce beau projet et prendre plus de recul. Finalement, merci à Emmanuel pour avoir conduit la défense privée avec un bel équilibre pour que celle-ci soit sérieuse sans être trop stressante, productive mais néanmoins confortable.

Fred, sans toi, il y a peu de chance que ce projet ait pu fonctionner ou en tous cas se finir en moins de dix ans, je te dois une sacrée chandelle. Par ailleurs, ta concentration et ton efficacité au travail m'ont vraiment impressionné. Je pense que tu as su me transférer une partie de ces qualités, à moins que ce soit la proximité de la fin de thèse. Dans le doute, on dira que c'est grâce à toi ! Merci pour les séjours de spatialisation et merci d'avoir été un chouette partenaire de bureau qui, comme moi, n'hésitait pas à jurer quand quelque chose n'allait pas. Impossible de travailler sans cela.

Merci à François et Nicolas pour l'aide dans le développement des nouveaux modules sur HETEROFOR. Paradoxalement, alors que les journées de travail étaient souvent très chargées, je revenais de chacun de mes passages à Montpellier dans le même état d'esprit qu'après une semaine de vacances. J'espère quand même que vous ne travaillez pas à ce rythme-là toute l'année.

A toute l'équipe d'EFOR, je vous dis un grand merci de m'avoir accueilli au sein de votre groupe de vie. Merci d'avoir répondu sans sourciller aux hérésies que j'ai pu poser comme question. J'aurais aimé pouvoir vous apporter un peu plus de connaissance en climatologie mais peut-être cela arrivera plus tard, n'hésitez pas ! En dehors du travail, merci pour votre humanité, vous êtes un groupe dans lequel on se sent directement intégré et qui défend de belles valeurs. Un merci particulier à François pour les semaines de mesures de terrain, on aura vécu, vu, mangé et bu de belles choses. Merci, Françoise, pour ton travail si précieux durant ces quatre années. Si la vie était si agréable en EFOR, c'est en grande partie grâce à toi. Isabelle, merci d'avoir été compréhensive en fin d'année mais surtout pour les discussions plus personnelles, c'est gai de pouvoir écouter et se confier dans le milieu professionnel également. Morgane, merci pour ton aide, un jour je serai organisé comme toi, c'est (presque) sûr et merci à tous les autres, ce fût un vrai plaisir de vous côtoyer.

A l'équipe du Mercator, merci aussi. On peut compter sur le doigt d'une main le nombre de mes passages annuels que certaines mauvaises langues ont tenté de lier avec les afterworks mais malgré cela je me suis à chaque fois senti comme à la maison. J'aurai mieux réussi à montrer mes qualités sociales que professionnelles avec vous, espérons que ce ne soit que partie remise.

Merci aux membres de l'ACELI et des différents groupe d'action pour la transition. Nos réunions étaient des petits îlots de fraîcheur bienvenus pour rompre le rythme parfois un peu linéaire de la recherche. Quel plaisir également de se sentir utile au sein de son université.

Merci aussi à Frédéric, Hans, Frank, Anthony, Sergei sans qui la concentration aurait été nettement plus difficile.

Impossible de terminer mes remerciements sans mentionner mes proches. Alo, merci du fond du cœur pour ton indéfectible soutien, ton courage et ta patience. Ça y est, c'est fini ! Ah oui, merci aussi pour tes beaux graphes. Merci à tous mes colocataires de Kraainem, amis de l'ode secret et d'ailleurs, vous ne vous rendez sans doute pas compte à quel point votre capacité à me faire rapidement mettre de côté le travail une fois la journée terminée m'aura été bénéfique. Finalement, merci à ma famille qui me soutient depuis toujours et qui a, une fois encore, su répondre présent aux bons moments.

# NOTICE

Parts of this thesis (2 chapters) are published in peer-reviewed journals, as indicated below:

- **Chapter 3**

de Wergifosse L, André F, Beudez N, de Coligny F, Goosse H, Jonard F, Ponette Q, Titeux H, Vincke C, Jonard M (2020) HETEROFOR 1.0: a spatially explicit model for exploring the response of structurally complex forests to uncertain future conditions–Part 2: Phenology and water cycle. Geosci. Model Dev. 13(3): 1459-1498.

- **Chapter 4**

de Wergifosse L, André F, Goosse H, Caluwaerts S, de Cruz L, de Troch R, Jonard M (2020) $CO_2$ fertilization, transpiration deficit and vegetation period drive the response of mixed broadleaved forests to a changing climate in Wallonia. Ann. For. Sci. 77(3): 1-23.

# CONTENTS

# ABBREVIATION LIST

- (N)AE: (Normalised) Average Error
- CMIP: Coupled Model Intercomparison Project
- CORDEX: Coordinated Regional Downscaling Experiment
- CUE: Carbon Use Efficiency
- DBH: Diameter at Breast Height
- DGVM: Dynamic Global Vegetation Model
- ERA5: Fifth Reanalysis of the European Centre for Medium-Range Weather Forecasts
- (M)EW: (Maximum) Extractable Water
- FAO: Food and Agriculture Organization of the United Nations
- FLM: Forest Landscape Model
- GCM: Global Circulation Model or Global Climate Model
- GHG: Greenhouse Gas
- GPP: Gross Primary Production
- HCB: Height of Crown Base
- IBM: Individual-Based Model
- ICP Forests: International Cooperative Programme on Assessment and Monitoring of Air Pollution Effects on Forests
- IPCC: Intergovernmental Panel on Climate Change
- LAI: Leaf Area Index
- LCI: Light Competition Index
- LTER: Long Term Ecological Research Network
- NFI: National Forest Inventory
- NPP: Net Primary Production
- PEP725: Pan European Phenological Project
- PFT: Plant Functional Type
- P-M: Penman-Monteith
- RCM: Regional Climate Model
- RCP: Representative Concentration Pathway
- (N)RMSE: (Normalised) Root Mean Square Error
- SPAC: Soil Plant Atmosphere Continuum
- TD: Transpiration Deficit
- USDA: United States Department of Agriculture
- VP: Vegetation Period
- VPD: Vapour Pressure Deficit
- WUE: Water Use Efficiency

# FOREWORD

This project finds his roots in a working group on the impact of climate change emanating from the ELI2020 initiative (Topic A. What are the climate change impacts on hydrosphere, ecosystems, biodiversity, biogeochemical cycles, agriculture, and health? How are the natural systems responding to observed climate change and expected to respond to projected climate change scenarii?). My two supervisors, Mathieu Jonard and Hugues Goosse who are working in the fields of forest modelling and climatology, decided to launch a project to study the impact of climate change on forest growth, which would benefit from their complementary expertise.

With a bachelor in Geography and a master in Climatology, and after completing a master thesis with Hugues Goosse, my polyvalent and multidisciplinary profile seemed to fit with this study project and we decided to build a PhD project together.

The initial idea was to simulate the future evolution of European temperate forest dynamics according to different climate scenarios while accounting for the different uncertainty sources along the modelling process. With time, the aim of my thesis progressively shifted from the uncertainty characterisation to the assessment of the stand structure impact on forest response to climate change, given the particularities of the tree growth model used.

In Europe, forests cover approximatively 35% of land area (Korhonen et al., 2020) and offer a vast amount of goods and services: wood and non-wood production, biodiversity conservation, soil and water protection, carbon storage, recreation (Hassan et al., 2005; Haines-Young and Potschin, 2018). Environmental modifications induced by climate change are already affecting forest growth and dynamics and threaten the provision of these ecosystem services. Warmer temperatures have induced a lengthening of the growing season in temperate and boreal climate (Menzel *et al*., 2006; Jeong *et al*., 2011; Fu *et al*., 2014; Park *et al*., 2016) and shifts in the latitudinal and altitudinal species distribution (Delzon *et al*., 2013; Rigling *et al*., 2013). More frequent and severe drought episodes have locally led to productivity decline (Boisvenue and Running, 2006; Ruiz-Benito *et al*., 2014; Charru *et al*. 2017), defoliation (Carnicer *et al*., 2011) and vitality loss (Allen *et al*., 2010; Greenwood *et al*., 2017), which in turn have favoured biotic and abiotic disturbances (Carvalho *et al*., 2011; Seidl *et al*., 2011; Jactel *et al*., 2021).

Given the future climate projections, it is likely that these trends will accelerate in the future and have an impact on European forest state (Lindner *et al*., 2014). However, whether the stands are located at the warm, cold or dry margin of their tree species distribution range, they are not expected to be affected the same way (Jump *et al*., 2006; Goldblum, 2010; Martin-Benito and Pederson, 2015; Dulamsuren *et al*., 2017). In addition, the stand characteristics (specific composition, density, development stage and structure) and soil properties (water retention capacity, chemical richness) will also modify the response to climate change, which complicates the projections of the future forest state.

While the soil and climate conditions can hardly be modified to adapt forests to future conditions, stand characteristics can be modulated by forest practices. A promising approach to increase the forest resilience to abiotic and biotic stressors is to favor uneven-aged structure and species mixture (Thompson et al., 2009; Oliver et al., 2015). Models able to simulate the response of structurally-complex stands to climate change are therefore crucial to elaborate new management systems favoring forest resilience.

In this project, using an individual-based and spatially explicit tree growth model, I seek to bring some light to the question: “How climate change will affect oak and beech tree growth in European temperate forests and how this response will be modulated by the local soil, stand and climate conditions?”

# CHAPTER 1

# STATE OF THE ART

## 1. DEFINITION OF THE STUDIED SYSTEM

### 1.1. DEFINITION OF THE FOREST ECOSYSTEM AND ITS COMPONENTS

In this first section, I define the notions of forest, the studied system, and how it will be considered in the project. Indeed, even if trees are a major element of it, a forest is more than a simple cluster of trees. The notion of ecosystem allows to encompass that complexity. According to the definition of the Convention on Biological Diversity, "*A forest ecosystem can be defined at a range of scales. It is a dynamic complex of plant, animal and micro-organism communities and their abiotic environment interacting as a functional unit, where trees are a key component of the system. Humans, with their cultural, economic and environmental needs are an integral part of many forest ecosystems*". According to this definition, the forest ecosystem is a multi-component, entangled system dominated by trees and composed of a biotic component with plants, animals, bacteria and fungi, and an abiotic component forming the habitat, which consists in the physicochemical environment (Bargali, 2018).

Another important notion in the forestry area is the concept of site. Skovsgaard and Vanclay (2008) propose two definitions, a general one stating that the site corresponds to "*a geographic location that is considered homogeneous in terms of its physical and biological environment*" and a second one, more forestry-oriented, considering that a "*site is usually defined by the location's potential to sustain tree growth, often with a view to site-specific silviculture*". In other terms, the site is the combination of soil, climate, topography and vegetation characteristics that drives the forest productivity potential so that two similar sites experiencing the same management should have the same productivity (Skovsgaard and Vanclay, 2013). One might consider only the physical environment (soil and climate) to define the site but, as forest productivity is dependent on tree species (site index hypothesis) and stand structure, we choose to include the stand component in our site definition. In my thesis, I attempt to simulate the response of a system (the forest ecosystem) to an external disturbance (climate change) and to analyse how this response depends on the site characteristics.

Given the multiple spatial and temporal scales that govern the ecosystem functioning (Levin, 1992; Chave, 2013), apprehending all the ecosystem complexity is not possible. Furthermore, a model is always a simplification of the reality and, consequently, several ecosystem components and processes will always be coarsely represented or even absent in a model. The biotic component of the ecosystem considered in this study is restricted to the ensemble of individual trees and the understorey vegetation taken as a whole. Therefore, animals, bacteria and fungi are not taken into account even if some of the processes in which they are involved are considered. The physicochemical environment is constituted of the soil and the atmosphere. The biotic component and the physicochemical environment are dynamic elements continuously interacting.

Inversely, the site characteristics are generally considered as static or representative of a long period and I separated them in three components: soil, climate and stand. According to the USDA, the soil is "*a natural body comprised of solids (minerals and organic matter), liquid, and gases that occurs on the land surface, occupies space, and is characterized by one or both of the following: horizons, or layers, that are distinguishable from the initial material as a result of* *additions, losses, transfers, and transformations of energy and matter or the ability to support rooted plants in a natural environment*" (Soil Survey Staff, 2014). In my thesis, the soil is seen as the layer between the bedrock and the atmosphere where plants grow, and which is divided in different horizons displaying the following homogeneous properties: thickness, bulk density, coarse fraction, texture (proportion of sand, silt and clay), hydraulic properties (saturated, field capacity and wilting point water content), and root distribution. The root distribution in the soil depends both on the soil properties (soil depth, texture and coarse fraction) and the type of vegetation but it will be considered here as part of the soil component. Given the relatively slow changes occurring in the soil, considering the soil physical characteristics constant during the time period used for simulations is a reasonable approximation (Cools and De Vos, 2013).

The climate as defined by the IPCC is the "*statistical description of the weather in terms of the mean and variability over a period of time ranging from months to thousands or millions of years*". Indeed, climate conditions are characterized by an important temporal variability due to its highly non-linear and chaotic nature (Lorenz, 1963) and the interactions of daily, seasonal and decadal cycles. In order to represent all this variability in a fixed value, it must be described over an appropriate timescale. In the study, the variables accounted for are the air temperature, relative humidity, short-wave incident radiation, rainfall, wind speed and wind direction, averaged over 30 year-periods as advocated by the World Meteorological Organization.

For a tree species in a pure even-aged stand, the site productivity can be characterized based on the dominant height (height of the 100 highest trees per hectare) at a given age (site index hypothesis). In addition to these two variables (dominant height and age), stand density, tree size distribution and species proportion as well as the spatial aggregation of trees by size and species must also be taken into account to properly describe heterogeneous stands (Del Rio et al., 2015). The stand density indicates how the resources are shared among trees in an even-aged stand. As a first approximation and to some extent, stand density can be reduced without affecting to the total stand productivity, which allows the remaining trees to receive more ressources (thinning response hypothesis, Skovsgaard and Vanclay, 2008). When the density reduction is too high, the productivity drops because the remaining trees cannot benefit from all the available ressources. Stand density can be estimated based on the stem number per unit area, the basal area or the leaf area index (LAI).Then, the species composition must be accounted for with information on the different species present and their relative abundance, usually with regards to the basal area (sum of the individual trunk section at breast height per hectare). To characterize a stand, the tree size distribution is also crucial and provides information on the mean development stage in even-aged stands and on the complexity of the structure in uneven-aged stands (Barbeito et al., 2009). Not only the vertical tree distribution but also the spatial pattern affect the local conditions undergone by individual trees. The later represents whether the trees of the same species and/or cohort are aggregated intimately or patch-wise, which can be represented by different indices (e.g. Clark and Evans, 1954; Pielou, 1959). In this study, I use the basal area, the beech and oak proportion in basal area, the mean *dbh* (diameter at breast height) and the standard deviation of *dbh* to represent respectively the stand density, species composition, development stage and structural complexity. The choice to use the *dbh* standard deviation instead of that of the height is done for practical reasons as *dbh* is usually measured for all trees of the stand whereas the height is often monitored only for a subset of trees and given that both variables are linked. All these properties evolve with time as trees grow and die, and as forest management or mortality occur but I define the stand as the state of these variables at the start of the study period (the initial stand conditions). To limit the influence of potentially diverging stand properties, simulations do not exceed 15 years in this project.

### 1.2. DEFINITION OF THE STUDY ZONE

Now that the studied system is defined, I will introduce the zone of interest: the deciduous temperate forests located on the European continent. According to the last FAO "State of Europe's forests" survey, realized in 2020, European forests represent a territory of 227 million ha covering 35% of the emerged territories, without considering Russia. At the continental scale, 46% of the forests are dominated by coniferous, 37% by broadleaved species and the remaining 17% by mixed forests (Korhonen et al., 2020). Only 30% of these forests, mainly coniferous-dominated ones, are monospecific while the majority of forests comprise two to five different species (Lier et al., 2020). The main tree genus found in Europe are pine, spruce, fir, beech, oak and birch (Mauri et al., 2017; Buras and Menzel, 2019) that together represent 84% of the forest growing stock. About 28% of European forests are uneven-aged and most of them are deciduous or mixed forests. The even-aged forests are mainly at an intermediate development stage (i.e. they stand between 20 and 90 % of the recommended rotation age). Finally, 94% of forests are considered as semi-natural (i.e. they display characteristics of natural ecosystems but are not undisturbed forests or they are old plantations that have not experienced intensive management for a long period), 2% are undisturbed forests and 4% are plantations (Korhonen et al., 2020).

Different ecological zones are found in Europe (Fig. 1.1). They can be characterised by their mean air temperature: polar, boreal, temperate and subtropical that can be further subdivided according to the precipitation regime (FAO, 2012a). The temperate region displays four to eight months of average temperature over 10°C. This zone, the main in terms of area, covers all the continent from West to East and has its Southern margin on the North border of Spain, Italy and Greece and its Northern on the South border of Scandinavia (Fig. 1.1). When the coldest month displays values over 0°C, the zone is called temperate oceanic and temperate continental when it is below 0°C. The first zone is found closer to the Atlantic coast and, for this reason, displays higher rainfall levels and a lower annual temperature amplitude. The typical vegetation cover of both regions is deciduous broadleaved forests. Further East, when evapotranspiration exceeds transpiration, the temperate steppe region is found. There, the very low rainfall prevents the establishment of vegetation other than grass and low shrubs. Finally, the mountainous temperate region is located at high altitudes, dominated by coniferous or mixed coniferous-deciduous forests and characterized by 1 to 4 months with negative temperature and elevated rainfall due to the positive relationship between precipitation and altitude observed in Europe (Basist *et al.*, 1994; Johnson and Hanson, 1995).

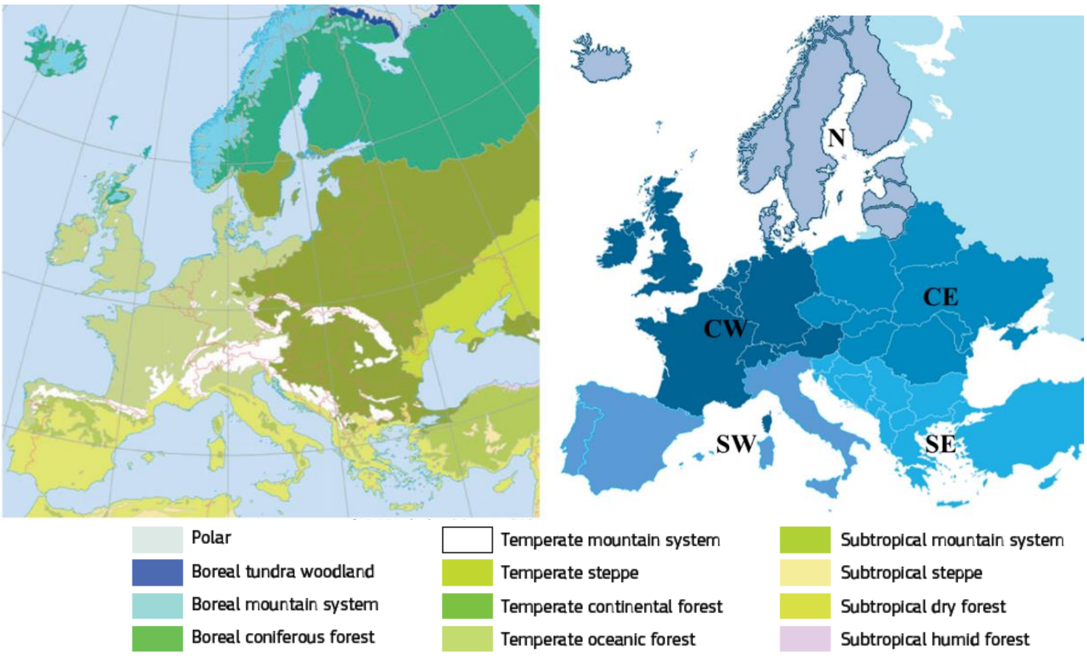

**Figure 1.1: Map of the different ecological zones in Europe according to FAO (2012b) (left) and geographical division of Europe according to political boundaries in Northern (N), Central-West (CW), Central-East (CE), South-West (SW) and South-East (SE) zones (right)**

Due to the competition with other landcovers, European forests are not evenly distributed across the continent. 31% of the European forest area is located in the Northern (N) countries that are sparsely-populated and display a climate too cold for agriculture while between 14 and 20% of the area is found in each of the following parts of the continent: Central-West (CW), Central-East (CE), South-West (SW) and South-East (SE) (Fig. 1.1). However, due to differences in growing stock density, CW and CE countries, representing together most of the European temperate zone, share the largest parts of growing stock (27 and 33% respectively), followed by N (26%), with values largely superior to SW and SE countries (3 and 11%) (Korhonen et al., 2020).

Moreover, although a typical vegetation can be assigned to the different ecological zones, a much larger diversity is present in each of them. For example, 66% of the forested area in Northern Europe, which is mainly located in the mainly coniferous boreal domain, is actually coniferous forest while the temperate continental and oceanic zones in CW and CE countries display only a slightly larger proportion of deciduous than coniferous forests. This peculiarity can be explained by the forest management history of Europe. In the early-Holocene, after the last glacial period, forests in Europe probably extended over 80% of the continent surface (Bradshaw and Sykes, 2014; Zanon et al., 2018). Since mid-Holocene, humanity has started to modify the European landscape (Kaplan et al., 2009). According to different studies using palynological records (e.g. Edwards et al., 2017; Zanon et al., 2018), the forest cover has thus decreased to reach a minimum around 1850 (Meyfroidt and Lambin, 2011). This shrinkage originates from the growth of European population and the ensuing increase of wood consumption to cook and heat, the forest removal for new agricultural areas, as well as the diversification of timber use (for house, ship construction, charcoal) (McGrath et al., 2015). Since 1850, European forests have gained territory to reach their current land surface. This afforestataion accompanied the yield increases in agriculture generated by technological advancements as well as a change in the perception of the forest (Kaplan et al., 2012). Indeed, Mather (1992) pointed out that similar conditions in many different European countries led to this transition from the reduction to an expansion of the forest land: an increase in the wood demand that lead to a scarcity of the forest resources and the perception of a forest crisis. These conditions generally triggered, in turn, a consideration of the forest for its economic and protective values and the subsequent implementation of conservation and intensive management policies (Mather, 1992; Meyfroidt and Lambin, 2011). The production-oriented management modified the species composition of European forests, favouring monospecific plantations of fast-growing coniferous at the expense of broadleaved species, explaining the current situation.

However, with the appearance of close-to-nature forest management promoting mixed and uneven-aged, a reverse trend promoting more heterogeneous forests is occurring throughout Europe. Between 2005 and 2015, 1% of the monospecific forest area was turned into stands with two to five species (Lier et al., 2020). Similarly, the percentage of uneven-aged stands has increased in Europe (Zeller et al., 2021). Quantifying this increase at the continental scale is difficult as definitions of "(un)even-aged" can change from one country to the other. Still, the two first surveys "State of Europe's forests" realised in 2003 and 2007 estimated the percentage of uneven-aged forests to be 17 and 13% compared to 32 and 25% found in the last two surveys (2015 and 2020). Finally, broadleaved forests undergo a sustained increase. Between 2010 and 2020, at the continental scale, the part of deciduous forests in the total forest area went from 27 to 37% at the expense of coniferous and mixed forests in similar proportions (San-Miguel-Ayanz et al., 2011; Korhonen et al., 2020).

The deciduous forests of the European temperate zone is dominated by two genus: fagus (European beech, *Fagus Sylvatica* L.) and quercus (pedunculate oak, *Quercus robur* L. and sessile oak, *Quercus petraea* (Matt.) Liebl) (Fig. 1.2). As stated earlier, this forest type represents a bit more than half (with an increasing trend) the area of the European temperate forests, which, in turn, represents the main growing stock of Europe's forests.

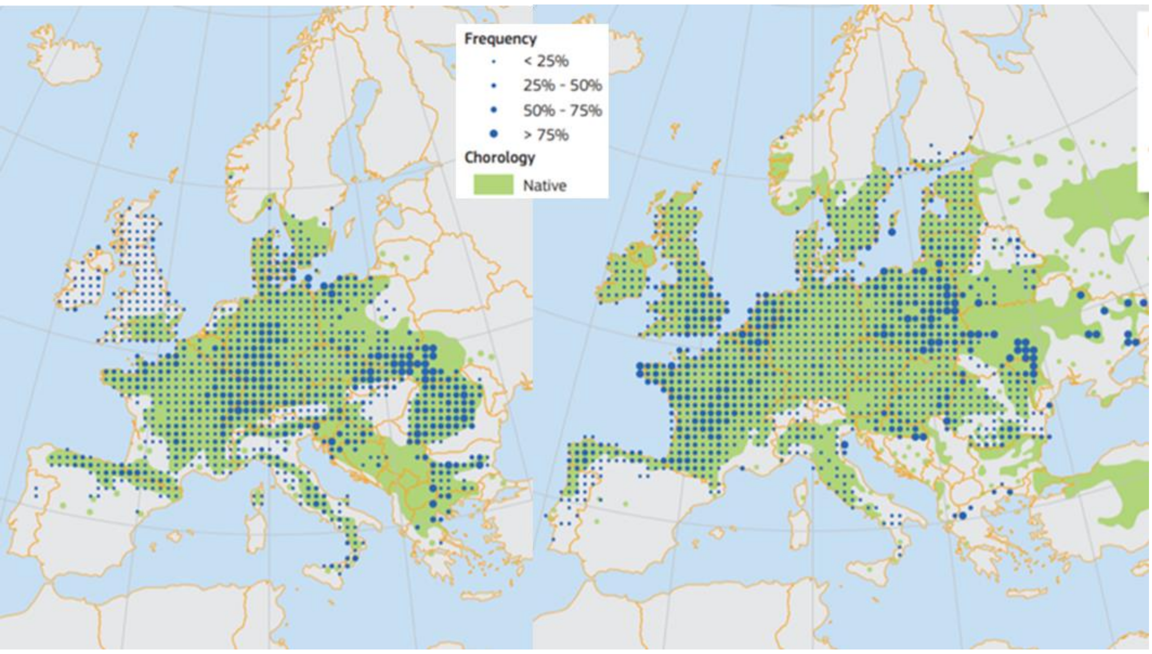

**Figure 1.2: Species distribution of European beech (left) and pedunculate oak (right) represented by the frequency of occurrences in observations from National Forest Inventories (maps from the European atlas of forest tree species by San Miguel et al., 2016)**

## 2. RECENT AND FUTURE CLIMATE CHANGE

Changes in environmental conditions can modify the forest state and dynamics. In some cases, this response is temporary and the forest will return to its initial state but in others, modifications can be irreversible and the forest will evolve towards a new equilibrium. Climate evolves continuously according to different natural cycles like the daily, seasonal and pluri-annual cycles, for which forests are adapted. However, due to the continuous release of greenhouse gas in the atmosphere since the industrial revolution, substantial changes in the European climate have been observed at unprecedented rates. The air temperature datasets HadCRUT4 (Morice et al., 2012), NOAA Global Temp v5 (Karl et al., 2015) and GISTEMP v4 (Lenssen et al., 2015) estimate that the temperature during the last decade (2010-2019) was between 0.94 and 1.03°C warmer than during the second half of 19th century (1850-1899) at the global scale and between 1.68 and 1.86°C higher over Europe. Rainfall monitoring is more recent and changes are more spatially variable compared to temperature but, according to E-OBS dataset (Haylock et al., 2008), a significant annual precipitation decrease was detected up to 90 mm per decade in the Iberian Peninsula, between 1960 and 2015, while rainfall increased over most of Scandinavia for the same period with values as high as 70 mm per decade. In terms of variability, an increase in drought frequency and severity was registered between 1950 and 2015 (particularly between 1981 and 2015) over Southern Europe in summer and spring. Inversely, lower frequency and severity of drought was monitored in Northern Europe, particularly during spring and winter (Spinoni et al., 2017).

In the future, the downscaled climate projections based on the results from 10 simulations including five different global climate models (GCM) and six regional climate models (RCM) predict that all European regions are expected to undergo substantial warming in all seasons of the year. Compared to the period 1971-2000, the likely increase (66% of the projection distribution) in mean annual temperature at the horizon 2071-2100 amounts between 1.4 and 4.1°C for the scenario RCP4.5 (moderate scenario) and between 2.7 and 6.2°C for the scenario RCP8.5 ("business-as-usual"). The spatial warming pattern displays the highest temperature increase in the Southern region in summer (Juny to August) and in Northern and Eastern Europe during winter (December to February) (Fig. 1.3). In addition, more frequent and long heat waves are expected in summer particularly in Southern and Western Europe (Jacob et al., 2014).

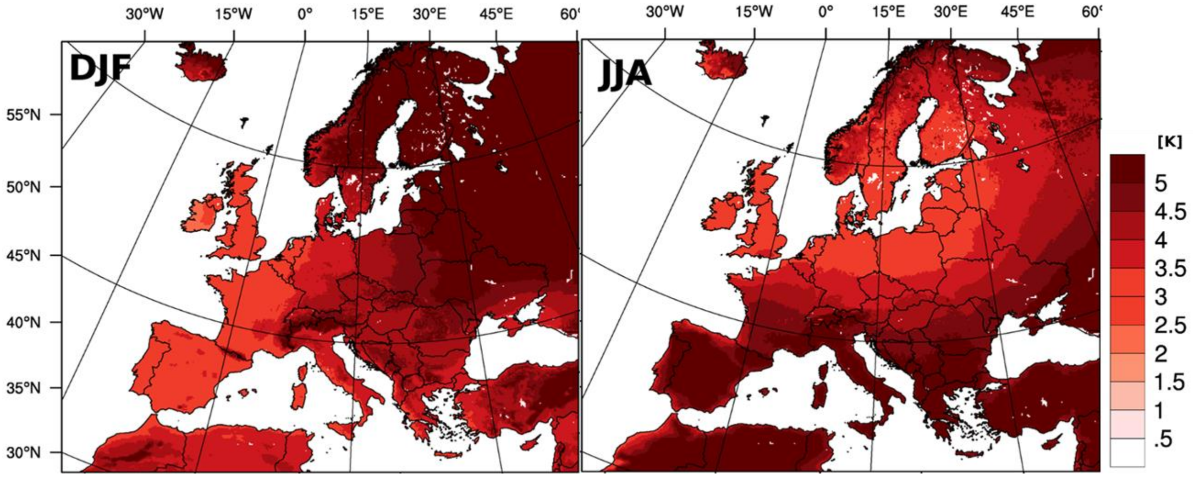

**Figure 1.3: Projected changes of seasonal mean temperature in winter (December to February) and summer (Juny to August) for 2071–2100 compared to 1971–2000 for scenario RCP8.5 downscaled by the EURO-CORDEX project based on 10 simulations from 5 different GCM and 6 RCM (Jacob et al., 2014)**

The future change in yearly precipitation is less marked than that of temperature with the continent divided in two parts: Southern Europe that will experience less rainfall and Central and North-Eastern Europe higher rainfall with a corridor with non-significant change approximately linking the North-West part of France and Albania. Overall, the range of precipitation change will extend from -10 to +17% and -21 to +32% under the scenario RCP4.5 and 8.5, respectively. Behind this trend, a general tendency is observed with more precipitation in winter and less in summer over most of the continent (Fig. 1.4) (Jacob et al., 2014).

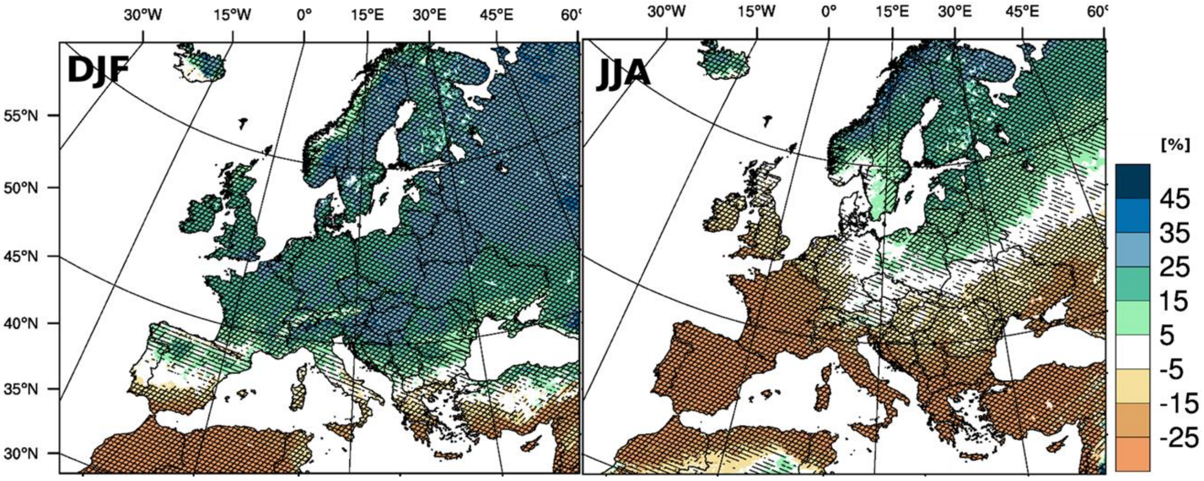

**Figure 1.4: Projected changes of seasonal precipitation in winter (December to February) and summer (Juny to August) for 2071–2100 compared to 1971–2000 for scenario RCP8.5 downscaled by the EURO-CORDEX project based on 10 simulations from 5 different GCM and 6 RCM (Jacob et al., 2014)**

To assess the robustness of the projections, the signal-to-noise ratio is often used. It is calculated as the ratio between the change in decadal means of a variable divided by the standard deviation of the projections from different GCMs. Values superior to one depict a robust signal. For temperature, the signal-to-noise ratio is always superior to one in winter and summer over Europe considering the EURO-CORDEX projections. Regarding rainfall, only 22% of Europe, mainly in the South-Western part, displays a robust signal (decrease) in precipitation (Matte et al., 2019). For the CMIP5 ensemble, almost all models agree on a rainfall increase in winter but considerable differences appear in summer with models predicting annual rainfall changes from -180 to +100 mm (Fig. 1.5 right) (McSweeney et al., 2015).

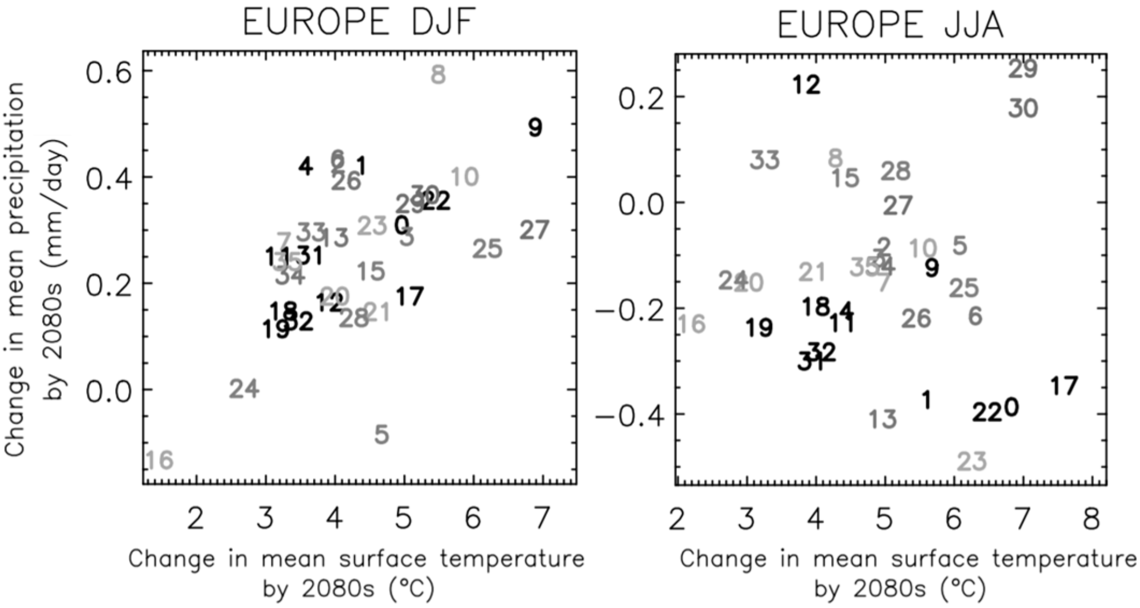

**Figure 1.5: Average change in mean temperature and precipitation in winter (December to February) and summer (Juny to August) projected by the different models of the CMIP5 ensemble by 2080 (McSweeney et al., 2015).**

## 3. OBSERVED RESPONSE OF THE FOREST ECOSYSTEM TO CLIMATE CHANGE

### Phenology

The transition from bud dormancy to budburst is a complex process that includes a sequence of phases where chemical and environmental (mainly air temperature) factors successively prevent the bud opening until the right conditions are met (Chuine et al., 2016). In autumn, environmental (mainly photoperiod and air temperature but also drought, ozone or pest and pathogens) and hormonal factors interact to trigger the leaf fall, which is also affected by the leaf development age (Lim et al., 2007). Given the central role of climate conditions in these processes, it is not surprising that phenology is affected by ongoing climate changes.

There are now numerous evidence that the warming experienced over the last decades has increased the length of the vegetation period in temperate deciduous forests. *In situ* as well as satellite observations have pointed out advances in tree leafing between 2.5 and 5.2 days/decade in the last decades (Chmielewski and Rötzer, 2001; Zhou et al., 2001; Stockli and Vidale, 2004; de Beurs and Hennebry, 2005; Menzel et al., 2006; Jeong et al., 2011; Fu et al., 2014). This advance considerably decreased or was even reversed between 2000 and 2012 (Fu et al., 2014; Wang et al., 2015; Park et al., 2016) probably due to the reduced air temperature warming (so-called global warming hiatus) (Piao et al., 2019). Observations show as well a delay in tree yellowing with values between 0.2 and 1.8 day/decade but in a less marked and more heterogenous way (Menzel et al., 2006; Jeong et al., 2011; Liu et al., 2016) that was also paused during the period 2000-2012. This lengthening of the growing period has enhanced forest productivity due to a longer period of photosynthetic activity (Park et al., 2016; Crabbe et al., 2016; Kolář et al., 2016).

Paradoxically, the earlier leaf onset induced by warmer temperature has also increased the occurrence of spring frost damage in Europe. Observations show that such damages depend on the species response to warming with the more opportunistic (quick response to temperature) being the most affected (Vitasse et al., 2014; Hänninen et al., 2016; Ma et al., 2018; Liu et al., 2018; Zohner et al., 2020).

**Water stress**

Transpiration transfers water from the soil, across the tree and to the atmosphere through leaf stomata. Carbon acquisition also occurs through these openings, linking the tree carbon and water cycles. Under dry conditions, when the evaporative demand is not met by soil water availability, the water flux can be reduced by a partial closure of stomata, which also limits the carbon uptake. Tree species that quickly reduce stomatal conductance when they experience water stress like beech are called isohydric species. In case of prolonged drought episodes, the insufficient photosynthesis reduces the stock of non-strucural carbohydrates and can lead to death through carbon starvation (Fig. 1.6). Inversely, anisohydric species like oak keep their stomata open for a larger range of water stress, reducing the risk of carbon starvation. For these species, the risk during extreme drought is the appearance of hydraulic failure and irreversible damage to xylem vessels transporting water, weakening considerably the tree (Fig. 1.6) (McDowell et al., 2008; Allen et al., 2010; Anderegg et al., 2013; Klein, 2014). On the field, this distinction is less marked and evidences of hydraulic conductivity loss are ubiquitous in case of drought-induced mortality while signs of carbon starvation are not as common (Adams et al., 2017).

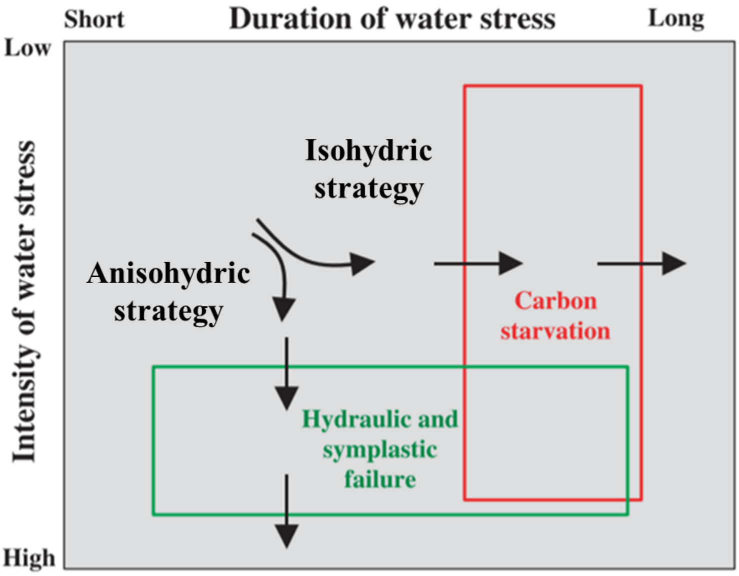

**Figure 1.6: Theoretical differentiation of isohydric and anisohydric strategies and their relationship to the type of drought. Adapted from McDowell et al. (2008).**

Since the middle of the XXth century, the coupled effect of warmer temperature and changes in the seasonal rainfall regime has increased the atmospheric evaporative demand and led to more frequent and/or severe summer drought over all Europe excepted in Scandinavia and Iceland (Spinoni et al., 2017). In 2003 and 2018, two important drought events occurred in many European forests. A strong reduction of forest productivity was registered during these events (Ciais et al., 2005; Bréda et al., 2006; Granier et al., 2007; Bastos et al., 2020; Schuldt et al., 2020).

Higher mortality rates are also documented during extreme drought events (Williams et al., 2013; Neumann et al., 2017; Greenwood et al., 2017). However, quantifying the influence of lower magnitude drought events is difficult as mortality is usually a complex and long-term process that comprises predisposing, inciting and contributing factors like drought and heat stress, fire, windstorm, pests and diseases (Franklin et al., 1987; Hartmann et al., 2018; Losseau et al., 2020). In addition, in managed forests like those found in temperate European region, dying and dead trees are removed during thinning and cutting operations, which blurs the signal. Then, disentangling the effect of drought episodes on the temporal evolution in tree mortality from that of management and normal forest dynamics is challenging.

Long-term monitoring studies show relatively constant or slightly increasing mortality rates over time for oak and beech. Using data from 276 plots in Switzerland covering a time span over one century, Etzold et al. (2019) showed that mortality rates of beech and oak (1.3 and 2.0%/yr, respectively) remained unchanged or even decreased over the last 50 years. The ICP level II Forests programm that records defoliation levels (a contributing factor of tree mortality) over nearly 15.000 sites across Europe display very limited mortality increase of 2.4 and 2.2% over 20 years for beech and oak, respectively (Timmerman et al., 2020).

### Species distribution

Northern and upward movements have been locally detected as a response to rising temperatures at both the cold and warm margins of tree species distributions. These so-called migrations are the results of seed dispersal and changes in the competition patterns between species and can be initiated or facilitated by management practices (Bolte et al., 2010; Bussotti et al., 2015).

Over the entire Swiss Alps, an upward shift of the tree line (mainly coniferous species but also beech) has been found to be primarily driven by land abandonment but was also related to a change in temperature (Gehrig-Falser et al., 2007). Similarly, in North-Eastern Spain, beech was found on average 70 m higher at high altitude (1600-1750 m) between 1945 and 2003 in response to a 1.5°C warming (Penuelas and Boada, 2003). Simultaneously, holm oak progressively replaced beech at lower altitudes (800-1400m) (Penuelas et al., 2007). The same trend was highlighted in French Alps with pubescent oak replacing pine forests (Rigling et al., 2013).

At the cold margin of their distribution, holm oaks have colonised northward at rates between 22 and 57 m/yr (Delzon et al., 2013) while the beech competitive ability was significantly strengthened in spruce-beech mixed stands in Southern Scandinavia (Bolte et al., 2010) and Central Europe (Sedmakova et al., 2019).

### Natural disturbances

Natural disturbances are usually differentiated in biotic and abiotic disturbances. In Europe, the main abiotic disturbances are windthrow and wildfires that both affected approximatively 0.11% of the forest area per year while the main biotic agent of disturbance is the bark beetle that damaged 0.02% of timber volume each year between 1850 and 2000 (Schelhaas et al., 2003). While being natural phenomena, the damage considerably increased (between +2.6 and +5.3%/yr) over the last decades dut to anthropogenic climate change (Schelhaas et al., 2003; Dupire et al., 2017; Gregow et al., 2017; Fernandez-Carrillo et al., 2020). Warmer and dryer conditions facilitate the proliferation of bark beetles and the occurrence of wildfires. These effects were particularly strong in older stand with high proportion of conifers (Seidl et al., 2011). Interestingly, outbreaks of all disturbance types show strong temporal synchronization, which highlights an intertwined relationship (Senf and Seidl, 2018).

The succession of warm periods experienced during the last decade has triggered a considerable increase in insect outbreak in Europe and Northern America, particularly in coniferous forests (Millar and Stephenson, 2015; Venäläinen et al., 2020; Koontz et al., 2021). For example, in Central Europe, before 2015, around 7% of the harvested wood volume was infested by insects. This proportion has dramatically increased over the last five years to reach 70% in 2019 , which can be related to the massive bark beatle attack on Norway spruce stands that occurs since 2018 (Fernandez-Carillo et al., 2020).

### Productivity

The different factors presented (vegetation period length, water stress, forest movements and disturbance occurrence) coupled to the anthropogenic increase in atmospheric $CO_2$ concentration and in nitrogen deposition have generated changes in the forest productivity. Since the middle of 20th century, a global increase of forest productivity has been observed, increasing the land carbon sink (Boisvenue and Running, 2006; Bontemps et al., 2011; Fernandez-Martinez et al., 2017). The increase in forest productivity is mainly attributed to the $CO_2$ fertilizing effect and, secondarily, to the lengthening of the vegetation period (Bellassen et al., 2011; Zhu et al., 2016; Penuelas et al., 2017). The increase in productivity has slowed down in the last decades (Charru et al., 2017) because of the reduced air temperature warming that stopped or even reversed the lengthening of the vegetation period between 2000 and 2014 (e.g. Park et al., 2016) and due to a fertilizing effect of $CO_2$ constrained by the nitrogen availability (Wang et al., 2020). Interestingly, productivity and mortality are two intertwined processes with mortality affecting negatively stand productivity and decreases in productivity being a first step toward mortality (Dobbertin, 2005; Cailleret et al., 2017).

## 4. IMPACT OF SITE PROPERTIES ON THE FOREST FUNCTIONING AND RESPONSE TO CLIMATE CHANGE

Locally, the trends in productivity are much more contrasted with numerous documented cases of decreasing (e.g. Jump et al., 2006; Sarris et al., 2007; Scharnweber et al., 2011; Ruiz-Benito et al., 2014), increasing (e.g. Becker et al., 1994; Bergès et al., 2000; Charru et al., 2010, Bontemps et al., 2011) or varying (e.g. Boisvenue and Running, 2006; Spiecker et al., 2012; Zang et al., 2014) productivity changes due to difference in site characteristics. Indeed, the site conditions modify the forest response to climate change and can be divided in three main components: climate, soil and stand. While the effects of the two first components are relatively well known and straightforward, the influence of some of the stand charcateristics on the forest response to climate change is much less understood.

As developed earlier, the effect of a climate warming is not the same whether a tree is located at the upper or lower temperate distribution range of its species. This is also true for rainfall. Dryer conditions in sites that already experience water stress will be more detrimental than in wetter sites (e.g. Jump et al., 2006; Pasho et al., 2011). This hypothesis was verified, among others, by Martin-Benito and Pederson (2015), who showed that, along a gradient from cold and dry sites to warm and wet, tree growth was more correlated to rainfall in the dryer sites than the wet ones and high summer temperature had a stronger negative effect in the warm than the cold sites.

Soil physical properties can dampen the negative effect of water stress on forest productivity and mortality when they display greater soil depth and subsequent rooting depth and water holding capacity (Phillips et al., 2016; Kostić et al., 2021). In addition, as stated previously, a limited nutrient availability can considerably constrain the $CO_2$ fertilizing effect. Then, forests growing on nutrient-richer soils with a large water reserve, facilitating mineral uptake, could be less negatively or even positively affected by climate change.

The stand characteristics can be further subdivided into different components: tree species composition (identity and diversity effects), stand structure and density. Tree species identity simply represents the difference in functional traits between species (Table 1.1). Beech trees are known to be drought and waterlogging sensitive but have a strong shade tolerance and recover quickly after drought events. Inversely, oaks are much less affected by drought and waterlogging (especially sessile oak regarding drought and pedunculate oak regarding waterlogging) but have higher light requirements and their recovery period after drought is longer (Jonard et al., 2011; Scharnweber et al., 2011; Scherrer et al., 2011; Vanhellemont et al., 2019). Coupled to a high shade tolerance, the faster growth and more regular seed production of beech (Gazol and Ibanez, 2010; Del Rio et al., 2014) compared to oak make them better competitor under non-limiting climate and soil conditions (Petritan et al., 2017; Rubio-Cuadrado, 2018). Therefore, under such conditions, regular interventions favouring oaks must be conducted to conserve mixed oak and beech stands. On the other hand, oak trees dominate in dry sites and on poorly-drained soils regularly experiencing saturation (Scharnweber et al., 2013). Regarding disturbances, both species are relatively resistant to pests and pathogens compared, for example, to coniferous stands.

However, the deeper root system of oaks makes them more resistant than beech to windstorms (San-Miguel-Ayanz et al., 2016).

**Table 1.1: Comparison of the functional traits of beech and oak based on the European Atlas of forest species (San-Miguel-Ayanz et al., 2016) and the Fichier écologique des essences (Petit et al., 2017)**

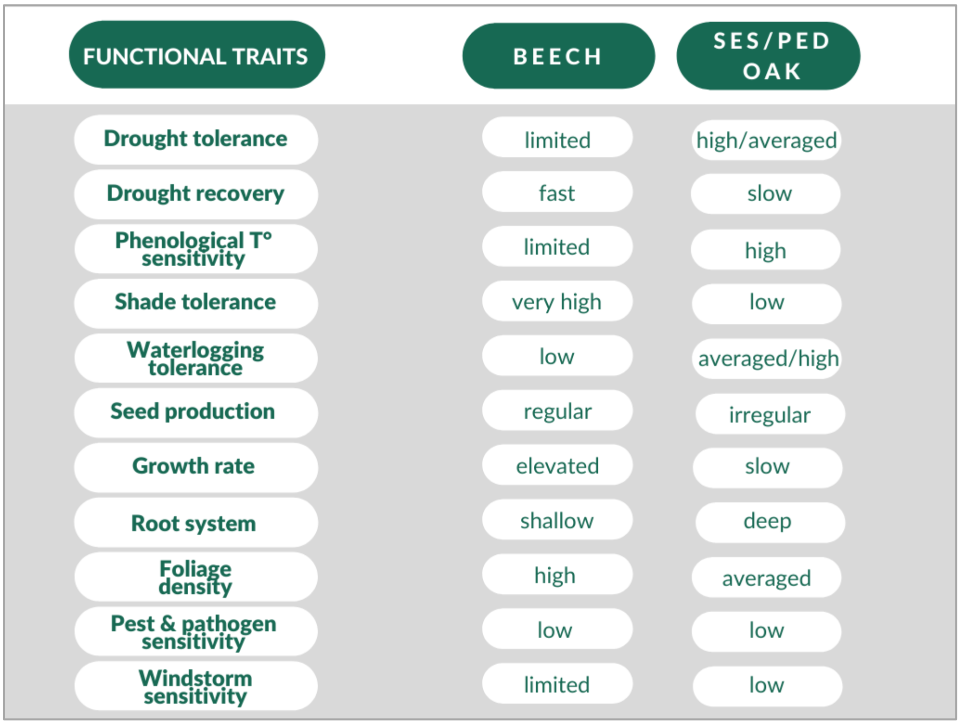

| FUNCTIONAL TRAITS | BEECH | SES/PED OAK |
|---|---|---|
| Drought tolerance | limited | high/averaged |
| Drought recovery | fast | slow |
| Phenological T° sensitivity | limited | high |
| Shade tolerance | very high | low |
| Waterlogging tolerance | low | averaged/high |
| Seed production | regular | irregular |
| Growth rate | elevated | slow |
| Root system | shallow | deep |
| Foliage density | high | averaged |
| Pest & pathogen sensitivity | low | low |
| Windstorm sensitivity | limited | low |

Competition is not the only process that two co-existing species experience. The inter-species differences in functional traits can temporally and spatially differ resource acquisition between the two species, optimising resource use and decreasing competition (complementarity process). In addition, the access to resource of a species can also be facilitated by the presence of another species for example through hydraulic soil water uplift or nutrient fixation (facilitation) (Grossiord 2019; Bello et al. 2019). As a result, even if the question is still debated, more and more studies show that mixed stands display increased resistance to drought (Pretzsch et al., 2013; Anderegg et al., 2018; Steckel et al., 2020), productivity loss (Liang et al., 2016; del Rio et al., 2016), biotic and abiotic disturbances (Silva Pedro et al., 2015; Jactel et al., 2017; Jactel et al., 2021) compared to monospecific stands. In addition, species diversity coupled to stand heterogeneity also increases the forest resilience. Indeed, disturbances usually do not affect similarly trees from different species and at different development stages and favour productive and/or resistant species (the so-called selection effect) (Wardle, 2001; Lefcheck et al., 2015). Finally, given the greater susceptibility of tall trees to windstorms, drought and pest attacks, the presence of a developed second tree layer allows a faster replacement of dead trees and smoothens the transition (Brockerhoff et al., 2017; Seidl et al., 2017). Linked to this effect, the stand spatial aggregation influences the degree of intra-specific competition as well as inter-specific complementarity whether the trees of a same species and with similar dimensions are clumped or homogeneously scattered (Sterba et al., 2018).

Compared to species diversity, the influence of stand structural complexity (variability in individual tree girth and height) on forest functioning has been considerably less studied (Ali, 2019). One of the reason for this is that structural complexity is linked to other stand properties and consequently, its effect is more difficult to isolate. For example, stands with different tree species and high density usually display more complex structure (Forrester and Bauhus, 2016; Soares et al., 2016). In addition, only individual-based tree growth models can integrate and study this stand feature. At the individual scale, the stand structural complexity modifies how individual trees are affected by climate change as resource competition is a very local process strongly depending on the size, age or social status of a tree relatively to its neighbours. Dominant trees benefit from a better light access but suffer more from drought than understorey trees due to their higher vulnerability to hydraulic stress and their crowns particularly exposed to atmospheric conditions (Bennett et al., 2015; McDowell and Allen 2015). Inversely, the lower radiation, wind and temperature during the warm period decreases the evaporative demand experienced by smaller trees while warmer temperature in spring accelerates budburst (Carl et al., 2018; De Frenne et al., 2019; Zellweger et al., 2019). The micro-environmental conditions felt by a tree also influence how it will allocate carbon for growth. At the stand scale, correlations between structural complexity and productivity have been highlighted but with mixed results. Some papers found out a negative effect of structure complexity on forest productivity (e.g. Binkley et al., 2013; Luu et al., 2013; Cordonnier et al., 2015; Bourdier et al., 2016; Soares et al., 2016) and others a positive effect (e.g. Zhang and Chen, 2015; Dănescu et al., 2016 ; Bohn and Huth, 2017; Ercanli, 2018). These contrasting results could be explained as the relationship depends on other variables. Indeed, positive relationships are preferentially found in mixed stands or in mature stands but rather negative ones in monospecific or young ones (Zeller and Pretzsch, 2019). The mechanisms suggested to explain the positive relationship are the niche complementarity as, for example, higher root densities are found in structured stands (Bolte et al., 2013; Grote et al., 2016) and the selection effect as described earlier. The negative relationship could be due to the assymetric light competition between dominant and suppressed trees that makes the productivity reduction of understory trees exceed the productivity gain of overstory (Ali, 2019).

Finally, stand density is a product as well as a direct measurement of the resource competition level in a stand and consequently, of the tree interactions, whether they are competition, complementarity or facilitation (Forrester and Bauhus, 2015). Therefore, it can strongly affect the forest response, for example, to the summer dryer conditions (Bello et al., 2019). One of the difficulty when accounting to the stand density effect through a comparison of established forests is that the management and disturbance history are usually unknown so that the density is not guaranteed to be the result of tree interactions (Forrester and Bauhus, 2015).

## 5. ADAPTING FOREST MANAGEMENT TO CLIMATE CHANGE

In a rapidly-changing environment, tree species populations can either persist through adaptation to new conditions, through migration to remain in their ecological niche or extirpate (extinct locally) (Aitken et al., 2008). The migration speed that would allow tracking the rate of future climate change is usually considered as unrealistic in natural conditions, especially for non-pioneer species like oak and beech that do not rely on wind for their seed dispersal (Dobrowski et al., 2013; Saltré et al., 2013), even if mammals or birds can accelerate their migration (Johnson and Web, 1989). Observations of intra-species and even intra-population genetic variations in functional traits have provided strong evidences of tree adaptation to local environmental changes (Savolainen et al., 2007; Aitken et al., 2008; Franks et al., 2014). However, due to the lack of data for genetic and physiological tree responses to climate change, it is very difficult to make assumptions on the future tree adaptive ability (Ruiz-Benito et al., 2020).

To avoid the negative consequences or even take advantage of potential benefits of climate changes, managers can adapt forests to cope with the future conditions. The climate and soil components can hardly be modified but forestry practices can modify the stand specific composition, structure and density. Specific composition can be modified through the planting of exogenous trees or regeneration strategies favouring particular species while the structure and density can be changed by different cutting strategies. As a result, the forester must decide among an ensemble of options (species selection, artificial *vs.* natural regeneration and silvicultural treatment towards even *vs.* uneven-aged stands) and, in the same time, consider the site constraints including ungulate density, the possible climate changes and future disturbance occurrence (Bauhus et al., 2013). Given the complexity of this multifactorial problem and the very long timescale for its application, foresters need guidelines to test suitable management strategies. However, while forestry practices for pure, even-aged stands have been studied for decades (Del Rio et al., 2015), foresters lack recommendation regarding rotation age or target dbh in mixed forests, which depend on the present species and site conditions (Bravo-Oviedo et al., 2014; Pach et al., 2018). As it is impossible to test *in situ* all silvicultural options for each site conditions and climate scenario, models able to implement innovative forestry practices are a good alternative to address these questions.

Nowadays, as shown in the first section, there is a trend toward turning coniferous and even-aged stands to mixed uneven-aged stands according to the close-to-nature and continuous-cover forestry. Indeed, given the uncertainty in the magnitude of global changes and how they will locally be expressed (Lindner et al., 2014), more and more foresters favour more diverse sites to reduce the risk of general dieback in spite of the lack of knowledge regarding mixed forest management. Progressively converting monocultures to mixed forests and even-aged to uneven-aged forest and favouring the settlement of drought-tolerant species can take a long time during which dieback can occur (Elkin et al., 2015). As a result, other adaptative practices that can be directly implemented, like intensified thinning or a reduction of harvesting dimension are regularly suggested (Youssefpour et al., 2017; Cosofret and Bouriaud, 2019). Indeed, thinned stand productivity is less affected during drought episodes due to a reduced competition for water among remaining trees (D'Amato et al., 2013; Sohn et al., 2016). However, this option is often considered as temporary because the thinning mitigating effect rapidly decreases with time and can therefore only have a limited impact if the thinning does not occur more or less at the same time as the droughts (D'Amato et al., 2013; Elkin et al., 2015).

## 6. REPRESENTATION OF SPATIAL HETEROGENEITY IN FOREST GROWTH MODELS

Different approaches can be undertaken to study the impact of future environmental changes on forests: long-term monitoring, environment-modifying experiments and modelling. While the two first are useful to document and understand the physiological processes, they do not cover all the ecological conditions on which climate change will apply and they cannot be used to test all the interactions between the processes nor to cover all the possible future conditions. On the other hand, models are based on the knowledge acquired from these approaches and try to represent them through mathematical equations. By doing so, they simplify the reality but enables one to test any future conditions.

Predicting the future response of European forests to climate changes can be done using different modelling approaches, designed to answer particular questions at specific scales and from different types of data (Ruiz-Benito et al., 2020). With an approach based on plant functional types (PFTs) (Cramer, 2001) requiring limited data for initialization, the dynamic global vegetation models (DGVMs) have been regularly used to estimate the impact of climate change on the European or global forest (Cramer et al., 2001; Poulter et al., 2011; Luyssaert et al., 2018). While essential to obtain continental or global estimates of carbon exchanges, their predictions are however locally associated with considerable uncertainties (Huntzinger et al., 2017). Indeed, models calibrated with coarse and global datasets do not provide reliable results at the local scale (Schwalm et al., 2010). At the regional scale, the forest landscape models (FLMs) provide information on how climate change affects long-term forest dynamics accounting for large-scale disturbances but have generally a simplified eco-physiological process description and stand spatial representation due to their large spatial and temporal perspective (Reyer, 2015 ; Shifley et al., 2017). Such models are appropriate to tackle forest management issues at the regional and landscape levels but not to analyse the site conditions and the stand structure and composition effects on forest response to climate change. Finally, process-based stand models were designed to account for the influence of local conditions on tree growth. The first generation of these models simplified the spatial representation by considering an averaged tree that represents the whole stand (stand models) and focused mainly on the process representation. This approach considerably reduces data and computation requirements and displays good predictive ability in pure even-aged forests (typically plantations) but hardly manage to simulate heterogeneous (mixed and uneven-aged) stands, which limits their use as 67% of European forests are composed of two or more species and 28% are uneven-aged (Korhonen et al., 2020).

A significant part of the stand structure and composition is accounted for within cohort-based models as they integrate the vertical component of the stand heterogeneity (Pretzsch et al., 2015). These models appeared as a partial response to the oversimplified spatial representation of stand-based models and extend their potential application area with only a limited increase in data requirements. Accordingly, cohort-based models have been applied on large numbers of sites from inventory and monitoring networks (e.g. NFI, ICP). Still, the assumption of horizontal homogeneity in cohort-based models does not allow accounting for the fact that trees compete for resource locally and adapt their development according to the local conditions, positively or negatively influenced by neighbouring trees (Berger et al., 2008). Yet, these processes can only be captured by models integrating horizontal heterogeneity and the relative position of trees (spatially-explicit models).

As a result, individual-based (IBM) and spatially-explicit models were developed. These models combine a detailed process representation with a spatial approach allowing to take individual variability, local environment and tree adaptive behaviour into account as well as forestry practices. This framework is also ideal for model calibration and evaluation as measurements at the individual and stand scale can both be compared to model predictions. However, given the important data requirements for the model initialization and the consequent computation time, this is usually only achieved on a restricted number of sites. In turn, this decreases the model genericity, which can become particularly problematic when the model is used in conditions where it was not tested previously.

**Table 1.2: Comparison of the concepts used in different individual-based models (HETEROFOR is described as it was at the start of my PhD) and their spatial scale (S=stand, C=cohort, I=individual, I*=individual target tree, GP=grid point). Abbreviations used in for describing transpiration (P-M= Penman-Monteith, SPAC = Soil-Plant-Atmosphere Continuum)**

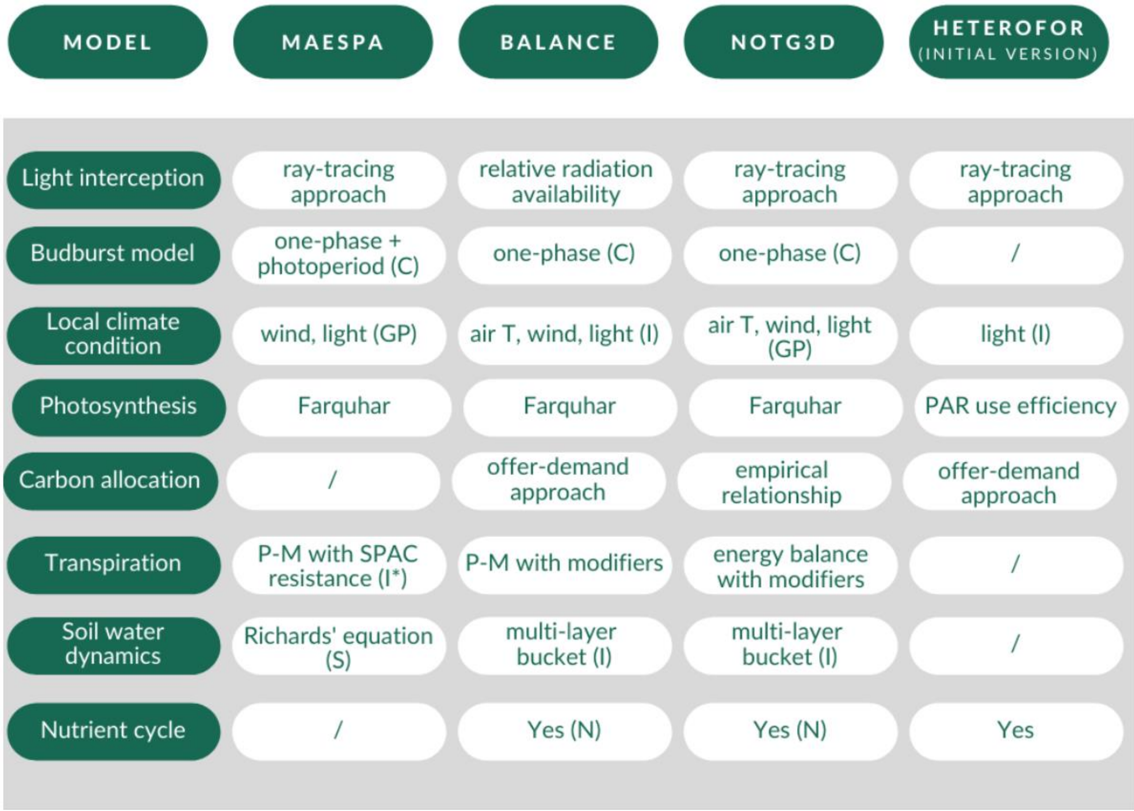

| MODEL | MAESPA | BALANCE | NOTG3D | HETEROFOR (INITIAL VERSION) |
|---|---|---|---|---|
| Light interception | ray-tracing approach | relative radiation availability | ray-tracing approach | ray-tracing approach |
| Budburst model | one-phase + photoperiod (C) | one-phase (C) | one-phase (C) | / |
| Local climate condition | wind, light (GP) | air T, wind, light (I) | air T, wind, light (GP) | light (I) |
| Photosynthesis | Farquhar | Farquhar | Farquhar | PAR use efficiency |
| Carbon allocation | / | offer-demand approach | empirical relationship | offer-demand approach |
| Transpiration | P-M with SPAC resistance (I*) | P-M with modifiers | energy balance with modifiers | / |
| Soil water dynamics | Richards' equation (S) | multi-layer bucket (I) | multi-layer bucket (I) | / |
| Nutrient cycle | / | Yes (N) | Yes (N) | Yes |

To account for the main tree growth processes affected by climate change, IBMs should integrate a process-based description of phenology, light interception, water and nutrient cycling as well as carbon allocation. According to the review conducted by Pretzsch et al. (2015) on 54 forest growth models able to represent species mixing, only three out of the 11 individual-based and spatially-explicit models integrated simultaneously radiation, water cycling and phenology modules: MAESPA (Duursma and Medlyn, 2012; Duursma, 2008), BALANCE (Grote and Pretzsch, 2002; Rötzer et al., 2010) and EMILION (Bosc et al., 2000). However, the latter is specific to pine species only. In addition to the mentioned models, the recent NOTG-3D (Simioni et al., 2016) also includes the mentioned modules. Even if the models displays the same features, they all present different advantages and disadvantages.

Regarding light interception, MAESPA and NOTG3D use a ray tracing approach that allows to calculate the energy intercepted for numerous grid points in the tree foliage for the first and at the organ scale for the second depending on a season-dependent sun trajectory. Compared to the other models, light interception is more roughly estimated in BALANCE as the proportion of available radiation is estimated according to a competition index updated three times per year and calculated for different tree crown layers. For all three models, the light interception module allows an individual differentiation of the intercepted radiation. Budburst is calculated similarly in the three models with functions that accumulate warm temperatures (and a photoperiod effect for MAESPA) to trigger budburst simultaneously for all the individuals of the same species. The representation of local climate conditions is rather detailed in the three models with a differentiation of the air temperature (excepted for MAESPA), wind and radiation at different grid points for MAESPA and NOTG3D and crown layers for BALANCE (Fig. 1.7).

Regarding photosynthesis and transpiration, the standard Farquhar equation and an energy balance with modifiers approach are used in all models even though the second is achieved through the classical Penman-Monteith equation in MAESPA and BALANCE but with a new approach for NOTG3D. However, differences emerge from how local climate conditions are accounted for in each model. MAESPA has a very detailed description of the water cycle with the representation of the soil-plant-atmosphere continuum (SPAC) and the use of Richard's equations to calculate soil water movements. However, due to the complexity of the water balance module and to limit the computation time, the model requires that the user chooses only a few representative trees to run the model on. An extrapolation at the stand scale is done after. This can potentially limit how the horizontal heterogeneity is included in the model. Inversely, BALANCE and MAESPA consider individualised multi-layer buckets that allow to differentiate water available for each individual tree but this approach prevent to consider exchange or facilitation mechanisms between neighbouring trees.

The process of carbon allocation is represented with a considerably higher level of detail in BALANCE that accounts for mineral nutrition and tree dimensions than in NOTG3D or MAESPA as the first uses empirical relationships and the process is simply absent in the second. The approach of BALANCE has the advantage to take into account at least some of the competition effect on carbon allocation. Finally, nutrient cycle is relatively simply implemented in BALANCE and NOTG3D that is limited to the nitrogen cycle. The main concepts these models rely on and the spatial level at which they are applied are presented in the Table 1.2. Moreover, their representation of tree structure is displayed in Fig. 1.7.

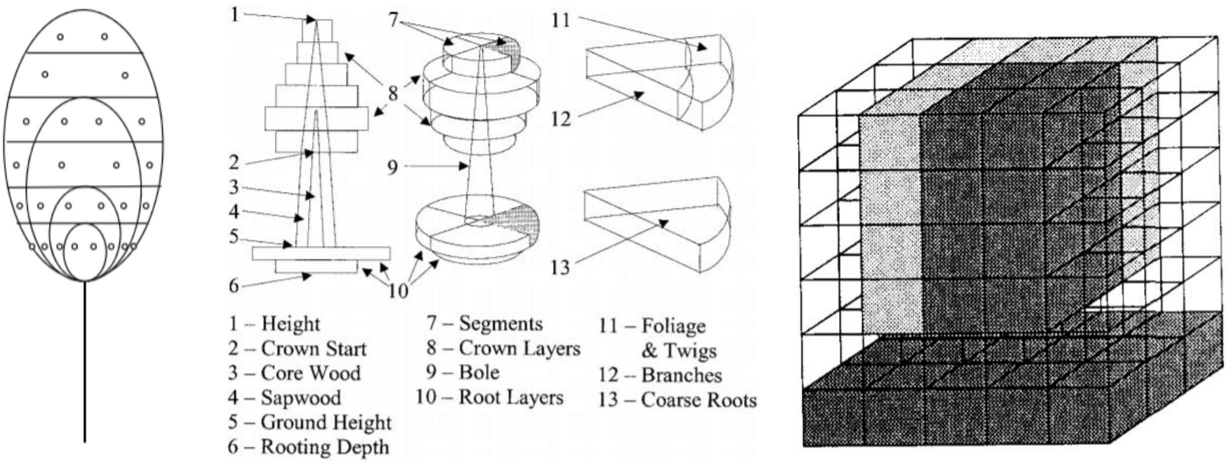

**Figure 1.7: Representation of tree structure in MAESPA that calculates aboveground processes to a number of gridpoints (typically 72) (left; Duursma and Medlyn, 2012), BALANCE, which calculation levels vary from the stand scale to the crown and root layers (middle; Grote and Pretzsch, 2002) and NOTG3D that divides the space into a 3D grid of voxels, containing leaves, roots or soil (right; Simioni et al., 2000).**

MAESPA and NOTG-3D are both very useful tools for analysing outcomes of ecophysiological experiments and study the interactions between ecophysiological processes in uneven-aged and heterogeneous stands but their interest to produce long-term projections is limited since MAESPA does not consider carbon allocation and dimensional growth and NOTG-3D does it empirically. BALANCE has a more comparable level of description between the different processes. As a result, it can theoretically be used for long-term projection studies in complex stands. Still, some processes that are expected to become of greater importance in the context of climate change are represented in a relatively simple way in the model. First, the persistence of the fertilizing effect of $CO_2$, one of the major sources of uncertainty in the projections of forest productivity (Reyer, 2015) is closely linked to the nutrient availability. Yet, the absence of links between soil water movements and nutrient availability and the focus on nitrogen alone in BALANCE could limit the predictive ability of the model for this process. Second, one-phase phenological models are efficient at predicting budburst in conditions close to those on which they were calibrated. However, for species at the warm margin of their species distribution area and as soon as endodormancy break observations are available to calibrate the model, two-phase models should be preferred for long-term simulations (Chuine et al., 2016). Finally, water uplift from low to more superficial horizons, which is one of the mechanisms of facilitation between different species in mixed stands and whose importance is expected to increase in the future due to dryer summer conditions (Domec et al., 2010; Zapater et al., 2011; Pretzsch et al., 2013), cannot be simulated in bucket models that only consider downward soil water movements.

Given the limitations of the three existing models and above all to have a perfect control on the model development, we decided to adapt HETEROFOR, an individual-based and spatially-explicit model which, at the beginning of my thesis, was able to simulate individual tree growth based on local light conditions using the radiative transfer module SAMSARALIGHT (sect. 1.3.3 in Chap. 2) and a PAR use efficiency approach (sect. 1.3.4 in Chap. 2) coupled to a carbon allocation module (sect. 1.3.6 in Chap. 2). The adaptation mainly consisted in the creation of several modules to describe phenology (sect. 1.3.2 in Chap. 2), water balance (sect. 1.3.10 in Chap. 2), respiration (sect. 1.3.5 in Chap. 2) and photosynthesis (sect. 1.3.4 in Chap. 2).

# OBJECTIVES

The objective of my PhD thesis is to estimate tree growth response to climate change taking the local soil, stand and climate conditions into account as well as the intra-stand heterogeneity. I focus on the response of the two main broadleaved species in Europe (sessile/pedunculate oak and European beech) considering different greenhouse gas (GHG) emission scenarios and a large range of ecological conditions and stand structures across Europe.

Hereafter, I make a series of hypotheses related to this objective.

**How climate change will affect oak and beech tree growth in European temperate forests?**

The expected warmer temperatures will continue to lengthen the vegetation period due to faster heat accumulation during the forcing period, leading to earlier budburst and a slower coldness accumulation in autumn, delaying leaf senescence. However, the vegetation period lengthening could slow down with time as the chilling accumulation could be delayed with milder winters and the photoperiod effect could dampen the senescence change. Then, the effect of warmer temperatures, coupled or not to lower summer rainfall, would increase both the averaged and extreme water stress levels as heat waves and extreme dry events are likely to become more frequent. Warmer temperatures could also favour maintenance respiration. The increase in vegetation period would have a positive effect on forest productivity opposed to the negative effect of higher water stress and respiration. Finally, the increase in atmospheric CO2 concentration could enhance productivity due to both a fertilizing effect and a reduction of water stress through stomatal control.

**How this response will be modulated by the local soil, stand and climate conditions?**

As the positive and negative effects generated by environmental changes are modulated by the local site conditions, hypotheses on the influence of the different site components (climate, soil and stand) on the forest response to climate change are formulated.

Climate

In Southern warmer sites experiencing summer rainfall reduction, I expect a dominance of the negative water stress and respiration effects that could be reinforced if the lengthening of the vegetation period becomes constrained. Inversely, in the cooler Northern and mountainous sites, the positive effect of a longer vegetation period on forest productivity would be dominant.

Soil

The impact of water stress could be mitigated in deep soils able to accumulate large amounts of water during winter.

Stand

Given their higher drought sensitivity and shallow root system, the water stress effect is likely to be greater in beech- than oak-dominated stands. Then, stands with higher density where resource competition and growth potential are important, both negative and positive effects would be intensified. Similarly, negative and positive effects on forest growth would be enhanced in even-aged stands while more complex stands with separated niches would rather buffer these effects.

To fulfil the main study goal and test these hypotheses, some intermediate objectives must be reached. First, a modelling tool able to account for the climate change effect on tree growth at the individual scale and valid for a large diversity in ecological conditions and stand structures is needed (I). Then, this model has to be evaluated to know its strength and limit and assess the uncertainty associated with the projections (II). Finally, the ultimate objective is to simulate oak and beech growth response to climate change in contrasted site and assess how it is modulated by the site components (climate, soil and stand) (III). The main originalities of this project are the creation of a new model that combines both a high level of spatial details and a process-based approach and its use to understand how site conditions and, particularly, stand characteristics, can modify the forest response to climate change.

## 1. ADAPTATION OF THE INDIVIDUAL-BASED MODEL HETEROFOR TO ACCOUNT FOR THE IMPACT OF CLIMATE CHANGE IN HETEROGENEOUS FORESTS

To simulate the climate change effects on tree growth and their interactions, a process-based approach is needed. In addition, reproducing the complexity of forest functioning in heterogeneous forests requires models with a detailed spatial representation (individual-based and spatially-explicit models) to account for the variability among trees (species, size, shape), the local environment (availability of resources) and the tree adaptive ability to these conditions (Berger et al., 2008). Very few models combine a detailed spatial representation with a process-based approach. It was therefore decided to develop a new approach in order to have a perfect control on the code and select the concepts adapted to my objectives.

Given the high data requirements for the initialization and calibration of such detailed models, they are often calibrated on a restricted number of well-documented sites. Yet, I plan to calibrate the model on a large diversity of site conditions benefiting from the data collected in long-term monitoring networks (ICP Forests, LTER). Indeed, calibrating a process-based model on a large range of ecological conditions increases its genericity and its predictive ability under unexperienced climate conditions.

Developing a modelling tool is not only an essential step in my PhD study but also an objective in itself for the research team in which I do my PhD. Indeed, this model is used in other studies. Furthermore, a new model is a good opportunity to test the sensitivity of the conclusions of existing studies to the model used and to compare the results of different models in order to improve them.

## 2. EVALUATION OF THE MODEL PREDICTIVE ABILITY

Structuring and integrating the existing knowledge into process-based models and calibrating it over a large panel of environmental conditions grants the model some reliability but this is not sufficient. The ability to reproduce the various processes and the tree growth must also be evaluated. A good evaluation of a forest growth model consists in a qualitative appraisal of the model biological realism and of the appearance of emergent properties as well as a quantitative assessment of the different energy, carbon and water fluxes (Soares et al., 1995). In practice, this is rarely the case as forest growth models are generally evaluated on integrative growth variables, for which data are easily available.

My objective is to combine a detailed evaluation of the processes on a couple of highly-documented sites with a more integrative assessment of the model performances on a large diversity of site and stand conditions. Among others, the aim of the detailed evaluation is to compare the model options in order to select the most appropriate concepts while the purpose of the large-scale evaluation is to check the model validity on a large diversity of ecological conditions, which is a guarantee of reliability for the simulations.

## 3. SIMULATION OF OAK AND BEECH INDIVIDUAL GROWTH RESPONSE TO CLIMATE CHANGE

With a model thoroughly evaluated, future projections of tree growth can be performed for a set of temperate broadleaved stands according to different scenarios. The use of various global and regional climate models and climate change scenarios accounts for some of the uncertainty related to climate projections (uncertainty in climate modelling and in the future GHG emission paths) while other uncertainty sources are also considered such as the persistence of the $CO_2$ fertilizing effect.

A first objective is to simulate the temporal changes in net primary production (NPP) according to various GHG emission scenarios and to identify the main drivers of this evolution. Since climate internal variability often blurs the climate change signal and since site conditions strongly influence NPP, a second objective is to differentiate the long-term trend in NPP from the inter-annual and inter-site variations. Then, a third objective is to quantify how the site components (stand, soil and climate) affect NPP and its response to climate change with a focus on the stand effect (species composition, stand density, development stage and structural complexity) that represents the leeway the forester has to adapt to climate change.

# RESEARCH STRATEGY

The research strategy is based on a modelling approach, which consists first in the adaptation of a model suitable for structurally-complex stands, then in the processing of the data necessary to run the model and finally in simulations to evaluate the model and explore the possible response of heterogeneous forests to climate change (Fig. 1.8).

## 1. MODELLING TOOL CREATION AND CALIBRATION

For my thesis, I contributed to adapt HETEROFOR, an individual-based and spatially-explicit model to better account for the sensitivity of tree growth to climate by adding a phenological and hydrological module while my colleagues created the respiration module and operated the connection with the photosynthesis module of CASTANEA. Regarding phenology, I implemented three budburst routines: two accounting for chilling and forcing periods and one considering just forcing. This allows the user to choose the best model regarding their calibration data and the location of the study site (models including chilling perform better in warmer conditions). Leaf yellowing was described as primarily driven by photoperiod while leaf fall was function of frost and wind. The water cycle was described by considering rainfall partitioning in throughfall and stemflow, water movements between soil horizons (Darcy law) and the various components of evapotranspiration using the Penman-Monteith equation. For both modules (phenology and hydrology), the processes can be described either at the tree or the stand scale (option to be selected by the user).

For Wallonia, the three budburst routines were calibrated based on observations from the phenology monitoring network PEP725 using the Phenology Modelling Platform (Chuine et al., 2013). Due to the data scarcity, the calibration and evaluation of leaf yellowing and fall were based on the same dataset (ICP Forests level II plots). At the European scale, I used the parameters of Duputié et al. (2015). While the hydrological module does not require any calibration, the function describing the individual height growth as well as the conversion of the gross primary production into NPP must be parameterised. At the regional (Wallonia) and then at the European scale, these functions were fitted based on repeated tree measurements in long-term forest monitoring plots (mainly ICP Forests level II plots) considering a calibration and validation datasets.

## 2. DATA PROCESSING

To make simulations and evaluate the model, case studies must be selected among highly-documented sites in order to have access to the soil, stand and climate data necessary for the initialization, calibration and evaluation. In a first step, six oak and/or beech stands located in Wallonia were used for a detailed evaluation of the model processes and a first simulation study. Then, 36 case studies distributed in Europe were selected among the level II plots of ICP Forests or other long-term monitoring sites (e.g. LTER). The site selection was made based on data availability with the aim of covering a large range of ecological conditions and stand types. The objective of this second step was to obtain a model valid for a large diversity of sites and to make projections for the future in contrasted conditions at the European scale.

Three different input files are required to run the model: a climate file with hourly meteorological observations, a soil file with information on the different soil horizons and a stand file with some general characteristics and the dimensions and relative coordinates of all trees. I fitted many allometric relationships and used them to replace missing data.

For the projections of tree growth, future climate time series for three different climate scenarios (RCP2.6, 4.5 and 8.5) were created. They are based on the outputs of one regional climate model for the six Walloon sites and on two RCMs for the 36 European sites that have been bias-corrected. For the Walloon simulations, a simple multiplicative or additive factor was applied to the projections while for the European simulations, a quantile mapping procedure that corrects the whole variable distribution was used.

## 3. SIMULATION STUDIES

The simulations carried out during my PhD thesis were achieved either in a model evaluation perspective or for predicting tree growth response to climate change. At the regional scale (Wallonia), I evaluated the capacity of the model to predict the vegetation period length (budburst and leaf development, leaf yellowing and fall), the water fluxes (throughfall, individual tree transpiration, deep drainage) as well as the soil water dynamics. At the European scale, less data were available. Thus, the evaluation focused rather on the model ability to reproduce height and radial growth as well as phenology.

Simulation experiments were carried out for the two sets of case studies. The first simulation set-up was a methodological proof of concept realised on the Walloon sites. Forest growth (NPP) was simulated from 2010 to 2100 under three greenhouse gas emission scenarios (RCP2.6, 4.5 and 8.5) and compared to the growth simulated during a reference period (1976-2005). Each year, a new simulation was launched starting from the same initial stand. Stand characteristics were therefore reinitialized each year keeping thereby the focus on the climate impact, in contrast to multi-year simulations which could have given rise to diverging stand characteristics with time. Two assumptions were considered regarding the persistence of the $CO_2$ fertilization effect (constant vs increasing atmospheric $CO_2$ concentration) as well as two thinning modalities. To further investigate the site effect on the NPP variability, a similar set of one-year simulations was ran for the historical period (1976-2005) by combining the climate, soil and stand input files of all the monitoring plots according to a full factorial design (6 soil types x 6 stands x 4 climates x 30 years). This allowed us to decompose the site variability in its components (soil, stand, climate).

At the European scale, in addition to the 36 sites studied (*real* sites), I also selected subsets of stands, soils and climates representative of the diversity of oak and beech growth conditions in Europe to create a set of *virtual* sites. In this step, I focused less on the inter-annual variability of productivity but rather on the influence of site conditions on the forest response to climate change. Two consecutive 15-year simulations were conducted for an historical period (1976-1990, 1991-2005) and for a period in the future (2071-2085, 2086-2100) according to two GHG emission scenarios (RCP 4.5 and 8.5). All the 15-year simulations started with the same initial conditions. For a given period (historical or future), the stand conditions were therefore reinitialized after 15 years. During these 15-year periods, I applied the same thinning operations as those which occurred during the monitoring period. By making 15-year simulations, the results less depend on recent cuttings or disturbances than with one-year simulations. Moreover, it also prevents that stand characteristics differ too much with time among RCP scenarios. Indeed, with longer simulation periods, the direct climate change impact could be partly confounded with an indirect effect due to a divergence in stand evolution.

It is important to note that between the time the simulations were performed at the Walloon (Chap. 4) and European (Chap. 5) scale, the stomatal conductance formulation was modified (see sect. 1.3.4 and 1.3.10 in Chap.2). In the first, the stomatal conductance for water vapour was not coupled to that for $CO_2$ while they were coupled in the second simulation set.

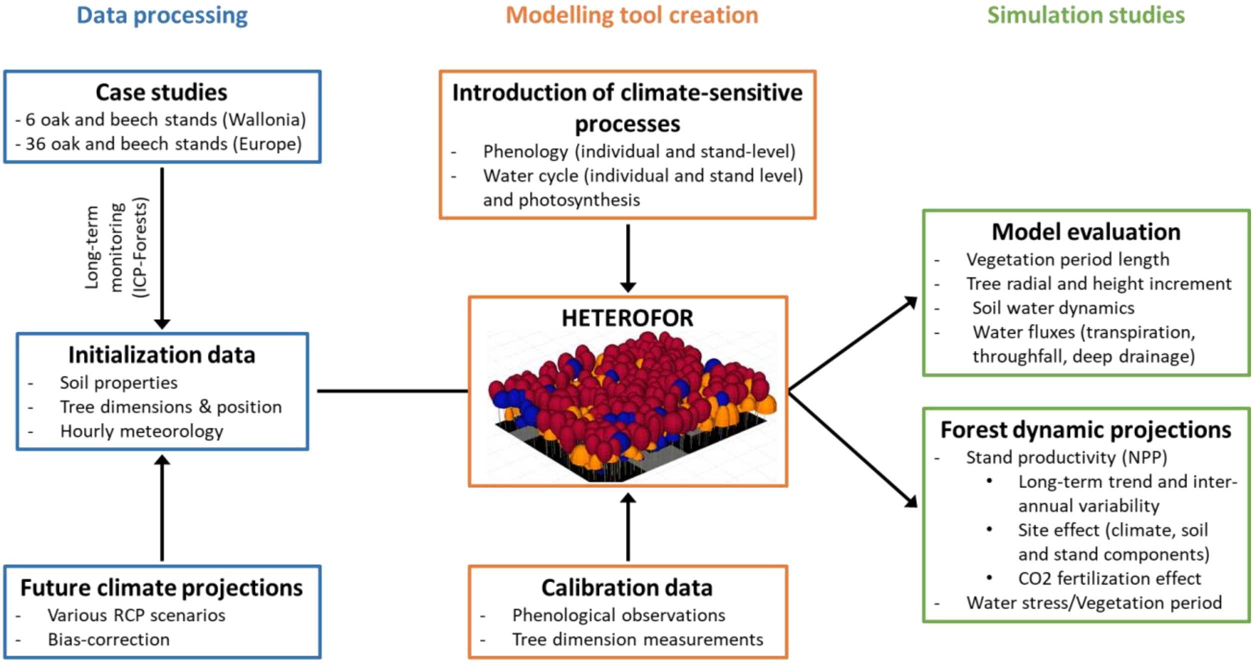

**Figure 1.8: Conceptual diagram describing the research strategy.**

# THESIS OUTLINE

The PhD manuscript is organised in six chapters including this introduction (*Chapter I*). *Chapter II* is centred on the description of the model HETEROFOR used in the project and how it was parameterized. In *Chapter III*, I focus on the evaluation of the phenology and water balance modules integrated in HETEROFOR and discuss to what extent they integrate the individual variability and the influence of the stand structure on these processes. *Chapter IV* consists in a first application of the model on a set of Walloon sites to simulate the forest response to climate change with the objective of identifying the main drivers of the forest productivity change and variability. In *Chapter V*, I extend the methodology of the Chapter IV at the European scale, with a focus on the influence of site conditions, and particularly of the stand structure, on the forest response to climate change. Finally, the main findings of the project are summarized and perspectives for future research are opened in the *Chapter VI*.

# Chapter 2

# MODEL DEVELOPMENT AND PARAMETERIZATION

## 1. MODEL DESCRIPTION

### 1.1. MODEL DEVELOPMENT HISTORY

At the start of my thesis, HETEROFOR consisted in a hybrid model predicting individual tree growth based on light competition and using the radiation and carbon efficiency concepts. In this first version of the model, the radiation intercepted by each tree was calculated by the SAMSARALIGHT library (Courbaud et al., 2003; André et al., submitted) and converted into GPP and NPP. Based on the functional balance concept and using allometric relationships, NPP was allocated to the different tree compartments (Jonard et al., 2020). My contribution to the model was to create the phenological module and to participate in the development of the water cycle module (de Wergifosse et al., 2020a). In parallel, Frédéric André and Mathieu Jonard coupled HETEROFOR to the photosynthesis routine of CASTANEA after adapting it to the tree level (Dufrêne et al., 2005) and created a temperature-dependent respiration routine (Jonard et al., 2020). Mathieu Jonard also developed a tree nutrition and nutrient cycling that still must be calibrated and tested (Fig. 2.1). As the description of the model is split into several articles, I have gathered the different parts below (see 1.3).

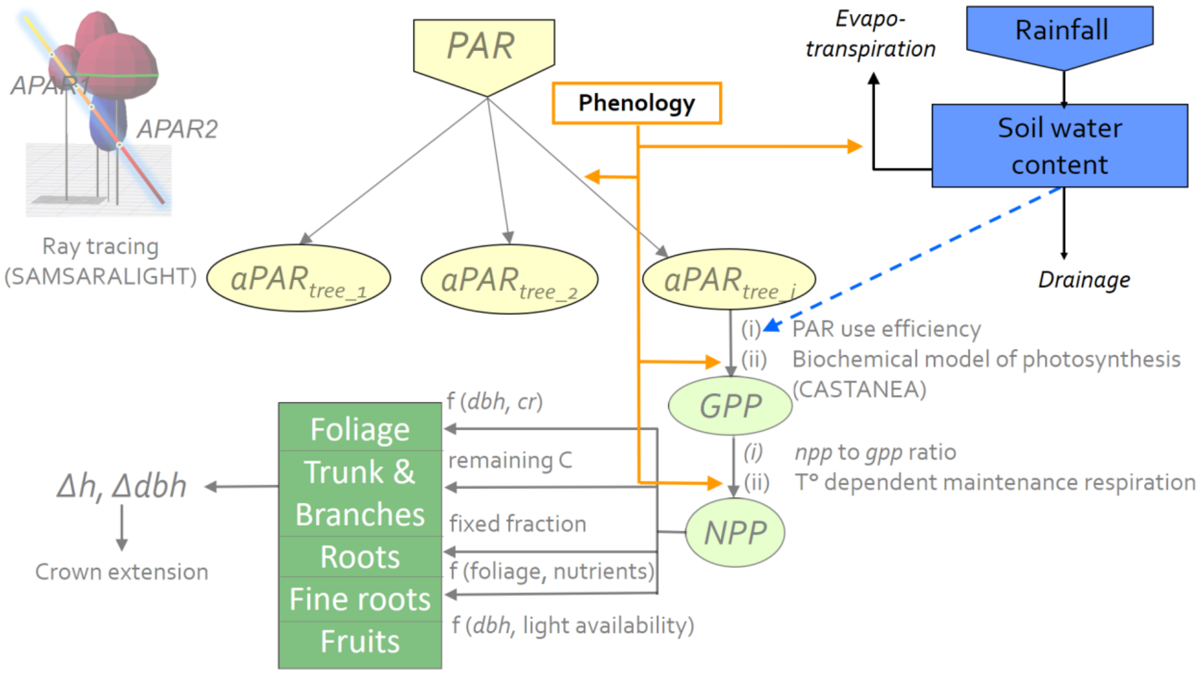

**Figure 2.1: Conceptual diagram of the HETEROFOR model with the part developped during my thesis highlighted (non-shaded components).**

### 1.2. OVERALL OPERATION OF THE HETEROFOR MODEL (FROM JONARD ET AL., 2020)

HETEROFOR is a model integrated in the CAPSIS (Computer-Aided Projection for Strategies in Silviculture) platform dedicated to forest growth and dynamics modelling (Dufour-Kowalski et al., 2012). HETEROFOR uses the CAPSIS execution system and its framework to run simulations and display the results. When running simulations with HETEROFOR, CAPSIS creates a new project in which the variables describing the forest state are stored at a yearly time step, starting from the initial forest characteristics (initial step). Some variables (foliage state, water fluxes, npp and gpp) are stored at an hourly or daily time step in java objects created annually. This information is accessible to the user through exports (see user manual in the supplements of Jonard et al., 2020). Although some data structures and methods are shared with other models integrated in CAPSIS, the initialisation and evolution procedures are specific to HETEROFOR. (Jonard et al., 2020, p. 907-908)

For the initialization, HETEROFOR loads a series of files containing tree species parameters, input data on tree (location, dimensions and chemistry), soil (chemical and physical properties) and open field hourly meteorological data. These data are used to create trees and soil horizons at the initial step. The tree is divided in three structural compartments (branch, stem, root) and three functional ones (leaf, fine root and fruit). Then, HETEROFOR predicts tree growth at a yearly time step based on underlying processes modelled at finer time steps and at different spatial levels. (Jonard et al., 2020, p. 907-908)

After the initialization step, and at the end of each successive yearly time step, the phenological periods for each deciduous species (leaf development, leaf colouring and shedding) are defined for the next step from meteorological data. When no hourly meteorological measurements are available, the vegetation period is defined by the user who provides the budburst and the leaf shedding dates. Knowing the key phenological dates and the rates of leaf expansion, colouring and falling, the foliage state of the deciduous species is predicted with a daily time step during the year. It is characterized by the proportions of leaf biomass and of green leaves relatively to complete leaf development, which are key variables to simulate energy, water and carbon fluxes within the forest ecosystem. The proportion of green leaves impacts photosynthesis, leaf respiration and tree transpiration, as these processes are not active anymore on discoloured leaves which however still intercept solar radiation and rainfall. Based on a ray tracing approach, the SAMSARALIGHT library of CAPSIS (Courbaud et al., 2003) calculates the proportions of solar radiation absorbed by the trunk and the crown of each individual tree and the radiation transmitted to the ground on average over the whole vegetation period (simplified radiation budget) or hourly for several key dates (detailed radiation budget). Predicting how solar energy is distributed within the forest ecosystem is necessary to estimate foliage, bark and soil evaporation, tree transpiration and leaf photosynthesis. (Jonard et al., 2020, p. 907-908)

Every hour, HETEROFOR performs a water balance and updates the water content of each horizon. Rainfall is partitioned in throughfall, stemflow and interception (André et al., 2008a; 2008b and 2011). Part of the rainfall reaches directly the ground (throughfall) while the rest is intercepted by foliage and bark. They both have a certain water storage capacity, which varies with precipitation and evaporative fluxes. When the foliage is saturated, the overflow joins the throughfall flux whose proportion increases. As the bark saturates, water flows along the trunk to form stemflow. Throughfall and stemflow supply the first soil horizon (forest floor) with water while soil evaporation and root uptake deplete it. The water evaporation from the soil (as well as from the foliage and the bark) is calculated with the Penman-Monteith equation based on the solar radiation absorbed by each component. Using the same equation, individual tree transpiration is estimated by determining the stomatal conductance from tree characteristics, soil water potential and meteorological conditions. The distribution of root water uptake among the soil horizons is done according to the soil water potential and the vertical distribution of fine roots. Water exchanges between soil horizons are considered as water inputs (capillary rise) or outputs (drainage). This soil water transfers are calculated based on the soil water potential gradient according to the Darcy law and using pedotransfer functions to determined soil hydraulic properties. By default, HETEROFOR calculates the water fluxes at the stand scale by aggregating individual fluxes (i.e. tree transpiration) or tree properties (e.g. foliage and bark capacity, stemflow proportion). With this option, all trees are taking up water in the same soil horizons assuming that soil water is redistributed homogeneously between two hourly time steps. However, the user can choose an alternative option to calculate all the water fluxes at the individual level. In this case, the model distributes the total soil volume in individual soil volumes (called pedon) and performs a water balance for each one. Contrary to the default option assuming a homogeneous horizontal water redistribution, the alternative option supposes no water redistribution among pedons. (Jonard et al., 2020, p. 907-908)

The user can choose to calculate the gross primary production of each tree (*gpp*) either based on a radiation use efficiency approach distinguishing sunlit and shaded leaves (yearly time step) or using the Farquhar et al. (1980) model (hourly time step). The latter is analytically coupled to the stomatal conductance model proposed by Ball et al. (1987). The photosynthesis is computed using the Library CASTANEA also present in CAPSIS (Dufrêne et al., 2005). This calculation requires the proportions of sunlit and shaded leaves, the direct and diffuse photosynthetically active radiation (*PAR*) absorbed per unit leaf area and the mean soil water potential. At the end of the vegetation period, *gpp* is converted to net primary production (*npp*) after subtraction of growth and maintenance respiration. Maintenance respiration is either considered as a proportion of *gpp* (depending on the crown to stem diameter ratio) or calculated hourly for each tree compartment by considering the living biomass, the nitrogen concentration and a Q10 function for the temperature dependency following Ryan (1991) as in Dufrêne et al. (2005). Carbon allocation is done once a year at the end of the vegetation period which allows to update tree dimensions for the next yearly time step during which tree size does not change. Carbon is allocated in priority to foliage and fine roots by ensuring a functional balance between carbon fixation and nutrient uptake through a fine root to leaf biomass ratio depending on the tree nutritional status (Helmisaari et al., 2007). Allometric relationships are then used to describe carbon allocation to structural components (trunk, branches and structural roots) and to derive tree dimensional growth (diameter at breast height, total height, height to crown base, height of maximum crown extension, crown radii in 4 directions) while considering competition with neighbouring trees. (Jonard et al., 2020, p. 907-908)

Knowing the chemical composition of the tree compartments for a given tree nutrient status, HETEROFOR computes the individual tree nutrient requirements based on the estimated annual growth rate and deduces the tree nutrient demand after subtraction of the amount of re-translocated nutrients. In parallel, the potential nutrient uptake (soil nutrient supply) is obtained by calculating the maximum rate of ion transport towards the roots (by diffusion and mass flow). The actual uptake is then determined by adjusting the tree nutrient status and growth rate so that tree nutrient demand matches soil nutrient supply. The nutrient limitation of tree growth is achieved through the regulation of photosynthesis, maintenance respiration and through the effect of the tree nutrient status on fine root allocation. (Jonard et al., 2020, p. 907-908)

The soil chemistry is characterized at the tree or stand scale for the various soil horizons defined by the user. In each soil horizon, the chemical composition of the soil solution is in equilibrium with the exchange complex and the secondary minerals. It receives the nutrients coming from atmospheric deposition, organic matter mineralization and primary mineral weathering, and is depleted by root uptake and immobilization in micro-organisms. The chemical equilibrium within the soil solution, with the exchange complex or the minerals is updated yearly with the PHREEQC geochemical model (Charlton and Parkhurst, 2011) coupled to HETEROFOR through a dynamic link library. (Jonard et al., 2020, p. 907-908)

## 1.3. DETAILED MODEL DESCRIPTION

### 1.3.1 Initialization (from Jonard et al., 2020 and André et al., submitted)

To initialize HETEROFOR, the relative position ($x, y, z$) and the main dimensions of each tree must be provided, including the following: girth at breast height ($gbh$; in cm), height ($h$; in m), height of maximum crown extension ($hlce$; in m), height to crown base ($hcb$; in m) and crown radii in the four cardinal directions ($cr$; in m). (Jonard et al., 2020, p. 908)

Based on these variables, each tree is positioned within the stand and is represented in 3D by geometrical forms. The trunk is described as a cylinder until the height to crown base with a diameter corresponding to the diameter at breast height. Crowns may be depicted considering either single ellipsoid (shape 'E'), two half-ellipsoids representing the lower and the upper parts of the crown (shape 'B'), paraboloid (shape 'P') or conical (shape 'C') geometric representations. For each of these shapes, the crown may be either trunk-centered ('c') or decentered ('d'). Furthermore, in order to account for the crown plasticity in response to competition, more complex crown forms considering eighths of ellipsoids (shape 'M'), fourths of paraboloids (shape 'Pm') or fourths of cones (shape 'Cm') are also implemented, resulting in a total of 11 possible crown types in HETEROFOR. Crowns of broadleaved species are usually depicted with ellipsoidal crown shapes while paraboloid and conical shapes are used to represent coniferous crowns. (André et al., submitted)

During the initialization phase, the biomass of each tree compartment is calculated according to the equations used for carbon allocation (see sect. 1.3.6). If available, site specific allometric equations can also be used to calculate initial biomasses of tree compartments. When data on fruit litterfall are available, a file providing the amount of fruit litterfall per year and per tree species can be loaded and used to adapt the allometric equations predicting fruit production at the individual level. When the water balance module is activated, a file must be loaded describing the following soil horizon properties: thickness ($th$ ; in mm), the coarse fraction (in m³ of stone by soil m³), bulk density ($\rho_b$; in kg of fine earth by soil m³), the sand, silt and clay content (g by g of fine earth), the organic carbon content ($C_{org}$; in mg by g of fine earth), the fine root proportion ($f$; in %) and, optionally, the saturated, field capacity and wilting point water contents ($\theta_{\mathrm{s}}$, $\theta_{\mathrm{fc}}$, $\theta_{\mathrm{wp}}$; in m³ by soil m³) that are calculated otherwise. A hourly meteorology file must also be provided describing the following variables: incident shortwave radiation ($RAD$; in W.m$^{-2}$), air temperature ($T$; in °C), rainfall ($R$; in mm), relative humidity ($RH$; in %) and wind speed ($WS$; in m.s$^{-1}$). Finally, the user must provide the nutrient concentrations of the current leaves (N, P, K, Ca and Mg) for each tree species. These foliar concentrations are then used to estimate the tree nutrient status for each major nutrient. When the tree nutrition and nutrient cycling module is not activated, these concentrations are kept constant throughout the simulation. (Jonard et al., 2020, p. 908-909)

### 1.3.2 Phenology

The phenological module aims at predicting the temporal variation of the foliage status during the vegetation period. From budburst, leaf biomass progressively increases until a maximum value, then remains constant and finally decreases during leaf fall. This temporal evolution is characterized by the proportion of leaf biomass relatively to its maximum value at full leaf development. In addition, two types of leaves are distinguished: green and discoloured leaves. The green leaf proportion is the ratio between the green leaf and the maximum leaf biomass. These two foliage properties are key variables to simulate energy, water and carbon fluxes within the forest ecosystem. Photosynthesis and tree transpiration are dependent on the proportion of green leaves since they are not active anymore on discoloured leaves. When leaves start yellowing, they still intercept rainfall while their photosynthetic activity and transpiration are progressively reduced.

The following phenological phases are distinguished, in chronological order:

- Chilling period or endodormancy: accumulation of coldness that breaks the bud dormancy. It is initiated at the chilling starting date ($t_0$) and ends at the forcing starting date ($t_1$).
- Forcing period or ecodormancy: accumulation of heat that initiates the leaf development in the bud and leads to the budburst (budburst date = $t_{2a}$).
- Leaf development: progressive growth of the leaves from budburst to the complete leaf development (leaf development date = $t_{2b}$).
- Ageing: accumulation of coldness that is initiated at the ageing starting date ($t_3$) and ends at the yellowing starting date ($t_{4a}$).
- Yellowing: loss of photosynthetic activity linked to the decrease of day length. This phase ends at the yellowing ending date ($t_{4b}$).
- Falling: the fall of the dead leaves starts ($t_{5a}$) when less than 60% of the leaves are still green and continues until the leaf fall ending date ($t_{5b}$).

Since the phenological timing can vary considerably between species, the phenology dates are calculated for each tree species separately. Intra-specific differences are also likely to occur according to the size or social status (Cole and Sheldon, 2017) and can be optionally accounted for as described later.

The phenological module is optional in HETEROFOR. Activating the phenology requires an hourly meteorological file. If not activated, the model uses the budburst and leaf fall dates provided by the user, which are identical for all years and tree species.

The principle behind the whole phenology module is similar for each phase. A *state* variable is increasing progressively growing at a *rate* depending on meteorological conditions (air temperature). When the phase *state* reaches a certain *threshold*, the start of a new phase is triggered, except for the leaf yellowing and fall that are partly simultaneous.

A two-phase model considering chilling and forcing is implemented to calculate the average budburst date ($t_{2a}$). The model starts to operate when the day of year corresponds to the chilling starting date ($t_0$). At this moment, the daily chilling rate ($R_c$) is calculated according to a response function to temperature. Two different response functions can be chosen. The first, called optimum, considers minimum, maximum and optimal temperatures regarding the accumulation of coldness according to the following equation based on Hänninen (1990):

$$R_c = \begin{cases} 0, \; T \leq T_{min} \\ \frac{T-T_{min}}{T_{opt}-T_{min}}, \; T_{min} < T \leq T_{opt} \\ \frac{T-T_{max}}{T_{opt}-T_{max}}, \; T_{opt} < T \leq T_{max} \\ 0, \; T \geq T_{max} \end{cases} \tag{1}$$

with $T_{min}$, $T_{max}$ and $T_{opt}$, the minimum, maximum and optimal temperatures (°C), respectively,

$T$, the daily average temperature (°C).

The second response function to temperature uses a sigmoid function (Chuine, 2000):

$$R_c = \begin{cases} \frac{1}{1+e^{Ca(T-Cc)^2+Cb(T-Cc)}}, \; -5 \leq T \leq 10 \\ 0, \; T > 10 \; or \; T < -5 \end{cases} \tag{2}$$

with $Ca$, $Cb$ and $Cc$ (°C), chilling parameters.

This rate is summed each day until reaching the chilling threshold ($C^*$) that triggers the forcing process and sets the forcing starting date ($t_1$) to the current day. Regarding the forcing period, the forcing rate ($R_f$) is calculated using another sigmoid equation (Chuine, 2000):

$$R_f = \begin{cases} \frac{1}{1+e^{Fb(T-Fc)}}, & T > T_{b\_for} \\ 0, & T \leq T_{b\_for} \end{cases} \tag{3}$$

with $Fb$ and $Fc$ (°C), forcing parameters,

$T_{b\_for}$, the base temperature for forcing.

The budburst is activated when the sum of the daily forcing rates reaches the forcing threshold ($F^*$).

A simplified one-phase version is implemented as well that only considers forcing similarly to the two-phase model (Eq. 3). In this case, the forcing starting date ($t_1$) must be provided.

As the module was calibrated based on observations carried out on trees representative of the stand, the predicted budburst starting date is expected to be that of an average tree. Since, at this date, the leaf expansion of some trees has already started in real conditions, the model shifts the budburst date to correspond to that of the earliest trees. This budburst shift, *t2a_shift*, is equal to half the period between the budburst of the first and the last tree and must be provided by the user for the various tree species. By doing so, leaf development starts early for all trees which follow a same average evolution when belonging to a same tree species.

The three temperature response functions presented were calibrated and evaluated as explained in Chap. 3. In the simulations at the Walloon scale, the one-phase phenological version was selected (see Chap. 4). Finally, the optimum function temperature was slightly updated for the simulations at the European (Chap. 5) because a European parameter set from Duputié et al. (2015) was used that relied on the equation from Wang and Engel (1998):

$$R_c = \begin{cases} 0, & T < T_{min} \\ \frac{2(T-T_{min})^{\alpha}(T_{opt}-T_{min})^{\alpha}-(T-T_{min})^{2\alpha}}{(T_{opt}-T_{min})^{2\alpha}}, & T_{min} \leq T \leq T_{max} \\ 0, & T_{max} < T \end{cases} \tag{4}$$

with $\alpha = \frac{\ln(2)}{ln\left(\frac{T_{max}-T_{min}}{T_{opt}-T_{min}}\right)}$

Once the budburst starting date ($t_{2a}$) is calculated, the equations for the subsequent phenological variables are the same. The leaf development rate ($R_{ld}$) is cumulated daily until the leaf development threshold ($LD^*$) is reached. It is computed according to:

$$R_{ld} = \begin{cases} T, & T > 0 \\ 0, & T \leq 0 \end{cases} \tag{5}$$

where $T$ is the daily average temperature of the current day (°C).

The leaf proportion (*leafProp*, g g$^{-1}$) is calculated daily for each tree species (*sp*) according to

$$leafProp_{sp\_t} = \frac{\sum_{t2a}^{t} R_{ld}}{LD^*} \tag{6}$$

with $t$, the current day.

As many studies have shown that budburst in the understory occurs earlier than in the overstory and ascribed this primarily to ontogeny (Gill et al., 1998; Seiwa 1999a; Seiwa, 1999b; Augspurger and Bartlett, 2003; Schieber, 2006; Vitasse, 2013), we implemented an option to make the phenology size-dependent (*phenology at tree level)*. With this option, the leaf development is first triggered in the smallest trees of each tree species and then progressively in the tallest ones according to their height. At the stand level, the option '*phenology at tree level*' provide exactly the same leaf development than the default option but the difference appears at the tree scale. The default option assumes that all trees of a same species initiate budburst at the same time and display the same progressive leaf development while the alternative one supposes that trees break down one after the other depending on their size. Both assumptions are quite rough as the budburst and senescence periods vary a lot among the individuals of a same species in a same site (Delpierre et al., 2017) and tree size explains only a part of the variability (Marchand et al., 2020) but other variables (genetics, water availability) also affect it (Delpierre et al., 2017).

With the option '*phenology at tree level*', the leaf proportion of each tree ($leafProp_{tree\_t}$) is updated daily ($t$) between the budburst starting date ($t_{2a}$) and the budburst ending date ($t_{2b}$) based on the leaf proportion calculated at the stand scale for the corresponding tree species ($leafProp_{sp\_t}$):

$$leafProp_{tree\_t} = \begin{cases} 1, & \frac{\sum_1^{tree} a_{leaf}}{A_{leaf}} \leq leafProp_{sp\_t} \\ 0, & \frac{\sum_1^{tree} a_{leaf}}{A_{leaf}} > leafProp_{sp\_t} \end{cases} \tag{7}$$

with *tree*, the tree of interest (note that the trees are sorted by ascending order based on their height),

$a_{leaf}$, the tree leaf area (m²),

$A_{leaf}$, the total stand leaf area (m²).

A fixed date, defined according to Dufrêne et al. (2005), is considered for the start of the ageing process ($t_3$). This process does not alter leaf quality but is a prerequisite for leaf yellowing ($t_{4a}$) that is initiated when the cumulated daily ageing rate ($R_{age}$) equals the ageing threshold ($A^*$), with

$$R_{age} = \begin{cases} T_{b\_age} - T, & T < T_{b\_age} \\ 0, & T \geq T_{b\_age} \end{cases} \tag{8}$$

with $T_{b\_age}$, the base temperature for ageing (°C).

The leaf yellowing calculation gives the green leaf proportion, *greenProp* (g g$^{-1}$), which provides the fraction of remaining green leaves compared to the maximum green leaf amount for each tree species. It is set to 1 before the start of yellowing, and then decreases with day length according to the following equation:

$$greenProp_{sp\_t} = greenProp_{sp\_t-1} * \left(\frac{DL_t - DL_{min}}{DL_{t4a} - DL_{min}}\right)^y \tag{9}$$

with $DL_t$ and $DL_{t4a}$, the day lengths (hours) for the current day and $t_{4a}$, respectively,

$DL_{min}$, the minimum day length (hours) value over the year, and

y, a leaf yellowing parameter.

The day length (hours) is calculated according to Teh (2006):

$$DL = \frac{24}{\pi} * acos\left(-\frac{\sin(\delta) * \sin(\lambda)}{\cos(\delta) * \cos(\lambda)}\right) \tag{10}$$

where $\lambda$ is the site latitude (rad) and $\delta$, the solar declination (rad) determined as $\delta = -\frac{23.45 * \pi}{180} * cos\left(2\pi \frac{DOY + 10}{365}\right)$

and *DOY* is the day of year (i.e., Jan 1=1, Jan 2=2, Feb 1=32…).

The yellowing phase ends when the green leaf proportion drops below a threshold, called yellowing threshold, Y*, indicated by the model user in the species file. The leaf fall ($t_5$) is set to start rapidly after yellowing initiation, namely, when *greenProp* reaches 0.60, considering that leaves no longer photosynthetically active can quickly fall.

The falling rate ($R_{fall}$) is calculated daily and is used to update *leafProp* for each tree species. It depends on the wind and frost episodes. While the frost weakens the leaf petiole, the wind can break it and take away the leaf. For this reason, *leafProp* is determined as follows for each day *t*:

$$leafProp_{sp\_t} = leafProp_{sp\_t-1} - f_{ampl} * WS * R_{fall} \tag{11}$$

with $f_{ampl}$, a frost amplifier coefficient fixed to 1 before the occurrence of five consecutive hours with air temperature below 0°C and is then set to 2 and 3 for oak and beech, respectively,

$WS$ is the daily average wind speed (m $s^{-1}$),

$R_{fall}$ is the falling rate (s $m^{-1}$ $d^{-1}$) calibrated as described in sect. 2.1.

According to Eq. (11), $leafProp_{sp\_t}$ progressively decreases from 1 to 0 but it cannot take a value below $greenProp_{sp\_t}$, accounting for the fact that green leaves are not expected to fall. Finally, when all leaves have fallen, the trees enter in the leafless period until the budburst of the following year.

As for leaf development but with a reverse order, the option ‘*phenology at tree level’* first triggers the leaf yellowing and fall in the taller trees and then in the smaller ones in order to reproduce the observations reported by Gressler et al. (2015). This options daily updates the green leaf and leaf proportions of each tree ($greenProp_{tree\_t}, leafProp_{tree\_t}$) between the yellowing starting date ($t_{4a}$) and the falling ending date ($t_{5b}$) based on the green leaf and leaf proportions calculated at the stand scale for the corresponding tree species ($greenProp_{sp\_t}, leafProp_{sp\_t}$):

$$greenProp_{tree\_t} = \begin{cases} 1, & \frac{\sum_{n}^{tree} a_{leaf}}{A_{leaf}} \leq greenProp_{sp\_t} \\ 0, & \frac{\sum_{n}^{tree} a_{leaf}}{A_{leaf}} > greenProp_{sp\_t} \end{cases} \tag{12}$$

$$leafProp_{tree\_t} = \begin{cases} 1, & \frac{\sum_{n}^{tree} a_{leaf}}{A_{leaf}} \leq leafProp_{sp\_t} \\ 0, & \frac{\sum_{n}^{tree} a_{leaf}}{A_{leaf}} > leafProp_{sp\_t} \end{cases} \tag{13}$$

with *tree*, the tree of interest (note that the trees are sorted by descending order based on their height),

$a_{leaf}$, the tree leaf area ($m^2$),

$A_{leaf}$, the total stand leaf area ($m^2$).

The option ‘*phenology at tree level’* gives the opportunity to compare two contrasted hypotheses regarding individual tree phenology and to evaluate to which extent it has an impact on tree growth.

### 1.3.3 Light interception (from André et al., submitted)

The SAMSARALIGHT library used to model the transfer of solar radiation through the canopy is based on a radiative transfer model developed by Courbaud et al (2003) which was later progressively improved and implemented in the Capsis platform (Ligot et al, 2014). Based on a ray tracing approach, SAMSARALIGHT calculates the proportions of solar radiation absorbed by the trunk and the crown of each individual tree and the radiation transmitted to the ground on average over the whole vegetation period (simplified radiation budget) or hourly for several key dates (detailed radiation budget). In the following, only the simplified radiation budget is described since only this option was used during my PhD thesis. SAMSARALIGHT is particularly suitable for uneven-aged and mixed forests as it provides both the energy intercepted by each tree or tree part (i.e., crown, crown part and/or trunk) and the distribution of irradiance on the ground, while requesting a limited number of input parameters. In SAMSARALIGHT, the stand area is subdivided into cells arranged as a regular grid on the ground and the model describes how the energy of light beams pointing to the center of each of these cells attenuates as they penetrate into the canopy. (André et al., submitted)

In SAMSARALIGHT, the first step is the creation of beams from the incident radiation measured at a meteorological station representative of the climate of the study site. The measured global radiation is partitioned into direct and diffuse energies, through coefficients either fixed to arbitrary values or derived from empirical equations accounting for atmospheric clearness through the global-to-extraterrestrial radiation ratio as proposed by Erbs et al (1982) or Jacovides et al (2010). Direct and diffuse energies are then distributed among beams. Direct beams are generated for regular hour angle intervals along the mean solar path for each month of the growing season according to astronomic laws providing the sun height angle and the sun azimuth for each hour angle (Bonhomme, 1993). Direct energy is then shared between the beams in proportion to the sinus of their height angle. Diffuse beams are created at regular azimuth and elevation intervals on the sky hemisphere and diffuse energy is shared between the beams according to either the ’Uniform Overcast Sky’ (UOC) or the ’Standard Overcast Sky’ (SOC) distributions (Moon and Spencer, 1942). The former distribution assumes identical radiation flux from all sky direction while the latter considers variation as a function of height angle, with larger radiation flux from sky directions towards the zenith. (André et al., submitted)

In a second step, each generated beam is pointed to the center of each cell and inter- sections with intercepted trees are calculated. Based on crown geometric representations, an entry point and an exit point are determined for each beam intersecting a crown (see Courbaud et al (2003) and Ligot et al (2014) for computation details). Not considered in the initial version of the model, trunks may now be optionally represented as cylinders which, in contrast to crowns, do not transmit light and interrupt the path of beams. (André et al., submitted)

In a third step, the energies intercepted by each tree and transmitted to the ground are calculated using either the turbid medium or the porous envelop approaches. The turbid medium approach assumes that radiation extinction inside a crown (or a crown part) follows that of a monochromatic ray through an homogeneous medium, which is described by the Lambert-Beer law. According to this law, light transmission is a function of the medium absorption coefficient and of the light path length inside the medium ($l$, m). In the case of a canopy, the absorption coefficient may be expressed as the product of a coefficient of extinction ($k$, -) depending on the leaf and branch orientation and spatial distribution, *LAD* and a clumping index ($\Omega$, -) accounting for the aggregation of leaves and branches, leading to the following formulation:

$$\frac{I_{out}}{I_{in}} = exp(-k \cdot \Omega \cdot LAD \cdot l) \tag{14}$$

where $I_{in}$ and $I_{out}$ are the irradiances at the entry point and at the exit point, respectively. The path length within the crown (or the crown part) is given by the distance between the beam entry and exit points. The determination of the other parameters will be discussed below. (André et al., submitted)

Two options are possible for determining *LAD*, either fixing it to a specific value ($\text{LAD}_{constant}$ option) or modeling it by considering the specific leaf area (*SLA*, $\text{m}^2\text{kg}^{-1}$) variation depending on the vertical position within the canopy ($\text{LAD}_{model}$ option). Based on observations and literature references (e.g., Fellner et al, 2016; Forrester et al, 2017; Leuschner and Meier, 2018), SLA is assumed to decrease from the bottom of the canopy to its top.

Therefore, when considering the $LAD_{model}$ option, the crown SLA for a given tree is evaluated by linear interpolation of reference SLA values for the top ($SLA_{top}$, $m^2kg^{-1}$) and for the bottom ($SLA_{bottom}$, $m^2kg^{-1}$) of the canopy as a function of crown height level. The top and bottom of the canopy are determined based on the mean height of the lower/upper crown part of the *n* lowest and highest trees in the vicinity of the target tree, respectively. LAD is obtained by multiplying the SLA by the leaf biomass (see Eq. 30) and by dividing it all by the crown volume derived by applying the ellipsoid, the paraboloid or the cone volume formula depending on the crown form. (André et al., submitted)

In contrast to the turbid medium analogy, the porous envelop approach was formulated considering a fixed crown openness (*p*, -), not depending on the light path distance through the crown neither on foliage density or arrangement. In this case, radiation interception inside the crown (or the crown part) may be expressed as:

$$\frac{I_{out}}{I_{in}} = p \tag{15}$$

When intercepted by a crown (or a crown part), the energy of a beam is decremented by the quantity determined according to the chosen approach and, in parallel, the energy intercepted by the corresponding crown (or crown part) is incremented by this quantity. This beam radiation extinction occurs for the successive trees traversed by the beam until it reaches the target cell. In case a beam hits a trunk, the trunk intercepted energy is incremented by the remaining energy of the beam and the beam energy is set to zero. After processing of all the beams for each cell, the total radiation reaching a ground cell is given by the sum of the remaining energies of the beams coming from all sky directions, and the total energy intercepted by a tree part (i.e., crown, crown part or trunk) equals the sum of the energies intercepted from the different beams. Besides this actual energy interception by trees, potential energy interception is also determined for each tree and corresponds to the energy that would have been intercepted by this tree in the absence of its neighbors. The ratio between actual and potential interception may be considered as a light competition index (*LCI*, -). For the sake of computing efficiency, the algorithm has been optimized in order to, for each beam, limit beam-tree interception computations only to trees likely to effectively intercept that beam. We refer to Courbaud et al (2003) for details about this optimization technique. Furthermore, virtual wrapping of the plot as a torus is implemented in the model to avoid erroneous radiative balance around plot borders. It allows repetition of the plot in every direction and, thereby, avoids overestimation of incident radiation coming for the edges and provides exact radiation balance at the stand level (see Courbaud et al (2003)). Finally, speedup of the algorithm was recently achieved through parallelization of the radiative balance computations for the different cells. (André et al., submitted)

#### 1.3.4 Gross primary production (from Jonard et al., 2020)

The annual gross primary production of each tree (*gpp* in kgC $yr^{-1}$) is calculated either based on a *PAR* use efficiency (*PUE*) approach (Monteith, 1977) or using the photosynthesis method of the CASTANEA model (Dufrêne et al., 2005). For the first option, the only input needed by the model is the mean monthly global radiation. The second option requires hourly meteorological data and the activation of the water balance calculation. In any case, a series of intermediate variables are needed to calculate *gpp*. (Jonard et al., 2020, p.909-910)

For the *PUE* approach, the model uses the solar radiation absorbed by each tree during the vegetation period (*aRAD* in MJ $yr^{-1}$*),* *aRAD* is then converted in *PAR* (*aPAR* in mol photons $yr^{-1}$) by supposing that 46% of the solar radiation (*RAD*) is *PAR* and that 1 MJ is equivalent to 4.55 moles of photons. The diffuse and direct components of *aPAR* are also considered (*aPAR*$_{diff}$ and *aPAR*$_{dir}$ in mol photons yr$^{-1}$). While all the leaves receive diffuse *PAR*, only sunlit leaves absorb direct *PAR*. To estimate the sunlit leaf proportion (*Prop*$_{sl}$) at the tree level, HETEROFOR uses an adaptation of the classical stand-scale approach based on the Beer-Lambert law (Teh, 2006):

$$Prop_{sl} = \frac{1-\exp(-k \cdot LAI)}{k} \qquad (16)$$

with $k$, the extinction coefficient,

$LAI$, the leaf area index (m² m$^{-2}$).

At the individual scale, the leaf area index is calculated by dividing the tree leaf area (*a*$_{leaf}$ in m$^2$) by the crown projection area (*cpa* in m²). The value obtained is then multiplied by the light competition index (*LCI* in MJ MJ$^{-1}$) to account for the shading effect of the neighbouring trees:

$$Prop_{sl} = \frac{1-\exp\left(-k \cdot \frac{a_{leaf}}{cpa}\right)}{k} \cdot LCI \qquad (17)$$

where LCI is the ratio between the absorbed radiation calculated with and without neighbouring trees in SAMSARALIGHT. LCI ranges from 1 (no light competition) to 0 (no light reaching the tree).

To adapt the *PAR* use efficiency concept (*PUE*) at the tree level, we considered a distinct *PUE* for sunlit (*sl*) and shaded (*sh*) leaves and calculated an average *PUE* weighted as follows:

$$pue = \frac{aPAR_{diff} \cdot (Prop_{sl} \cdot PUE_{sl} + Prop_{sh} \cdot PUE_{sh}) + aPAR_{dir} \cdot PUE_{sl}}{aPAR} \qquad (18)$$

This *pue* is then used to calculate *gpp* based on *aPAR* and a reducer accounting for water stress ($red_{water}$):

$$gpp = aPAR \cdot pue \cdot red_{water} \qquad (19)$$

The default value of $red_{water}$ is 1 but, when the water balance module is activated, it is set to the ratio between the actual and the potential (i.e., considering no soil water limitation) tree transpiration ($t_{actual}$ and $t_{pot}$, in l per year). This ratio estimates the fraction of the vegetation period during which stomata are partially or totally closed due to limitation in soil water availability. Since this ratio is always lower or equal to 1, a correction factor is applied to avoid introducing a bias.

$$red_{water} = \frac{t_{actual}}{t_{pot}} \cdot corr \qquad (20)$$

*gpp* can also be estimated using the photosynthesis method of CASTANEA (Dufrêne et al., 2005). This method consists in the biochemical model of Farquhar et al. (1980) analytically coupled with the approach of Ball et al. (1987) that linearly relates stomatal conductance to the product of the carbon assimilation rate by the relative humidity. The slope of this relationship varies between 0 and 1 with the soil water availability characterized in HETEROFOR based on a decreasing exponential function of the mean soil water potential (see Eq. 115 in section 1.3.10). The formulation of Ball et al. (1987) was slightly adapted to the tree level by accounting for the influence of tree height (Schäfer et al., 2000). Indeed, leaf water potential increases with leaf height and induces a decrease in stomatal conductance (Ryan and Yoder, 1997). (Jonard et al., 2020, p.909-910)

The photosynthesis routine requires, at an hourly time step, the direct and diffuse *PAR* absorbed per unit leaf area. The direct *PAR* is intercepted only by sunlit leaves and is obtained by multiplying the hourly incident *PAR* (µmol photons m$^{-2}$ s$^{-1}$) by the proportion of direct *PAR* absorbed by sunlit leaves. For a tree, this proportion is by default fixed for the whole vegetation period and calculated as the ratio between the direct *PAR* absorbed per unit sunlit leaf area during the vegetation period (in mol photons.m$^{-2}$.yr$^{-1}$) and the incident *PAR* cumulated over the same period (in mol photons m$^{-2}$ yr$^{-1}$). A similar procedure is used for the diffuse absorbed *PAR*, except that it is related to the total leaf area. When using the detailed version of SAMSARALIGHT, the proportions of direct/diffuse *PAR* absorbed per unit leaf area change every hour during the day and depending on the phenological stage. The photosynthesis routine of CASTANEA also requires the foliar nitrogen concentration to estimate the maximal carboxylation rate (Dufrêne et al., 2005). (Jonard et al., 2020, p.909-910)

### 1.3.5 Growth and maintenance respiration (from Jonard et al., 2020)

$gpp$ is converted to annual net primary production ($npp$ in kgC yr$^{-1}$) using either a ratio (Eq. 21) or after subtraction of growth ($gr$) and maintenance respiration ($mr$) (Eq. 22) according to the theory of respiration developed by Penning de Vries (1975). (Jonard et al., 2020, p.910-911)

$$npp = gpp \cdot r_{npp\_gpp} \tag{21}$$

$$npp = gpp - mr - gr \tag{22}$$

Mäkelä and Valentine (2001) showed that the *npp* to *gpp* ratio, also called carbon use efficiency (CUE) changes with some tree characteristics (tree height and age) while others highlighted the influence of air temperature or social status (DeLucia et al., 2007; Collalti and Prentice, 2019). Based on simulated *gpp* and *npp* reconstructed by using the model in reverse mode (see sect. 1.3.9), we tested the impact of several variables characterizing tree dimensions and shape (height, height of crown base, *dbh*, crown radius, crown volume, crown to stem diameter ratio, aboveground volume or biomass) as well as the influence of competition using the LCI and the annual mean temperature on the *npp* to *gpp* ratio. (Jonard et al., 2020, p.910-911)

$$r_{npp\_gpp} = a + b\ dbh_{cm} + c\ {dbh_{cm}}^2 + d\ h + e\ h^2 + f\ \frac{h}{dbh_m} + g\ Dd_{index} + i\ \frac{h-hcb}{h} + j\ ln(LCI) + k\ MAT \tag{23}$$

with *dbh* and *h* characterising the tree size,

*h/dbh*, $Dd_{index}$, $\frac{h-hcb}{h}$ describing the tree shape independently of its size (slenderness, crown horizontal and vertical extension),

*LCI*, the light competition index varying between 0 (no light reaching the tree) and 1 (no competition),

*MAT*, the mean annual air temperature,

*a* to *k*, fitting parameters.

More precisely,

$$DdIndex = \frac{\mathrm{Dd}}{Dd_{pred}} \tag{24}$$

with $Dd$, the crown to stem diameter ratio determined from the tree mean crown radius ($cr_{mean}$ in m) and diameter at breast height (*dbh* in m),

$Dd_{pred}$, the crown to stem diameter ratio predicted based on the girth at breast height (*gbh* in cm):

$$Dd_{pred} = \alpha + \beta \cdot gbh + \gamma \cdot \frac{1}{gbh} + \delta \cdot \frac{1}{gbh^2} \tag{25}$$

In Eq. (22), maintenance respiration is calculated for each tree by summing the maintenance respiration of each compartment estimated from the nitrogen content of its living biomass and considering a $Q_{10}$ function for the temperature dependency. During daytime, the inhibition of foliage respiration by light is taken into account by considering that this inhibition reduces respiration by 62% (Villard et al., 1995).

$$mr = \sum_{comp.} \left( b_{comp.} \cdot f_{living} \cdot [N] \cdot R_{T_{ref}} \cdot Q_{10\_organ}{}^{\frac{T-T_{ref}}{10}} \right) \tag{26}$$

with $b_{comp.}$, the tree compartment biomass (kg of organic matter),

$f_{living}$, the fraction of living biomass,

$[N]$, the nitrogen concentration (g kg$^{-1}$),

$R_{T_{ref}}$, the maintenance respiration per g of N at the reference temperature (15°C),

T, is the air temperature for aboveground tree compartments or the soil horizon temperature for roots. Root maintenance respiration is estimated for each soil horizon separately.

The fraction of living biomass is fixed to 1 for leaves and fine roots or equals the proportion of sapwood for the structural tree compartments. The sapwood proportion is derived from the sapwood area ($a_{sapwood}$ in cm$^2$) determined based on an empirical function of the tree compartment diameter ($\emptyset_{comp.}$ in cm):

$$a_{sapwood} = a + b \cdot \emptyset_{comp.} + c \cdot \emptyset_{comp.}{}^2 \tag{27}$$

Growth respiration is the sum of the tree compartment growth respiration which is proportional to their biomass increment (see sect. 1.3.6):

$$gr = \sum_{comp.} \left( R_{gr} \cdot \Delta b_{comp.} \right) \tag{28}$$

where $R_{gr}$ is the growth respiration per unit biomass increment (kgC kgC$^{-1}$). (Jonard et al., 2020, p.910-911)

### 1.3.6 Carbon allocation and dimensional growth (from Jonard et al., 2020)

For each tree, the *npp* and the carbon retranslocated from leaves and roots ($rt_{leaf}$ and $rt_{fine\ root}$in kgC yr$^{-1}$) are distributed among the various tree compartments at the end of the year. $rt_{leaf}$ and $rt_{fine\ root}$ are determined as follows :

$$rt_{leaf\ or\ fine\ root} = b_{leaf\ or\ fine\ root} \cdot \delta_{leaf\ or\ fine\ root} \cdot rtr_{leaf\ or\ fine\ root} \tag{29}$$

where $b_{leaf}$ and $b_{fine\ root}$ are the tree leaf and fine root biomasses (kgC), $\delta_{leaf}$ and $\delta_{fine\ root}$ are the leaf and fine root turnover rates (kgC kgC$^{-1}$ yr$^{-1}$), and $rtr_{leaf}$ and $rtr_{fine\ root}$ are the leaf and fine root retranslocation rates (kgC kgC$^{-1}$).

$b_{leaf}$ is estimated with an allometric equation based on the stem diameter at breast height (*dbh* in cm) and on the crown to stem diameter ratio (*Dd*):

$$b_{leaf} = \alpha \cdot dbh^{\beta} \cdot Dd^{\gamma} \tag{30}$$

$b_{fine\ root}$ is deduced from the leaf biomass using the fine root to leaf ratio ($r_{fine\ root\ to\ foliage}$):

$$b_{fine\ root} = b_{leaf} \cdot r_{fine\ root\_leaf} \tag{31}$$

$r_{fine\ root\_leaf}$ takes a value between a minimum ($r_{fine\ root\_leaf\_min}$) and maximum ($r_{fine\ root\_leaf\_max}$) ratio depending on the tree nutritional status, in accordance with the concept of functional balance (Mäkela 1986). This means that a higher ratio is used (more carbon allocation to fine roots) when tree suffers from nutrient deficiency. For each nutrient, a candidate ratio is obtained based on a linear relationship depending on the nutritional status. The ratio increases when the nutritional status deteriorates and this effect is more pronounced for nitrogen (N) > phosphorus (P) > potassium (K) > magnesium (Mg) > calcium (Ca). Among the candidate ratios, the maximum is retained in order to account for the fact that the most limiting nutrient has the dominant effect. For each nutrient, the nutritional status is bounded between 0 and 1 and calculated based on the foliar concentrations (provided in the inventory file) and on the optimum and deficiency thresholds (Mellert and Göttlein, 2012). (Jonard et al., 2020, p.911-913)

$$Status(Nutrient) = \frac{[Foliar\ Nutrient] - Deficiency}{Optimum - Deficiency} \tag{32}$$

The leaf and fine root litter amounts ($s_{leaf}$ and $s_{fine\ root}$ in kgC yr$^{-1}$) are estimated based on the turnover rate taking into account the retranslocation:

$$s_{leaf\ or\ fine\ root} = b_{leaf\ or\ fine\ root} \cdot \delta_{leaf\ or\ fine\ root} \cdot \left(1 - rt_{leaf\ or\ fine\ root}\right) \tag{33}$$

Allocation priority is given to leaves and fine roots. The carbon allocated to leaves corresponds to the annual leaf production ($p_{leaf}$ in kgC yr$^{-1}$) which is equal to the amount of leaves fallen the previous year plus the leaf biomass change ($\Delta b_{leaf}$ in kgC yr$^{-1}$):

$$p_{leaf} = b_{leaf_{t-1}} \cdot \delta_{leaf} + \Delta b_{leaf} \tag{34}$$

where $\Delta b_{leaf}$ is determined by :

$$\Delta b_{leaf} = b_{leaf_t} - b_{leaf_{t-1}} \tag{35}$$

with $b_{leaf_{t-1}}$ and $b_{leaf_t}$ being the tree leaf biomasses corresponding to the previous and the current years, respectively.

The fine root production is then estimated according to the same logic:

$$p_{fine\ root} = b_{fine\ root_{t-1}} \cdot \delta_{fr} + \Delta b_{fr} \tag{36}$$

where $b_{fine\ root_{t-1}}$ is provided by Eq. (31).

When the carbon allocated to leaf and fine root is higher than the *npp* plus the retranslocated carbon (suppressed trees with low *gpp* and *npp* for their size), the leaf and fine root productions are recalculated so that they do not exceed 80% of the available carbon. (Jonard et al., 2020, p.911-913)

Then, the fruit production ($p_{fruit}$ in kgC yr$^{-1}$) is estimated with an allometric equation similar to Eq. (30) and is considered directly proportional to the light competition index since fructification is known to be favoured when tree crowns are exposed to the sun (Greene et al., 2002; Davi et al., 2016). A threshold *dbh* ($dbh_{threshold}$ in cm) is fixed below which no fruit production occurs. (Jonard et al., 2020, p.911-913)

$$p_{fruit} = \alpha \cdot LCI \cdot (dbh - dbh_{threshold})^{\beta} \tag{37}$$

In this equation, the parameter α takes a default value or is adapted based on the fruit production of the year (when the file with the amount of fruit litterfall per year and per tree species is loaded).

Part of the carbon is also used to compensate for branch and root mortality. The branch mortality ($s_{branch}$ in kgC yr$^{-1}$) is described based on a turnover rate or with an equation of the same form as Eq. (30) while the structural root mortality ($s_{root}$ in kgC yr$^{-1}$) is obtained using a turnover rate. (Jonard et al., 2020, p.911-913)

After subtracting the leaf, fine root and fruit productions and the root and branch senescence, the remaining carbon is allocated to structural tree compartment growth:

$$\Delta b_{structural} = npp + rt - p_{leaf} - p_{fine\ root} - p_{fruit} - s_{branch} - s_{root} \tag{38}$$

At this stage, the remaining carbon is partitioned between the above- and below-ground parts of the tree according to a fixed root to shoot ratio ($r_{root\_shoot}$):

$$\Delta b_{structural\_above} = \frac{\Delta b_{structural}}{(1 + r_{root\_shoot})} \tag{39}$$

$$\Delta b_{structural\_below} = \Delta b_{structural} - \Delta b_{structural\_above} \tag{40}$$

The increment in aboveground structural biomass is then used to determine the combined increment in *dbh* and total height ($h$ in m) based on an allometric equation used to predict aboveground woody biomass (Genet et al., 2011; Hounzandji et al., 2015):

$$b_{structural\_above} = \alpha + \beta(\,dbh^2 \cdot h)^{\gamma} \tag{41}$$

Deriving this equation and rearranging terms gives:

$$\Delta b_{structural\_above} = \beta\gamma(\,dbh^2 \cdot h)^{\gamma-1}\Delta(\,dbh^2 \cdot h) \tag{42}$$

$$\Delta(\,dbh^2 \cdot h) = \frac{\Delta b_{structural\_above}}{\beta\gamma(\,dbh^2 \cdot h)^{\gamma-1}} \tag{43}$$

The development of the left term provides:

$$\Delta(\,dbh^2 \cdot h) = (dbh + \Delta dbh)^2 \cdot (h + \Delta h) - dbh^2 \cdot h \tag{44}$$

which can be further developed to isolate $\Delta h$:

$$\Delta h \cong \frac{\Delta(\,dbh^2 \cdot h)}{dbh^2} - \frac{h \cdot \Delta dbh^2}{dbh^2} \tag{45}$$

From Eq. (45), we know that the height increment can be expressed as a function of $\frac{\Delta(\,dbh^2 \cdot h)}{dbh^2}$. In the following, we refer to it as the height growth potential ($\Delta h_{pot}$) since it corresponds to the height increment if all the remaining carbon was allocated to height growth. Contrary to the other term of Eq. (45) $\left(\frac{h \cdot \Delta dbh^2}{dbh^2}\right)$ which is unknown, this height growth potential can be evaluated at this step by dividing the result of Eq. (43) by *dbh²*. However, depending on the level of competition for light and on the tree size, only part of this height growth potential will be effectively realized for height increment. For each tree species, an empirical relationship predicting height growth from the height growth potential, the light competition index and the tree size (*dbh* or height) was therefore fitted based on successive inventory:

$$\Delta h = a + b\ LCI + c\ \Delta h_{pot} + d\ \Delta {h_{pot}}^2 + e\ h + f\ h^2 + g\ dbh + error \tag{46}$$

The *dbh* increment is then determined by rearranging Eq. (44):

$$\Delta dbh = \sqrt{\frac{\Delta(\,dbh^2 \cdot h) + dbh^2 \cdot h}{(h + \Delta h)}} - dbh \tag{47}$$

The increments in root, stem and branch biomass are obtained as follows:

$$\Delta b_{root} = r_{root\_shoot} \cdot \Delta b_{structural\_above} \tag{48}$$

$$\Delta b_{stem} = f \cdot \rho \cdot ((dbh + \Delta dbh)^2 \cdot (h_{stem} + \Delta h_{stem}) - dbh^2 \cdot h_{stem}) \tag{49}$$

$$\Delta b_{branch} = \Delta b_{structural\_above} - \Delta b_{stem} \tag{50}$$

with $\rho$, the stem volumetric mass (kgC m$^{-3}$),

$h_{stem}$, the stem height (m)

$f$, the form coefficient (m$^3$ m$^{-3}$).

The stem height ($h_{stem}$) is defined as the total tree height ($h$, m) for evergreen species and Larix and as the Delevoy height ($h_{del}, m$), corresponding to the height at which stem diameter is half the diameter at breast height, for the other deciduous species. (Jonard et al., 2020, p.911-913)

The form coefficient (f) is formulated as follows based on Deleuze et al. (2014b):

$$f = \frac{\pi^2 \cdot Vol_{stem}}{\mathrm{h}_{stem} \cdot (gbh/100)^2}\left(1 - \frac{1.30}{h}\right)^2 \tag{51}$$

in which the stem volume ($Vol_{stem}$, m$^3$) is expressed as:

$$Vol_{stem} = Vol_{tree} \cdot Stem_{frac} \cdot \mathrm{Corr} \tag{52}$$

with $Vol_{tree}$ (m$^3$), the tree total volume,

$Stem_{frac}$ (-), the fraction of the tree volume belonging to the stem,

$Corr$ (-), a correction factor accounting for the considered cutting circumference.

The three terms of Eq. (52) are determined through:

$$Vol_{tree} = \frac{h \cdot (gbh/100)^2}{4 \cdot \pi} \frac{a + b \cdot \frac{\sqrt{gbh/100}}{h} + c \cdot \frac{h}{gbh/100}}{\left(1 - \frac{1.30}{h}\right)^2} \tag{53}$$

$$Stem_{frac} = \mathrm{d} + \mathrm{e} \cdot \log\left(\frac{h_{step}}{h - h_{step}}\right) + \mathrm{f} \cdot \frac{\sqrt{gbh/100}}{h} + \frac{g}{gbh/100} \tag{54}$$

$$Corr = \left(1 - \frac{C_{cut}{}^3}{gbh^3}\left(1 - \frac{1.30}{h}\right)^3\right) \tag{55}$$

where a, b, c, d, e, f and g are species specific parameters,

$\mathrm{h}_{step}$ (m) is the step height, corresponding to the height at which the first sharp decrease of stem circumference is observed,

$\mathrm{C}_{cut}$ (cm) is the cutting circumference, set to zero for evergreen species and Larix for which stem height corresponds to total tree height and set to $gbh/2$ for the other deciduous species whose stem height is defined as the Delevoy height (see above). (Jonard et al., 2020, p.911-913)

Finally, $\mathrm{h}_{step}$ is obtained using:

$$h_{step} = (\alpha + \beta \cdot gbh) \cdot h \tag{56}$$

where $\alpha$ and $\beta$ are species specific parameters.

The branch and root biomasses are then distributed in 3 categories defined based on the diameter: small branches/roots < 4 cm, medium branches/roots between 4 and 7 cm, coarse branches/roots > 7 cm. The proportions of small, medium and coarse branches/roots are determined based on equations of the same form as those presented in Hounzandji et al. (2015) for oak branches. Until we can adjust these equations on appropriate data sets, the parameters of Hounzandji et al. (2015) are also used for beech branches and for oak and beech roots. The distribution in root categories has no impact on the functioning of the model since this information is not used elsewhere. This is just a model output that the user can ignore or consider as a whole. (Jonard et al., 2020, p.911-913)

### 1.3.7 Crown extension (from Jonard et al., 2020)

Depending on whether the competition with the neighbouring trees is taken into account or not, the crown dynamics can be described by two different approaches. When local competition is not considered (distance-independent approach), change in crown dimensions are derived from $dbh$ or height increment based on empirical relationships:

$$\Delta hcb = hcb\% \cdot \Delta h \tag{57}$$

$$\Delta hlce = (hcb + \Delta hcb) + hlce\% \cdot \big(h - (hcb + \Delta hcb)\big) - hlce \tag{58}$$

$$\Delta cr = Dd_{pred} \cdot \frac{\Delta dbh}{200} \tag{59}$$

where $hcb\%$ is the proportion of the total height corresponding to the height to crown base estimated according to

$$hcb\% = a + b\ girth + c\ LCI + d\ LCI^2 \tag{60}$$

$hlce\%$ is the proportion of the crown length corresponding to $(hlce - hcb)/(h - hcb)$, the distance from the crown base to the height of largest crown extension ($hlce$, m) obtained from

$$hlce\% = a + b\ gbh + c * LCI + d * gbh * LCI \tag{61}$$

$\Delta cr$ is the change in crown radius (in m) whatever the direction;

$Dd_{pred}$ is the crown to stem diameter ratio estimated by Eq. (25). (Jonard et al., 2020, p.913-914)

Alternatively, the changes in crown dimensions can be described based on the competition with the neighbouring trees (distance-dependent approach). The space around a target tree is divided into 4 sectors according to the 4 cardinal directions (North between 315° and 45°, East between 45° and 135°, South between 135° and 225°, West between 225° and 315°). In each sector, the tree which is the closest to the target tree is retained as a competitor if its height is higher than the $hcb$ of the target tree. Beyond a certain distance (i.e., two times the maximal crown radius: 10 m), no competitor is considered. For each main direction, the model calculates an $hlce$ at equilibrium ($hlce_{eq}$ in m) for the target tree. This $hlce$ at equilibrium is located between a minimum ($hcb$ in m) and a maximum ($hlce_{max}$ in m). $hlce_{max}$ is obtained by determining the higher intersection between the potential crowns of the target tree and the competitor. The potential crown of a tree is the crown that this tree would have had in absence of competition and is considered as having the shape of a half ellipsoid centred on the tree trunk and with the semi-axis lengths equal to the tree potential crown radius ($cr_{pot}$ in m, see below) and to the crown length ($h - hcb$). $hlce_{eq}$ is positioned between the minimum and the maximum values according to the competition intensity estimated based on the target tree and the competitor heights ($h_{target}$ and $h_{comp}$ in m) as well as the $hcb$ of the target tree:

$$hlce_{eq} = hcb + (hlce_{max} - hcb) \cdot max\left(0, min\left(1, \frac{h_{comp} - hcb}{h_{target} - hcb}\right)\right) \tag{62}$$

The four values of $hlce_{eq}$ are then averaged ($hlce_{eq\_mean}$).

Finally, the change in $hlce$ is determined as follows:

if $hlce < hlce_{eq\_mean}$,

$$\Delta hlce = \min(\Delta hlce_{max}, hlce_{eq\_mean} - hlce) \tag{63}$$

else,

$$\Delta hlce = \max(-\Delta hlce_{max}, hlce_{eq\_mean} - hlce) \tag{64}$$

where $\Delta hlce_{max}$ is the maximum change in $hlce$ allowed by the model.

The change in $hcb$ is obtained with the same logic:

if $hcb < hcb_{eq\_mean}$,

$$\Delta hcb = \min(\Delta hcb_{max}, hcb_{eq\_mean} - hcb) \tag{65}$$

else,

$$\Delta hcb = \max(-\Delta hcb_{max}, hcb_{eq\_mean} - hcb) \tag{66}$$

where $hcb_{eq\_mean}$ is the $hcb$ estimated from the tree height based on $hcb\%$ (Eq. 60).

(Jonard et al., 2020, p.913-914)

The change in the four crown radii is calculated based on crown radii at equilibrium ($cr_{eq}$ in m) which are estimated by considering the competitive strength of the target and neighbouring trees. For a given direction, $cr_{eq}$ is calculated based on the potential (free growth) crown radius of the target tree ($cr_{pot\_target}$ in m) and of its competitor ($cr_{pot\_comp}$ in m), the distance between the two trees ($d$ in m) and the crown overlap ratio ($r_{overlap}$ in m m$^{-1}$):

$$cr_{eq} = \frac{cr_{pot\_target}}{cr_{pot\_target} + cr_{pot\_comp}} \cdot d \cdot r_{overlap\_target} \tag{67}$$

The potential crown radius ($cr_{pot}$) of a tree if determined by:

$$cr_{pot} = \frac{dbh}{200} \cdot Dd_{pred} \cdot sh \tag{68}$$

where $Dd_{pred}$ is the crown to stem diameter ratio estimated by Eq. (25) and $sh$ is a coefficient allowing to shift from the mean to the maximum $Dd_{pred}$.

The crown overlap ratio is estimated by considering neighbouring trees of the same species two by two and by calculating the ratio between the sum of their crown radii and the distance between the corresponding tree stems. This overlap ratio accounts for the capacity of a tree species to penetrate in neighbouring crowns. (Jonard et al., 2020, p.913-914)

The change in crown radius is then determined as follows for each direction:

if $cr < cr_{eq}$,

$$\Delta cr = \min(\Delta cr_{max}, cr_{eq} - cr) \tag{69}$$

else,

$$\Delta cr = \max(-\Delta cr_{max}, cr_{eq} - cr) \tag{70}$$

with $\Delta cr_{min}$ and $\Delta cr_{max}$ being respectively the minimum and the maximum change in $cr$ allowed by the model. They are obtained similarly as $cr_{pot}$:

$$\Delta \mathrm{cr}_{max} = \frac{\Delta dbh}{200} \cdot Dd \cdot sh \tag{71}$$

(Jonard et al., 2020, p.913-914)

### 1.3.8 Tree harvesting and mortality (from Jonard et al., 2020)

During the simulation, thinning can be achieved at each annual step either (i) by selecting the trees from a list or a map or according to tree characteristics (tree species, age, *dbh*, height), or (ii) by defining the number of trees to be thinned per diameter class using an interactive histogram, or (iii) by loading a file listing the trees that must be thinned. In addition, the thinning methods developed for GYMNOS and QUERGUS are compatible with HETEROFOR. They allow to reach a target basal area, density or relative density index by thinning from below or from above or by creating gaps (Ligot et al., 2014). (Jonard et al., 2020, p.914)

When the *npp* of a tree is not sufficient to ensure a normal leaf and fine root development (for suppressed trees and/or after a severe drought), the leaf biomass is reduced and induces a defoliation which is estimated as follows:

$$Def = \frac{b_{leaf} - b_{leaf\_corr}}{b_{leaf}} \cdot 100 \tag{72}$$

where $b_{leaf}$ and $b_{leaf\_corr}$ are respectively the leaf biomass estimated with Eq. (30) and the leaf biomass corrected to match the available carbon (see sect. 1.3.6). (Jonard et al., 2020, p.914)

Tree mortality occurs when trees reach a defoliation of 90%, considering that a tree with less than 10% of its leaves is in an advanced stage of decline and is unlikely to recover (Manion, 1981). Hence, HETEROFOR takes into account the mortality resulting from carbon starvation due to light competition and/or water stress (stomatal closure). (Jonard et al., 2020, p.914)

### 1.3.9 Growth reconstruction (from Jonard et al., 2020)

HETEROFOR was adapted to allow the user to run it in reverse mode starting from the known increments in *dbh* and *h* to reconstruct individual *npp* using exactly the same parameters and equations as in the normal mode. To achieve a reconstruction, an inventory file with tree measurements must be loaded to create the initial step. From this initial step, the reconstruction tools can be launched and requires another inventory file with tree measurements achieved one or several years later. Based on these two inventories, HETEROFOR calculates the mean *dbh* and *h* increments for each tree and use the model equations to reconstruct each step and evaluate among other individual *npp*. The *npp* is obtained by re-arranging Eq. (38) in which the carbon allocated to the structural biomass is calculated from the *dbh* and *h* increments using Eq. (42), (40) and (39). The carbon allocated to leaf, fine root and fruit production is determined respectively with Eq. (34), (36) and (37) while the amount re-translocated from leaves and roots before senescence is evaluated with Eq. (29). Finally, the terms of Eq. (38) accounting for the leaf and fine root litter were determined with Eq. (33). In addition to two stand inventories, the reconstruction tool also requires a file listing the trees which were cut or died between the two inventory dates and the last year during which they were present in the stand. (Jonard et al., 2020, p.914)

### 1.3.10 Water balance

The water balance module operates at an hourly time step and simulates the partitioning of incident rainfall into the main forest water fluxes and pools, namely, interception (i.e., water storage on foliage and bark, and evaporation), throughfall, stemflow, water movements between soil horizons and deep drainage, transpiration and soil water uptake in the different soil horizons, and soil evaporation (Fig. 2.2).

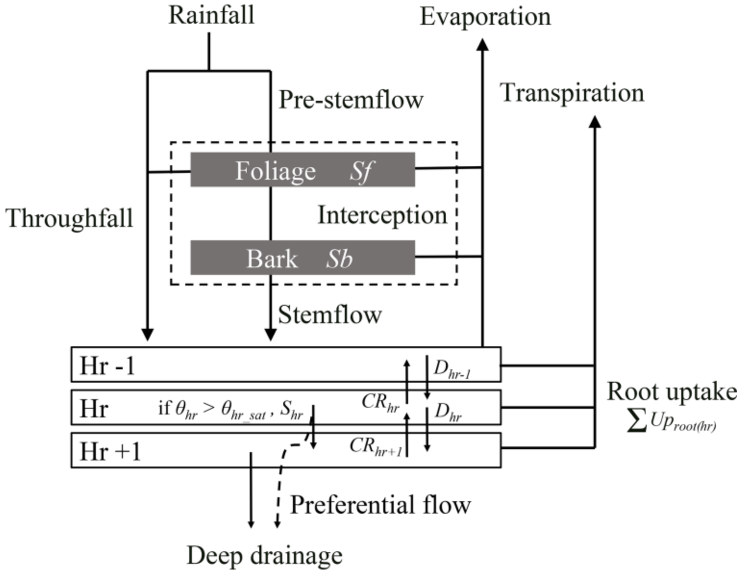

**Figure 2.2: Schematic representation of the water fluxes and pools in the water balance module. Rainfall is divided into throughfall reaching directly the forest floor and a pre-stemflow component intercepted by the foliage and the bark. Once the foliage and bark are saturated, the water surplus increases the throughfall flux and flows along the branches and the trunk to generate stemflow. The throughfall and stemflow fluxes enter in the upper part of the soil and then, move from one horizon to the other according to the Darcy's law. For a soil horizon *hr*, the water input fluxes can be the drainage from the upper horizon ($D_{hr-1}$) and the capillary rise from the lower horizon ($CR_{hr+1}$) that depend on the water potential gradient between the concerned horizons and on their hydraulic conductivity. The output fluxes are the drainage ($D_{hr}$) and the capillary rise ($CR_{hr}$), the root water uptake ($UP_{root(hr)}$) and the surplus ($S_{hr}$) that appears when the horizon water content exceeds the saturated water content. One part of this latter flux can directly leaves the system as deep drainage (*DD*) when preferential flow is considered, in addition to the water drainage of the last horizon. In parallel, water evaporates from foliage, bark and soil and is taken up by roots to enable tree transpiration. The evapo-transpiration fluxes are all calculated with the Penman-Monteith equation.**

Surface runoff and groundwater level rise are not yet considered in the current HETEROFOR version. Instead, when saturation is reached in a soil layer, the water surplus is transferred to the horizon below or is lost when occurring in the last horizon.

In a first step, the parameters considered as constant during the leaved and leafless periods are estimated. Then, the various water fluxes are calculated at an hourly time step. The default option for the water balance module calculates the water fluxes at the stand level by summing properties estimated at the tree level (maximum foliage and bark storage capacities, throughfall and stemflow proportions). For this option, tree transpiration is calculated at the tree level and summed at the stand scale. Stand transpiration is then used to estimate root water uptake in the different soil horizons assuming that all trees are taking up water in the same reservoirs in which soil water is redistributed homogeneously between two hourly time steps. This hypothesis can be justified by soil anisotropy, which induces a higher horizontal than vertical soil conductance. This is justified since water movements through the same horizon depend only on its own hydrological properties while the presence of one horizon with a low conductance can slow down vertical water movement in the upper horizons (Todd and Mays, 2005). Moreover, as sediments are preferentially deposited on their longest side, the vertical conductance is decreased with regards to the horizontal one (Cristiano et al., 2016) so that the ratio of the horizontal *vs* vertical conductance ranges between 2 and 10 in alluvial soils and amounts to 100 in clay soils (Todd and Mays, 2005).

The user can select an alternative option '*activate fine spatial resolution*' to perform water balance on an individual scale. In this case, all the water fluxes (throughfall, stemflow, foliage, bark and soil evaporation, transpiration, water uptake, soil water movements and drainage) are calculated at the individual level. For this option, the model distributes the total soil volume in individual soil volumes (called pedon).

The pedon area ($a_{pedon}$) is determined proportionally to the leaf area of the associated tree (but is limited to two times its crown projection):

$$a_{pedon} = \frac{a_{leaf}}{A_{leaf}} . A_{stand} \qquad (73)$$

with $a_{leaf}$, the tree leaf area (m²)

$A_{leaf}$, the total stand leaf area (m²)

$A_{stand}$, the total stand area (m²)

In sparse stands, all the stand area is not allocated to the trees and the remaining area is considered as a pedon without any associated tree. With the fine spatial resolution, the model performs a water balance for each tree pedon and also for the remaining pedon (without tree). Contrary to the default option, the alternative option supposes no water redistribution among pedons. This hypothesis could become more appropriate than the perfect redistribution hypothesis when soil dries (Friedman and Jones, 2001), at least beyond the air entry value (Assouline and Or, 2006). The two options allow the user to test two contrasted hypotheses regarding soil water redistribution in the horizontal dimension. In the following description, variables calculated at the stand scale are represented with capital letters while lowercase letters are used for variables at the tree level. In some cases, when the equation is the same at the tree and the stand level, the variables are represented only with capital letters to avoid unnecessary duplications.

**Foliage and bark storage capacity**

The maximum foliage storage capacity of a tree ($c_{foliage\_max}$, l) is calculated by multiplying the foliage storage capacity of the corresponding tree species by the tree leaf area:

$$c_{foliage\_max} = a_{leaf} \cdot c_{foliage\_sp} \qquad (74)$$

with $c_{foliage\_sp}$, the foliage storage capacity for the species *sp* (mm or l per m² of leaf).

To obtain it at the stand level ($C_{foliage\_max}$, l), the model sums the maximum foliage storage capacity of all the trees.

Bark storage capacity depends on season (i.e., leafed and leafless periods) and on tree species. It is derived from a linear model proposed by André et al. (2008a) predicting the individual stemflow (*sf*, l) produced during a rain event as a function of tree girth (*gbh*, cm) and rainfall amount (*R*, mm):

$$sf = a + b . gbh + c . R + d . gbh . R + \tau + \delta + \varepsilon \qquad (75)$$

where $a$ (l), $b$ (l $\mathrm{cm}^{-1}$), $c$ ($\mathrm{m}^2$) and $d$ ($\mathrm{m}^2\ \mathrm{cm}^{-1}$) are fixed effect parameters varying with tree species and season, $\tau$ and $\delta$ are random factors characterizing the tree and the rain event variability and ε account for the residuals.

As it multiplies the rainfall amount in Eq. (75), the term "$c + d.gbh$" may be interpreted as an estimate of the stemflow rate ($sf_{rate}$, l $\mathrm{mm}^{-1}$). In parallel, André et al. (2008a) determined the rainfall threshold for stemflow appearance ($R_{min}$, mm), defined as the amount of rainfall required to produce stemflow at the base of the trunk. This threshold was found to be independent of tree size while it depends on both season and tree species. Multiplying the $sf_{rate}$ estimations by $R_{min}$ values for the corresponding species and season provides estimates of the tree bark storage capacity ($c_{bark}$, l), namely, the amount of water accumulated on branch and trunk bark before stemflow occurs at tree base:

$$c_{bark} = (c + d \cdot C130) \cdot R_{min} \tag{76}$$

The individual $c_{bark}$ estimates are then summed over all trees of a same species for each season to determine leafless ($ll$) and leaved ($ld$) stand bark storage capacity ($C_{bark\_sp\_ll}, C_{bark\_sp\_ld}$, l). As shown by André et al. (2008a), the seasonal variation of the bark storage capacity is not significant since the corresponding changes in the three parameters (c, d and Rmin) offset each other. We maintained, however, the distinction between seasons since the parameters of Eq. (75) were also used to estimate throughfall and stemflow proportions (described hereafter), which are clearly season-dependent.

**Throughfall and stemflow proportions**

For a given tree, the proportion of stand rainfall reaching the ground at the base of the trunk as stemflow may be calculated by dividing the stemflow rate (see above) by the pedon or stand area ( $a_{pedon}\ or\ A_{stand}$, $\mathrm{m}^2$) depending on the selected option (tree *vs* stand scale water balance):

$$\%sf = \frac{c+d\cdot C130}{a_{pedon}}\ or\ \frac{c+d\cdot C130}{A_{stand}} \tag{77}$$

For the water balance at the stand scale, the stemflow proportion per tree species is then calculated separately for the leafless and the leaved periods ($\%SF_{sp\_ll}$, $\%SF_{sp\_ld}$) by summing the corresponding tree stemflow proportions. The stemflow proportion is also calculated at the stand scale for each period ($\%SF_{ll}$, $\%SF_{ld}$). Finally, tree and stand level throughfall proportions are obtained directly from the stemflow proportions:

$$\%\mathrm{tf}_{\mathrm{ll}} = 1 - \%sf_{\mathrm{ll}}\ \text{ or }\ \%\mathrm{TF}_{\mathrm{ll}} = 1 - \%SF_{\mathrm{ll}} \tag{78}$$

$$\%\mathrm{tf}_{\mathrm{ld}} = 1 - \%sf_{\mathrm{ld}}\ \text{ or }\ \%\mathrm{TF}_{\mathrm{ld}} = 1 - \%SF_{\mathrm{ld}} \tag{79}$$

**Absorbed radiation proportions**

During the leaved period, the radiation absorbed by the trees is provided by the SAMSARALIGHT library either for the whole period (simplified radiation balance, default option) or for every hour of key phenological dates (detailed radiation balance, alternative option). It may be determined either by considering absorption by tree crowns as a function of leaf area density and ray path length through the crown by applying the Beer-Lambert law, or by specifying relative crown radiation absorption coefficients for each species. At the tree scale, the proportion of incident radiation absorbed per unit of leaf area during the vegetation period ($\%aRAD_{tree\_canopy\_m^2}$) is calculated as the ratio of the radiation absorbed by the crown over the whole vegetation period ($aRAD_{tree\_crown}, MJ$) divided by the corresponding incident radiation ($RAD$, MJ $\mathrm{m}^{-2}$) and the tree leaf area:

$$\%aRAD_{tree\_leaf\_m^2} = \frac{aRAD_{tree\_crown}}{RAD\cdot a_{leaf}} \tag{80}$$

At the stand scale, this proportion is obtained by summing the radiation absorbed by each crown and dividing it by the incident radiation and the leaf area of the whole stand:

$$\%aRAD_{stand\_leaf\_m^2} = \frac{\sum_{tree} aRAD_{tree\_crown}}{RAD \cdot A_{leaf}} \tag{81}$$

Similarly, the proportion of incident radiation absorbed per unit of bark area is obtained, at the tree and stand scales respectively, by

$$\%aRAD_{tree\_bark\_m^2} = \frac{aRAD_{tree\_trunk}}{RAD \cdot a_{bark}} \tag{82}$$

with $aRAD_{tree\_trunk}$, the radiation absorbed by the trunk of a given tree (MJ),

$a_{bark}$, the tree bark area (m²)

$$\%aRAD_{stand\_bark\_m^2} = \frac{\sum_{tree} aRAD_{tree\_trunk}}{RAD \cdot A_{bark}} \tag{83}$$

with $A_{bark}$, the stand bark area (m²)

At both scale (tree and stand), the proportion of incident radiation transmitted to the understorey is the transmitted radiation ($transRAD,$ MJ $m^{-2}$), determined as the difference between the incident radiation and the radiation absorbed by the tree(s), divided by the incident radiation:

$$\%transRAD = \frac{transRAD}{RAD} \tag{84}$$

The radiation transmitted to the understory is then partitioned into the radiation intercepted by the ground vegetation and that reaching the soil by applying Beer-Lambert law considering the ground vegetation leaf area index (described later in *Ground vegetation transpiration and soil evaporation*).

In the following sections, all these proportions are used to estimate the hourly absorbed or transmitted radiations based on the hourly incident radiation.

For the leafless period, the proportions of incident radiation intercepted by the trunks and the branches and transmitted to the understory are obtained based on the Beer-Lambert law using the bark area index (i.e. bark surface divided by the stand or pedo area, *BAI*, $m^{2\ -2}$) calculated from the bark biomass, density and thickness:

$$\%aRAD_{bark\_m^2} = \frac{1-\exp(-k \cdot BAI)}{BAI} \tag{85}$$

$$\%transRAD = \frac{\exp(-k \cdot BAI)}{BAI} \tag{86}$$

**Interception and evaporation of water stored on foliage and bark**

Based on the preceding calculations, the water balance module starts updating the different water fluxes and pools for every hourly time step. First water evaporation from foliage and from bark is computed using the Penman Monteith (P-M) equation (Monteith, 1965) at the tree or stand scale. The latent heat flux density is calculated as follows:

$$\lambda.E = \frac{\Delta R + \frac{\rho.c_p.VPD}{r_a}}{\Delta + \gamma\left(\frac{r_a + r_s}{r_a}\right)} \tag{87}$$

with $\lambda.E$: latent heat flux density (W $m^{-2}$),

$\lambda$: water latent heat of vaporization = 2454000 J $kg^{-1}$ (Teh, 2006),

$\gamma$: psychometric constant = 0.658 mbar $K^{-1}$ (Teh, 2006),

$\Delta$: slope of the saturated vapour pressure curve (mbar $K^{-1}$):

$$\Delta \approx \frac{de_s(T)}{dT} = \frac{25029.4 \cdot exp\left[\frac{17.269.T}{T+237.3}\right]}{(T+237.3)^2}, \tag{88}$$

$\rho$: moist air density = 1.209 kg $m^{-3}$,

$c_p$: moist air specific heat capacity = 1010 J $kg^{-1}$ $K^{-1}$,

$T$: air temperature (°C),

$R$: absorbed radiation per unit of leaf or bark area (Watt per m² of leaf/bark),

$r_a$: aerodynamic resistance (s $m^{-1}$), the inverse of aerodynamic conductance, ga:

$$r_a = \frac{1}{g_a} \tag{89}$$

$r_s$: surface resistance (s $m^{-1}$), the inverse of surface conductance, $g_s$:

$$r_s = \frac{1}{g_s} \tag{90}$$

$VPD$: the vapour pressure deficit (mbar or hPa) calculated as follows based on the air temperature and the relative humidity:

$$VPD = e_s(T) - e_r \tag{91}$$

with $e_s$: saturated vapour pressure (mbar):

$$e_s(T) = 6.1078 \, . \, exp\left[\frac{17.269T}{T+237.3}\right] \tag{92}$$

$e_r$: air vapour pressure (mbar):

$$e_r = \frac{RH}{100} . e_s(T_r) \tag{93}$$

where $RH$ is the relative humidity ($10^{-2}$ hPa $hPa^{-1}$)

The radiation absorbed hourly per unit of leaf area ($h\_aRAD_{leaf\_m^2}$, W.$m^{-2}$) is obtained by multiplying the proportion of incident radiation absorbed per leaf area unit by the hourly incident radiation ($h\_RAD$, W $m^{-2}$):

$$h\_aRAD_{leaf\_m^2} = \%aRAD_{leaf\_m^2} \cdot h\_RAD \tag{94}$$

Similarly, the hourly absorbed radiation per unit of bark area ($h\_aRAD_{bark\_m^2}$, W.$m^{-2}$) is obtained by multiplying the proportion of incident radiation absorbed by the bark by the hourly incident radiation:

$$h\_aRAD_{bark\_m^2} = \%aRAD_{bark\_m^2} \cdot h\_RAD \tag{95}$$

The aerodynamic resistance is defined as the inverse of the aerodynamic conductance, which represents the ease for a water vapour molecule to get away from its original location once it has been evaporated. Similarly, the surface resistance is the inverse of surface conductance that represents the ease for water molecules to migrate through the surface-air interface. The aerodynamic resistance depends mainly on wind speed and turbulence while the surface resistance is a function of the water diffusivity through the surface.

According to Teh (2006) and depending on the scale considered (tree or stand), the mean canopy air resistance may be obtained by integrating the canopy air conductance ($g_a$, m.s$^{-1}$) values estimated at 11 height levels between the mid-crown or mid-canopy height and the dominant height for the foliage and between half of the total or dominant height and the dominant height for the bark:

$$g_a = 0.006 \cdot \sqrt{\frac{WS}{l_{sp}}} \tag{96}$$

with $l_{sp}$, the mean leaf width,

$WS$, the wind speed (m s$^{-1}$).

The mid-canopy height is determined as the mid-height between the dominant height of the stand ($hd$, m), defined as the mean total height of the 100 biggest trees per ha, and the canopy base height ($hcb$, m), defined as the mean height to crown base of the 100 smallest trees per ha. At the tree scale, the integration is done between the mid-crown height and the total height for the foliage and between half of the total height and the total height for the bark.

$WS$ is estimated at the different heights ($h$, m) based on the dominant height wind speed ($WS_{hd}$, m s$^{-1}$) and on the wind speed attenuation coefficient ($\alpha$):

$$WS = WS_{hd} \cdot e^{-\left[\alpha \cdot \left(1 - \frac{h}{hd}\right)\right]} \tag{97}$$

where $WS_{hd}$ is calculated according to Jetten (1996) based on the measured wind speed and its height of measurement:

$$WS(h) = WS(z_m) \cdot \frac{ln\left[{(z_e - d_m)}/{z_{0m}}\right]}{ln\left[{(z_m - d_m)}/{z_{0m}}\right]} \cdot \frac{ln\left[{(h - d_f)}/{z_{0f}}\right]}{ln\left[{(z_e - d_f)}/{z_{0f}}\right]} \tag{98}$$

with $h$ is the height at which wind speed is estimated (in this case the dominant height),

$z_e$ is the reference height (m) fixed to 50 m,

$z_m$ is the wind speed measurement height (2.5 m),

$d_m$ is the surface roughness height (m) of the meteorological station fixed to 0.08 m,

$z_{0m}$ is the zero plane displacement (m) of the meteorological station fixed to 0.015 m,

$d_f$ is the surface roughness height (m) of the forest and estimated as $0.75 \cdot hd$ and

$z_{0f}$ is the zero plane displacement (m) of the meteorological station fixed to $0.1 \cdot hd$.

While no surface resistance is considered for the foliage evaporation (infinite conductance), the bark conductance (m s$^{-1}$) depends on the bark storage at the previous time step ($prevS_{bark\_sp}$, l) and the bark storage capacity ($C_{bark\_sp}$, l) according to

$$g_{s\_bark\_sp} = g_{s\_bark\_min} + (g_{s\_bark\_max} - g_{s\_bark\_min}) \cdot \frac{prevS_{bark\_sp}}{C_{bark\_sp}} \tag{99}$$

The latent heat flux density is then converted to hourly water evaporation ($EV$, l per hour per m² of leaf):

$$EV_{foliage\ or\ bark\_m^2} = \frac{\frac{\lambda.E}{\lambda}}{d_{H2O}} \cdot 1000 \cdot 60 \cdot 60 \tag{100}$$

with $E$, the mass of water evaporated (kg m$^{-2}$ s$^{-1}$) and

$d_{H2O}$, the water density (998 kg $m^{-3}$)

Hourly tree or stand foliage evaporation ($EV_{foliage\_stand}$, $l.h^{-1}$) is obtained by multiplying $EV_{foliage}$ from Eq. (100) by the tree or stand leaf area:

$$EV_{foliage} = EV_{foliage\_m^2} \cdot (a_{leaf}\ or\ A_{leaf}) \tag{101}$$

Similarly, hourly evaporation from bark ($EV_{bark}$, l $h^{-1}$) is determined separately for each tree or tree species by

$$EV_{bark} = EV_{bark\_sp\_m^2} \cdot (a_{leaf}\ \ or\ A_{bark_{sp}}) \tag{102}$$

where $A_{bark\_sp}$ is the bark area for the tree species *sp* ($m^2$).

Evaporation from foliage and from bark cannot be larger than the corresponding amounts of water stored on these surfaces, namely, $S_{foliage}$(l) and $S_{bark\_sp}$ (l) (see next section). Therefore, the following conditions are set:

$$EV_{foliage} = \min(EV_{foliage}, S_{foliage}) \tag{103}$$

$$EV_{bark} = \min(EV_{bark}, S_{bark\_sp}) \tag{104}$$

***Partitioning of rainfall into interception, throughfall and stemflow***

Rainfall passing through the canopy can be intercepted by the foliage, the branches and the stems of the tree(s). These reservoirs saturate progressively and the water then flows along the trunks to the tree base(s) to produce stemflow or drips from the canopy to the ground as throughfall. For some of the parameters (i.e., storage capacities, stemflow proportions) showing contrasting values depending on the season, the leaved and the leafless periods are distinguished to describe these processes. In addition, several intermediate state variables are considered, namely:

- tree or stand rainfall ($R_{tree\ or\ stand}$, l) $= R \cdot (A_{pedon}\ or\ A_{stand})$; (105)
- foliage storage ($S_{foliage}$, l) corresponding to the amount of water stored on the tree or stand foliage;
- previous stand foliage storage ($prevS_{foliage}$, l) being the tree or stand foliage storage at the previous time step;
- remaining foliage storage capacity ($RemC_{foliage}$, l), defined as

  $$RemC_{foliage} = C_{foliage} - (prevS_{foliage} - EV_{foliage}) \tag{106}$$

- non-intercepted rainfall ($unintR$, l).

For the leaved period, the foliage storage and the non-intercepted rainfall are updated at every time step considering various cases:

```
if ($RemC_{foliage} > 0$) {
    if ($RemC_{foliage} > R_{tree\ or\ stand}$) {
        $S_{foliage} = prevS_{foliage} - EV_{foliage} + R_{tree\ or\ stand}$
        $unintR = 0$ }

    else {
        $S_{foliage} = C_{foliage}$
        $unintR = R_{tree\ or\ stand} - RemC_{foliage}$}

else {
    $S_{foliage} = C_{foliage}$
    $unintR = R_{tree\ or\ stand}$}
```

For the leafless period, we have $C_{foliage} = 0$, which gives $unintR = \ R_{tree\ or\ stand})$

Throughfall and stemflow fluxes are then calculated separately for the leaved and leafless periods. For both periods, tree or stand throughfall and pre-stemflow ($preSF,$ l) are considered as complementary fractions of the non-intercepted rainfall. Pre-stemflow is the amount of rain deviated towards the branches and the trunk but not necessarily reaching the base of the trunk due to storage and evaporation losses. At the stand level, pre-stemflow is estimated separately for each tree species.

$$TF_{tree\ or\ stand} = \%\mathrm{TF} \cdot unintR \tag{107}$$

$$preSF_{tree\ or\ sp} = \%SF \cdot unintR \tag{108}$$

At this stage, the following state variables are used:

- the tree or species bark storage ($S_{bark},$ l) = amount of water stored in the bark of a given tree or in that of all the trees of a same tree species,
- the previous tree or species bark storage ($prevS_{bark},$ l) = tree or species bark storage at the previous time step;
- the remaining bark storage capacity of a given tree or species ($RemC_{bark}$, l)*:*

$$RemC_{bark} = C_{bark} - (prevS_{bark} - EV_{bark}) \tag{109}$$

Similarly as above for foliage storage and non-intercepted rainfall, various cases are distinguished to hourly update the bark storage and the stemflow volume ($SF$, l) of each tree or species:

```
if ($RemC_{bark} > 0$) {
        if ($RemC_{bark} > preSF$) {
                $S_{bark} = prevS_{bark} - EV_{bark} + preSF$
                $SF = 0$ }
        else {
                $S_{bark} = C_{bark}$
                $SF = preSF - RemC_{bark}$}
else {
        $S_{bark} = C_{bark}$
        $SF = preSF$}
```

At the stand scale, stemflow is obtained by summing stemflow fluxes over the tree species:

$$SF_{stand} = \sum_{sp} SF_{sp} \tag{110}$$

**Tree transpiration**

As for evaporation from foliage and bark, the Penman Monteith equation (see Eq. 87) is used to estimate hourly tree transpiration during the vegetation period. In this case, the radiation absorbed per unit of leaf area by each tree ($h\_aRAD_{tree\_leaf\_m^2}$, Watt per m² of leaf) is considered and is obtained by:

$$h\_aRAD_{tree\_leaf\_m^2} = \%aRAD_{tree\_leaf\_m^2} \cdot \ h\_RAD \tag{111}$$

The individual aerodynamic resistance is determined from Eq. (96) to Eq. (98) applied between the height of largest crown extension ($h_{lce}$, m) and the dominant height. The individual surface resistance ( $r_{s\_foliage}$, s m$^{-1}$) is defined as the inverse of the foliage stomatal conductance ($g_{s\_foliage}$, m s$^{-1}$). In the model version 1.0 presented in Jonard *et al.* (2020)

and de Wergifosse *et al.* (2020a), the water balance was calculated before photosynthesis, and the stomatal conductance for water was estimated based on a potential x modifier approach considering soil and climate conditions as well as individual tree characteristics (HETEROFOR 1.0) and did not depend on atmospheric $CO_2$ concentration. In the new model version 1.1, the two processes (water balance and photosynthesis) were more closely coupled and the stomatal conductance for water balance was calculated in the same way as for the photosynthesis (see sect. 1.3.4) using the formulation of Ball *et al.* (1987) adapted to the tree level by accounting for the influence of tree height (Schäfer *et al.*, 2000). This modification allows taking the effect of atmospheric $CO_2$ concentration on stomatal conductance for water transpiration into account.

As the first version of the model was used for the chapters 3 and 4, we described below the potential x modifier approach for estimating stomatal conductance which was however not anymore used for the new simulations (chapter V). This approach allows to account for the increase in stomatal conductance with radiation and for the negative effect of increasing vapour pressure deficit and soil water potential (Granier and Breda, 1996; Tuzet et al., 2003; Buckley, 2017). For similar soil and climate conditions, the stomatal conductance is acknowledged to be higher for trees with a larger sapwood to leaf area ratio and to decreases with crown height as stomata of top leaves close earlier to avoid cavitation when water stress occurs (Ryan and Yoder, 1997; Schäfer et al., 2000).

$$r_{s\_foliage} = \frac{1}{g_{s\_foliage}} \tag{112}$$

$$g_{s\_foliage} = g_{s0\_foliage} \cdot \frac{a_{sapwood}}{a_{leaf}} \cdot \frac{1}{h_{lce}} \cdot M_{radiation} \cdot M_{soil\ water} \cdot M_{vpd} \tag{113}$$

with $g_{s0\_foliage}$: the reference stomatal conductance (m $s^{-1}$),

$\frac{a_{sapwood}}{a_{leaf}}$: the sapwood to leaf area ratio ($m^2$ $m^{-2}$) calculated at the tree level (see Eq. 27 in sect. 1.3.5),

$M_{radiation}$: the radiation modifier = $\frac{h\_aRAD_{tree\_leaf\_m^2}}{h\_aRAD_{tree\_leaf\_m^2} + p_{radiation}}$, (114)

where $p_{radiation}$ is a parameter characterizing stomatal response to radiation.

$M_{soil\ water}$: the soil water modifier = $e^{-p1_{SW}(pF-2.5)^{p2_{SW}}}$ when $pF > 2.5$, 1 otherwise (115)

where $pF$ (cm) is the base-10 logarithm of the mean soil water potential ($\phi$) (mean value of the various horizons weighted based on root proportion, see below in the "root water uptake" section for calculation details of the soil water potential) and $p1_{SW}$ and $p2_{SW}$ are two parameters characterizing the stomatal response to soil water potential.

$M_{vpd}$, the $VPD$ modifier = $1.0 - p_{VPD} \cdot \ln VPD$. (116)

where $p_{VPD}$ is a species-dependent parameter characterizing stomatal response to vapour pressure deficit.

The latent heat flux density (W $m^{-2}$) determined by applying this parametrization to Eq. (87) is then converted to tree transpiration ($TR_{tree}$, l $h^{-1}$) using the same approach as for foliage evaporation that was described in Eq. (100) and Eq. (101). Finally, $TR_{tree}$ is corrected by multiplying it by the proportion of green leaves (*greenProp*) and by the fraction of leaves not covered with water ($1 - \frac{S_{foliage}}{C_{foliage}}$), considering that transpiration occurs from photosynthetically active and dry leaves only.

***Ground vegetation transpiration and soil evaporation***

The Penman Monteith equation is also used to estimate ground vegetation transpiration and soil evaporation at the tree and stand scale. For this purpose, the radiation transmitted to the understory is subdivided for each time step into the radiation absorbed by per unit of leaf area of the ground vegetation ($h\_aRAD_{grd\_veg\_m^2}$, Watt per m² of leaf) and the radiation absorbed by the soil ($h\_aRAD_{soil\_m^2}$, W.m$^{-2}$) through application of the Beer-Lambert law:

$$h\_aRAD_{grd\_veg\_m^2} = \frac{\%transRAD \cdot rad \cdot (1 - \exp(-k \cdot LAI_{grd\_veg} \cdot greenProp_{stand}))}{LAI_{grd\_veg} \cdot greenProp_{stand}} \tag{117}$$

$$h\_aRAD_{soil\_m^2} = \%transRAD \cdot rad \cdot \exp\left(-k \cdot LAI_{grd_{veg}} \cdot greenProp_{stand}\right) \tag{118}$$

where $k$ is the extinction coefficient fixed to 0.5 (Teh, 2006), $LAI_{grd\_veg}$ is the leaf area index of the ground vegetation calculated as the difference between the ecosystem LAI and the tree or stand LAI, $greenProp_{stand}$ is the proportion of remaining green leaves at the stand level.

The energy effectively available for soil evaporation is obtained by subtracting the soil heat flux density ($G$, W m$^{-2}$) from $h\_aRAD_{soil\_m^2}$. $G$ is estimated based on the temperature gradient and the soil thermal conductivity ($K$, fixed to 0.25 W m$^{-1}$ K$^{-1}$) as follows:

$$G = K * \frac{T_{surf} - T_{int}}{th_{org}/_{100}} \tag{119}$$

with $T_{surf}$ (°C), the temperature at the soil surface, considered as equal to air temperature ($T$)

$T_{int}$ (°C), the temperature at the interface between the organic layers and the mineral soil (see supplementary materials in Jonard et al., 2020 for more information on the way $T_{int}$ is obtained),

$th_{org}$ (m), the thickness of the organic layer.

For ground vegetation transpiration and soil evaporation, the aerodynamic resistance is computed by applying Eq. (96) to (98) between the ground level and the dominant height.

The surface resistances of the ground vegetation ($r_{s\_grd\_veg}$) and of the soil ($r_{s\_soil}$) are the reciprocals of the ground vegetation and soil conductances, respectively. The ground vegetation conductance ($g_{s\_grd\_veg}$, m s$^{-1}$) is estimated based on the same approach as $g_{s\_foliage}$ for tree transpiration while the soil conductance ($g_{s\_soil}$, m s$^{-1}$) depends on the relative extractable water (see below for computation details) of the forest floor at the previous time step ($prevREW_{forest\_floor}$):

$$g_{s\_soil} = g_{s\_soil\_min} + (g_{s\_soil\_max} - g_{s\_soil\_min}) \cdot prevREW_{forest\_floor} \tag{120}$$

The latent heat flux density (W m$^{-2}$) is then converted to ground vegetation transpiration ($TR_{grd\_veg}$, l h$^{-1}$) and soil evaporation ($EV_{soil}$, l h$^{-1}$) using the same approach as for tree transpiration and foliage evaporation, Eq. (100) and Eq. (101).

### Soil hydraulic properties

The modelling of water uptake distribution among soil horizons and of water transfer from a horizon to another requires estimates of the hydraulic properties for all soil horizons. The relationship between the soil water content ($\theta$, m$^3$ m$^{-3}$) and the absolute matric potential ($h$, cm) is described by the van Genuchten function

$$\theta = \theta_r + S \cdot (\theta_s - \theta_r) \tag{121}$$

that can be rearranged under the form

$$S = \frac{\theta - \theta_r}{\theta_s - \theta_r} \text{ and} \tag{122}$$

$$S = [1 + (\alpha|h|)^n]^{-\left(1 - \frac{1}{n}\right)} \tag{123}$$

with $\theta_r$, the residual water content (m$^3$ m$^{-3}$),

$\theta_s$, the saturated water content (m$^3$ m$^{-3}$),

*S*, the relative water content

α and $n$, two parameters

The Mualem-van Genuchten function allows to estimate the soil hydraulic conductivity based on the relative water content and the saturated conductivity.

$$K = K_0 \left( S^{\lambda} \left\{ 1 - \left(1 - S^{n/_{n-1}}\right)^{1 - \frac{1}{n}} \right\}^2 \right) \tag{124}$$

with *K*, the hydraulic conductivity (cm day$^{-1}$),

$K_0$, the saturated conductivity (cm day$^{-1}$) and

$\lambda$, a parameter.

These two functions (Eqs 64 and 65) partly share the same parameters which are estimated based on soil horizon properties (i.e., organic carbon content, $C_{org}$, particle size distribution). For organic horizons, values from Dettmann et al. (2014) are used for α, n and λ (α = 0.251, n = 1.75, λ = 0.5) and the equation of Päivänen (1973) for Sphagnum peat is considered for $K_0$.

$$K_0 = 10^{\left(-2.321 - 13.22 \cdot \rho_b \cdot \frac{1000}{1000000}\right) \cdot 24 \cdot 60 \cdot 60} \tag{125}$$

with $\rho_b$ = bulk density (kg m$^{-3}$)

For mineral horizons, pedotransfer equations elaborated by Weynants et al. (2009) are used:

$$\ln \alpha = -4.3003 - 0.0097 \cdot clay + 0.0138 \cdot sand - 0.0992 \cdot C_{org} \tag{126}$$

$$\ln(n - 1) = -1.0846 - 0.0236 \cdot clay - 0.0085 \cdot sand + 0.0001 \cdot sand^2 \tag{127}$$

$$\ln K_0 = 1.9582 + 0.0308 \cdot sand - 0.6142 \cdot \rho_b - 0.1566 \cdot C_{org} \tag{128}$$

$$\lambda = -1.8642 - 0.1317 \cdot clay + 0.0067 \cdot sand \tag{129}$$

with *clay* and *sand*, the clay and sand content of the soil (10$^{-2}$ g g$^{-1}$) respectively

$C_{org}$, the organic carbon content of the soil (g kg$^{-1}$) and

$\rho_b$, the bulk density (g cm$^{-3}$).

**Water uptake distribution among soil horizons**

Once tree and ground vegetation hourly transpiration has been calculated, the module sums transpiration on all trees for the stand approach and add the ground vegetation transpiration to obtain the hourly stand transpiration, corresponding to the stand water uptake. Then, tree or stand water uptake is distributed among the horizons according to a method described in Couvreur et al. (2012). This method assumes that water absorption occurs preferentially in horizons where the water potential (matric potential, *h*, plus a gravimetric component), $\phi$, is higher. Moreover, it considers that the amount of water uptake is proportional on the one hand to the difference between the horizon water potential and the averaged water potential weighted by the fine root proportion of the whole soil profile and on the other hand to the fine root proportion of the horizon. This can be transcribed as:

$$UP_{root(hr)} = UP_{root}.\mathrm{f}_{hr} + K_{comp}\,.3600.\left(\phi_{hr} - \sum_{hr=1}^{N}\phi_{hr}.\mathrm{f}_{hr}\right).10.\mathrm{f}_{hr}.\left(A_{pedon}\ or\ A_{stand}\right) \tag{130}$$

with $UP_{root}$ and $UP_{root(hr)}$, the total water uptake and the water uptake of the *hr* horizon respectively (l h$^{-1}$),

$f_{hr}$, the fine root proportion of the horizon *hr*,

$K_{comp}$, the compensatory conductivity set to 1.10$^{-9}$ (s$^{-1}$),

$\phi_{hr}$, the horizon water potential (cm).

The right term of Eq. (130) is null when integrated on all the horizons. Then, it does not change the total amount of water uptake but it refines its distribution. Moreover, this method can generate water uplift that can occur when the top horizons are much drier than the deep ones.

**Water balance of the soil horizons**

At the tree and stand scale, the module performs an hourly water balance for each soil horizon *hr* (numbered from the topsoil) and updates its water content ($\theta_{hr}$, m$^3$ m$^{-3}$) as follows:

$$\theta_{hr} = \theta_{hr\_prev} + \frac{(IN_{hr} - OUT_{hr})}{998 \cdot V_{hr}} \tag{131}$$

with $\theta_{hr\_prev}$, the water content of the *hr* horizon at the previous time step (m$^3$ m$^{-3}$),

$V_{hr}$, the volume of the *hr* horizon (m$^3$),

$IN_{hr}$, the sum of the input water fluxes (l) and

$OUT_{hr}$, the sum of the output water fluxes (l).

The input fluxes are the drainage ($D$, l) and the water surplus ($S$, l) from the upper horizon (*hr-1*) and the capillary rise ($CR$, l) from the lower horizon (*hr+1*) described hereafter and represented in Fig. 2.2:

$$IN_{hr} = D_{hr-1} + S_{hr-1} + CR_{hr+1} \tag{132}$$

The output fluxes are the drainage, the soil evaporation ($E_{soil}$, l), the root water uptake ($UP_{root}$, l) and the capillary rise from the current horizon (*hr*) (Fig. 2.2):

$$OUT_{hr} = D_{hr} + EV_{soil(hr)} + UP_{root(hr)} + CR_{hr} \tag{133}$$

The water transfer ($WT$, $l$) between the horizon $hr$ and $hr+1$ (considered as drainage if directed downward or as capillary rise if directed upward) is estimated with the Darcy law and the average conductivity between the horizons is calculated according to the upwind scheme that takes into account the horizon water potential (e.g. An and Noh, 2014).

$$WT = \frac{K_{hr,hr+1}}{24} \cdot \left(\frac{\Delta h_m}{\Delta z} + 1\right) \cdot (A_{pedon} \; or \; A_{stand}) \cdot 100 \tag{134}$$

with $$K_{hr,hr+1} = \begin{cases} K_{hr+1}, \; \phi_{hr+1} > \phi_{hr} \\ K_{hr}, \; \phi_{hr+1} \leq \phi_{hr} \end{cases} \text{(cm day}^{-1}\text{)} \tag{135}$$

$$\frac{\Delta h_m}{\Delta z} = \frac{|h_{hr+1}| - |h_{hr}|}{\frac{th_{hr} + th_{hr+1}}{2} \cdot 100} \tag{136}$$

where $th$ (m) is the horizon thickness.

To ensure the mass conservation, a variable time step ($\Delta t$, s) is considered based on a stability criterion derived from the Peclet number.

$$\Delta t = \frac{\theta_{hr_{prev}} \cdot th_{hr}}{10 \cdot \frac{K_{hr}}{100 \cdot 24 \cdot 3600}} \tag{137}$$

This criterion is calculated for each horizon and the minimum value is retained. Still, the mass conservation is tested for the whole soil profile at the end of each hour. If the water balance error exceeds 0.01 mm, the time step is divided by 10 (with 1000 as a maximum). The hourly water transfer is then obtained by cumulating the discretized values of water transfer.

For the top horizon, $D_{hr-1}$ is initialized at $TF + SF$ and $CR_{hr}$ is set to 0. For the current horizon, if $WT \geq 0$, $D_{hr} = WT$, else $D_{hr} = 0$ and $CR_{hr+1} = -WT$.

Soil evaporation occurs only in organic horizons. The amount of water evaporated from the horizon $hr$ ( $EV_{soil(hr)}$, l) is obtained by taking the minimum value between the remaining water to evaporate ($remEV_{soil(hr)}$, l) and the volume of extractable water in the horizon ($VEW_{hr} = EW_{hr} \cdot (A_{pedon}$ or $A_{stand})$, l). For the upper organic horizon, $remEV_{soil(hr)}$ is initialized to the total amount of water evaporated from the soil and is progressively decremented by subtracting $EV_{soil(hr)}$ for the deeper organic horizons:

$$remEV_{soil(hr)} = remEV_{soil(hr-1)} - EV_{soil(hr-1)} \tag{138}$$

In both mineral and organic horizons, if the water balance leads to a soil horizon water content higher than saturation, the soil horizon water content is set to the value of the saturated water content and a surplus is calculated. Part of this surplus is passed to the next horizon ($S_{hr-1}$) while the rest is considered as preferential flows and is added to the deep drainage ($DD$).

$$S_{hr-1} = IN_{hr} - \left(\theta_{s\_hr} - \theta_{hr\_prev}\right) \cdot V_{hr} \cdot 998 \cdot (1 - \nu_{hr}) - OUT \tag{139}$$

with $\nu_{hr}$, the additional coarse fraction of the horizon ($m^3$ $m^{-3}$), not accounted for in the bulk density.

The deep drainage is calculated as the sum of $D_{hr}$ and $S_{hr-1}$ of the last horizon plus the preferential flows.

Before passing to the next horizon, $D_{hr-1}$ takes the value of $D_{hr}$ and $CR_{hr}$ the value of $CR_{hr+1}$.

**Absolute and relative extractable water**

The absolute extractable water ($EW$, mm) is defined as the amount of water stored in the soil that can be used by the plants:

$$EW = \sum_{hr=1}^{n} \left(\theta_{hr} - \theta_{\mathrm{wp}\_hr}\right) \cdot th_{hr} \cdot (1 - \nu_{hr}) \tag{140}$$

where $\theta_{wp\_hr}$ is the water content of the soil horizon at the wilting point (m³ m⁻³),

$\nu_{hr}$ is the additional coarse fraction of the horizon (m³ m⁻³), not accounted for in the bulk density,

$th_{hr}$ is the horizon thickness (mm).

The relative extractable water ($REW$, mm) corresponds to the ratio between this value of extractable water and the reference extractable water at the field capacity ($EW_{ref}$, mm):

$$REW = \frac{EW}{EW_{ref}} \tag{141}$$

with $$EW_{ref} = \sum_{hr=1}^{n} \left(\theta_{\mathrm{fc}\_hr} - \theta_{\mathrm{wp}\_hr}\right) \cdot th_{hr} \cdot (1 - \nu_{hr}) \tag{142}$$

where $\theta_{fc\_hr}$ is the water content of the soil horizon at the field capacity (m³ m⁻³).

## 2. MODEL PARAMETERIZATION

### 2.1. PHENOLOGY

Two different sets of phenological parameters were used in the project. The first was created to evaluate the three phenological models implemented (two-phase optimum, two-phase sigmoid and one-phase) against observations from different sites in Wallonia (Chap. 3) and was used for the first simulation round at the Walloon scale with the one-phase model (Chap. 4). Then, for the simulation at the European scale (Chap. 5), I took advantage of an existing set of parameters from Duputié et al. (2015) considering a slightly modified version of the two-phase optimum model for oak and the two-phase sigmoid for beech.

The parameters used to calculate the start of budburst at the Walloon scale were determined using observations from the Pan European Phenology dataset (PEP725), which provides data about phenological observations across different European countries, though not in Belgium. We selected 129 sites on the western border of Germany covering the latitudes of our 6 study plots (49.5-51.0°N), for which the budburst dates of a representative tree were available at least between 1951 and 2015. The daily minimum, maximum and mean temperatures required to achieve the calibration came from the meteorological stations of the DWD Climate Data Center (Deutscher Wetterdienst). Phenological data from each site were assigned to the nearest meteorological station (5 different stations were sufficient). The calibration was carried out with the Phenological Modeling Platform software (Chuine et al., 2013). This module enables the user to perform a Bayesian calibration procedure using the algorithm of Metropolis et al. (1953). Some of the parameters can also be fixed. In our case, the chilling starting date of the two-phase model were fixed to the 1st of November of the previous year (e.g., Chiang and Brown, 2007; Roberts et al., 2015) in order to enhance the accuracy of the other parameter calibration. The length of the budburst period (necessary to determine the budburst shift), the leaf development, yellowing and falling rates were all adjusted from phenological observations conducted on 20 trees in the six Walloon study sites used to evaluate the model (Chap. 3). The parameter values can be found in Table 3.1. For this set, the parameters for common hornbeam were fixed to those of European beech given their similar morphology, which is a relatively rough approximation (Table 3.S1). However, the parameters for common hornbeam, as well as for many other tree species, were then adapted based on literature data by Frédéric André (Kramer et al., 1994a; Vitasse et al., 2011).

The parameter set from Duputié et al. (2015) to calculate budburst at the European scale was also calibrated from observations of the PEP725 dataset using PMP but on a larger number of countries and sites. Leaf yellowing and fall parameters were fitted with the observations provided for 13 ICP Forests study sites located in Belgium, Germany, France and Romania, which are part of the sites used for the simulation round at the European scale (Chap. 5).

### 2.2. LIGHT INTERCEPTION (FROM ANDRÉ ET AL., SUBMITTED)

The calibration of HETEROFOR light interception module was carried out by resorting to hemispherical photographs, which allowed assessing undercover radiation and its spatiotemporal variation. Observations were obtained in 19 uneven-aged forest stands in the Belgian Ardennes dominated by beech and sessile oak, covering a wide range of proportions of both species from pure beech stands to stands mainly dominated by oak. These measured quantities were then compared to model outputs so as to estimate parameters of the radiative transfer. The calibration exercise focused on the three main species found at the study sites, namely, sessile oak, European beech and common hornbeam, and parameters were estimated separately for each of the three species. So as to simplify the optimization process and to avoid instability and non-uniqueness issues, the values for some of the parameters were determined either based on literature or through separate fitting. (André et al., submitted)

Among the parameters, k and Ω are both factors of a same product and cannot be estimated separately without fixing one of them. As a result, Ω was set to 1, considering then no clumping of canopy elements within tree crowns. Therefore, k is the only optimized parameter for the ‘Turbid medium’ mode whereas in the case of the ‘Porous envelop’ mode, the canopy openness (p) is the only free parameter and has been optimized. (André et al., submitted)

The parameters were optimized resorting to a Bayesian procedure with iterative Markov Chain Monte Carlo (MCMC) carried out through the DiffeRential Evolution Adaptive Metropolis (DREAM) algorithm, using more specifically the DREAM(zs) version for greater efficiency (Vrugt, 2016). The R version of the algorithm implemented within the ‘BayesianTools’ package (Hartig et al, 2019) was used. (André et al., submitted)

The light interception module was calibrated while also considering tree growth based on stand inventory data (long-term monitoring plots in Wallonia). Two different optimization strategies were tested and compared. The first strategy consists in a two steps optimization, optimizing first the radiative balance parameters based on the radiation data and fixing then these parameters to the median value of their retrieved posterior distribution for the optimization of the tree growth parameters based on the stand inventory comparison data. The second strategy combined the optimization of both the radiative balance and the tree growth parameters using both sets of data in one single run. (André et al., submitted)

### 2.3. TREE GROWTH

The HETEROFOR model requires parameters most of which are species-specific. For the growth module, the HETEROFOR model was first calibrated for three deciduous species: indigenous oak, beech and hornbeam as described in Jonard et al. (2020). In the last year, prior to the simulations at the European scale (Chap. 5), additional species have been incorporated into the model: birch, common spruce, Douglas-fir, Scots pine, silver fir, sycamore maple, European larch, Atlas cedar, red oak, ash, cherry, small-leaved lime and chestnut. Some of these species parameters (e.g. specific leaf area, leaf size, leaf/needle turnover, leaf retranslocation, taper function, volume functions, drought sensitivity) were obtained directly from the literature on functional traits, tree ecophysiology or dendrometry. The parameters used for carbon allocation were obtained by fitting allometric relationships predicting, for example, leaf biomass or aboveground woody biomass from dbh and/or height. To make these adjustments, we benefited from biomass data gathered for meta-analyses (André and Ponette, 2003; André *et al.*, 2010; Falster *et al.*, 2015; Ung *et al.*, 2017; Schepaschenko *et al.*, 2017).

Then, for some other parameters, similarly to the phenological parameterization, two different parameter sets were used. The first was calibrated with individual observations from Walloon sites (see Jonard et al. 2020 for more details) and was used for the simulations at the Walloon scale (Chap. 4). The second was calibrated based on the observations from 36 ICP Forest sites across Europe. The simulations at the European scale described in Chap. 5 are based on this second set of parameters. The main parameters that changed from one parameter set to the other are those associated with relationships predicting some tree dimensions (crown base height and crown radius) based on dbh and/or tree height (Eq. 57 to 61), the parameters to estimate height growth (Eq. 47) and those to calculate the npp to gpp ratio (or CUE) (Eq. 23). A particularity of the height growth and npp to gpp ratio functions is that their calibration required to run the model using the reconstruction mode (see sect. 1.3.9). For this reason, the calibration results were evaluated in details as described in Chap. 5. Finally, the values of the first parameter set can be found in Table 2 of Jonard et al. (2020) while those of the second parameter set are located in Table 5.S5.

### 2.4. WATER CYCLE

For the water cycle module, most of the model parameters were taken directly from the literature and can be found in Table 3.1. As a result, there has been no significant parameter change during the project. For the soil hydraulic properties, the saturation $\theta_s$ was based on the 0.999 quantile of measured soil water contents when data were available. For horizon without soil water content sensor, $\theta_s$ was interpolated from the closest horizons. Then, the wilting point water content was determined using the obtained saturated water content and the Eq. (123) with a matric potential, $h$, of 15000. When no data were available, these values were determined according to pedotransfer functions (Eq. 121 to 129).

# Chapter 3

# HETEROFOR 1.0: A SPATIALLY EXPLICIT MODEL FOR EXPLORING THE RESPONSE OF STRUCTURALLY COMPLEX FORESTS TO UNCERTAIN FUTURE CONDITIONS – PART 2: PHENOLOGY AND WATER CYCLE

**Based on**

de Wergifosse L, André F, Beudez N, de Coligny F, Goosse H, Jonard F, Ponette Q, Titeux H, Vincke C, Jonard M (2020) HETEROFOR 1.0: a spatially explicit model for exploring the response of structurally complex forests to uncertain future conditions–Part 2: Phenology and water cycle. Geosci. Model Dev. 13(3): 1459-1498.

## ABSTRACT

*Climate change affects forest growth in numerous and sometimes opposite ways and the resulting trend is often difficult to predict for a given site. Integrating and structuring the knowledge gained from the monitoring and experimental studies into process-based models is an interesting approach to predict the response of forest ecosystems to climate change. While the first generation of models operates at stand level, one needs now spatially explicit individual-based approaches to account for individual variability, local environment modification and tree adaptive behaviour in mixed and uneven-aged forests supposed to be more resilient under stressful conditions. The local environment of a tree is strongly influenced by the neighbouring trees which modify the resource level through positive and negative interactions with the target tree. Among others, drought stress and vegetation period length vary with tree size and crown position within the canopy.*

*In this paper, we describe the phenology and water balance modules integrated in the tree growth model HETEROFOR (HETEROgenous FORest) and evaluate them on six heterogeneous sessile oak and European beech stands with different levels of mixing and development stages and installed on various soil types. More precisely, we assess the ability of the model to reproduce key phenological processes (budburst, leaf development, yellowing and fall) as well as water fluxes.*

*Two two-phase models differing regarding their response function to temperature during the chilling period (optimum and sigmoid functions) and a simplified one-phase model are used to predict budburst. The two-phase model with the optimum function is the least biased (overestimation of 2.46 days) while the one-phase model best accounts for the interannual variability (Pearson's r = 0.68). For the leaf development, yellowing and fall, predictions and observation are in accordance. Regarding the water balance module, the predicted throughfall is also in close agreement with the measurements (Pearson's r = 0.856, bias = -1.3%) and the soil water dynamics across the year is well-reproduced for all the study sites (Pearson's r comprised between 0.893 and 0.950, and bias between -1.81 and -9.33%). The model also* *well reproduced individual transpiration for sessile oak and European beech with similar performances at the tree and stand scale (Pearson's r of 0.84 – 0.85 for sessile oak and 0.88 – 0.89 for European beech). The good results of the model assessment will allow us to use it reliably in projection studies to evaluate the impact of climate change on tree growth in structurally complex stands and test various management strategies to improve forest resilience.*

---

## 1. INTRODUCTION

Climate projections for the future indicate a substantial increase in air temperature all over Europe (between 1.0 and 5.5°C depending on the greenhouse gas emission scenario) and changes in precipitation regime according to the region (Jacob et al., 2014; Kovats et al., 2014). Climate extremes (*e.g.* heat waves and droughts) are also predicted to increase in intensity and frequency (Dai, 2013; Jacob et al., 2018). These changing climate conditions affect forest growth and mortality (Allen et al., 2015; Teskey et al., 2015; Charru et al., 2017; Kornhuber et al., 2019) and have an impact on the provision of ecosystem services (Hassan et al., 2005; Shvidenko et al., 2005; Rasche et al., 2013). Among others, forests play an important role in regulating the climate system by sequestering carbon in biomass and soil (Myhre et al., 2013; Le Quéré et al., 2018) and by determining water and energy exchanges with the atmosphere through their evapotranspiration and land surface properties (e.g. albedo, roughness) (Bonan, 2008; Stocker et al., 2013).

Since climate change affects some tree growth processes positively and others negatively and given the interactions among factors as well as the feedback and acclimation mechanisms, it is not easy to predict the resulting effect on tree growth at a given site (Lindner et al., 2014; Herr et al., 2016). Knowledge about climate change has been acquired based on long-term monitoring studies that are limited to the observed changes (Bussotti and Pollastrini, 2017; Etzold et al., 2019) and on experiments of environment manipulation generally analysing one or two factors at a time on a limited period (Ainsworth and Long, 2005; Norby et al., 2010; Wolkovich et al., 2012; Meir et al., 2015). In order to apprehend the complex functioning of forest ecosystems, the use of process-based modelling is a complementary approach that allows integrating and structuring the existing knowledge and making extrapolations for unprecedented conditions like those projected for the coming decades.

Process-based models were originally built to predict forest growth response to environmental changes at stand level without accounting for management operations and canopy heterogeneity. Such models were therefore suitable for pure even-aged stands but hardly manage to simulate mixed and structurally-complex stands (Dufrêne et al., 2005; Pretzsch et al., 2007). Yet, nowadays, a promising way to adapt forests to climate change is to progressively turn them into uneven-aged and mixed stands using continuous cover forestry and natural-disturbance based management to improve their stress resistance and resilience (DeRose and Long, 2014; Messier et al., 2015; Anderegg et al., 2018). To account for the spatial heterogeneity, some process-based models were designed or adapted to simulate various tree cohorts (Collalti et al., 2016). However, this approach only considers the vertical dimension of spatial heterogeneity while implementing innovative forestry practices in structurally complex stands requires to account for the horizontal dimension through a spatially explicit approach at tree level (Pacala and Deutschman, 1995; Pretzsch et al., 2007; Berger et al., 2008; Bravo et al., 2019).

To reproduce the complexity of forest ecosystem functioning in mixed and structured forests, models must take individual variability, local environment and tree adaptive behaviour into account (Berger et al., 2008). Tree size and species influence physiological and morphological properties that in turn affect the main growth processes (Binkley et al., 2013). Considering average individuals is therefore a rough approximation and does not allow accounting for all the variability within a heterogeneous forest (Berger et al., 2008). Even in cohort-based approaches, tree grouping can only be done on a limited number of criteria that are not necessarily representative of the whole tree diversity. The local environment of a tree is strongly influenced by the neighbouring trees which modify the resource level through positive and negative interactions with the target tree (Grossiord et al., 2014). As trees compete for limited resources, neighbouring trees can decrease light, water and nutrient availability. Tree species can however develop strategies to avoid competition by using different temporal and spatial niches (complementarity, Grossiord, 2018). Positive interactions may also occur when the neighbouring trees improve the growing conditions of the target trees (facilitation, Pretzsch et al., 2013). Finally, trees adapt their morphology and physiological behaviour to the local environmental conditions by optimizing carbon allocation in order to maximise the acquisition of the limiting resource (Petritan et al., 2009; Yuang et al., 2019).

As this study focus on phenology and water cycling, we briefly review how these processes are influenced by tree characteristics and local environment. Phenology timing varies among tree species, which favours early-leafing species but can also expose them to late frosts (Lopez et al., 2008; Liu et al., 2018). Many studies report that leaf development starts earlier and leaf senescence occurs later in the understory compared to the overstory (Gill et al., 1998; Seiwa 1999a; Augspurger and Bartlett, 2003; Schieber, 2006; Vitasse, 2013; Gressler et al., 2015) which allows the understory trees to benefit from a longer growing period and consequently, to increase their productivity (Jolly et al., 2004). Warmer temperatures in the understory is one of the hypotheses advanced to explain this difference in budburst between under- and overstory (Augspurger and Bartlett, 2003; Schieber, 2006). Using a construction crane, Vitasse (2013) tested this hypothesis by transplanting seedlings of 5 tree species at 30 and 35 m height in the canopy. He observed that the budburst of the seedling growing at these heights was much earlier than that of the dominant trees. He concluded that the main factor to explain this difference in budburst is driven by ontogeny (tree age and height) as stated by Seiwa (1999b) and that the vertical profile in temperature within the canopy only plays a secondary role. To capture the differences in budburst between understorey and dominant trees, ontogeny must be taken into account in priority.

Drought stress occurs when trees cannot anymore adjust their water use to soil water availability, which reduces growth and can even lead to mortality at short or medium term due to hydraulic failure or progressive carbon starvation (McDowell and Allen, 2015; Meir et al., 2015; Greenwood et al., 2017). The stomatal control of water use varies among tree species and depends on tree size (Martínez-Vilalta and Lloret, 2016). In general, stomatal conductance decreases with tree height which can be related to the fact that taller trees experience higher hydraulic resistance, higher soil-to-leaf water potential differences and are more vulnerable to cavitation (Grote et al., 2016). For the same climate conditions above the forest canopy, water demand varies with the degree of crown shading (local microclimate) which depends on the crown position within the canopy (Bennett et al., 2015). All in all, dominant trees are more susceptible to drought stress and mortality since they are more exposed to stressful conditions (excessive radiation, high vapour pressure deficit and elevated temperature) and present a higher risk of cavitation (Grote et al., 2016; Rötzer et al., 2017). In addition, as dominant trees have higher evapotranspiration rates, the soil water reserves in their surroundings is more rapidly depleted which is however partly compensated by deeper rooting and horizontal water redistribution. These dominant trees reduced water availability for suppressed ones but, at the same time, decrease their evaporation demand. Complementarity in water use can occur when trees of different size and species take up water from different soil layers (Schwendenmann et al., 2015). This can also result in facilitation through hydraulic lift (Zapater et al., 2011). Mixed and structured stands promote facilitation and complementarity in water use but can also lead to faster exploitation of soil water reserves (Schäfer et al., 2018).

Modelling the complex functioning of heterogeneous forests is rather challenging. A more detailed representation of tree interactions comes at the price of a higher complexity, eventually lower robustness and longer computing times. One needs however spatially explicit individual-based models for gaining a mechanistic and comprehensive understanding of tree interactions and for comparing various spatial representations of stand structure in order to select the best one for the considered function (Berger et al., 2008; Bravo *et al.*, 2019). Among others, such models allow to take tree spatial configuration into account and distinguish between stands composed of the same trees but with a contrasted spatial aggregation (*e.g.* intimate *vs* patch-wise mixture). However, very few models of this type currently exist. For all these reasons, we decided therefore to develop a spatially explicit individual-based model called HETEROFOR for HETEROgeneous FOrest.

The processes regulating the carbon fluxes and the dimensional growth constitute the core of the HETEROFOR model and are described in Chap.2. Here, we focus on the description of two modules essential for predicting the impact of climate change on tree growth: phenology and water balance (Park et al., 2016; Choat et al., 2018). Phenology is described at the species level with the possibility to make it dependent on tree size. Water balance can be achieved at the tree level or at the stand level by aggregation of individual tree properties. We used data from long-term forest monitoring to evaluate the capacity of the model to reproduce key phenological phases (budburst, leaf development, yellowing and fall) and the soil water content dynamics as well as to estimate individual transpiration, stand throughfall and deep drainage. Evaluating each module separately is necessary to ensure the consistency of the whole model (Soares et al., 1995).

## 2. MATERIAL AND METHODS

### 2.1. MODEL DESCRIPTION

Section moved in the chapter 2 (sect. 1.3.2 for phenology and 1.3.10 for water cycle)

### 2.2. PARAMETER DETERMINATION

Section moved in the chapter 2 (sect. 2.1 for phenology and 2.4 for water cycle)

**Table 3.1: Description of the phenological and water balance module parameters for sessile oak and European beech and origin of their value**

| *Symbol* | *Description* | *Units* | *Value* | | *Origin* |
|---|---|---|---|---|---|
| | | | *Sessile oak* | *European beech* | |
| ***Storage capacity*** | | | | | |
| $c_{foliage\_sp}$ | foliage storage capacity | l per m² of leaf | 0.272 | 0.174 | André et al. (2008b) |
| $c_{bark\_sp\_ll}$ | bark storage capacity c parameter (leafless) | l mm$^{-1}$ | -9.08 | -9.53 | André et al. (2008b) |
| $d_{bark\_sp\_ll}$ | bark storage capacity d parameter (leafless) | l cm$^{-1}$ mm$^{-1}$ | 0.16 | 0.18 | André et al. (2008b) |
| $R_{\_min\_sp\_ll}$ | stemflow rainfall threshold (leafless) | mm | 6 | 1.5 | André et al. (2008b) |
| $c_{bark\_sp\_ld}$ | bark storage capacity c parameter (leaved) | l mm$^{-1}$ | -4.21 | -4.15 | André et al. (2008b) |
| $d_{bark\_sp\_ll}$ | bark storage capacity d parameter (leaved) | l cm$^{-1}$ mm$^{-1}$ | 0.08 | 0.09 | André et al. (2008b) |
| $R_{\_min\_sp\_ld}$ | stemflow rainfall threshold (leaved) | mm | 10.9 | 3.4 | André et al. (2008b) |
| ***Evaporation of water on foliage and trunk*** | | | | | |
| $l_{sp}$ | mean leaf width of the species *sp* | m | 0.08 | 0.07 | measured |
| $g_{s\_bark\_min}$ | bark minimum vapour conductance | m.s$^{-1}$ | 0.0077519 | | soil values x 100 |
| $g_{s\_bark\_max}$ | bark maximum vapour conductance | m.s$^{-1}$ | 0.125 | | soil values x 100 |
| ***Tree transpiration*** | | | | | |
| $g_{s0\_foliage}$ | reference stomatal conductance | m s$^{-1}$ | 308.4 | 281.9 | calibrated (Jonard et al., 2011) |
| $p_{radiation}$ | parameter of the stomatal response to radiation | W m$^{-2}$ | 37.2 | | calibrated (Jonard et al., 2011) |
| $p1_{sw}$ | parameter 1 of the stomatal response to soil water potential | adimensional | 0.127 | 0.527 | calibrated (Jonard et al., 2011) |
| $p2_{sw}$ | parameter 2 of the stomatal response to soil water potential | adimensional | 5 | 3 | calibrated (Jonard et al., 2011) |
| $p_{rew\_sensitivity}$ | parameter of the stomatal response to vapour pressure deficit | adimensional | -11.1 | -2.15 | calibrated (Jonard et al., 2011) |
| ***Soil evaporation*** | | | | | |
| $k$ | extinction coefficient | adimensional | 0.5 | | Teh (2006) |
| $g_{s\_soil\_min}$ | soil minimum vapour conductance | m s$^{-1}$ | 7.75E-05 | | Dufrêne (2005) |
| $g_{s\_soil\_max}$ | soil maximum vapour conductance | m s$^{-1}$ | 0.00125 | | Dufrêne (2005) |
| ***Phenology*** | | | | | |
| *Two-phase model (optimum chilling)* | | | | | |
| $t_0$ | chilling starting date | day of year | 305 (1st of November) | | Chuine (2000) |
| $T_{min}$, $T_{max}$, $T_{opt}$ | minimal, maximal and optimal chilling temperatures | °C | -35.08, 41.61, 0.26 | -9.89, 42.87, 2.85 | calibrated |
| $C^*$ | chilling threshold | °C | 50.25 | 5.82 | calibrated |
| $F_b$, $F_c$ | forcing parameters | adimensional | -0.07, 11.23 | -0.05, -1.43 | calibrated |
| $T_{b\_for}$ | base temperature for forcing | °C | -20.0 | | fixed |
| $F^*$ | forcing threshold | °C | 46.72 | 94.18 | calibrated |
| *Two-phase model (sigmoid chilling)* | | | | | |
| $t_0$ | chilling starting date | day of year | 305 (1st of November) | | Chuine (2000) |
| $C_a$, $C_b$, $C_c$ | chilling parameters | adimensional | 0.37, -6.48, -7.91 | 1.17, -29.21, -13.51 | calibrated |
| $C^*$ | chilling threshold | °C | 132.82 | 153.80 | calibrated |
| $F_b$, $F_c$ | forcing parameters | adimensional | 0.23, 13.17 | 0.19, 15.58 | calibrated |
| $T_{b\_for}$ | base temperature for forcing | °C | 0 | | Chuine (2000) |
| $F^*$ | forcing threshold | °C | 9.72 | 4.77 | calibrated |
| *One-phase model (no chilling)* | | | | | |
| $t_1$ | forcing starting date | day of year | 57 (26th of Feb) | 44 (13th th of Feb) | calibrated |
| $F_b$, $F_c$ | forcing parameters | adimensional | -0.12, 18.28 | -0.08, 11.77 | calibrated |
| $T_{b\_for}$ | base temperature for forcing | °C | 0 | | Chuine (2000) |
| $F^*$ | forcing threshold | °C | 12.88 | 28.12 | calibrated |
| $F^*$ | forcing threshold | °C | 46.72 | 94.18 | calibrated |
| *Other phases* | | | | | |
| *t2a_shift* | budburst shift | Days | 12.0 | 15.0 | calibrated |
| $LD^*$ | leaf development threshold | °C | 260.0 | 312.0 | calibrated |
| $t_3$ | ageing starting date | day of year | 213 (1st of August) | | Dufrêne et al. (2005) |
| $T_{b\_age}$ | base temperature for ageing | °C | 20.0 | | Dufrêne et al. (2005) |
| $A^*$ | ageing threshold | °C | 230.0 | | Dufrêne et al. (2005) |
| $y$ | leaf yellowing parameter | adimensional | 0.07557 | 0.1384 | calibrated |
| $Y^*$ | yellowing threshold | °C | 0.01 | | fixed |
| $R_{fall}$ | falling rate | s m$^{-1}$ d$^{-1}$ | 0.010 | 0.007 | calibrated |
| $F_{ampl}$ | frost amplifier coefficient | adimensional | 3.0 | 2.0 | calibrated |

## 2.3. SITE DESCRIPTION

Six sessile oak (*Quercus petraea* (Matt.) Liebl.) and European beech (*Fagus sylvatica* L.) stands located in Wallonia (Belgium) were used to evaluate the model. They all belong to long-term ecological research sites (Belgium LTER network). Three of them were located in Baileux and were monitored since 2001. The three other stands were part of the level II plot network of ICP Forests since 1998 and were located in Louvain-la-Neuve, Chimay and Virton. These sites were selected as their contrasted stand structure, species composition, soil and climate make them suitable for testing the ability of the model to account for structure complexity in various ecological conditions (at the regional scale).

### 2.3.1 Stand characteristics

The experimental site of Baileux was installed to study the impact of species mixture on forest ecosystem functioning (Jonard et al., 2006, 2007, 2008; André et al., 2008a, 2008b) and consisted of three plots. Two plots were located in stands dominated either by sessile oak or by European beech and the third one presents a mixture of both species. In these plots, sessile oak trees originated from a massive regeneration in 1880 and displayed the typical Gaussian distribution of even-aged stands, while European beech trees appeared progressively giving rise to an uneven-aged structure with all diameter classes represented. The stand in Chimay was an ancient coppice-with-standards, presently composed of mature sessile oak trees with an important hornbeam understorey. The stands in Louvain-la-Neuve and Virton were both more or less even-aged stands dominated by European beech but differed in their age, with much older trees in Louvain-la-Neuve than in Virton (130 *vs* 60 years old in 2009). All stand characteristics are provided in Table 3.2.

### 2.3.2 Soil properties

The Baileux, Chimay and Virton stands were all located on Cambisol but with some nuances, ranging from Dystric to the Calcaric variants in Chimay and Virton, respectively, while an Abruptic Luvisol was found in Louvain-la-Neuve (FAO soil taxonomy). All sites presented a moder humus, except Virton for which mull was observed. In Baileux, Chimay and Louvain-la-Neuve, the soil developed from the parent bedrock mixed with aeolien loess deposition that occurred at the interglacial period. In Virton, the soil originated only from the bedrock weathering. The parent materials were sandstone and shales, clayey sandstone and hard limestone bedrocks in Baileux, Chimay and Virton, respectively. In Louvain-la-Neuve, the soil was almost exclusively built from the loess deposits. These differences in parent material generated contrasted physical and chemical soil properties (Table 3.3).

The soil textures also varied significantly among sites. Based on the USDA taxonomy, the soil texture was silty clayey loam and silty loam in Baileux and Louvain-la-Neuve, respectively. In Chimay and Virton, finer soil textures were observed with a clayey loam and a clay texture, respectively. In relation to the texture, drainage was good in Baileux and Louvain-la-Neuve, while the presence of inflating clay triggered the appearance of a shallow water table during the wet period and drought cracks during summer in Chimay. In Virton, despite the high clay content in the lower horizons, drainage was good due to the existence of faults in the bedrock (Table 3.3).

Finally, stoniness and drainage influenced the estimate of the maximum extractable water reserve (Eq. 142 in Chap. 2 sect. 1.3.10). While the beech-dominated and mixed stands in Baileux and in Virton showed the lowest water reserve, the highest value was found in Louvain-la-Neuve, with intermediate values for the oak stand in Baileux and in Chimay (Table 3.3).

**Table 3.2: Initial stand characteristics for the main tree species and for the whole stands**

| Stand Inventory year | Species | Tree density (N/ha) | Basal Area ($m^2$/ha) | $C_{130}$ (cm) | Dominant Height (m) | LAI ($m^2/m^2$) |
|---|---|---|---|---|---|---|
| Baileux (oak) | Sessile oak | 187 | 16.2 | 100.6 (26.5) | 21.9 | |
| 2001 | European beech | 118 | 4.0 | 46.4 (35.6) | 15.5 | |
| | Common hornbeam | 152 | 1.3 | 31.4 (11.4) | 11.6 | |
| | Total | 468 | 21.6 | 63.7 (40.4) | 22.2 | 4.17 |
| Baileux (beech) | Sessile oak | 72 | 6.4 | 103.3 (18.1) | 23.0 | |
| 2001 | European beech | 217 | 16.5 | 87.5 (41.5) | 25.0 | |
| | Total | 297 | 23.1 | 90.3 (38.5) | 24.8 | 4.86 |
| Baileux (mixed) | Sessile oak | 118 | 12.9 | 115.5 (21.0) | 24.5 | |
| 2001 | European beech | 352 | 17.0 | 91.2 (39.3) | 25.7 | |
| | Common hornbeam | 9 | 0.1 | 22.6 (17.3) | 9.4 | |
| | Total | 484 | 30.0 | 101.2 (42.0) | 25.9 | 5.99 |
| Chimay | Sessile oak | 63 | 13.1 | 158.7 (35.0) | 20.4 | |
| 1999 | Common hornbeam | 634 | 5.3 | 30.5 (10.8) | 15.8 | |
| | Total | 697 | 18.4 | 42.4 (40.1) | 19.2 | 3.96 |
| Louvain-la-Neuve | Sessile oak | 21 | 4.7 | 165.9 (23.0) | 30.9 | |
| 1999 | European beech | 87 | 24.6 | 179.1 (53.6) | 32.1 | |
| | Total | 108 | 29.4 | 176.6 (49.6) | 32.9 | 6.34 |
| Virton | Sessile oak | 5 | 1.3 | 190.0 (10.0) | 24.1 | |
| 1999 | European beech | 340 | 16.8 | 70.9 (31.7) | 24.0 | |
| | Common hornbeam | 22 | 0.4 | 48.4 (15.4) | 14.5 | |
| | Total | 425 | 23.3 | 73.6 (36.0) | 24.0 | 6.93 |

**Table 3.3: Soil and meteorological characteristics of the different study sites (2001-2016 period)**

| Stand | Location | Altitude (m) | Soil type | Soil texture (USDA) | Max extractable water (mm) | Annual rainfall (mm) | Mean air temperature (°C) |
|---|---|---|---|---|---|---|---|
| Baileux (beech/mixed/oak) | 50°01’N, 4°24’E | 305-312 | Cambisol | Silt (clay) loam | 178/154/239 | 1075 | 9.8 |
| Chimay | 50°06’N, 4°16’E | 260 | Dystric Cambisol | Clay loam | 205 | 940 | 9.7 |
| Louvain-la-Neuve | 50°41’N, 4°36’E | 130 | Abruptic Luvisol | Silt loam | 450 | 818 | 11.0 |
| Virton | 49°31’N, 5°34’E | 370 | Calcaric Cambisol | Clay | 167 | 1060 | 9.9 |

### 2.3.3 Climate

Even if the same type of climate occurred all over Belgium (temperate oceanic), the study sites were located in different bioclimatic zones (Van der Perre et al., 2015). Louvain-la-Neuve was in the *Hesbino-brabançon* zone with the highest average temperatures (11.0°C) between 2001 and 2016 and the driest conditions (818 mm). Despite their close locations, Baileux and Chimay were part of different zones. Baileux was in “*Basse et moyenne Ardenne*” while Chimay was in “*Fagne, Famenne et Calestienne*”. Average temperatures are similar for both locations (i.e., 9.8°C in Baileux and 9.7°C in Chimay). Yet, a consistent difference in terms of precipitation is observed. Baileux being more elevated, it receives on average 1075 mm of precipitation each year while only 940 mm are measured in Chimay with respect to the rainfall-altitude relationship (Poncelet, 1956). Finally, Virton was part of the “*Basse Lorraine*” with elevated annual rainfall (1060 mm) and intermediate average temperature values (9.9°C) (Table 3.3).

For Chimay, Louvain-la-Neuve and Virton, we used data from the meteorological stations of the PAMESEB network. The records covered the 1999-2018 period. A tipping bucket located at 1 m height was used to monitor rainfall. Global radiation was registered with a pyranometer, air temperature with a resistance sensor thermistor, relative humidity with a psychrometer and wind speed with an anemometer. All these devices were placed at 1.5 m height. Data were collected at 12 min intervals and were then averaged hourly. For Baileux, an independent meteorological station managed by our laboratory was used to collect meteorological data since 2002. The devices were identical to those described before. Air temperature, relative humidity and rainfall were monitored at 1.5 m. Wind speed and global radiation were taken at 2.5 m above the ground.

## 2.4. MODEL EVALUATION

The various routines to calculate the budburst starting date were tested and the two-phase model with the optimum response function for chilling was retained for the evaluation of the water balance module as this approach performed better (see sect. 3.1.1).

### 2.4.1 Phenology

The phenological observations available on the level II sites of Chimay, Louvain-la-Neuve and Virton were used to evaluate the model predictions. These phenological observations were carried out on 20 dominant and co-dominant sessile oaks in Chimay (2012-2014) and 20 dominant and co-dominant European beeches in Louvain-la-Neuve and Virton (2012-2016) according to the ICP Forests manual (Beuker et al., 2016). They consisted of weekly observations of the percentage of budburst, yellowing and leaf fall depending on the season. As the model predicted the budburst for an average tree, we evaluated it with the budburst observations of the median tree. In addition, we visually assessed the agreement between the predicted and observed increase in leaf biomass proportion (*leafProp*) during the leaf development period and between the predicted and observed decrease in green leaf proportion (*greenProp*) and in *leafProp* during leaf yellowing and leaf fall, respectively. We did not perform a statistical evaluation for these latter variables as the corresponding processes were not calibrated independently in the model. Finally, as there were no data available for trees of different social status, we could not directly evaluate the option '*Phenology at tree level'*. We evaluated however its impact on tree growth predictions for the three stands in Baileux.

### 2.4.2 Water balance

Regarding the water balance module, the evaluation was conducted using variables integrating most of the processes described in the model. The observed throughfall, extractable water dynamics, individual transpiration and deep drainage (considered in the next section) were compared to model predictions. For the evaluation of the throughfall, extractable water and drainage predictions, we used simulations carried out at the stand scale since the corresponding observations cannot be related to a particular tree. Regarding individual tree transpiration, the approaches at the two scales were compared (tree *vs* stand).

For the evaluation of throughfall predictions, only independent throughfall data collected in Chimay, Louvain-la-Neuve and Virton between 2000 and 2016 were used as the rainfall partitioning routine was calibrated based on data from the Baileux forest (André et al., 2008a, 2008b). The collecting devices consisted of three long gutters connected to plastic barrels. The throughfall volume was measured weekly based on the height of water in the barrels. A log transformation of both the observations and the predictions was necessary to remove the heteroscedasticity.

Individual tree transpiration predictions were evaluated against sap flux measurements obtained using Granier type thermal dissipation sensors and based on a thermal dissipation approach (Granier, 1985). These measurements were taken every 15 minutes on 16 sessile oak and 16 European beech trees of different sizes in the three stands of Baileux between April and September 2003 (Jonard et al., 2011).

Extractable water (EW) was estimated based on Eq. (80) using soil water content measurements taken between 2005 and 2017 in Baileux and for the 2015-2018 period in the other sites. Soil water content was measured hourly using time-domain reflectometry (TDR) sensors (CS616, Campbell Scientific, Shepshed, UK) inserted into the main horizons (3 to 5 different soil depths depending on the site). Given some horizons were not equipped with TDR, MEW can differ slightly between the evaluation and the values displayed in Table 3.3. In order to decrease the influence of the soil disturbance due to the instrument installation, the first year of records was discarded. Indeed, Walker et al. (2004) showed that inserting a moisture sensor in a soil disturbed its hydraulic properties and water content during at least 9 months. The electrical signal from the TDR was transformed in relative dielectric permittivity and then converted into soil volumetric water content ($m^3$ $m^{-3}$) using the equation of Topp et al. (1980) for Baileux and resorting to our own calibration for the other sites (established based on gravimetric measurements of soil water content).

### 2.4.3 Drainage

Deep drainage can represent a large water output but is difficult to measure directly. Among the existing indirect approaches to estimate this component, we retained the mass-balance method using chloride ion ($Cl^-$) as tracer. This method has been widely used to estimate groundwater recharge (e.g. Bazuhair and Wood,1996; Ting et al., 1998; Scanlon et al., 2002) but can be applied to assess deep percolation as well (Willis et al., 1997). It relies on the fact that $Cl^-$ is not subject to any chemical transformations in the soil and undergoes only temporary storage in soil (Öberg, 2003). The only $Cl^-$ input in our study plots comes from throughfall and stemflow and can be determined from $Cl^-$ deposition data obtained from monthly chemical analyses of throughfall and stemflow samples. For the deep drainage, which constitutes the only output, the $Cl^-$ concentration is also obtained from monthly chemical analyses of soil solution collected with zero-tension lysimeters at 1 m depth in the three stands of Baileux between 2008 and 2016 and between 2013 and 2016 for the other sites. Deep drainage was estimated yearly by considering that the $Cl^-$ amount leaving the soil through drainage was equal to the $Cl^-$ input from throughfall and stemflow. As there is a clear annual pattern with a recharge and a discharge period in our study sites, the annual time step is therefore required to verify the hypothesis that chloride concentration in rainfall and in the soil are in a steady-state balance. Based on Eq. (83), the deep drainage flux was estimated and compared to our predictions.

$$Drainage = (Throughfall + Stemflow).\frac{[Cl]_{Througfall-Stemflow}}{[Cl]_{Drainage}} \quad (83)$$

with $[Cl]_{Throughfall\text{-}Stemflow}$, $Cl^-$ concentration in throughfall and stemflow and

$[Cl]_{Drainage}$, $Cl^-$ concentration in drainage water

### 2.4.4 Statistical analyses

To test the quality of the predictions, different statistical tests and indexes were used. The absolute bias, defined as the difference between the mean observation and prediction, and the relative bias, corresponding to the ratio between the absolute bias and the mean observation, were calculated to detect any over- or underestimation. To assess the precision of the predictions, the Root Mean Square Error (*RMSE*) was used and calculated as follows:

$$RMSE=\sqrt{\frac{\sum(obs-pred)^2}{n}} \quad (84)$$

with $n$ the number of observations.

When the range of values differed considerably for one variable between the different sites, the RMSE was divided by the range, i.e. the difference between the maximum and the minimum values. This Normalised Root Mean Square Error (*NRMSE*) is much more adapted for comparisons in these situations.

The agreement between observations and predictions was also evaluated with the Pearson's correlation coefficient (*r*) and with a regression test conducted to analyse the linear relationship between observed and predicted values. As both predictions and observations are subject to uncertainties, we used Deming regression. Then, we tested whether the regression line confidence interval (95%) included the identity line. These tests were realized with the mcr package in R.

# 3. RESULTS

## 3.1. EVALUATION OF MODEL PERFORMANCE

### 3.1.1 Phenology

On average, the budburst was best predicted with the two-phase model with the optimum response function for chilling (bias = 2.46 days compared with 8.23 and -5.88 days for the one-phase and two-phase with sigmoid response function for chilling models, respectively). However, this option was less appropriate to capture the inter-annual variations (Pearson's $r = 0.537$) than the one-phase model (Pearson's $r = 0.680$). The temporal variability was very poorly estimated with the two-phase model with the sigmoid response function for chilling, which displayed an inverse trend for the ranking among years (Pearson's $r = -0.277$) (Fig. 3.1b). Moreover, as this model was not able to trigger the end of the chilling period for some years in Louvain-la-Neuve (for European beech), all results for beech budburst on this site were considered as unreliable and were consequently not represented on Fig. 3.1. The predicted leaf development displayed a good agreement with observations (Fig. 3.2).

Simulated leaf yellowing and leaf fall were also evaluated by comparison with observations. While the leaf ageing threshold was taken from Dufrêne et al. (2005), the yellowing parameter determining the length of the yellowing period was adjusted with the five years of data from Chimay (sessile oak), Louvain-la-Neuve and Virton (European beech). Therefore, only the yellowing start was independently evaluated. The prediction of the start of the yellowing displayed a low absolute bias (2.7 days) and *RMSE* (7.0 days). However, a weak correlation (0.056) was found between predictions and observations (data not shown).

For the temporal dynamics of leaf yellowing and leaf fall, the agreement between model predictions and observations was just assessed visually since the parameter regulating these processes (yellowing, falling rate and falling frost amplifier) were adjusted with the same data. The overall agreement was good. The simulated decrease of green leaf proportion was similar for all sites as the photoperiod reduction is identical for each site and year (Fig. 3.3a, c and e). The only noticeable difference came from the yellowing starting date, which depended on air temperature. For Chimay (sessile oak), a close agreement was found between predictions and observations. For Louvain-la-Neuve (European beech), predictions were correctly centred but the predicted trend was more abrupt and the start of the decrease displayed some delay, except in 2012. For Virton (European beech), the decreasing trend was correctly displayed but the decrease start was less precise in 2016 (Fig. 3.3e).

(a) Two-phase model with optimum response function for chilling

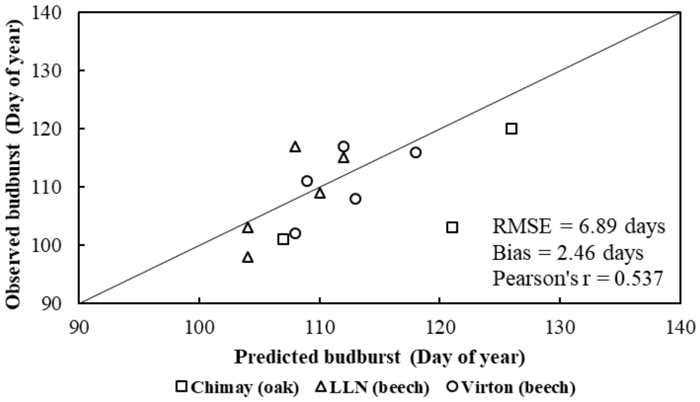

(b) Two-phase model with sigmoid response function for chilling

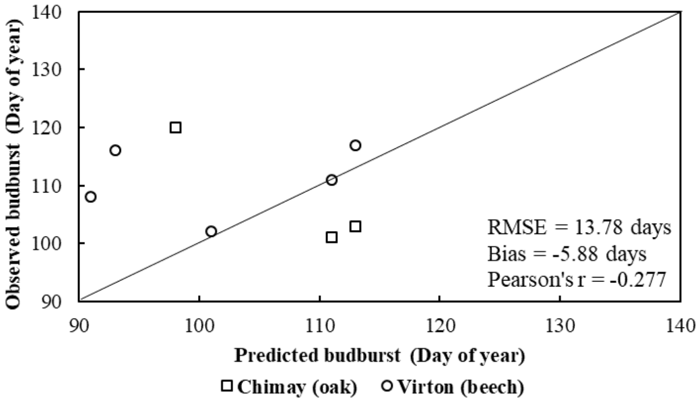

(c) One-phase model (no chilling)

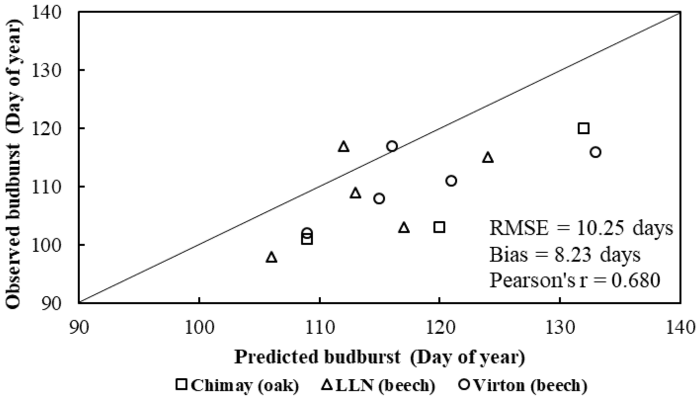

**Figure 3.1: Comparison of the observed and predicted budburst of the median tree in Chimay, Virton and Louvain-la-Neuve for the three phenological variants implemented. The quality of the predictions is indicated by the *RMSE*, the absolute bias and the Pearson's correlation coefficient (*r*).**

Concerning the leaf fall, the temporal dynamics was correctly represented in Chimay (sessile oak). In Louvain-la-Neuve (European beech), the model predicted a slightly too slow decrease in leaf proportion in 2012 and 2015. For the other years, the observed and predicted leaf proportion matched well even if the predicted start of the fall appeared later than in the observations for some years. In Virton (European beech), the predictions were well centred with regards to the observations but the decrease in leaf proportion was a bit too fast in 2012 (Fig. 3.3b, d and f).

(a) Chimay (oak)

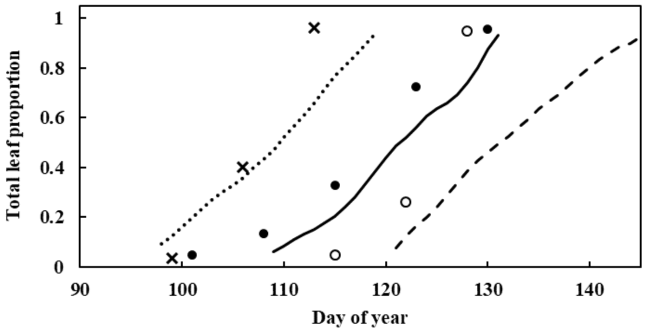

(b) Louvain-la-Neuve (beech)

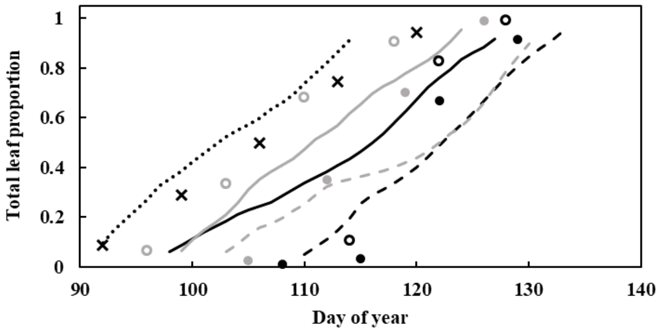

(c) Virton (beech)

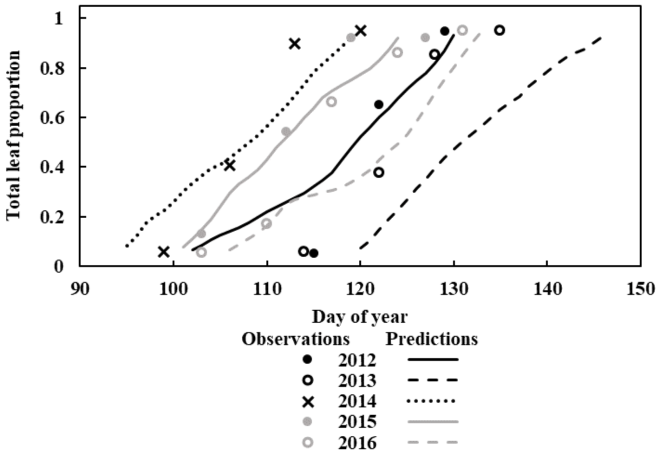

**Figure 3.2: Observed and predicted increase in leaf proportion in Chimay, Louvain-la-Neuve and Virton during the budburst and leaf development phase (data from 2012-2016). Observations are missing in Chimay for 2013, in Louvain-la-Neuve for 2012 and 2013 and in Virton for 2013.**

The option '*phenology at tree level'* was used to test if the agreement between predicted and observed basal area increment could be improved. With the default phenology option, HETEROFOR tended to overestimate the growth of dominant trees and underestimate that of suppressed trees (Jonard et al., 2020). With the option '*phenology at tree level*', this bias was partially resorbed. The slope of the Deming regression went from 0.74 to 0.84 for sessile oak and from 0.79 to 0.88 for European beech, being much closer to the identity line (Fig. 3.S3). This was however at the price of slightly lower Pearson's correlation.

(a) Chimay (oak) - yellowing

(b) Chimay (oak) - falling

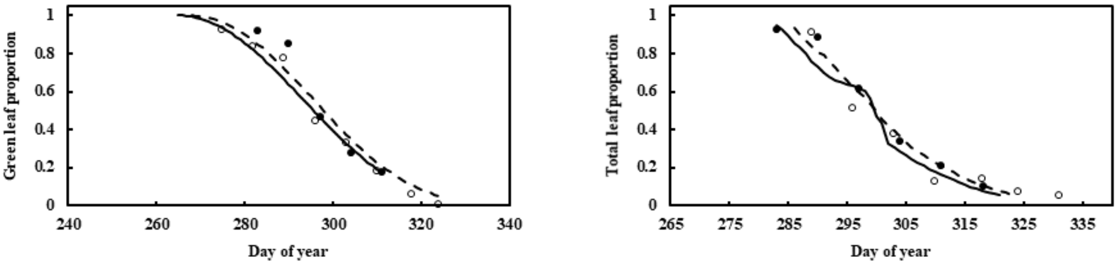

(c) Louvain-la-Neuve (beech) - yellowing

(d) Louvain-la-Neuve (beech) - falling

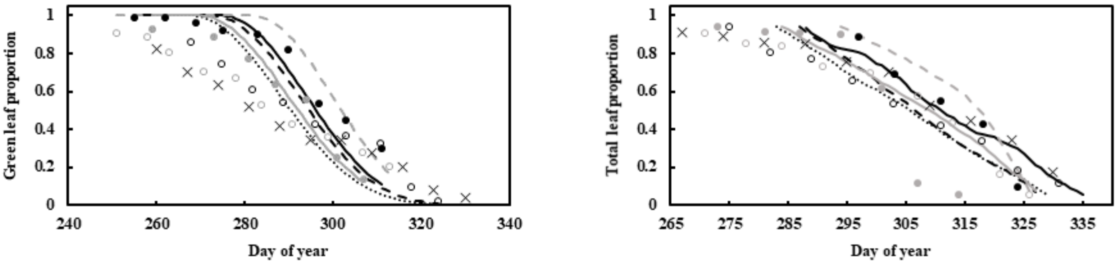

(e) Virton (beech) - yellowing

(f) Virton (beech) - falling

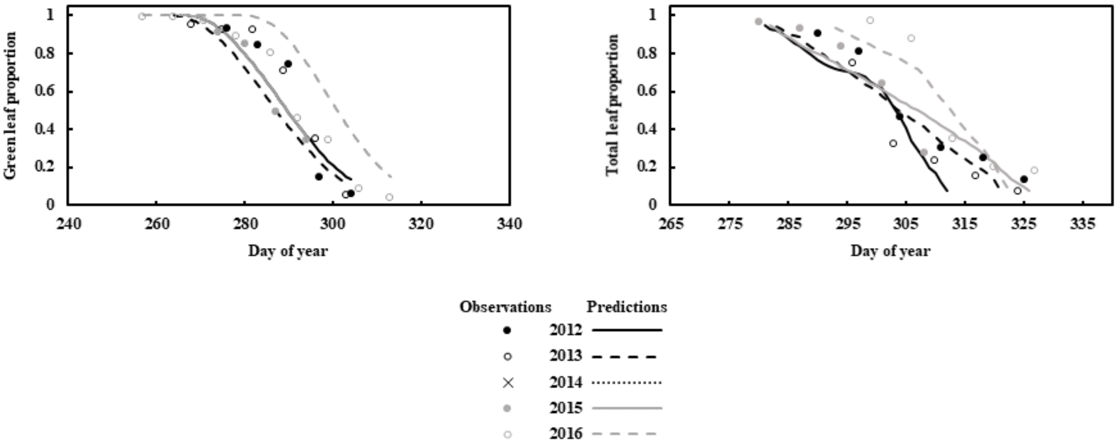

**Figure 3.3: Observed and predicted temporal dynamics in leaf yellowing and in leaf fall in Chimay, Louvain-la-Neuve and Virton (data from 2012-2016). Yellowing is represented by the decrease in green leaf proportion (left) and leaf fall by the decrease in total leaf proportion (right).**

### 3.1.2 Water balance

For each site, the main water fluxes affecting the water balance were calculated daily, summed up and the annual values were averaged for the 2002-2016 period (Table 3.4). Depending on the site, 65 to 78% of the rainfall reached the floor as throughfall and 6 to 13% as stemflow. The remaining 16 to 22% was intercepted by the tree foliage and the bark and evaporated. Then, 31 to 45% of the water received as rainfall returned in the atmosphere through tree transpiration. The remaining 26 to 44% were lost from the ecosystem through drainage.

### 3.1.3 Rainfall partitioning

Rainfall partitioning was correctly reproduced by the HETEROFOR model. Across all considered sites (Virton, Chimay and Louvain-la-Neuve), the mean bias of throughfall predictions was very limited (-1.3%) and non-significant (*P* value of the paired *t*-test = 0.316). The confidence interval of the linear relationship between the logarithm of the observed and predicted throughfall contained the identity line corresponding to the perfect match (upper part of Fig. 3.4). The correlation between predictions and observations amounted to 0.86 and the *RMSE* to 16.62 mm which corresponded to

34.2% of the mean througfall (48.6 mm). The separate examination of the different sites revealed that throughfall in Virton (European beech) were very well predicted but that a slight underestimation of the throughfall predictions in Chimay (sessile oak) was compensating an overestimation of similar magnitude in Louvain-la-Neuve (European beech) (Fig. 3.S1).

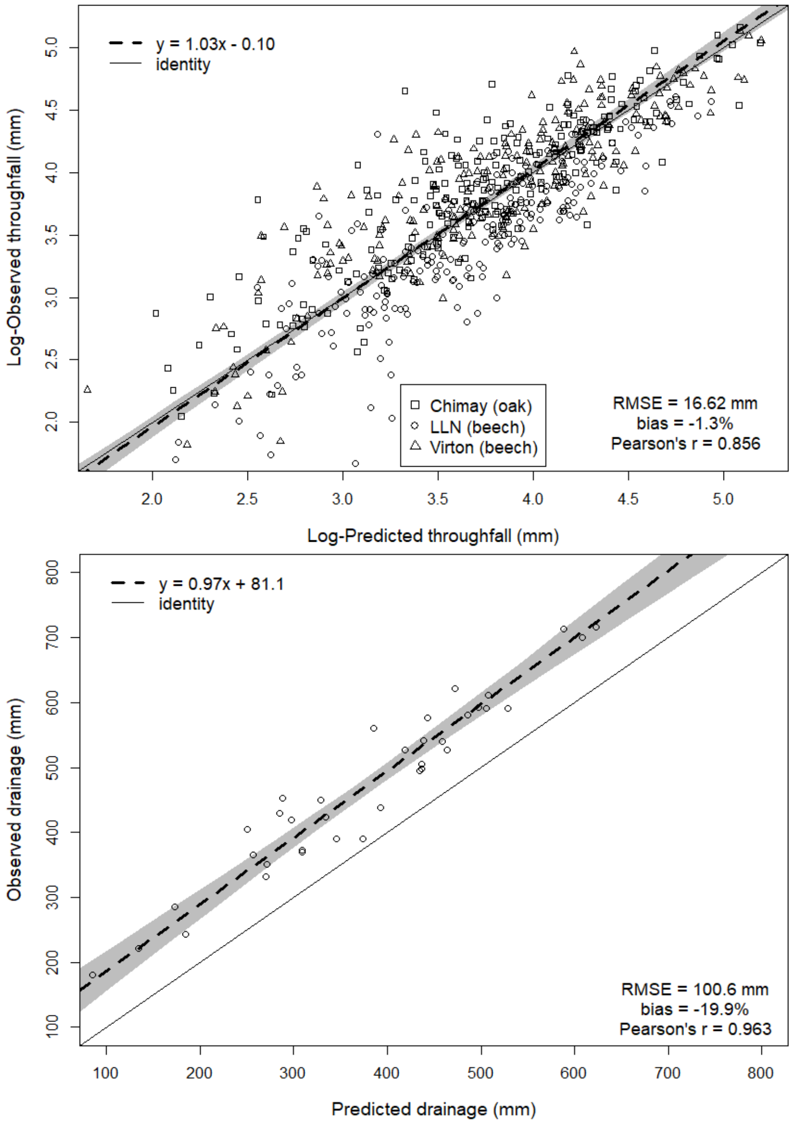

**Figure 3.4: Comparison of the log-transformed observed and predicted monthly throughfall in Chimay (oak), Louvain-la-Neuve (beech) and Virton (beech) between 2000 and 2016 (upper part) and comparison of observed and predicted annual drainage in all study stands between 2008 and 2016 (lower part). The quality of the non-transformed predictions is indicated by the *RMSE*, the relative bias and the Pearson's correlation coefficient (*r*). The shaded area represents the confidence interval of the Deming regression (95%) of observations on predictions and the solid line corresponds to the identity line.**

### 3.1.4 Transpiration

The model well reproduced individual transpiration for sessile oak and European beech in the Baileux site (in 2003) with similar performances at the tree and stand scale (Pearson's r of 0.84 – 0.85 for sessile oak and 0.88 – 0.89 for European beech). For European beech, the tree approach corrected the slight bias observed with the stand approach due to an overestimation of high transpiration values. Regarding sessile oak, the small underestimation of transpiration remained whatever the scale considered (Fig. 3.5).

(a) Oak trees with water balance at stand scale (b) Beech trees with water balance at stand scale

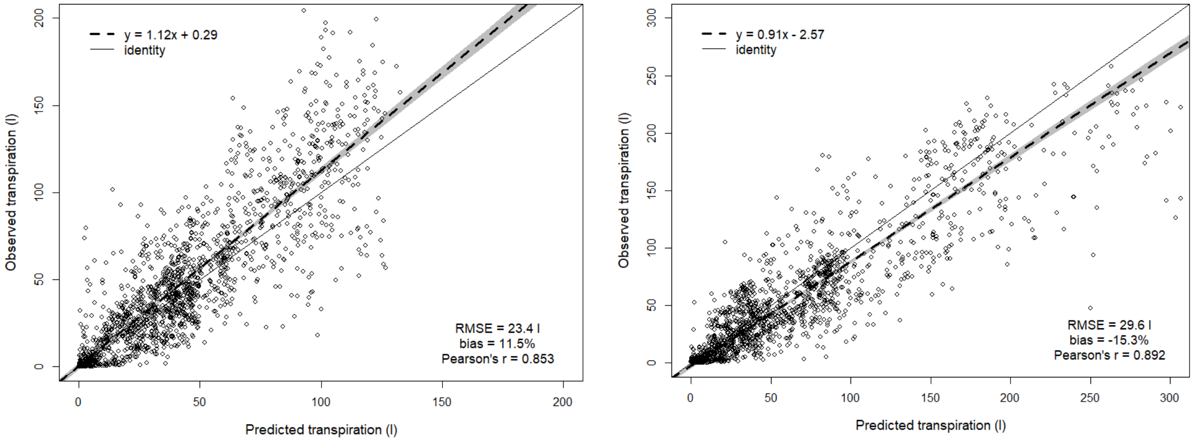

(c) Oak trees with water balance at tree scale (d) Beech trees with water balance at tree scale

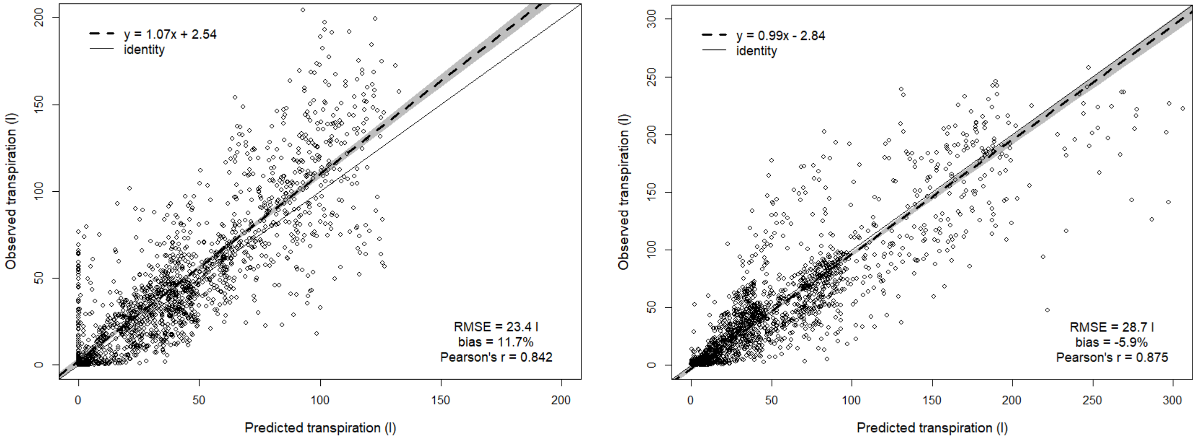

**Figure 3.5: Comparison of the observed and predicted daily transpiration of sessile oak and European beech in 2003 considering the tree and the stand scale for the water balance calculation. The quality of predictions is indicated by the *RMSE*, the relative bias and the Pearson's correlation coefficient (*r*). The shaded area represents the confidence interval of the Deming regression (95%) of observations on predictions and the solid line corresponds to the identity line.**

### 3.1.5 Soil water content

As the temporal variation of the extractable water was affected by all the water fluxes, it was used to check the performances of the water balance module (Fig. 3.6). A clear seasonal pattern appeared. At the beginning of the vegetation period, the extractable water values (*EW*) were highest. Then, tree and ground vegetation transpiration progressively depleted the water reserve which was partly recharged with rainfall events. Depending on their frequency, duration and intensity, the decline in *EW* was more or less pronounced and available water could reach levels close to zero. For all the sites, the Pearson's correlation between observed and predicted relative extractable water ranged from 0.893 to 0.950. These high correlation values and the graph inspection show that the seasonal pattern was precisely reproduced by the HETEROFOR model. *NRMSE* values range from 10.54 to 13.96% while relative bias values were around -2 and -3% in Baileux-oak, Baileux-mixed and Chimay and close to -8 and -9 % in Baileux-beech, Louvain-la-Neuve and Virton. These higher negative bias in the latter stands originated mainly from the model underestimation of the high values of *EW* (i.e. during wet periods). Despite these similar statistical results, the amount of extractable water in Virton displayed some peculiarities with regards to the other stands. Indeed, the observed *EW* levels fluctuated considerably more than in the other sites with frequent peaks both for high and low values that were not represented by the model. Finally, apart from Virton where some discrepancy between observations and predictions can be pointed out, the model quality did not decrease in Chimay or Virton during the 2018 summer that was categorized as exceptionally dry by the Royal Meteorological Institute of Belgium. The comparison of the tree and stand approach in 2003 indicates that the extractable water calculated at the tree scale progressively deviated from that obtained at the stand scale during the course of the vegetation period and became slightly lower, especially in Baileux-oak and Baileux-mixed (Fig. 3.S2). On these graphs, one may notice the heterogeneity in extractable water within the various stands.

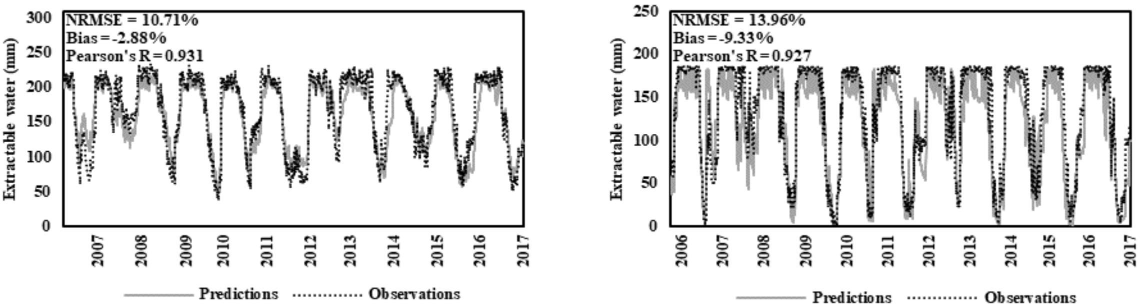
(a) Baileux-oak

(b) Baileux-beech

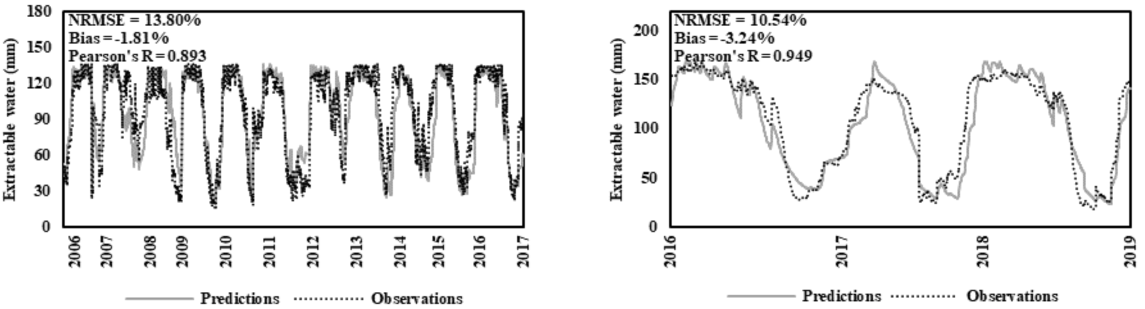
(c) Baileux-mixed

(d) Chimay

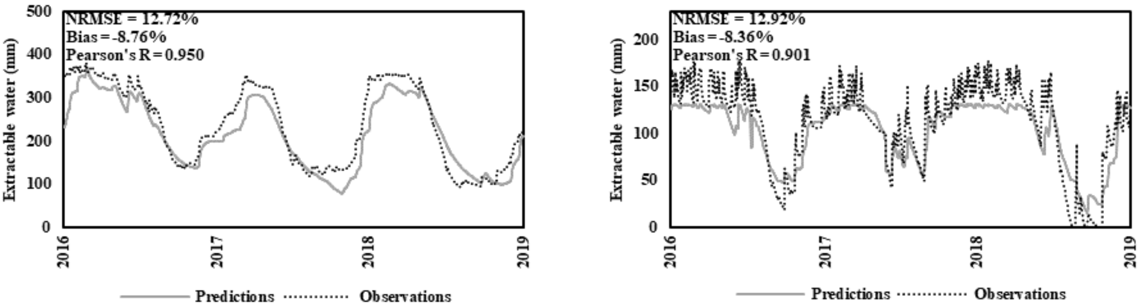
(e) Louvain-la-Neuve

(f) Virton

**Figure 3.6: Temporal dynamics of observed and predicted extractable water amount (mm) in the various stands. The prediction quality is indicated by the *NRMSE*, the relative bias and the Pearson's correlation coefficient (*r*).**

### 3.1.6 Drainage

The predicted deep drainage was compared with estimates calculated on a yearly basis using Cl as a tracer. The *RMSE* (100.6 mm) and the bias (-19.9%) were quite large but a surprisingly good correlation was found between the predicted and estimated drainage (Pearson's *r* = 0.963). Due to the systematic bias, the identity line was not within the confidence interval of the Deming regression despite a regression slope of 0.97 (lower part of Fig. 3.4).

## 4. DISCUSSION

In order to predict the impact of global changes on forests, it is crucial to integrate and structure the existing knowledge in process-based models. However, this first step is not sufficient. A detailed documentation of the models as well as an evaluation of their performances are also needed in order to use them knowing exactly their strengths and limits. While most models were described in scientific articles or reports, their evaluation was often limited to one or two sites used to illustrate the model functioning and was generally based on integrative response variables such as radial tree growth

(Vanclay and Skovsgaard, 1997; Schmidt et al., 2006). Yet, to provide robust predictions of tree growth under changing conditions, the model must be able to accurately reproduce not only the observed tree growth but also the intermediate processes describing resource availability (light, water and nutrient) (Soares et al., 1995). In the following section, we discuss the quality of the predictions for two main drivers of tree growth (phenology and water balance) in relation with the concepts used to describe them.

### 4.1. PHENOLOGY

The two-phase model with the optimum response function for chilling was the least biased variant for predicting budburst. However, the one-phase model including only the forcing period better captured the inter-annual variability. While the bias is likely to originate from the model calibration (data used for calibration were observations from western Germany) and could be corrected, the ability of the model to predict temporal variability is more representative of its structural quality. The gap between observations and predictions can seem high. Yet they are comparable to the considerable observation uncertainty, which amounts, for budburst, typically to an order of magnitude of one to two weeks (Liu et al., 2021). It is common that models accounting only for the forcing period better represent the observations of budburst temporal variability (Leinonen and Kramer, 2002; Fu et al., 2014; Basler, 2016). Two reasons can explain this. First, in areas where the chilling requirements are always met as in Western Europe, the chilling parameters are not enough constrained by the observations and therefore more difficult to calibrate. When few phenological observations are available, taking the chilling into account increases the model complexity without improving the accuracy of the predictions (Leinonen and Kramer, 2002; Fu et al., 2014). Secondly, two-phase models predict the break of endodormancy (end of chilling) and the start of budburst while they are only calibrated from budburst observations. When endodormancy break observations are used for the calibration, the chilling parameters are estimated more accurately (Chuine et al., 2016) but these data are difficult to obtain and consequently very scarce (Jones et al., 2013).

Similarly to Chuine et al. (2016), we advise to use a two-phase model (with the optimum response function for chilling) when endodormancy break observations are available or for long-term simulations with climate conditions beyond the range used for the model calibration. For example, for trees located at the southern margins of their species distribution area, the expected rise in winter temperature could prevent the fulfilling of their chilling requirements and inhibit budburst (Clark et al., 2014). This phenomenon would only be captured by a two-phase model. When few phenological data are available for calibration, one-phase model should be preferred, especially for simulations with climate conditions similar to those used for the calibartion. This highlights the importance of having both one and two-phase options to describe budburst. Most process-based models listed in Table 3.5 had however only one phenological variant except 4C.

A possible improvement of the two-phase phenological models would be to integrate the photoperiod effect on budburst. Indeed, some recent studies have shown evidences that photoperiod can compensate for a lack of chilling temperature that would prevent the buds to open and for an early frost episode that would trigger budburst before winter (Vitasse and Basler, 2013; Pletsers et al., 2015). This mechanism is particularly present for late-successional species like beech and oak trees and is regularly cited as a key element to simulate the phenology under climate change (Basler and Körner, 2012). Some models tried to account for the photoperiod effect simply by replacing chilling by photoperiod (Kramer, 1994b; Schaber and Badeck, 2003) but, in this way, failed to represent the combined effect of these variables. Recently, a few models integrating the compensatory effect of photoperiod on chilling have appeared. However, these models include more phenological parameters for similar predictive ability (Gauzere et al., 2017). It remains indeed difficult to disentangle the co-varying effect of chilling and day length with *in situ* measurements (Flynn and Wolkovich, 2018) since photoperiod variations only occur for sites with different latitudes where other confusing factors play a role as well (Primack et al., 2009). Therefore, many data is necessary to calibrate these models. Then, we decided to privilege the accuracy of our phenological model to a more process-based approach but we are looking forward for improvements in these kinds of models and a more consensual body of literature.

The better growth predictions obtained for the small trees when the phenology was calculated at the individual scale highlights the importance of the “phenological avoidance strategy” displayed by understory trees. This had already been mentioned by Lopez et al. (2008) who observed that early-leafing species received between 45 and 80% of their photon flux during the budburst period. Moreover, a simulation study showed that a one (two) week lengthening of the understory vegetation period with regards to the overstory in both spring and autumn generated a productivity increase of 32% (55%) on such a short period (Jolly et al., 2004).

### 4.2. WATER BALANCE

In a first step, the annual water fluxes predicted by HETEROFOR were compared to measurements and predictions of other studies (Table 3.4). Then, some water fluxes were individually evaluated when data was available. Finally, some potential improvement of the water balance module were discussed.

Various studies were taken from the literature to compare our water module predictions with observations. They cover a range of annual rainfall comprised between 425 and 1476 mm (Table 3.4), which is comparable to what can be found in Belgium. The proportions of rainfall converted to stemflow obtained with HETEROFOR (6.1 to 13.1%) are within the range reported in the literature (0.6 to 20.4%). This large observation spectrum comes from the important seasonal (higher stemflow proportion in winter than during the vegetation period) and species differences (stemflow importance is higher for beech than oak trees), which features are accounted for in HETEROFOR. However, the mean value from the literature (7.3% of rainfall) is close to the average value for the six study sites (10.3%). The proportions of intercepted rainfall (15.9 to 22.0%) and throughfall (64.8 to 78.0%) are also consistent with the ranges reported in other studies (1.9 to 31.0% and 59.8 to 83.1%). Moreover, we observed a good matching between the average values (respectively 19.5 and 73.8% from literature and 19.4% and 70.2% for our study sites). For transpiration, the range found in the literature is large (14.8 to 52.3% for an average value of 31.9%), which is not surprising since inter-annual and inter-site variabilities are high for this variable (Schipka et al., 2005; Vincke et al., 2005). The predicted transpiration proportions are less variable (31.2 to 44.9%) and their average value of 36.0% is slightly superior to the mean observed transpiration (31.9%). Regarding drainage, no direct measurements can be made; all the estimates from the literature come from indirect methods or modelling also subject to uncertainties. The range of drainage values reported in the literature (13 to 70%) is very large and contains that obtained with HETEROFOR (26.3 to 44.2%). The mean predicted drainage (39.7%) is close to the mean value of the literature (37.5%). By this comparison with the water fluxes reported in the literature, we show that HETEROFOR provides plausible estimates of the various components of the water cycle.

**Table 3.4: Predicted annual water fluxes and the corresponding percentage of rainfall in brackets for the different study sites during the period 2002-2016. The minimum, maximum and mean values from literature are indicated with the number of studies (n) they are based on. The studies taken into account were restricted to sites dominated by beech or by oak in temperate regions with similar meteorological conditions. Data from the same site were averaged so that long monitoring studies do not influence too much the average value.**

| Site/Study | Rainfall (mm) | Stemflow (mm) (%R) | Throughfall (mm) (%R) | Interception (mm) (%R) | Transpiration (mm) (%R) | Drainage (mm) (%R) |
|---|---|---|---|---|---|---|
| Baileux-beech | 1059 | 124 (11.7) | 728 (68.7) | 207 (19.5) | 366 (34.5) | 428 (40.4) |
| Baileux-mixed | 1059 | 139 (13.1) | 686 (64.8) | 233 (22.0) | 331 (31.2) | 432 (40.8) |
| Baileux-oak | 1059 | 94 (8.9) | 763 (72.0) | 202 (19.1) | 343 (32.4) | 465 (43.9) |
| Chimay | 897 | 55 (6.1) | 700 (78.0) | 143 (15.9) | 351 (38.7) | 384 (42.3) |
| Louvain-la-Neuve | 800 | 81 (10.1) | 545 (68.1) | 174 (21.8) | 353 (44.9) | 206 (26.3) |
| Virton | 1014 | 123 (12.1) | 705 (69.5) | 186 (18.3) | 361 (34.4) | 464 (44.2) |
| Van der Salm (2004) oak | 725 | - | - | 177 (24.4) | 338 (46.6) | 123 (17.0) |
| Van der Salm (2004) beech | 891 | - | - | 241 (27.0) | 356 (40.0) | 138 (15.5) |
| Min literature value | 425 | 5.0 (0.6) | 209.9 (59.8) | 19.0 (1.9) | 117.5 (14.8) | 82.0 (13.0) |
| Max literature value | 1476 | 162.0 (20.4) | 864.0 (83.1) | 241.0 (31.0) | 397.0 (52.3) | 626.0 (70.0) |
| Mean literature value | 805.2 | 44.3 (7.3) | 514.6 (73.8) | 109.2 (19.5) | 263.5 (31.9) | 312.1 (37.5) |
| n | | 9 (20) | 13 (23) | 12 (23) | 24 (22) | 11 (13) |

Papers included in the literature review: Cepel, 1967. Aussenac, 1968. Aussenac, 1970. Lemée, 1974. Nagy, 1974. Szabo, 1975. Aussenac and Boulangeat, 1980. Matzner and Ulrich, 1981. Rowe, 1983. Bücking and Krebs, 1986. Gerke, 1987. Giacomin and Trucchi, 1992. Neal et al., 1993. Leuschner, 1994. Ulrich et al., 1995. Heil, 1996. Tarazona et al., 1996. Bellot and Escarre, 1998. Didon-Lescot, 1998. Herbst et al., 1998. Nizinski and Saugier, 1998. Forgeard et al., 1980. Granier et al., 2000. Bent, 2001. Michopoulos et al., 2001. Knoche et al., 2002. Mosello et al., 2002. Dripps, 2003. Bastrup-Birk and Gundersen, 2004. Hanson et al., 2004. Ladekarl et al., 2005. Schipka et al., 2005. Vincke et al., 2005. Carlyle-Moses and Price, 2006. Christiansen et al., 2006. Roberts and Rosier, 2006.Schmidt, 2007. Herbst et al., 2008. Staelens et al., 2008. Ahmadi et al., 2009. Müller and Bolte, 2009. Risser et al., 2009. Gebauer et al., 2012.

Comparing predicted and observed throughfall is interesting to evaluate the water balance module since throughfall is an integrative variable depending on the water storage capacity of foliage, on evaporation, and on the proportion of stemflow. The good agreement between observations and predictions indicates that the partitioning of rainfall when passing through the canopy and the evaporation of the water intercepted by foliage and bark are well described. Among the different models of the Table 3.5, no one accounts separately for stemflow and throughfall but other models not included in the list consider the two fluxes separetly (e.g. Gotilwa+ and Castanea). Yet, separating throughfall and stemflow is important, especially for structurally-complex stands. In these stands, rainfall interception cannot be simulated based on a mean foliage storage capacity and a mean partitioning between throughfall and stemflow since these parameters vary with stand composition and structure. Our tree-level approach estimating foliage storage capacity and stemflow proportion based on individual tree characteristics allows to overcome this difficulty. Moreover, if one wants to accurately describe the nutrient cycle, partitioning rainfall is essential as nutrient concentrations in stemflow and throughfall can be 10 to 100 times higher than in rainfall due to dry and wet deposition and canopy exchange (Levia and Herwitz, 2000; André et al., 2008c; van Stan and Gordon, 2018). Even if the rainfall partitioning can still be improved from a theoretical perspective (e.g., including canopy drainage after rain events or the impact of wind on the foliage storage capacity like in Hörmann et al. (1996) or Muzylo et al. (2009)), we chose to limit the level of complexity in order to avoid calibration difficulties.

HETEROFOR satisfyingly reproduced individual tree transpiration with similar prediction quality for the tree and stand approach regarding the water balance calculation. For European beech, the water balance calculation at the tree scale allowed even correcting the small bias which appeared with the stand approach (Fig. 3.5). The year selected for the simulation (2003) was particularly dry and hot during summer, which allowed to cover a large range of meteorological and soil water conditions. It is indeed interesting to test the tree approach under dry conditions since horizontal water redistribution is much less efficient in this case.

Twenty to thirty percent of the transpiration variability remained unexplained by the model, which can be partly ascribed to model inaccuracies but also to the large uncertainty associated with the sap flux measurements. Among others, the measurements made by Jonard et al. (2011) did not take the azimuthal variation of the sap flux into account since only one sensor per tree was installed.

This first evaluation of tree transpiration predictions indicates that no loss of precision occurred with the tree scale approach while this detailed spatial representation could have increased the variability of transpiration predictions since it generated some heterogeneity in soil water availability (Fig. 3.S2). These good results show that the water balance calculation at the tree scale provides a promising tool to better understand the individual variability and local environment effects on tree water use and sensitivity to drought. This must be considered in a dynamics of continuous improvement of the model and will require more transpiration measurements and in-depth comparisons of predictions and observations.

The amount of extractable water (*EW*), directly influenced by tree transpiration and soil evaporation, is also a key element of the water cycle, driving, among others, the drought resistance of a stand. The temporal dynamics of *EW* was well captured by HETEROFOR as evidenced by the high correlations (Pearson's coefficient comprised between 0.893 and 0.950) between observed and predicted *EW* for the various study sites (Fig. 3.6). These correlations are within the high end of the range reported for similar models. With the BALANCE model, Gröte and Pretzsch (2002) obtained a Pearson's correlation of 0.85 between the observed and predicted soil water content of the upper soil (0-20 cm horizon) in a beech forest in Germany (Freising). Applying BALANCE on three broadleaved stands of oak or beech in Germany, Rötzer et al. (2005) were also able to correctly reproduce soil water content dynamics but they mentioned a significant decrease in the quality of predictions during the 2003 drought due to an overestimation of the soil drying, which was not observed with HETEROFOR in 2018. Comparing the observed soil water content at various soil depths with that predicted by the 4C model in mixed oak and pine forest (Brandeburg, Germany), Gutsch et al. (2015) obtained Pearson's correlations ranging from 0.59 to 0.74. In an oak stand in Tennessee (USA), Hanson et al. (2004) compared the ability of nine process-based forest models to reproduce soil water dynamics in the 0-35 cm horizon of the soil and obtained correlations ranging from 0.81 to 0.96.

In the study of Hanson et al. (2004), relative bias was evaluated as well for soil water content and ranged between -1.3 and 4.0%. These values are comparable to those found in this study yet a bit lower. Furthermore, discrepancies between predicted and observed *EW* occurred during limited periods. Several reasons can be advanced to explain them. Errors in the prediction of the budburst date can result in a too early or too late restarting of tree transpiration and induce an inaccurate depletion of the soil extractable water during the vegetation period. In order to distinguish this error source from the others, one could force the model with the observed budburst date. This option is however not yet implemented in the model. The lack of agreement between observed and predicted *EW* could also be ascribed to the strong heterogeneity of soil properties in forest ecosystems. Similarly, local rainfall events recharging soil extractable water during summer (often associated with thunderstorms) are sometimes not correctly taken into account when missing meteorological data (due to failed sensors or other technical problems) are replaced by rainfall data of a meteorological station further away.

Simplifications and errors in the model conception may also generate divergence between observations and predictions. However, this structural uncertainty can be limited by selecting the most appropriate concepts. HETEROFOR predicts water transfer between soil horizons using the Darcy law. We tried to implement an approach of intermediate complexity between simple bucket models and the Richards equations. From a theoretical point of view, the Richards approach is the most state-of-the-art but requires very long calculation times (Fatichi et al., 2016) and is usually implemented in models specifically dedicated to water flow simulations (in Table 3.5, only one of the models, MAESPA, use them). Forest ecosystem models generally use simpler approaches such as the bucket model declined in a large variety of forms (Table 3.5). These models consider one or several buckets with a specified water storage capacity that is filled with rainfall and is emptied by evapotranspiration. If the soil water content is at field capacity, water is transferred to the underlying layer and finally lost by drainage. Improved versions can account for transfer between buckets in unsaturated conditions using the Darcy law (leaky bucket model).

Our water transfer routine discretises the soil in horizons whose thickness varies from a few centimetres (upper horizons) to half a meter (deeper horizons). Compared to the numerical resolution of Richards equation which requires thin soil layers (1 to 2 cm), our vertical discretisation of the soil profile is quite coarse and inaccurately predict the advance of the wetting front. As the tree transpiration and photosynthesis depend on the soil water conditions of the whole soil profile, this inaccuracy has very limited implications on the simulated tree growth. In our approach, water transfer during a time step is calculated based on the horizon water potentials estimated at the end of the previous time step. As such, the model makes the hypothesis that the water content does not change significantly during the time step, which is certainly not the case close to the wetting front and cannot ensure mass conservation. In order to limit this problem, the model uses an adaptive time step estimated based on the Peclet number described in Eq. (77). This allows to ensure mass conservation.

Finally, another reason that could explain the discrepancy between predictions and observations is the presence of macropores that cause preferential flows. These water fluxes defined as water movements in the soil along preferred pathways that bypass the soil matrix (Hardie et al., 2011) can be generated by soil shrinkage, root growth, chemical weathering, cycles of freezing and thawing or bioturbation (Aubertin, 1971). These macropores are more frequent in forest soils than in agricultural soils as the latter are often ploughed and homogenized. They are however difficult to characterize given their strong spatial heterogeneity in both vertical and horizontal directions (Aubertin, 1971). Adaptations of the Richards equations can be used to account for the preferential flows (dual porosity and dual permeability) but require a good characterisation of soil macropores (not possible to achieve routinely in forest soils given their heterogeneity) and are still more complicated to solve than the classical Richards equations. We implemented in the model the transfer of the soil water surplus (when water saturation is reached) to the underlying horizon and the possibility to redirect part of this surplus as deep drainage to account empirically for preferential flows. Indeed, preferential flows in macropores become significant only when rainfall exceeds the water infiltration rate in the soil matrix and accumulates in the soil surface. The fraction of the water surplus considered as preferential flows is an empirical parameter reflecting the macroporosity of the site.

**Table 3.5: Comparison of the spatial scale (S=stand, C=cohort, I=individual, I*=individual target tree) and concepts used for describing phenological and hydrological processes in HETEROFOR and in other individual and cohort-based models. Backslash is used to distinguish the various model options. Abbreviations used in for describing transpiration (P-M= Penman-Monteith, SPAC = Soil-Plant-Atmosphere Continuum)**

| Model | Spatial resolution | Phenology | | Water balance | | | |
|---|---|---|---|---|---|---|---|
| | | Budburst model | Individual variability | Rainfall partitioning | Canopy micro-climate variations | Transpiration | Soil water dynamics |
| HETEROFOR | Individual | one-phase/ two-phase (C) | Y (C) | Y (C) | wind, light (I) | P-M with modifiers (S) | Darcy model + mass conservation (S) |
| HETEROFOR<br>- tree-scale phenology<br>- fine resolution water | Individual | one-phase/ two-phase (C) | Y (I) | Y (I) | wind, light (I) | P-M with modifiers (I) | Darcy model + mass conservation (I) |
| BALANCE$^{a,b}$ | Individual | one-phase (C) | Y (I) (yellowing) | N | air T°, wind, light (I) | P-M with modifiers (I) | multi-layer bucket (I) |
| HYBRID$^{c}$ | Individual | parallel chilling forcing (C) | N | N | light (I) | plot conductance and energy balance (S) | single-layer bucket (S) |
| iLand$^{d}$ | Individual | two-phase (C) | N | N | light (I) | P-M with modifiers (S) | single-layer bucket (S) |
| MAESPA$^{e,f}$ | Individual | one-phase + photoperiod (C) | N | N | wind, light (I) | P-M with SPAC resistance (I*) | Richards equation (S) |
| NOTG-3D$^{g}$ | Individual | one-phase (C) | N | N | air T°, wind, light (I) | energy balance with modifiers (I) | multi-layer bucket (I) |
| 4C$^{h,i}$ | Cohort | promot.-inhibit. and others (C) | N | N | light (C) | P-M and others with modifiers (C) | multi-layer bucket (C) |
| ANAFORE$^{j}$ | Cohort | two-phase (C) | N | N | wind, light (C) | P-M with SPAC resistance (C) | spilling multi-layer bucket (C) |
| PSIM-DNDC$^{k}$ | Cohort | one-phase + photoperiod (C) | N | N | air T°, light (C) | Carbon demand driven with modifiers (C) | Darcy model (S) |
| 3D-CMCC$^{l,m}$ | Cohort | one-phase (C) | N | N | light (C) | P-M lookalike function with modifiers (C) | single-layer bucket (S) |

**a**. Grote and Pretzsch, 2002 **b**. Rötzer et al., 2010 **c**. Friend et al., 1997 **d**. Seidl et al., 2012 **e**. Duursma and Medlyn, 2012 **f**. Duursma, 2008 **g**. Simioni et al., 2016 **h**. Gutsch et al., 2015 **i**. Model description on 4C website **j**. Deckmyn et al., 2008 **k**.Grote et al., 2011 **l**. Collalti et al., 2014 **m**. Collalti et al., 2016

The performances of the soil water transfer routine can also be checked based on the deep drainage flux. In this study, we compared the deep drainage estimated with HETEROFOR and with the chloride mass balance approach. The mean drainage predicted with HETEROFOR was 379 mm per year while the average drainage obtained with the chloride approach amounted to 472 mm per year, which corresponds to a bias of -19.9%. The correlation between the two types of estimate amounted to a Pearson's coefficient of 0.963, with a *RMSE* value of 100.6 mm. These values depict a constant negative bias in the predictions that can easily be seen on the lower part of Fig. 3.4. It is hard to tell whether the gap originates from the model or the method used to estimate drainage from the chloride approach. It is more likely that the bias must be ascribed to both. Indeed, on the one hand, even if the use of chemical tracers to estimate drainage or groundwater recharge is commonly used (Scanlon et al., 2002), its application remains subject to uncertainties. First, the chloride method supposes that the main chloride source is rainfall and that the other sources can be neglected (Murphy et al., 1996). This hypothesis is not always fulfilled due to anthropogenic chloride introduction (road salting, wastewater) or when chloride is present in the bedrock (Ping et al., 2014). Then, preferential flows have been regularly highlighted as an error source since the associated water fluxes are not well sampled by zero-tension lysimeters (Tyler and Walker, 1994; Nkotagu, 1996). Finally, this method displays better results when rainfall and soil water is richer in chloride (e.g., sites close to the sea with high marine deposits or with low drainage flux) because the chemical analyses are more accurate for higher concentrations (Sammis et al., 1982; Grismer et al., 2000).

On the other hand, modelling errors could explain the bias presence. One of them could be the overestimation of the transpired water amount. However, deep drainage tends to produce during winter while transpiration only takes place during the vegetation period (spring and summer). Therefore, if transpiration was overestimated we should observe an underestimation of the EW during spring and summer (low values), which is not the case (Fig. 3.6).

Hanson et al. (2004) measured deep drainage at the watershed level by accounting for rainfall and stream flow outputs and compared their measurements with the predictions of several models. Their multi-model comparison displayed similar *RMSE* (65.5 to 225.6 mm) and relative bias (-27.6 to 20.5 %) values but the Pearson's coefficient displayed by HETEROFOR is definitely located in the high tail of the study range (0.61 to 0.95). However, the performances of their models are not strictly comparable to ours since the reference method for estimating drainage differs (Sammis et al., 1982; Grismer et al., 2000; Obiefuna and Orazulike, 2011).

### 4.3. SIMULATING PHENOLOGY AND WATER BALANCE IN HETEROGENEOUS STANDS

Increasing the functional trait diversity and promoting uneven-aged stands are among the management strategies that foresters can use to make their forests more resistant to stressful conditions and more resilient after a disturbance (Pedro et al., 2015; Jactel et al., 2017; Anderegg et al., 2018). With the growing interest for mixed and uneven-aged stands, various attempts have been made to better account for stand structure in process-based forest models. Some of these models present very detailed 3D representations of individual tree structure but describe generally only specific physiological processes (e.g. LIGNUM, EMILION, MAESPA). Such models are very useful tools for analysing outcomes of eco-physiological experiments and obtain a better understanding of specific eco-physiological processes (e.g. drought sensitivity) in structurally complex stands. Since they are generally computationally expensive and applied to one or a limited number of individuals, they can however not be used for simulating long-term forest dynamics according to various climate and forest management scenarios. Other individual-based models can be applied on all the trees of a stand in long-term simulations but at the cost of a coarse representation of physiological processes (e.g. SORTIE/BC). These models are interesting to analyse tree growth dynamics in heterogeneous forests but are less suitable for taking into account the changing environment. Since they simplify stand structure representation, cohort-based models can afford a detailed process-based description of the main processes involved in tree growth (e.g. 4C, ANAFORE, PSIM-DNDC, 3D-CMCC, see Table 3.5 for model characteristics). Here, the compromise is made on the spatial representation which accounts for the vertical gradient in growing conditions but not for the horizontal heterogeneity. Such models can indeed not distinguish between stands composed of the same trees but with various degrees of spatial aggregation (e.g. intimate *vs* patch-wise mixture). Similarly, some individual-based models choose to sacrifice the horizontal heterogeneity of some processes (e.g. iLand and Hybrid that calculate most of the water balance at stand scale, see Table 3.5 for model characteristics).

To simulate the impact of management in heterogeneous forests under changing conditions, we developed a spatially explicit individual-based approach designed to account for individual variability, local environment and adaptive behaviour of trees (Berger et al., 2008). The compromise was not achieved by strongly reducing the complexity of a particular aspect (spatial representation, process description or spatial or temporal coverage) but instead we tried to develop a balanced approach in which each aspect is described with the same level of complexity.

Among the existing individual-based models, BALANCE and NOTG-3D are close to HETEROFOR since they were designed according to the same philosophy. They present however some substantial conceptual differences (Table 3.5). Except BALANCE for leaf yellowing, HETEROFOR is the only model determining budburst, leaf yellowing and fall at the tree level. While rainfall partitioning is only calculated in HETEROFOR, the spatial representation of local climate conditions in the canopy is finer in BALANCE and NOTG-3D that consider different canopy layers or voxels. Regarding transpiration, HETEROFOR and BALANCE implement the widely used Penman-Monteith equation while it is determined as part of detailed energy budget in NOTG-3D. Finally, they all describe soil water dynamics at the individual scale but HETEROFOR displays a more mechanistic approach for describing soil water transfer among horizons (bucket *vs* Darcy model).

In HETEROFOR, some processes were described at two spatial scales (tree or stand level) in order to have the opportunity to compare the two approaches and choose the most appropriate one depending on the pursued objective. The phenological timing is species dependent and can optionally vary with tree size. This option (phenology at tree level) is interesting since it accounts for both the ontogeny effect and the vertical gradient in climate conditions. With this option, a longer vegetation period is assigned to the understory compared to the overstory, which allows improving radial growth predictions by correcting the growth underestimation in small trees and the overestimation in bigger ones (Fig. 3.S3). This first attempt to describe phenology at tree scale is quite empirical and incomplete and could be adapted in the future as knowledge on inter-individual phenology differences improves (e.g. Delpierre et al., 2017; Marchand et al., 2020). Individual phenology observations for trees of all social status will be necessary to better calibrate and evaluate this module in an iterative cycle of model improvement.

For the water balance, HETEROFOR accounts for a direct tree size effect on stomatal conductance (stomatal conductance is inversely proportional to the height of largest crow extension) and for an indirect effect on the sapwood to leaf area ratio whose both components depends on tree size (sect. 1.3.4 in Chap. 2). In addition, individual transpiration is a function of the radiation intercepted by the tree, the local wind speed and of the soil water availability. Finally, the tree adaptive behaviour to the local environment is described by an adaptation of the foliage biomass to local competition conditions and by specific leaf area varying with crown position within the canopy (sect. 1.3.6 and 1.3.7 in Chap. 2). Whatever the considered scale (tree or stand), HETEROFOR was able to correctly reproduce individual tree transpiration. Additional sap flux measurements as well as a characterization of the horizontal soil water content heterogeneity (using GPR technique for example) would be very useful to further evaluate the model performances and still enhance its ability to describe the complex hydrological functioning of heterogeneous forest. Among the possible improvements, mortality representation could be enhanced by considering hydraulic failure during severe droughts (Martin-StPaul et al., 2017). Another model improvement would be to take the interaction between the water cycle and the phenology into account by integrating a drought effect on budburst, leaf yellowing and fall as reported in some observation studies (Sanz-Perez and Castro-Diez, 2010; Xie et al., 2018).

## 5. CONCLUSION

In this paper, two key modules of HETEROFOR are described in details and evaluated in 4 sites / 6 stands. The phenological module correctly predicts the leafed period, which is essential to simulate light interception by trees, evapotranspiration, photosynthesis and respiration. With the hydrological module, HETEROFOR properly estimates rainfall interception, individual transpiration, soil water and deep drainage. Reproducing correctly the soil water dynamics is necessary to adequately predict photosynthesis since stomatal conductance closely depends on it. In addition, the description of the nutrient cycling requires accurate estimates of the water fluxes since water is the main vehicle for nutrient transport.

Our spatially explicit individual-based approach allows describing phenology and water balance in structurally-complex stands by partly accounting for the tree size effect on phenology and on tree transpiration, for the local environment modification (radiation and water availability) and for the adaptive behaviour of trees to local conditions (e.g. tree leaf area). Given the complexity of the functioning of heterogeneous forests, there are still a lot of ways to explore to improve the model, which will be done progressively as part of an iterative approach based on the prediction comparison with observations. Our model will also be used to compare various spatial representation scales (tree, cohort, stand) and determines the most appropriate one depending on the considered process and the pursued objective.

Simulating properly resource availability is necessary to produce robust predictions of tree growth under changing climate conditions. The next steps will be to extend the model validation to other European sites (see Chap. 5) to cover a larger range of ecological conditions and to use HETEROFOR to simulate stands dynamics under various management options and climate scenarios.

## 6. SUPPLEMENTARY MATERIALS

### Table 3.S1: Description of some model parameters for European hornbeam (regarding light interception, respiration, carbon allocation and tree dimension increment) and origin of their value.

| *Symbol* | *Description* | *Units* | *Value* | **Origin** |
|---|---|---|---|---|
| ***Light interception*** | | | | |
| $k$ | extinction coefficient | $m^{-1}$ | 1.10 | fitted with light measurements |
| ***Respiration*** | | | | |
| $r_{npp\_gpp}$ | parameters of the npp to gpp ratio function (α/β in Eq. 8) | | 0.65/0.0 | fitted with tree growth data of the study sites |
| $R_{Tref}$ | maintenance respiration per g of N at reference temperature (15°C) | mol $CO_2$ $gN^{-1}$ $h^{-1}$ | 5.15E-05 | fitted with tree growth data of the study sites |
| ***Carbon allocation*** | | | | |
| $b_{leaf}$ | parameters of the leaf biomass function (α/β/γ in Eq. 15) | kgC | 15.382/1.34/0.00 | Jonard *et al.* (2006) |
| $b_{structural\_above}$ | parameters of the aboveground structural biomass (α/β/γ in Eq. 26) | kgC | 0.0/533.1/0.996 | fitted with data from André and Ponette (2003) |
| $f$ | stem form factor (0.5) | $m^3$ $m^{-3}$ | 0.515 | fitted with data from André and Ponette (2003) |
| $\rho$ | stem volumetric mass | kgC $m^{-3}$ | 858.53 | fitted with data from André and Ponette (2003) |
| $s_{branch}$ | parameters of the branch mortality function (α/β/γ as in Eq. 15) | kgC | 0.00037/2.170/0.0 | fitted with data from André and Ponette (2003) |
| $p_{fruit}$ | parameters of the fruit production function (α/β in Eq.22) | kgC | 0.005/2.17 | fitted with litterfall data from the study sites |
| $dbh_{threshold}$ | threshold dbh for fruit production | cm | 5.0 | field observations |
| **Tree dimension increment** | | | | |
| *hlce%* | fraction of the height corresponding to the largest crown extension | m $m^{-1}$ | 0.505 | fitted with tree inventory data from the study sites |
| *hcb%* | fraction of the height corresponding to the crown base | m $m^{-1}$ | 0.392 | fitted with tree inventory data from the study sites |
| *Dd* | parameters of the crown to stem diameter function (α/β/γ/δ in Eq. 10) | m $m^{-1}$ | 10.17/0/1674/0 | fitted wih tree inventory data from the study sites |

(a) Chimay (oak)

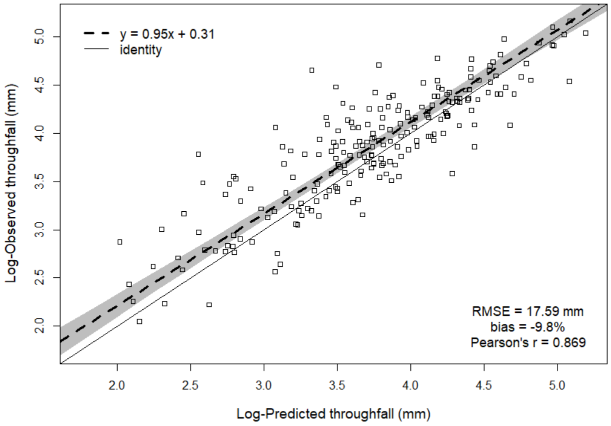

(b) Louvain-la-Neuve (beech)

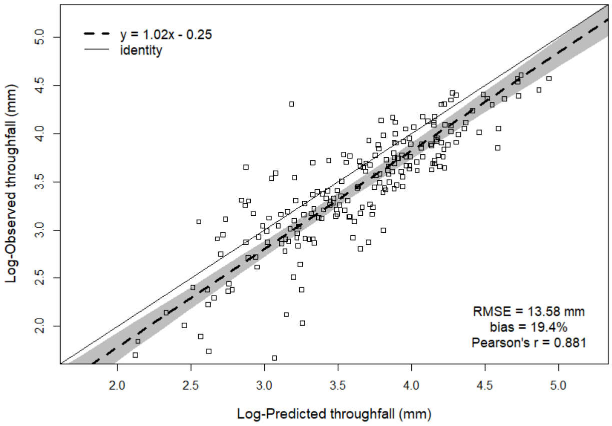

(c) Virton (beech)

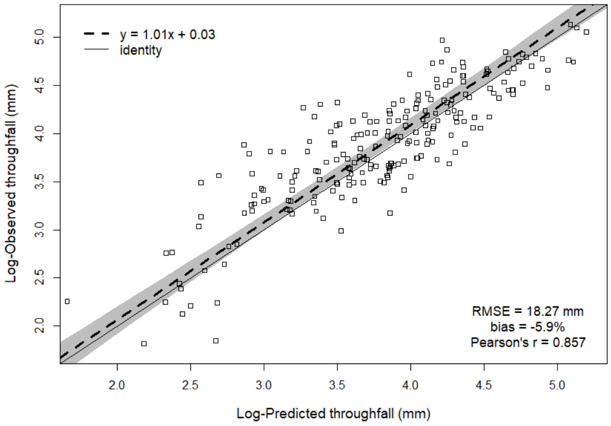

**Figure 3.S1: Comparison of the log-transformed observed and predicted monthly throughfall in Chimay (sessile oak), Louvain-la-Neuve (European beech) and Virton (European beech) between 2000 and 2016. The shaded area represents the confidence interval of the Deming regression (95%) of observations on predictions and the solid line corresponds to the identity line.**

(a) Baileux-beech

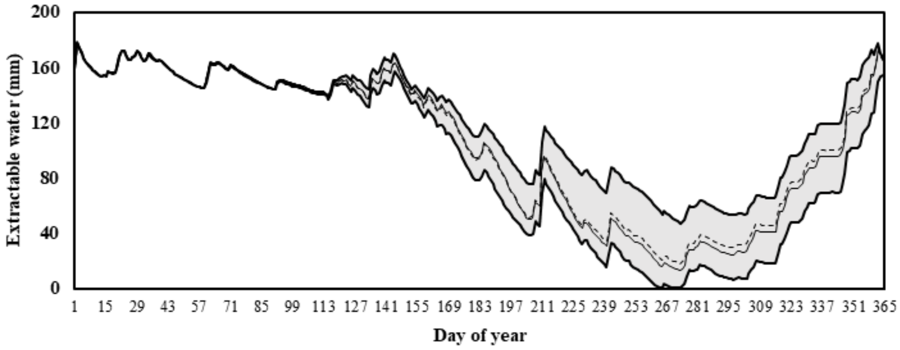

(b) Baileux-mixed

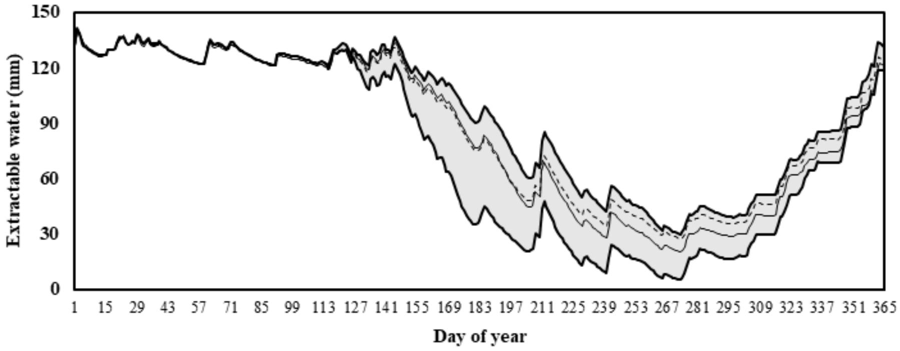

(c) Baileux-oak

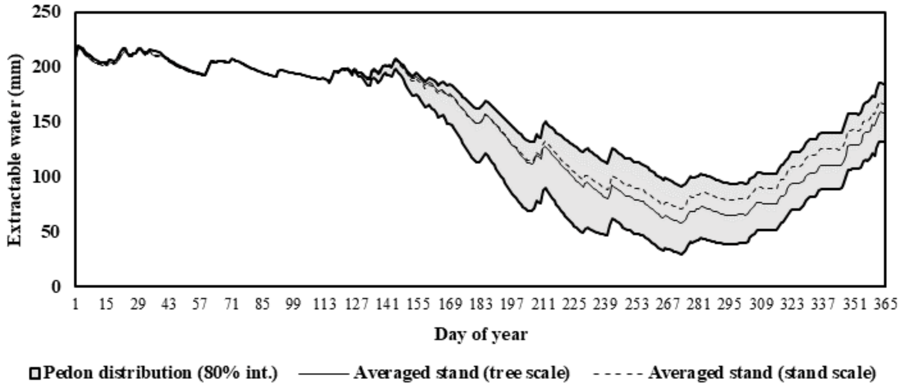

**Figure 3.S2: Temporal dynamics of soil extractable water simulated with the tree approach in the three stands of Baileux for 2003. The shaded area represents the 80% confidence interval of the values obtained for the various pedons. For comparison, the mean extractable water calculated with the stand approach is represented with a dashed line.**

(a) oak trees with phenology at stand scale (b) Beech trees with phenology at stand scale

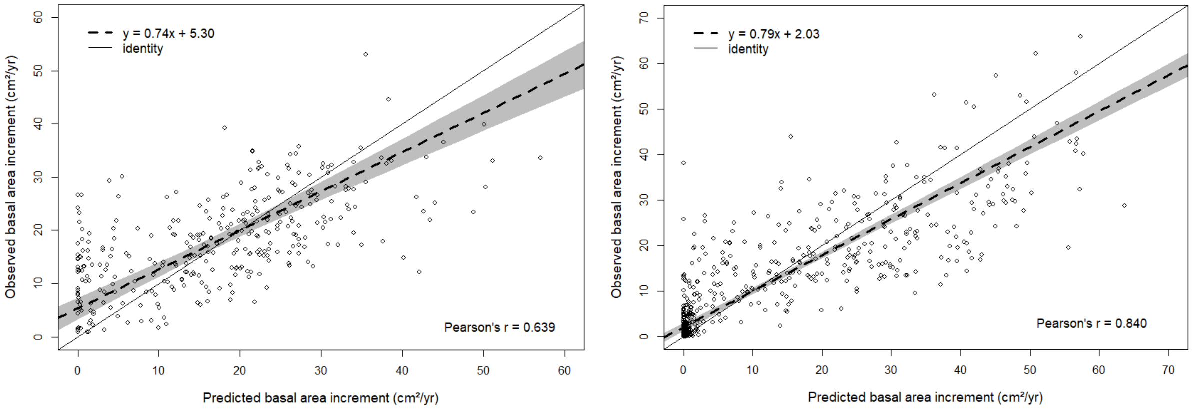

(c) Oak trees with phenology at tree scale (d) Beech trees with phenology at tree scale

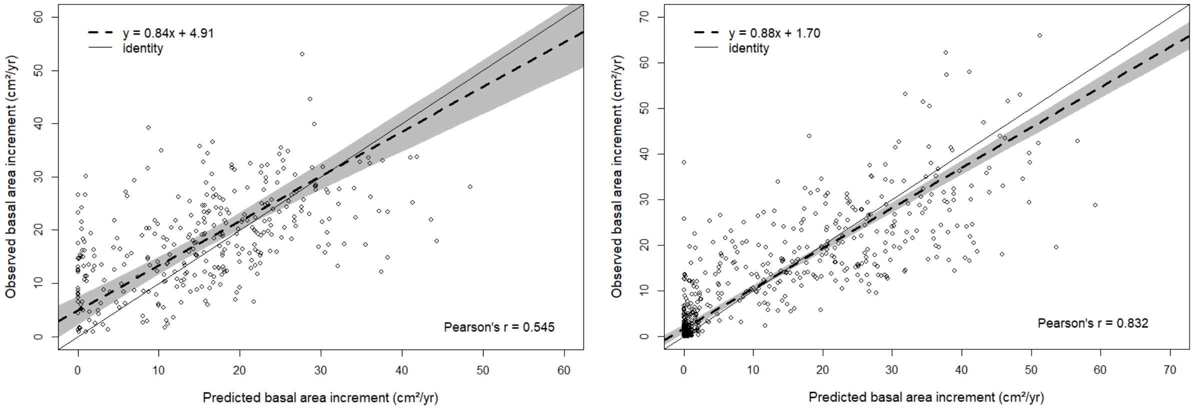

**Figure 3.S3: Comparison of observed and predicted basal area increments for sessile oak and European beech considering the two phenology modalities (tree vs stand scale). The quality of predictions is indicated by the *RMSE*, the relative bias and the Pearson's correlation coefficient (*r*). The shaded area represents the confidence interval of the Deming regression (95%) of observations on predictions and the solid line corresponds to the identity line.**

# Chapter 4

## $CO_2$ FERTILIZATION, TRANSPIRATION DEFICIT AND VEGETATION PERIOD DRIVE THE RESPONSE OF MIXED BROADLEAVED FORESTS TO A CHANGING CLIMATE IN WALLONIA

**Based on**

de Wergifosse L, André F, Goosse H, Caluwaerts S, de Cruz L, de Troch R, Jonard M (2020) $CO_2$ fertilization, transpiration deficit and vegetation period drive the response of mixed broadleaved forests to a changing climate in Wallonia. Ann. For. Sci. 77(3): 1-23.

## ABSTRACT

*Context: Forest net primary production (NPP) reflects forest vitality and is likely to be affected by climate change.*

*Aims:Simulating the impact of changing environmental conditions on NPP and two of its main drivers (transpiration deficit and vegetation period) in six Belgian stands and decomposing the site effect.*

*Methods: Based on the tree growth model HETEROFOR, simulations were performed for each stand between 2011 and 2100 using three climate scenarios and two* $CO_2$ *modalities (constant vs time-dependent). Then, the climate conditions, soils and stands were interchanged to decompose the site effect in these three components.*

*Results: In a changing climate with constant atmospheric* $CO_2$*, NPP values remained constant due to a compensation of the negative effect of increased transpiration deficit by a positive impact of longer vegetation periods. With time-dependent atmospheric* $CO_2$*, NPP substantially increased, especially for the scenarios with higher greenhouse gas (GHG) emissions. For both atmospheric* $CO_2$ *modalities, the site characteristics modulated the temporal trends and accounted in total for 56 to 73% of the variability.*

*Conclusion: Long-term changes in NPP were primarily driven by* $CO_2$ *fertilization, reinforced transpiration deficit, longer vegetation periods and the site characteristics.*

## 1. INTRODUCTION

Forests affect the climate in various and complex ways, through biophysical and biogeochemical effects. They can have a warming or a cooling effect depending on the way they modify albedo and evapotranspiration compared to other land covers (Bonan, 2008; Stocker et al., 2013). In addition, forest ecosystems decrease the concentration of atmospheric carbon dioxide ($CO_2$) by carbon storage in the soil and in tree biomass (Myhre et al., 2013; Le Quéré et al., 2018). On another hand, most of the processes involved in forest ecosystem functioning are climate sensitive (Parmesan and Yohe, 2003; Kint et al., 2012; Charru et al., 2017). Climate changes could therefore seriously affect forest dynamics and the provision of ecosystem services (Temperli et al., 2012; Mina et al., 2017) that in turn affect climate (Seidl et al., 2014; Thom et al., 2017).

Many environmental manipulation experiments and monitoring studies have highlighted the effects of atmospheric $CO_2$ concentration, air temperature and soil water availability on forest net primary production (NPP). The fertilizing effect of atmospheric $CO_2$ was pointed out from free-air or chamber $CO_2$ enrichment experiments (Ainsworth and Long, 2005; Ainsworth and Rogers, 2007; Thompson et al., 2017). Norby et al. (2005) found that NPP increased by 20-25% when the $CO_2$ level was elevated to 550 ppm. On the long run, however, this increase was constrained by nutrient availability (Norby et al., 2010; Warren et al., 2015).

Furthermore, global remote sensing and local observational studies have shown that the increase in air temperature tends to advance the budburst date and therefore lengthens the vegetation period (Menzel et al., 2006; Jeong et al., 2011; Richardson et al., 2013; Park et al., 2016; Flynn and Wolkovich, 2018) and favours NPP (Baldocchi, 2008; Dragoni et al., 2011; Richardson et al., 2013; Fu et al., 2017). Moreover, respiration and photosynthesis, which have an opposite effect on biomass production, are both stimulated by warmer temperatures (Zhang et al., 2017).

Concerning water availability, it is well known that soil water deficit during the vegetation period triggers stomatal closure and reduces carbon assimilation. In addition, it reduces the mineralization, uptake and transport of nutrients (Bréda et al., 2006; Lisar et al., 2012; Osakabe et al., 2014). Syntheses and meta-analyses of rainfall experiments generally report decreases in photosynthesis, NPP, aboveground biomass and soil respiration (Wu et al., 2010; Paschalis et al., 2020). During prolonged water stress periods, tree mortality may occur due to hydraulic failure or carbon starvation (McDowell et al., 2008; Adams et al., 2017). For instance, a particularly drastic rainfall exclusion experiment conducted during a five-year period in a Mediterrannean broadleaf forest (*Q. ilex*, *A. unedo* and *P. latifolia*) led to a 15% decrease in soil water content, lowered the aboveground biomass production by 83% and increased mortality rate by 46% (Ogaya and Peñuelas, 2007). Similarly, different studies have highlighted the same trends but with a lower effect during the 2003 drought (Ciais et al., 2005; Bréda et al., 2006; Granier et al., 2007).

The Intergovernmental Panel on Climate Change (IPCC) has adopted different greenhouse gas (GHG) emission scenarios called Representative Concentration Pathway (RCPs). Two commonly-used scenarios are RCP4.5 and RCP8.5 and feature $CO_2$ concentrations of 540 and 940 ppm in 2100, respectively. Regarding Atlantic Europe (see Fig. S1 in Jacob et al., 2014), the climate projections for the two abovementioned scenarios at the end of the 21st century are characterised by an increase in air temperature (between +1.3 °C and +4.2 °C), changes in annual precipitation (-1% to +9%), in high-temperature extremes, in drought events, and by a decrease in summer precipitation (-5 to -25%) compared to the 1971-2000 period (Jacob et al., 2014; Kovats et al., 2014; Jacob et al., 2018).

The projected climate changes are likely to alter the forest dynamics (Lindner et al., 2014). However, the resulting trend is difficult to estimate due to the opposite and interacting effects of climate on the processes regulating forest productivity. To estimate tree growth in unprecedented conditions, process-based models (PBM), which integrate knowledge from in-situ experiments, are recommended since they allow the integration of a wide range of effects (Pretzsch et al., 2015). However, the future forest evolution will not be uniform but is more likely to be site-dependent. Indeed, the different components of the site effect - climate, soil and stand - can modify the forest response to changing conditions (Holdridge, 1967; Tucker et al., 2008; Steenberg et al., 2015) and therefore PBM must account for them.

The response of a given tree species to climate change depends on the local climate (first component of the site effect). For sites at the upper limit of the temperature distribution range of a tree species, an increase in temperature would be detrimental for the development of this tree species while it could be positive in colder sites. The same reasoning also holds for a rainfall reduction, which could induce water stress more frequently on drier sites but could be beneficial on wetter ones. In Wallonia, an increase in temperature of 2 °C would confine European beech (*Fagus Sylvatica* (L.)) in its tolerance limits while sessile oak (*Quercus petraea* (Matt.) Liebl.) would remain in optimal growing conditions (Petit et al., 2017). The climate change effect can then be modulated by the soil properties. Indeed, greater soil depth and water holding capacity decrease the negative impact of drought events on NPP (Phillips et al., 2016). Finally, the stand characteristics generate differences in the forest response to climate change. Different effects constitute the stand effect: the tree species identity and diversity and the stand structure and density. The tree species identity effect simply depicts that all tree species do not exhibit the same functional traits such as phenological timing (Vitasse et al., 2009; Cole and Sheldon, 2017) or drought sensitivity (Leuzinger et al., 2005; Scherrer et al., 2011). Consequently, they display different phenological and stomatal responses to a rise of temperature (Primack et al., 2009) and a change in soil water content or in $CO_2$ levels (Medlyn et al., 2001; Jonard et al., 2011; Raftoyannis and Radoglou, 2002). Additionally, when these tree species coexist in the same stand, the response to climate change is even more difficult to predict since it can be affected by complementarity, facilitation and selection effects (Grossiord, 2019; Bello et al., 2019a). For instance, Anderegg et al. (2018) observed that mixing species with a high diversity of hydraulic traits decreases their sensitivity to drought. On the other hand, an intensive water use by some tree species mixtures could lead more rapidly to water stress (Pretzsch and Biber, 2016). The stand structure modifies the response to climate change since trees respond differently depending on their size, age or social status. Dominant trees seem to be more sensitive to climatic stress than dominated ones, which can be explained by a higher vulnerability to hydraulic stress (McDowell and Allen, 2015) and a stronger exposition to atmospheric conditions (Bennett et al., 2015). When soil water availability decreases, small trees keep their stomata open for longer since the position of their crown within the canopy limits the evaporative demand (Carl et al., 2018). Finally, tree density also affects the stand response to climate change as it is positively related to stand leaf area index and, consequently, to evapotranspiration (Bello et al., 2019b). During drought events, thinned broadleaved stands generally exhibit a lower growth decrease due to reduced competition for water among remaining trees (Sohn et al., 2016). Understanding the effect of stand characteristics on forest response to climate change is essential since the forester can adapt it while the adaptability of the soil is much more limited and is practically inapplicable for the climate. In conclusion, sites subject to similar changes in climate conditions can display very different responses due to their climate, soil and stand characteristics. This was already pointed out based on observations by Boisvenue and Running (2006) and can be found in simulation studies (Reyer, 2015).

In order to produce realistic projections of NPP for the 21st century, one must take into account the future climate under various GHG emission scenarios, the soil properties and the stand characteristics. Yet, most of the currently-existing PBM are stand-scale models accounting for the climate and soil effects but only partly integrating the spatial and structural complexity of the stand. However, structurally-complex stands (uneven-aged and mixed) tend to be favoured by the foresters in order to improve the resilience of their forests (Bauhus et al., 2013; DeRose and Long, 2014). To simulate correctly such stands, spatially explicit and individual-based approaches are required (Seidl et al., 2005).

In this study, we will address the question of how and to what extent changing climate and $CO_2$ conditions will impact forest productivity in six contrasting and structurally-complex stands in Wallonia and assess how the site components and thinning operations modulate the response. To do so, we will use HETEROFOR (Jonard et al., 2020; de Wergifosse et al., 2020), a process-based tree growth model running at the individual level with different climate projections based on three GHG emission scenarios.

Wallonia is within a climatic zone that deserves more studies on the impact of climate change on forests since this effect is quite uncertain there for several reasons. Under the current climate conditions, Wallonia is located at the transition between areas where forest growth is limited by temperature, and consequently by the length of the growing period, in the North and by water availability in the South (Bastrup-Birk et al., 2016). In the future, warmer temperatures are expected all over Europe, a rainfall increase in the Northern temperature-limited areas and inversely a precipitation decrease in the Southern water-limited areas (IPCC, 2013; Kovats et al., 2014). Therefore, while most simulation studies agree that forest productivity should increase in Boreal forests and decrease or remain constant in Mediterranean area (Reyer et al., 2014; Reyer, 2015), to what extent Walloon forest productivity will be constrained by water availability, on average and during extreme events, is not a consensual issue. In addition, an increased water stress could be partly compensated by a longer vegetation period in the future.

More precisely, the objectives of the paper are

I. to simulate the temporal changes in the net primary production of six broadleaved stands in Wallonia (Belgium) and in two of its main drivers (transpiration deficit and vegetation period) under various GHG scenarios.
II. to differentiate the long-term trend from the inter-annual NPP variations and to evaluate the part of the NPP variability explained by transpiration deficit, vegetation period and atmospheric $CO_2$ concentration.
III. to assess to which extent these temporal trends are modulated by the site and how thinning affects transpiration deficit.
IV. to decompose the site effect in its three main components (climate, soil and stand) and see how they are accounted for by transpiration deficit and vegetation period.

## 2. MATERIAL AND METHODS

### 2.1. SITE DESCRIPTION

For the simulation study, six long-term monitoring plots installed in sessile oak (*Quercus petraea* (Matt.) Liebl.) and European beech (*Fagus sylvatica* (L.)) stands were selected as case studies representative of the broadleaved forest in Wallonia (Belgium). Three plots are located in an experimental site in Baileux (50°01'N 4°24'E) and have been monitored since 2001. The three other plots are part of the level II network of ICP Forests since 1998 (Ferretti and Fischer, 2013) and are located in Louvain-la-Neuve (50°41'N 4°36'E), Chimay (50°07'N 5°34'E) and Virton (49°32'N 5°34'E).

#### 2.1.1 Stand characteristics

The three plots in Baileux were installed to study how species mixtures influence the forest ecosystem functioning (Jonard et al. 2006, 2007, 2008; André et al. 2008a, 2008b, 2010, 2011). Two are located in nearly monospecific stands dominated either by sessile oak (hereafter called Baileux-oak) or by European beech (Baileux-beech) and the third one is in a balanced mixture of both tree species (Baileux-mixed) (Table 4.1).

The stand of Chimay originates from coppice-with-standards and is dominated by mature sessile oaks with a hornbeam understory. In Louvain-la-Neuve and Virton, European beech is the main tree species and is mixed with oaks. In Virton, other broadleaved species (maple, wild cherry, ash, hornbeam) are also present. All these stands cover a wide range in tree size (girth in 1999 or 2001: from 22.6 cm for hornbeam in Baileux-mixed to 190 cm for sessile oak in Virton), in stand density (basal area in 1999 or 2001: from 18.4 to 30.0 m².ha$^{-1}$) and in leaf area index (LAI) with values extending from 3.96 to 6.93 m².m$^{-2}$. Except for the Louvain-la-Neuve plot installed in an old even-aged beech forest, the study stands display complex structure in terms of species composition and tree age (Table 4.1).

**Table 4.1: Stand characteristics for the main tree species and for the whole stands.**

| Stand Inventory year (area) | Tree species | Tree density (N.ha$^{-1}$) | Basal area (m².ha$^{-1}$) | $C_{130}$ (cm) | Dominant height (m) | **Modelled** LAI (m².m$^{-2}$) |
|---|---|---|---|---|---|---|
| Baileux-oak | Quercus petraea | 187 | 16.2 | 100.6 (26.5) | 21.9 | |
| 2001 (0.9 ha) | Fagus sylvatica | 118 | 4.0 | 46.4 (35.6) | 15.5 | |
| | Carpinus betulus | 152 | 1.3 | 31.4 (11.4) | 11.6 | |
| | Total | 468 | 21.6 | 63.7 (40.4) | 22.2 | 4.17 |
| Baileux (beech) | Quercus petraea | 72 | 6.4 | 103.3 (18.1) | 23.0 | |
| 2001 (1.4 ha) | Fagus sylvatica | 217 | 16.5 | 87.5 (41.5) | 25.0 | |
| | Total | 297 | 23.1 | 90.3 (38.5) | 24.8 | 4.86 |
| Baileux (mixed) | Quercus petraea | 118 | 12.9 | 115.5 (21.0) | 4.5 | |
| 2001 (1.8 ha) | Fagus sylvatica | 352 | 17.0 | 91.2 (39.3) | 25.7 | |
| | Carpinus | 9 | 0.1 | 22.6 (17.3) | 9.4 | |
| | Total | 484 | 30.0 | 101.2 (42.0) | 25.9 | 5.99 |
| Chimay | Quercus petraea | 63 | 13.1 | 158.7 (35.0) | 20.4 | |
| 1999 (1.3 ha) | Carpinus betulus | 634 | 5.3 | 30.5 (10.8) | 15.8 | |
| | Total | 697 | 18.4 | 42.4 (40.1) | 19.2 | 3.96 |
| Louvain-la-Neuve | Quercus petraea | 21 | 4.7 | 165.9 (23.0) | 30.9 | |
| 1999 (1.1 ha) | Fagus sylvatica | 87 | 24.6 | 179.1 (53.6) | 32.1 | |
| | Total | 108 | 29.4 | 176.6 (49.6) | 32.9 | 6.34 |
| Virton | Quercus petraea | 5 | 1.3 | 190.0 (10.0) | 24.1 | |
| 1999 (1.4 ha) | Fagus sylvatica | 340 | 16.8 | 70.9 (31.7) | 24.0 | |
| | Carpinus betulus | 22 | 0.4 | 48.4 (15.4) | 14.5 | |
| | Total | 425 | 23.3 | 73.6 (36.0) | 24.0 | 6.93 |

Tree density is the number of trees per ha, basal area is the sum of the trunk radial area at 130 cm height per ha, $C_{130}$ is the average trunk circumference (cm) at an height of 130 cm, dominant height is the average height of the 100 biggest trees per ha and LAI (Leaf Area Index) is the sum of tree leaf areas expressed by unit ground area

### 2.1.2 Soil properties

The soils in Baileux and Chimay are cambisols with moder humus (FAO soil taxonomy) developed in a bedrock of sandstone and shales mixed with loess deposits while the soil in Louvain-la-Neuve is an abruptic luvisol with moder humus formed in loamy loess deposits from the interglacial period. Finally, the soil of Virton is a calcaric cambisol with mull humus; it originates from the weathering of a hard limestone bedrock (Table 4.2).

This large range of soils is reflected in the soil texture. According to the USDA taxonomy, the soil of Baileux is silty clay loam and that of Chimay is intermediate between silty clay loam and clay loam. The soil in Louvain-la-Neuve is silty loam due to its high silt content (62-75%). The highest clay fraction was registered in Virton and it is therefore a clayey soil (Table 4.2). The soil texture influenced the soil hydraulic properties. In Baileux and Louvain-la-Neuve, the high silt content ensures good drainage. In Chimay, the presence of inflating clay favours the appearance of a perched water table near the surface during winter and drought cracks in the warm and dry period. In Virton, in spite of elevated clay content, the existence of faults in the bedrock enables an efficient drainage.

The stoniness varies a lot among plots. Baileux-beech, Baileux-mixed and Virton have the higher coarse fraction (>50% in the deep horizons) while the soil in Louvain-la-Neuve contains hardly any large stones. The coarse fraction in the soils of Baileux-oak and Chimay is intermediate (between 30 and 45% at the bottom of the profile). These differences in soil texture and coarse fraction among sites lead to a great diversity (between 154 and 450 mm) of extractable water reserve on a 1.6 m depth. For example, the maximum extractable water (MEW) reserve in Louvain-la-Neuve is almost three times greater than that of Baileux-mixed and Virton (Table 4.2). A same soil depth of 1.6 m was retained for all site as it allows to account for most (if not all) the rooting zone and for the sake of comparability. The impact of using a same depth for all sites is limited since water uptake only occurs in the horizon where roots are present. In addition, the lower horizons of some sites are very stony and therefore the associated extractable water is limited.

### 2.1.3 Climate

Although entire Belgium being characterized by the same climate type (temperate maritime), the four sites of our study are all located in different bioclimatic zones (Van der Perre *et al.*, 2015), which highlights their climate diversity (Table 4.2). Louvain-la-Neuve is characterized by the warmest (11.0 °C) and driest (818 mm) climate. Despite their proximity, Baileux and Chimay display differences in terms of annual rainfall with 1075 mm in Baileux and 940 mm in Chimay probably due to the more elevated location of Baileux (between 305 and 312 m a.s.l.) than Chimay (260 m a.s.l.). However, yearly-average temperatures are similar in both locations (9.8 °C in Baileux and 9.7 °C in Chimay). Finally, Virton features high precipitation values (1060 mm) and an intermediate yearly-mean temperature of 9.9 °C (Table 4.2). Reference crop evapotranspiration was calculated for each site according to the FAO method (Allen et al., 1998) and showed a low variability (between 712 and 745 mm.year$^{-1}$) that can mainly be attributed to air temperature differences.

**Table 4.2: Soil and meteorological (2001-2016 period) characteristics of the different study sites.**

| Stand | Location | Bioclimatic zone | Altitude (m) | Soil type | Soil texture (USDA) | MEW over 1.6 m (mm) | Annual rainfall (mm) | Mean air temperature (°C) | Reference crop evapotranspiration (mm.year$^{-1}$) |
|---|---|---|---|---|---|---|---|---|---|
| Baileux (beech/mixed/oak) | 50°0’N, 4°2’E | Basse et moyenne Ardenne | 305-312 | Cambisol | Silt (clay) loam | 174/154/239 | 1075 | 9.8 | 712 |
| Chimay | 50°1’N, 4°2’E | Fagne, Famenne et Calestienne | 260 | Dystric Cambisol | (Silt) clay loam | 205 | 940 | 9.7 | 723 |
| Louvain-la-Neuve | 50°4’N, 4°4’E | Hesbino-brabançon | 130 | Abruptic Luvisol | Silt loam | 450 | 818 | 11.0 | 745 |
| Virton | 49°3’N, 5°3’E | Basse Lorraine | 370 | Calcaric Cambisol | Clay | 167 | 1060 | 9.9 | 726 |

## 2.2. SIMULATION EXPERIMENTS

### 2.2.1 Model description and performances

For the simulations, we used the individual-based, spatially explicit and process-based model HETEROFOR that has been implemented in the CAPSIS simulator (Dufour-Kowalski et al., 2012) and is especially convenient to simulate the evolution of structurally-complex stands. Hereafter, we present a brief overview of the model functioning limited to the description of the options retained for the simulation experiments carried out in this study. For a more in-depth description, we refer the reader to Chap.2.

To initialise the model, the user must provide different files: a tree species parameter file, an inventory (or stand) file with the tree coordinates and dimensions (tree circumference, total height, height to crown base, height of largest crown extension and crown radius in four cardinal directions), a soil file with the physical properties of each soil horizon (thickness, bulk density, coarse fraction, sand, silt, clay and organic carbon contents and fine root proportion) and a meteorology (or climate) file with hourly data for radiation, air temperature, precipitation, relative humidity and wind speed. After the initialization phase and at the end of each year, HETEROFOR calls the phenology routine that provides daily information concerning the foliage state for the coming year. From a fixed date, a sum of warm temperature is daily accumulated until reaching a threshold, which triggers the budburst and then, similarly, the progressive leaf expansion. From mid-summer, cold temperatures are accumulated until reaching a threshold, which triggers leaf yellowing occurring at a rate proportional to the photoperiod decrease. The leaf falling rate is calculated based on wind speed and accelerated in case of frost events. Phenology can be calculated at the species level or the individual scale to account for the extended vegetation period of understorey trees. In this study, we chose to calculate phenology at the species level. Once phenology is fixed, HETEROFOR calculates the proportion of solar radiation intercepted by each tree using the SAMSARALIGHT library based on a ray tracing approach (Courbaud et al., 2003). From the photosynthetically active radiation (PAR) absorbed per unit leaf area and the soil water potential updated hourly with a water balance routine, the gross primary production (GPP) of each tree is estimated hourly with the photosynthesis model of the CASTANEA library (Farquhar et al., 1980; Dufrêne et al., 2005). The individual NPP is then obtained by using a NPP to GPP ratio to take the growth and maintenance respiration into account. NPP is first allocated to foliage and fine roots by ensuring a functional balance and then to structural components using allometric equations, which allows deriving tree dimensional growth. The water balance routine accounts for rainfall partitioning in throughfall, stemflow and interception (André et al., 2008a), for tree transpiration and evaporation from foliage, bark and soil using the Penman-Monteith equation (Monteith, 1965), for root water uptake (Couvreur et al., 2012) and for soil water movements based on the Darcy law. This routine can be calculated at the stand or individual scale but calculation time considerably increases when the individual option is selected and consequently, we selected the stand scale in this study.

HETEROFOR was evaluated on the same sites as those used in this study. The evaluation of tree growth conducted in Jonard et al. (2020) demonstrated the model ability to reproduce size-growth relationships and individual radial growth. In the same study, the simulated GPP was related to the NPP reconstructed from tree growth measurement and this relationship displayed high Pearson's correlation coefficients (0.89 and 0.91 for Sessile oak and European beech, respectively). Regarding water balance evaluated in de Wergifosse et al. (2020), the model satisfactorily simulated the soil water content temporal dynamics (correlation coefficients between simulations and observations ranging from 0.83 to 0.95 according to the site) and the individual transpiration (0.85 and 0.89 for oak and beech, respectively). Finally, the budburst model previously described, a one-phase model based on the Uniforc model (Chuine, 2000), which simulates the forcing period, has been chosen among two other budburst models (two-phase models accounting for the forcing and chilling periods) implemented in HETEROFOR as it reproduced best the inter-annual variability. With this budburst model, vegetation period was on average simulated with a RMSE of 6.7 days (unpublished data).

The parameters needed to initialize the model are those described in the two model description papers (Table 2 in Jonard et al., 2020 and Table 3.1). Only for Virton, a higher NPP to GPP ratio is used in the species parameter file to account for differences not considered by the model (probably due to a higher site fertility). This ratio was fixed to 0.6 and 0.75 for Sessile oak and European beech, respectively. Yet, this parameterization difference is only applied in the first simulation experiment described below. Indeed, one of the objective of this first experiment is to estimate the future productivity of the site, for which as many site characteristics as possible must be integrated while the second simulations aimed at decomposing the site effects in its components without being affected by the parametrization.

### 2.2.2 First simulation experiment to highlight the climate change impact

One-year simulations were performed for different periods in order to assess the impact of climate change on stand NPP median value and variance, on transpiration deficit and on vegetation period (objectives I and II stated in the introduction) and to evaluate how site and thinning affected these changes (objective III). More specifically, each year, a new simulation was launched starting from the same initial stand. Stand characteristics were therefore reinitialized each year keeping thereby the focus on the climate impact, in contrast to multi-year simulations which could have given rise to diverging stand characteristics with time. Climate projections generated according to three Radiative Concentration Pathway (RCP) scenarios (see below) were used to run simulations on the 2011 – 2100 period while the 1976 – 2005 period (called "historical" period) was used as reference for comparisons with RCP scenarios.

One of the major uncertainties when simulating long-term forest productivity is whether or not the positive response of forest to rising $CO_2$ concentration can persist. Indeed, it has been shown that the induced productivity gain may progressively be reduced when other factors such as nutrient availability become limiting (Körner, 2006; Norby et al., 2010). In order to cover the range of possible tree responses, from a perfect acclimation to rising atmospheric $CO_2$ to no acclimation at all, the set of simulations was launched considering either a constant atmospheric $CO_2$ concentration (380 ppm) or time-dependent $CO_2$ concentrations corresponding to the RCP scenarios (Reyer et al., 2014). The first case can be seen as a response to increasing $CO_2$ concentration totally constrained by other limiting factors and the second as never constrained. Moreover, holding $CO_2$ concentration constant allowed us to have a better insight into the other climate effects.

The two simulation types were also run for each monitoring plot after applying a virtual thinning to reduce stand basal area by 25% and test the immediate thinning impact. The selection of thinned trees was made among the pool of trees that were effectively cut in each plot during the monitoring period. When the past thinning operations were insufficient to reach 25%, additional trees were randomly selected and removed.

### 2.2.3 Second simulation experiment to highlight and decompose the site effect

To further investigate the site effect on the NPP variability (objective IV stated in the introduction), a similar set of one-year simulations was ran for the historical period (1976-2005) by combining the climate, soil and stand input files of all the monitoring plots according to a full factorial design (6 soil types x 6 stands x 4 climates x 30 years). The simulations were performed for a constant atmospheric $CO_2$ concentration in order to limit the number of variation factors. Then, the simulations were repeated for the 2071-2100 period considering the RCP8.5 scenario to test whether the NPP variance decomposition is affected by climate change.

### 2.2.4 Climate projections

As a basis, the climate projections of the global climate model (GCM) CNRM-CM5 were used here. These global simulations were also included in the Coupled Model Intercomparison Project (CMIP5) on which the IPCC bases most of its conclusions (Fifth Assessment Report: IPCC, 2013; IPCC special report on 1.5 C: Masson-Delmotte, et al., 2018). However, the horizontal resolution of CNRM-CM5 is 1.4° (≃155 km), which did not allow us to make any distinctions between our study plots. In a first step, the CNRM-CM5 projections were therefore downscaled over the European domain using the Regional Climate Model (RCM) ALARO-0 (Giot et al., 2016; Termonia et al, 2018) following the guidelines of the Coordinated Regional Downscaling Experiment (CORDEX; Giorgi et al, 2009; Jacob et al, 2014). This dynamic downscaling consisted in using ALARO-0 over 50-km resolution areas forced at their boundaries by projections of CNRM-CM5. In a second downscaling step, the simulations over Europe with 50-km resolution were downscaled to a 4-km resolution over Belgium (Rummukainen, 2010).

The meteorological variables that served as input for HETEROFOR include hourly values of the longwave and shortwave radiations, air temperature, surface temperature, rainfall, specific humidity and wind speed. Finally, relative humidity was calculated based on temperature, specific humidity and atmospheric pressure. All values were taken at the grid points closest to the four sites for the historical period (1976-2005) and for the 2011-2100 period according to three RCP scenarios: RCP2.6, RCP4.5, RCP8.5. The scenario names depict the increase in radiative forcing in 2100 relative to preindustrial levels (+2.6 $W.m^{-2}$, +4.5 $W.m^{-2}$, +8.5 $W.m^{-2}$). The climate projections should be considered as sensitivity experiments. In other words, the climate changes rather than the absolute climate values are of importance as the model climatology (during the historical period) is known to differ from the observed one (Maraun and Widmann, 2018). However, for our case, there were important positive model biases in rainfall ranging from 7 to 35% when compared with the observed values at the considered sites. A bias correction was therefore performed (Maraun and Widmann, 2018). More specifically, for air and soil temperatures, data were corrected according to

$$x_{corr\_t} = x_{simul\_t} + (\overline{x_{obs}} - \overline{x_{simul}}) \quad (1)$$

with

$x_{corr\_t}$, the corrected value of a variable at time t

$x_{simul\_t}$, the variable simulated by the regional model at time t

$\overline{x_{obs}}$ and $\overline{x_{simul}}$, the average observed and simulated values for the period 2001-2016.

This method is, however, not suitable for variables which cannot take negative values. For these variables (radiation, rainfall, relative humidity and wind speeds), data were corrected using a multiplicative scaling

$$x_{corr\_t} = x_{simul\_t} \frac{\overline{x_{obs}}}{\overline{x_{simul}}} \quad (2)$$

The same correction was applied to the three RCP scenarios using $\overline{x_{obs}}$ and $\overline{x_{simul}}$ based on the period 2001-2016. The average corrected mean air temperature, rainfall and reference evapotranspiration are presented in Table 4.3 for the three RCP scenarios during the 2071-2100 period and also during the historical period.

**Table 4.3: Mean annual rainfall, air temperature and reference crop evapotranspiration for the historical period (1976-2005) and the various RCP scenarios (2071-2100). Mean values for the vegetation period (fixed from the 1$^{st}$ of May to the 30$^{th}$ of September) are indicated between brackets. For each site and climatic variable, same letters indicate that the scenarios are not statistically different (Student's t-test).**

| Stand | Rainfall (mm) | | | | Air temperature (°C) | | | | Reference crop evapotranspiration (mm) | | | |
|---|---|---|---|---|---|---|---|---|---|---|---|---|
| | Historical (1976-2005) | RCP2.6 (2071-2100) | RCP4.5 (2071-2100) | RCP8.5 (2071-2100) | Historical (1976-2005) | RCP2.6 (2071-2100) | RCP4.5 (2071-2100) | RCP8.5 (2071-2100) | Historical (1976-2005) | RCP2.6 (2071-2100) | RCP4.5 (2071-2100) | RCP8.5 (2071-2100) |
| Baileux | 1075$^{A}$ | 1066$^{A}$ | 1145$^{B}$ | 1161$^{B}$ | 9.78$^{A}$ | 10.49$^{B}$ | 11.56$^{C}$ | 13.12$^{D}$ | 681.4$^{A}$ | 699.6$^{A}$ | 730.9$^{B}$ | 760.1$^{C}$ |
| | (449)$^{A}$ | (439)$^{A}$ | (431)$^{A}$ | (435)$^{A}$ | (15.40)$^{A}$ | (16.09)$^{B}$ | (17.08)$^{C}$ | (18.40)$^{D}$ | (480.9)$^{A}$ | (494.2)$^{A}$ | (522.4)$^{B}$ | (538.5)$^{B}$ |
| Chimay | 940$^{AB}$ | 915$^{A}$ | 975$^{BC}$ | 995$^{C}$ | 9.74$^{A}$ | 10.48$^{B}$ | 11.55$^{C}$ | 13.10$^{D}$ | 689.1$^{A}$ | 706.6$^{A}$ | 739.3$^{B}$ | 767.1$^{B}$ |
| | (380)$^{A}$ | (379)$^{A}$ | (366)$^{A}$ | (372)$^{A}$ | (15.37)$^{A}$ | (16.06)$^{B}$ | (17.04)$^{C}$ | (18.35)$^{D}$ | (485.2)$^{A}$ | (498.5)$^{A}$ | (527.2)$^{B}$ | (541.9)$^{B}$ |
| Louvain-la-Neuve | 818$^{A}$ | 799$^{A}$ | 868$^{B}$ | 901$^{B}$ | 10.99$^{A}$ | 11.67$^{B}$ | 12.75$^{C}$ | 14.30$^{D}$ | 716.0$^{A}$ | 729.9$^{A}$ | 762.5$^{B}$ | 788.3$^{B}$ |
| | (354)$^{A}$ | (341)$^{A}$ | (352)$^{A}$ | (360)$^{A}$ | (16.71)$^{A}$ | (17.37)$^{B}$ | (18.37)$^{C}$ | (19.68)$^{D}$ | (502.0)$^{A}$ | (513.2)$^{AB}$ | (540.6)$^{BC}$ | (554.7)$^{C}$ |
| Virton | 1060$^{A}$ | 1013$^{A}$ | 1067$^{AB}$ | 1111$^{B}$ | 9.90$^{A}$ | 10.65$^{B}$ | 11.81$^{C}$ | 13.32$^{D}$ | 698.1$^{A}$ | 716.8$^{A}$ | 756.3$^{B}$ | 784.2$^{B}$ |
| | (391)$^{A}$ | (381)$^{A}$ | (345)$^{B}$ | (382)$^{A}$ | (15.93)$^{A}$ | (16.69)$^{B}$ | (17.79)$^{C}$ | (19.05)$^{D}$ | (495.0)$^{A}$ | (507.5)$^{A}$ | (542.2)$^{B}$ | (556.1)$^{B}$ |
| mean | 958$^{A}$ | 948$^{A}$ | 1014$^{B}$ | 1042$^{B}$ | 10.11$^{A}$ | 10.82$^{B}$ | 11.92$^{C}$ | 13.46$^{D}$ | 696.2$^{A}$ | 713.2$^{A}$ | 747.3$^{B}$ | 774.9$^{B}$ |
| | (394)$^{A}$ | (385)$^{A}$ | (374)$^{A}$ | (387)$^{A}$ | (15.85)$^{A}$ | (16.55)$^{B}$ | (17.57)$^{C}$ | (18.87)$^{D}$ | (490.8)$^{A}$ | (490.8)$^{A}$ | (533.1)$^{B}$ | (547.8)$^{B}$ |

### 2.2.5 Model simulation analysis

The HETEROFOR model generates many fluxes and stocks of carbon and water as outputs. For this study, we focus on the actual and potential tree transpiration (obtained without considering any limitation from soil water) to determine the transpiration deficit, the daily foliage status of each tree species to calculate the vegetation period length and the yearly NPP to characterize forest productivity.

From the daily foliage status, the yearly vegetation period length was defined as the number of days between the day the green leaf proportion reaches 50% (budburst period) until the day it drops below this threshold (yellowing and then falling periods). Annual stand NPP values ($gC.m^{-2}$) were simply the sum of individual tree NPP (gC) divided by the stand area ($m^2$), with NPP derived from GPP after accounting for the growth and maintenance respirations (sect. 1.3.5 in Chap. 2). The annual transpiration deficit was calculated for each tree as the difference between actual and potential transpiration (in L). Then, individual transpiration deficits were summed and divided by the stand area to obtain a transpiration deficit in mm. As described in Chap.2 (Eq. 113 in sect. 1.3.10), the stomatal conductance is considered as decreasing exponentially with the soil water potential in the model. Therefore, this difference depicts the transpiration deficit induced by the soil water limitation. Using the vegetation period and the transpiration deficit is interesting since these variables are sufficiently integrative to summarize the model functioning but not too general so that we can disentangle the effect of two main mechanisms through which climate change affects forest ecosystems functioning (phenology and water).

In order to compare stand NPP, transpiration deficit and vegetation period (objective I) among RCP scenarios and time periods (1976–2005 for past climate and 2011-2040, 2041-2070 and 2071-2100 for the future climate), we used two different statistical tests to assess whether the distributions were significantly different. An unpaired Mann-Whitney test (Wilcoxon, 1945) was performed when the two periods were not related (e.g. for the comparison of the 1976-2005 and 2041-2070), while a Wilcoxon signed-rank test (Wilcoxon, 1945) was used when comparing RCP scenarios for a same period. These tests were chosen given the non-normality of the investigated variables. The Wilcoxon signed-rank test was also adopted to assess the effect of thinning on transpiration deficit. In order to test the equality of variance among distributions, a Levene test was performed as it is less sensitive to non-normality than other commonly-used tests.

To differentiate the long-term effect of climate change on NPP from that of the inter-annual climate variability (objective II) while taking the site effect into account (objective III), a linear mixed model was fitted on the simulated stand NPPs of the first simulation experiment including both thinning modalities. For a same location, the thinned and unthinned stands were considered as two different sites in the linear mixed models We have chosen to use linear mixed models to account for the correlation structure of the simulated dataset and to avoid an over-parameterization of the model (for parsimony reasons). Some factors were important to consider to estimate their relative importance in explaining the NPP variability and to represent correctly the correlation structure of the data. However, we did not need to know accurately the value taken by each level of these factors, which, therefore, were considered as random and characterized with a limited number of parameters (one parameter per factor instead of one per factor level). In contrast, we wanted to accurately quantify the effects of other factors which were considered as fixed. For this reason, in the first mixed model, the temporal trend of each RCP scenario (*Time* x *Scenario*) is considered as a fixed effect and the site (*Site*) and its effect on the temporal trend (*Site* x *Time* x *Scenario*) as random factor effects. This model was applied for both atmospheric $CO_2$ modalities.

$$NPP \sim [Time \text{ x } Scenario]_{fixed} + [Site + Site \text{ x } Time \text{ x } Scenario + \epsilon]_{random} \quad (3)$$

The continuous variable characterising the time effect is the number of years since 2011. In this way, no effect of the RCP scenario is considered in 2011, which allowed us to avoid considering the scenario as a main effect.

Besides, we adjusted another linear mixed model containing yearly vegetation period (*VP*), transpiration deficit (*TD*) and atmospheric $CO_2$ concentration (CO2) as fixed effects in addition to the effects already considered in the previous model (Eq. 3) in order to assess the extent to which these three variables accounted for the site effect, the long-term trend and the inter-annual variability:

$$NPP \sim [Time \text{ x } Scenario + \ VP + TD + CO2]_{fixed} + [Site + Site \text{ x } Time \text{ x } Scenario + \epsilon]_{random} \quad (4)$$

This model was applied for both atmospheric $CO_2$ modalities, except that the atmospheric $CO_2$ concentration was logically not considered for the modality with constant atmospheric $CO_2$ concentration.

Using the outputs of the second simulation experiment, a linear mixed model was applied to decompose the site effect in its climate, soil and stand components (objective IV). Three random factors were used to characterise the site components.

$$NPP \sim [Climate + Soil + Stand + \epsilon]_{random} \quad (5)$$

Finally, to estimate how transpiration deficit and vegetation period accounted for the three components of the site effect, we fitted a linear mixed model containing these two drivers as fixed effects in addition to the effects considered in Eq. 5.

$$NPP \sim [VP + TD]_{fixed} + [Climate + Soil + Stand + \epsilon]_{random} \quad (6)$$

For all the effects in the various models, the partial $R^2$ was calculated as the difference between the $R^2$ of the model with and without the considered effect. This method assumes that the effects are independent. As, in reality, this not always the case, the sum of the partial $R^2$ can be lower than the $R^2$ of the full model. All the figures, statistical tests and linear mixed models were realised using R Studio software (RStudio Team, 2015).

## 3. RESULTS

### 3.1. OBJECTIVE I: CLIMATE CHANGE IMPACT ON NPP, TRANSPIRATION DEFICIT AND VEGETATION PERIOD

*Net primary production (NPP)*

The differences in NPP between the RCP scenarios were generally non-significant when the atmospheric $CO_2$ concentration was kept constant. For this modality, the only significant difference with the historical period occurred between 2041 and 2070 for the RCP4.5 and 8.5 scenarios and remained limited: an increase of 3 and 5%, respectively (Fig. 4.1a). The site-by-site examination of the NPP projections revealed that the only sites with a significant positive effect of the RCP scenarios were Baileux-oak (RCP4.5 between 2071 and 2100) and Chimay (RCP4.5 and 8.5 for the 2041-2070 period and RCP8.5 during the 2071-2100 period) (Fig. 4.S1).

For the simulations accounting for the time-dependent atmospheric $CO_2$, NPP increased significantly over time, especially for the scenarios with the higher $CO_2$ emission levels in 2100. Upon comparison with the historical period, NPP in 2071-2100 increased by 9%, 20% and 34% for RCP2.6, 4.5 and 8.5, respectively (Fig. 4.1b). The trends were similar for the different sites taken individually (Fig. 4.S2). The impact of climate change on NPP cannot be based solely on the change in its median value. The variability is a key component of the temporal evolution as well. However, as depicted by the boxplot width and whisker length of Fig. 4.1 and confirmed by the Levene tests, no consistent increase in NPP variability was observed in our simulations.

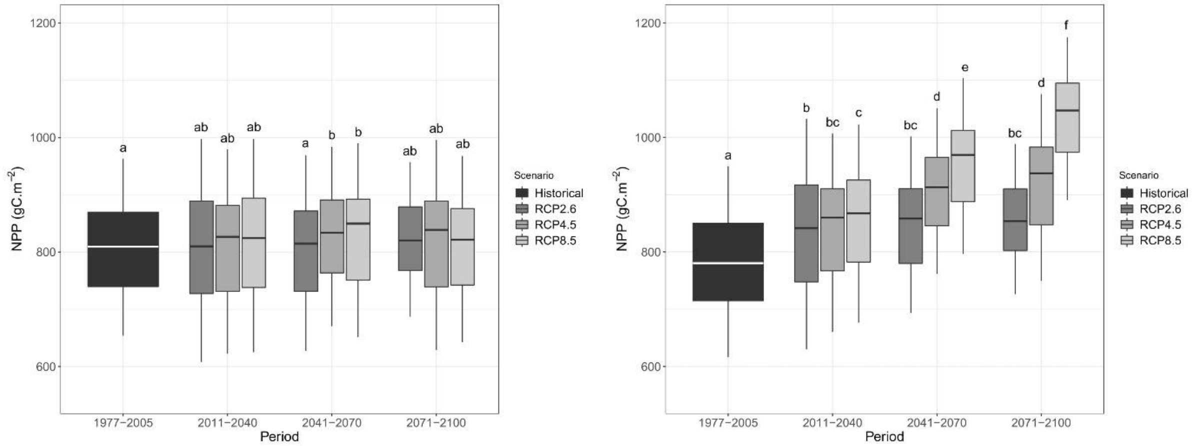
a. Constant atmospheric $CO_2$ concentration

b. Time-dependent atmospheric $CO_2$ concentration

**Figure 4.1: NPP comparisons among RCP scenarios and with the historical period (1976-2005) for three 30-year periods considering all the sites together, with constant (a) and time-dependent (b) atmospheric $CO_2$ concentrations. The horizontal line corresponds to the median, the box ends indicate the upper and lower quartiles and the whiskers show the values above and below these quartiles within 1.5 interquartile. Common letters indicate that the distributions are non-significantly different according to a paired Wilcoxon signed-rank (between scenarios of the same period) or an unpaired Mann-Whitney (between scenarios of different periods) tests.**

*Transpiration deficit*

The results obtained for transpiration deficit were identical for the constant and time-dependent atmospheric $CO_2$ concentration since the way stomatal conductance for water was calculated does not account for the atmospheric $CO_2$ concentration effect. Therefore, only those of the constant atmospheric $CO_2$ were presented (Fig. 4.2a). Transpiration deficit did not change in comparison with the historical period during the 2011-2040 period. During the next period, the RCP2.6 and 8.5 scenarios displayed a significant increase in transpiration deficit of 24% and 19%, respectively. For this period, the only inter-scenario difference occurred between RCP2.6 and 4.5. During the last period, all scenarios were different from each other and the RCP4.5 and 8.5 scenarios showed respectively a 21% and 42% increase in transpiration deficit compared to the historical period (Fig. 4.2a). The analysis of the temporal change in actual and potential transpiration enabled us to get a better insight in the origin of the transpiration deficit. It appeared that both variables were characterized by an increasing trend, but with a more pronounced one for potential transpiration. The augmentation in actual transpiration ranged from 2.7% to 10.2% during the last period (2071-2100) while the rise in potential transpiration varied from 3.4% to 19.8% (Fig. 4.S3).

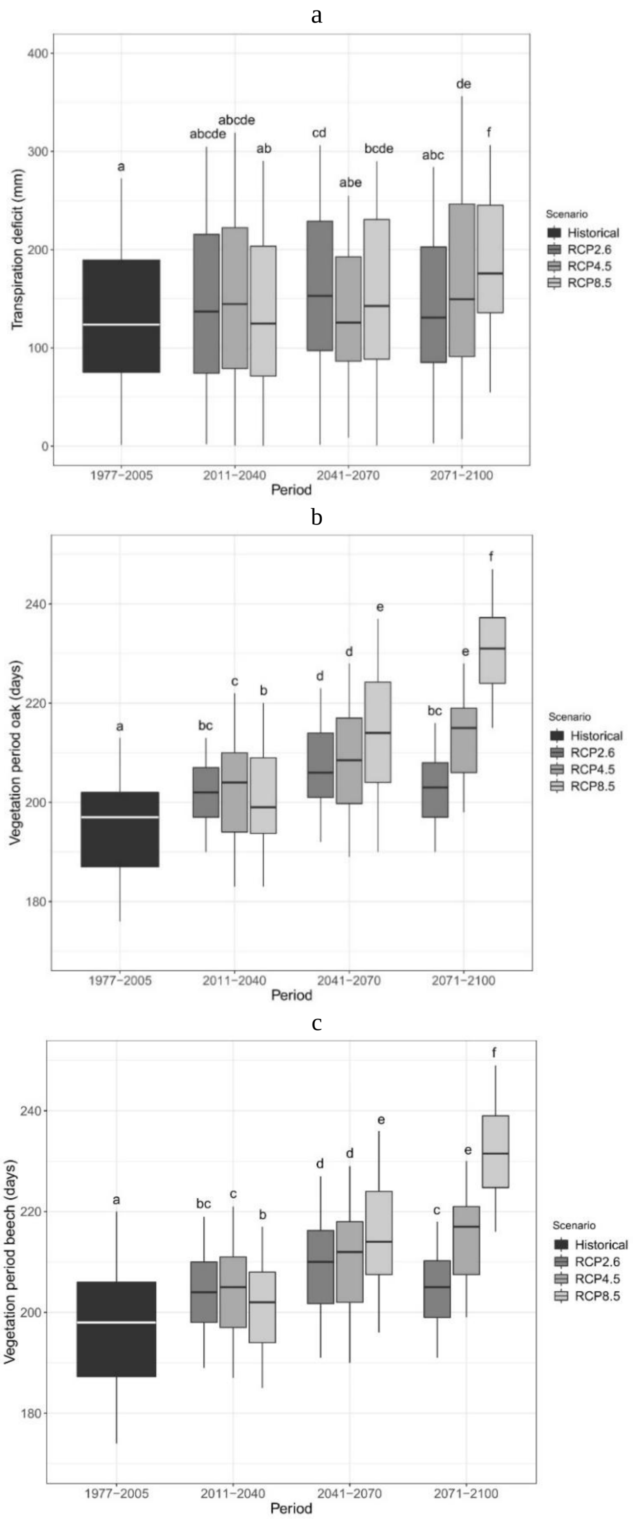

**Figure 4.2: Transpiration deficit (a), vegetation period of Sessile oak (b) and European beech (c) comparisons among RCP scenarios and with the historical period (1976-2005) for three 30-year periods considering all the sites together, with constant atmospheric $CO_2$ concentrations. The horizontal line corresponds to the median, the box ends indicate the upper and lower quartiles and the whiskers show the values above and below these quartiles within 1.5 interquartile. Common letters indicate that the distributions are non-significantly different according to a paired Wilcoxon signed-rank (between scenarios of the same period) or an unpaired Mann-Whitney (between scenarios of different periods) tests.**

*Vegetation period*

As phenology is not $CO_2$ dependent in the HETEROFOR model, no distinction was made between atmospheric $CO_2$ modalities. Even though, the length of the vegetation period differed between oak and beech (206 days for oak and 209 days for beech), its temporal change due to climate change was very similar for both tree species. The vegetation period length increased significantly with time for RCP4.5 and 8.5 while, for RCP2.6, it peaked between 2041 and 2070 before returning to the 2011 – 2040 level in 2071 - 2100. The increase of the vegetation period length (calculated with regards to the last period) amounted to 0.6, 1.8 and 5.3 days per decade for RCP2.6, 4.5 and 8.5, respectively (Fig. 4.2b and 4.2c).

### 3.2. OBJECTIVE II: LONG-TERM TREND AND INTER-ANNUAL VARIATIONS OF NPP

When a constant atmospheric $CO_2$ concentration was considered for the model described by Eq. 3, no mean temporal trend in NPP was detected (*Time* x *Scenario*) though the random effect associated to this trend (*Site* x *Time* x *Scenario*) explained 34% of the variability. This means that the temporal trend oscillated around 0, being slightly positive in some sites and slightly negative in others. The rest of the site effect accounted for 39% of the NPP variability and the unexplained variability amounted to 27% (Table 4.4a).

For the simulations with changing atmospheric $CO_2$ concentrations, we observed a significant positive temporal trend dependent on both the RCP scenario (*Time* x *Scenario*) and on the site (*Site* x *Time* x *Scenario*). These two effects accounted for 22% and 24% of the NPP variability, respectively. The remaining site effect explained 32% of the NPP variability while the unexplained variability was slightly lower than the simulations with constant $CO_2$, accounting for 23% of the NPP variability (Table 4.4b).

**Table 4.4: Estimate, standard error, *P*-value and partial $R^2$ of the parameters of the mixed linear model (Eq. 3: NPP ~ Time*Scenario + Site + Site*Time*Scenario) used to differentiate the temporal trend from the inter-annual variability in NPP ($gC.m^{-2}$) for all sites, periods and RCP scenarios considering constant (a) and time-dependent (b) atmospheric $CO_2$ concentration.**

| | Estimate | Standard error | *P*-value | Partial $R^2$ |
|---|---|---|---|---|
| a. Constant atmospheric $CO_2$ concentration | | | | |
| Fixed effects | | | | |
| *Intercept* | 764.70 | 39.99 | <.0001 | / |
| *Time* x *Scenario[2.6,4.5,8.5]* | [-0.06,-0.07,0.06] | [0.07,0.08,0.08] | 0.460 | 0.000 |
| Random effects | | | | |
| *Site* | 0 | 138.13 | / | 0.392 |
| *Site* x *Time* x *Scenario[2.6,4.5,8.5]* | 0 | [0.05,0.15,0.13] | / | 0.336 |
| *Residuals* | 0 | 84.19 | / | 0.272 |
| Total explained | / | / | / | 0.728 |
| b. Time-dependent atmospheric $CO_2$ concentration | | | | |
| Fixed effects | | | | |
| *Intercept* | 777.24 | 41.38 | <.0001 | / |
| *Time* x *Scenario[2.6,4.5,8.5]* | [0.32,1.06,2.52] | [0.08,0.09,0.10] | <.0001 | 0.216 |
| Random effects | | | | |
| *Site* | 0 | 142.97 | / | 0.316 |
| *Site* x *Time* x *Scenario[2.6,4.5,8.5]* | 0 | [0.10,0.22,0.27] | / | 0.239 |
| *Residuals* | 0 | 85.84 | / | 0.229 |
| Total explained | / | / | / | 0.771 |

### 3.3. OBJECTIVE III: INFLUENCE OF ATMOSPHERIC $CO_2$ CONCENTRATION, TRANSPIRATION DEFICIT, VEGETATION PERIOD, SITE AND THINNING ON NPP

*Relative importance of atmospheric $CO_2$ concentration, transpiration deficit, vegetation period and site in explaining NPP variability*

For both atmospheric $CO_2$ modalities, when comparing the linear mixed models containing only the temporal trend and the site effect (Eq. 3) with those including also transpiration deficit, vegetation period and atmospheric $CO_2$ concentration (Eq. 4), one can observe that these variables explained the temporal trend (*Time* x *Scenario*) and its modulation by the site (*Site x Time* x *Scenario*) as well as all the inter-annual variability (*Residuals*). In addition, their inclusion slightly lowered the variability associated to the rest of the site effect. When atmospheric $CO_2$ concentration was held constant, the transpiration deficit effect was negative with a partial $R^2$ of 0.58 while the vegetation period effect was positive with a partial $R^2$ of 0.025 (Table 4.5a). For the time-dependent atmospheric $CO_2$ simulations, the transpiration deficit and vegetation period effects had the same sign as for the constant atmospheric $CO_2$ modality but their partial $R^2$ was lower (0.43 and 0.016 respectively) since the atmospheric $CO_2$ concentration also explained a significant part of the variability (partial $R^2$ = 0.22, Table 4.5b).

**Table 4.5: Estimate, standard error, *P*-value and partial $R^2$ of the parameters of the mixed linear model (Eq. 4: NPP ~ Time*Scenario + VP + TD + CO2 + Site + Site*Time*Scenario) used to explain the NPP ($gC.m^{-2}$) variability based on transpiration deficit, vegetation period and $CO_2$ (only for time-dependent $CO_2$ modality) for all the sites, periods and RCP scenarios considering constant (a) and time-dependent (b) atmospheric $CO_2$ concentration.**

| | Estimate | Standard error | *P*-value | Partial $R^2$ |
|---|---|---|---|---|
| a. Constant atmospheric $CO_2$ concentration | | | | |
| Fixed effects | | | | |
| *Intercept* | 506.70 | 21.74 | <.0001 | / |
| *Time* x *Scenario[2.6,4.5,8.5]* | [0.01,0.04,0.09] | [0.04,0.05,7.64] | 0.748 | 0.000 |
| *Vegetation period* | 2.18 | 0.08 | <.0001 | 0.025 |
| *Transpiration deficit* | -1.30 | 0.01 | <.0001 | 0.582 |
| Random effects | | | | |
| *Site* | 0 | 55.69 | / | 0.365 |
| *Site* x *Time* x *Scenario[2.6,4.5,8.5]* | 0 | [0.05,0.12,26.5] | / | 0.026 |
| *Residuals* | 0 | 39.54 | / | 0.002 |
| Total explained | / | / | / | 0.998 |
| b. Time-dependent atmospheric $CO_2$ concentration | | | | |
| Fixed effects | | | | |
| *Intercept* | 358.68 | 23.56 | <.0001 | / |
| *Time* x *Scenario[2.6,4.5,8.5]* | [0.15,0.56,1.08] | [0.04,0.07,12.26] | 0.310 | 0.001 |
| *Vegetation period* | 2.48 | 0.08 | <.0001 | 0.016 |
| *Transpiration deficit* | -1.30 | 0.01 | <.0001 | 0.432 |
| *$CO_2$ concentration* | 0.261 | 0.03 | <.0001 | 0.220 |
| Random effects | | | | |
| *Site* | 0 | 56.38 | / | 0.299 |
| *Site* x *Time* x *Scenario[2.6,4.5,8.5]* | 0 | [0.05,0.11,42.5] | / | 0.031 |
| *Residuals* | 0 | 42.69 | / | 0.001 |
| Total explained | / | / | / | 0.999 |

*Thinning effect on transpiration deficit*

Transpiration deficit was much higher in beech-dominated (between 205 and 267 mm) than in oak-dominated stands (between 75 and 104 mm) and this was observed after thinning as well (Fig. 4.3). Thinning significantly decreased transpiration deficit in all situations (*P* value < 0.001). For the historical period, RCP2.6, 4.5 and 8.5, the transpiration deficit in the thinned oak-dominated stands was 30, 34, 32 and 39 mm lower than in the unthinned ones (Fig. 4.3a) while in beech-dominated stands, this decrease amounted to 65, 82, 76 and 91 mm, respectively (Fig. 4.3b). The relative decrease was, however, more similar between the two tree species with a decrease between 35 and 40% for oak and between 32 and 34% for beech.

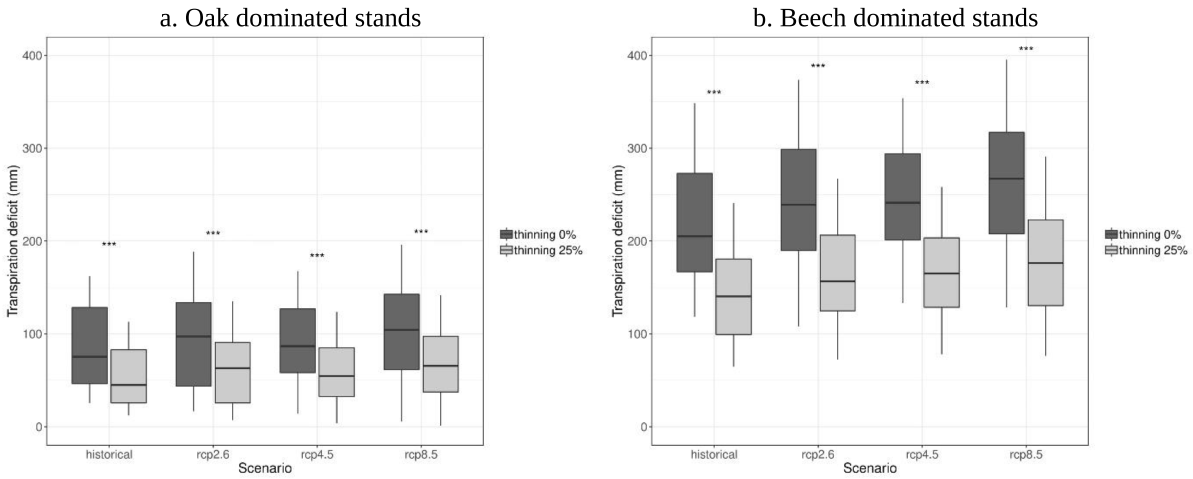
a. Oak dominated stands

b. Beech dominated stands

**Figure 4.3: Thinning effect on transpiration deficit for the historical period (1976-2005) and the three RCP scenarios (2011-2100) considering a constant atmospheric $CO_2$ concentration. Results are shown separately for oak dominated stands (Baileux-oak and Chimay) (a) and beech dominated stands (Baileux-beech, Louvain-la-Neuve and Virton) (b). Significance of the Wilcoxon test evaluating the thinning effect by climate scenario is represented as NS (non significant), * (p<0.05), ** (p<0.01) and ***(p<0.001).**

## 3.4. OBJECTIVE IV: DECOMPOSITION OF THE SITE EFFECT IN ITS CLIMATE, SOIL AND STAND COMPONENTS

The second simulation experiment, aiming at decomposing the site effect in its climate, soil and stand components, was performed for two contrasted periods and RCP scenarios (i.e., the 1977-2005 historical period *vs* the 2071-2100 period for the RCP8.5 scenario). As the results were quite similar among periods, only the results for the historical period are presented. The stand and soil partial $R^2$ were close and amounted to 0.321 and 0.264, respectively, and were much higher than that of the climate effect (0.016) (Eq. 5). Introducing the transpiration deficit and the vegetation period in the model (Eq. 6) accounted for nearly the entire climate (94%) and soil (98%) effects but only partly for the stand effect (7%). The consideration of these drivers also strongly reduced the unexplained part of the variability (from 40% to 7%). The transpiration deficit had a negative effect while the impact of vegetation period was positive, with a much higher partial $R^2$ for transpiration deficit (0.536) than for vegetation period (0.057) (Table 4.6).

**Table 4.6: Estimate, standard error, *P*-value and partial R² of the parameters of (a) the mixed linear model (Eq. 5: NPP ~ Stand + Soil + Climate) and (b) the mixed linear model (Eq. 6: NPP ~ VP + TD + Stand + Soil + Climate) used to decompose the site effect in its climate, soil and stand components in order to explain the NPP ($gC.m^{-2}$) variability for all the sites during the historical period, using simulations with constant atmospheric $CO_2$ concentration.**

| | Estimate | Standard error | *P*-value | Partial R² |
|---|---|---|---|---|
| a. Historical period | | | | |
| Random effects | | | | |
| *Stand* | 0 | 72.38 | / | 0.321 |
| *Soil* | 0 | 69.33 | / | 0.264 |
| *Climate* | 0 | 18.19 | / | 0.016 |
| *Residuals* | 0 | 82.57 | / | 0.397 |
| Total explained | / | / | / | 0.603 |
| b. Historical period | | | | |
| Fixed effects | | | | |
| *Intercept* | 305.11 | 39.94 | < .0001 | / |
| *Transpiration deficit* | -1.30 | 0.014 | < .0001 | 0.536 |
| *Vegetation period* | 3.45 | 0.067 | < .0001 | 0.057 |
| Random effects | | | | |
| *Stand* | 0 | 85.78 | / | 0.299 |
| *Soil* | 0 | 34.69 | / | 0.006 |
| *Climate* | 0 | 7.75 | / | 0.001 |
| *Residuals* | 0 | 46.04 | / | 0.072 |
| Total explained | / | / | / | 0.928 |

## 4. DISCUSSION

*What are the possible evolutions of broadleaved forest NPP according to different climate projections?*

At first glance, our results appear quite clear and easy to interpret. When the atmospheric $CO_2$ level was held constant, no long-term changes were observed but upon changing atmospheric $CO_2$, NPP increased up to 34% for the 2071-2100 period. However, using a process-based model with many different outputs gave us the opportunity to understand more deeply the underlying mechanisms.

Based on the bias-corrected downscaled climate projections of ALARO-0 for our four sites in Wallonia, mean air temperature is expected to be significantly higher during the 2071-2100 period compared to the historical period (from 0.7 °C to 3.4 °C) while mean annual rainfall would remain stable or increase a bit. During the vegetation period, rainfall would slightly decrease but this decrease would be significant only for Virton under RCP4.5 scenario (Table 4.3). According to our simulations, these changing climate conditions would substantially increase the vegetation period (Fig. 4.2b and 4.2c) since the budburst is triggered earlier when late winter temperatures are warmer while leaf yellowing occurs later under warm conditions. The decrease of the vegetation period length between 2041-2070 and 2071-2100 for RCP2.6 scenario might look surprising but it is simply generated by the scenario that projects a temperature peak around the middle of the 21st century and a subsequent progressive decrease. Some limitations concerning the phenology date simulations are discussed hereafter. First, the budburst model is a one-phase model that only accounts for the accumulation of warm temperature to trigger budburst while it is commonly accepted that a chilling period is a prerequisite for the start of forcing period (corresponding to the endodormancy break) and then budburst. However, when no observations of endodormancy break are available and the species considered are not located at the margin of their species distribution area, one-phase models are often preferred to more complex ones (Chuine et al., 2016). In addition, our approach does not account for the impact of photoperiod on budburst, which can become significant when chilling requirements are not met (Vitasse and Basler, 2013; Pletsers et al., 2015), the influence of late frost or water stress on the leaf development and senescence (Sanz-Perez and Castro-Diez, 2010; Fu et al., 2014; Morin and Chuine, 2014; Xie et al., 2018). However, as shown in the review of Piao et al. (2018), the modelling of these second order processes is extremely difficult and inaccurate because the interactions between these factors are still poorly known, observations are available only for a few phenological stages and environmental modifying experiments have not been conducted to disentangle such a complexity.

In addition to the strong impact of climate change on the vegetation period, the model simulates that the transpiration deficit could be moderately reinforced through an increased evapotranspiration (Fig. 4.2a). As the transpiration deficit was a stronger NPP driver than the vegetation period (Table 4.5 and 4.6), their opposite effects on the long-term trends in NPP had more or less the same magnitude and were compensating. However, the long-term NPP evolution was slightly affected by the site: it tended to be slightly negative (positive) in sites with a low (high) soil holding capacity and for drought-sensitive (-tolerant) tree species such as beech (oak) (Fig. 4.S1). Furthermore, by reducing the transpiration deficit, thinning contributed to make the climate change effect on NPP more positive. As the oak stomatal sensitivity to soil drying is lower than that of beech, the simulated impact of climate change was rather positive on oak and null on beech-dominated stands, which is consistent with simulation studies estimating that oak competitiveness could exceed that of beech under the projected future climate conditions in temperate European forests (Kint et al., 2012; Mette et al 2013; Zimmermann et al 2013; Rubio-Cuadrado et al 2018).

With our simulations, we were unable to distinguish between the transpiration deficit under constant and time-dependent atmospheric $CO_2$ concentration since the water balance is calculated before photosynthesis in HETEROFOR and the stomatal conductance for water does not depend on atmospheric $CO_2$ concentration contrary to that for $CO_2$ (Dufrêne et al., 2005; Jonard et al., 2020; de Wergifosse et al., 2020). Therefore, our transpiration simulations are more reliable for the constant atmospheric $CO_2$ modality. For the time-dependent $CO_2$ modality, tree transpiration is probably slightly overestimated so that the increase in the transpiration deficit could still be lower than that simulated with HETEROFOR which is already limited. According to our simulations, water stress on Walloon broadleaved forests should not drastically increased in the future.

As stated in the description of the first simulation experiment (section 2.2.2), the objective of running two similar sets of simulations with constant and changing atmospheric $CO_2$ concentrations was to define a possible range of NPP change depending on the way the fertilizing effect of $CO_2$ is constrained by other limiting factors. As soil water limitation was taken into account in the model, the more obvious constraint would come from the soil nutrient supply. The increased atmospheric $CO_2$ could potentially have no effect in sites where trees suffer from severe nutrient deficiencies. The $CO_2$ fertilization, on the other hand, would be manifested in full for stands with an optimal mineral nutrition (Oren et al., 2001 and Fernandez-Martinez et al., 2014). On average, this $CO_2$ fertilizing effect seems already constrained by nutrient availability since many European tree species, especially European beech and oak are experiencing significant deterioration of their foliar nutrition (Jonard et al., 2015). Therefore, among our study sites, the plots in Chimay, Virton and Louvain-la-Neuve that already display some latent deficiency regarding P concentrations (Titeux et al., 2018) should behave closer to the simulations with constant $CO_2$ than the Baileux plots which present better foliar nutrition. On another hand, one could also consider that a decreased soil water content would reduce nutrient availability and consequently NPP but this aspect is not taken into account in this study. However, as the simulated increase in transpiration deficit is limited, one can consider that the impact on nutrient availability would remain very low.

The dominant effect of the $CO_2$ fertilization in the long-term trend of forest productivity is consistent with similar studies. In his global review mainly focused on temperate and boreal forests in Europe and North America, Reyer (2015) showed that, for the simulation studies in which the atmospheric $CO_2$ levels were held constant, the simulated NPP change with regards to reference conditions varied between -20 and +33% for a median value of +5%. When both climate change and atmospheric $CO_2$ rise were taken into account, most of the simulated biomass production increased relative to the historical period. In our simulations, when the atmospheric $CO_2$ was maintained constant, the NPP increase ranged from 0.1 to 5.0% (Fig. 4.1a), which is close to the value pointed out in the abovementioned review. When the atmospheric $CO_2$ concentration changed, the NPP increase was between 7.8 and 34.2% (Fig. 4.1b), which is again in good agreement with Reyer (2015) that displayed a median value 20% higher than that of the historical period.

Fernandez-Martinez et al. (2014) analysed an extensive global dataset and showed that NPP was mainly determined by water availability, warm period length and nitrogen deposition. These results, which come from temporally averaged measurements and therefore reflect spatial rather than temporal patterns, can be considered as a spatial corollary of our results that highlight the significance of the same variables or related ones.

We have mainly discussed here the average impact of climate change. However, many papers highlight the importance of extreme heat and drought waves on tree growth and mortality (Fuhrer et al., 2006; Lindner et al., 2010; Allen et al., 2010; Teskey et al., 2015). These extreme events are important because tree functioning is a complex set of non-linear mechanisms where threshold exceedance can generate feedbacks and totally deregulate their functioning (Thompson, 2011; Reyer et al., 2015; D'Orangeville et al., 2018). In HETEROFOR, the leaf-level processes (photosynthesis, respiration, and transpiration) are climate dependent and take the impact of heat or drought waves into account, especially on tree growth. In addition, as most processes in HETEROFOR are calculated at the hourly time scale, temperature peaks are not smoothed as in models working at the daily or monthly time scale. The impact of these extreme climate events is, however, only partly accounted for since mortality by hydraulic failure and leaf shedding is not considered. Furthermore, tree mortality driven by pests and diseases which is often promoted by a succession of drought and heat waves (Allen et al., 2010) is not yet included in HETEROFOR. This could partly explain why we did not observe any changes in NPP variability in our simulations between the different scenarios and time periods. Moreover, as these elements are mostly detrimental, our simulation results should be seen as the upper estimates for NPP.

*What can be learnt from the decomposition of the NPP variability?*

The main originality of our study is the decomposition of the NPP variability, which allows estimating the relative importance of the temporal trend compared to the inter-annual variations and evaluating the extent to which site components (climate, soil and stand) could modulate the impact of climate change on NPP. The part of the NPP variability explained by the stand effect gives an idea of the leeway left to forest managers to adapt the forests to changing conditions. Furthermore, this is of primary concern for forest managers because NPP can be considered as closely related to the timber volume under the hypothesis of allometry conservation and as a good proxy for forest health and the provision of most of the ecosystem services (e.g. Costanza et al., 1998; Dobbertin, 2005; Costanza et al., 2007; Van Oudenhoven et al., 2012; Vargas et al., 2019).

When the atmospheric $CO_2$ was kept constant, no overall temporal trend was observed but considering a trend randomly changing with the site explained 34% of the variability (Eq. 3 and Table 4.4a). This random effect was ascribed to differences in soil water properties and in tree species sensitivity to drought and phenology since it almost totally disappeared when the transpiration deficit and the vegetation period were included in the linear mixed model (Eq. 4 and Table 4.5a). These factors accounted also for some of the site effect that decreased from 39.2 to 36.5%. The remaining 'unexplained' variability (27%) was mainly due to inter-annual climate variations since it totally vanished when the transpiration deficit and the vegetation period were added in the model (Table 4.4a, Table 4.5a). Among these two drivers, the transpiration deficit had a much greater explanatory power than the vegetation period (partial $R^2$ of 0.582 vs 0.025).

Using a time-dependent atmospheric $CO_2$ concentration generated a strong temporal trend. This temporal trend accounted for 22% of the NPP variability while its modulation by the site explained another 24% (Eq. 3 and Table 4.4b). The integration of the atmospheric $CO_2$ concentration, the transpiration deficit and the vegetation period in the linear mixed model made disappear the entire temporal trend and most of its variation among sites (3% remaining after the inclusion). The part of the variability explained by the atmospheric $CO_2$ concentration corresponded exactly to that associated to the temporal trend (22%) (Eq. 4 and Table 4.5b). The site-dependent component of the trend was mainly ascribed to differences in transpiration deficit among sites with a minor role also played by the vegetation period. The rest of the NPP variability associated to the site amounted to 30%. As for the constant atmospheric $CO_2$ modality, we considered that the remaining 'unexplained' variability (23%) was mainly due to inter-annual climate variations since it disappeared when the transpiration deficit and the vegetation period were added in the linear mixed model (Table 4.4b, Table 4.5b). In this case, the transpiration deficit had also a much higher explanatory power than vegetation period (43% *vs* 2%).

Interchanging the climate, soil and stand files for the historical period under constant $CO_2$ concentration allowed us to get a deeper understanding of the site effect. According to Table 4.6a (Eq. 5) when they were the only variables included, the stand and soil components had a similar contribution in explaining the site effect (32 and 26%, respectively) while the part explained by differences in climate among sites was very low (1.6%). This was however not surprising as we examined a broad range of soils and stands but a much narrower range of climates. Anyway, integrating the transpiration deficit and the vegetation period in the linear mixed model explained most of the soil effect (which dropped to 0.6%) but only a little part of the stand effect, which remained at 30% (Eq. 6 and Table 4.6b). These 30% represent the amount of freedom the forest managers have to influence the forest productivity under the current climate conditions. For the future, one must also consider the interaction between the site effect and the climate change (including atmospheric $CO_2$) whose relative importance in explaining the NPP variability is of the same order of magnitude than the site effect (Table 4.4). Foresters can also act on the transpiration deficit through tree species selection and thinning even if transpiration deficit is also strongly determined by climate conditions and soil water properties.

In all stands, thinning significantly decreased the transpiration deficit and this decrease was much more pronounced in beech-dominated stands. Still, the transpiration deficit levels before and after thinning were lower in oak-dominated than in beech-dominated stands (Fig. 4.3). This positive short-term effect of thinning on a stand response to drought was pointed out by various studies. For example, a Douglas-fir stand showed a decrease in evapotranspiration of 30 mm (17%) during the first year after thinning. This effect was progressively reduced during the next four years before evapotranspiration returned to its original level (Aussenac and Granier, 1988). For broadleaved species, a meta-analysis highlighted the potential of thinning to mitigate growth reduction during drought events by increasing soil water availability (Sohn et al., 2016). As a result, thinning seems to be an interesting practice to reduce the projected increase in transpiration deficit and its detrimental effect on tree growth, especially for drought-sensitive tree species. However, one must keep in mind that thinning has a transitory effect and that its impact on drought resistance progressively decreases (Guillemot et al., 2015; Sohn et al., 2016). Thinning abruptly modifies stand characteristics and forest functioning due to tree removal. Then, the remaining trees react by expanding their crown and increasing their growth rate benefiting from the higher availability of resources per tree. With time, the openings in the canopy close and the effect of thinning decreases. In this study, we simulate the first year after the thinning when its effect is maximal and when the tree dimensions (especially the crown extension) are still those that characterize a stand with a higher density. Finally, in addition to thinning, some efforts to promote oak regeneration could also be recommended to increase the stand resistance to drought as this tree species is more drought tolerant.

## 5. CONCLUSION

Understanding how NPP is going to be affected in the future due to environmental changes is crucial in order to create consistent climate change adaptation strategies and preserve the forest ecosystem services. This paper aimed at assessing, for six Belgian stands, the temporal change in NPP and in two of its main drivers: transpiration deficit and vegetation period length. Concomitantly, the influence of the $CO_2$ fertilization effect and the impact of thinning operations were evaluated. We did not detect any trend under the three contrasted GHG emission scenarios (RCP2.6, 4.5 and 8.5) when atmospheric $CO_2$ concentration was held constant but NPP showed a significant increase ranging from 9.4 to 34.2% for the time-dependent atmospheric $CO_2$ concentration. Behind the apparent lack of temporal trend in NPP for simulations with constant atmospheric $CO_2$ lies a compensatory effect of the transpiration deficit that slightly increased with time and had a pronounced negative effect on NPP and the vegetation period that became substantially longer but with a less marked impact on NPP. The site effect modulated these temporal trends and accounted for a substantial part of the NPP variability, which is encouraging for forest managers who have still a lot of possibilities to adapt their forest to changing conditions. Among others, thinning appeared very effective to decrease transpiration deficit, especially in beech-dominated stands. Forest practitioners could regularly decrease stand density or promote oak regeneration to limit the negative effect of the transpiration deficit. In the future, we plan to extend our methodology at the European scale to expand the validity of our results.

## 6. SUPPLEMENTARY MATERIALS

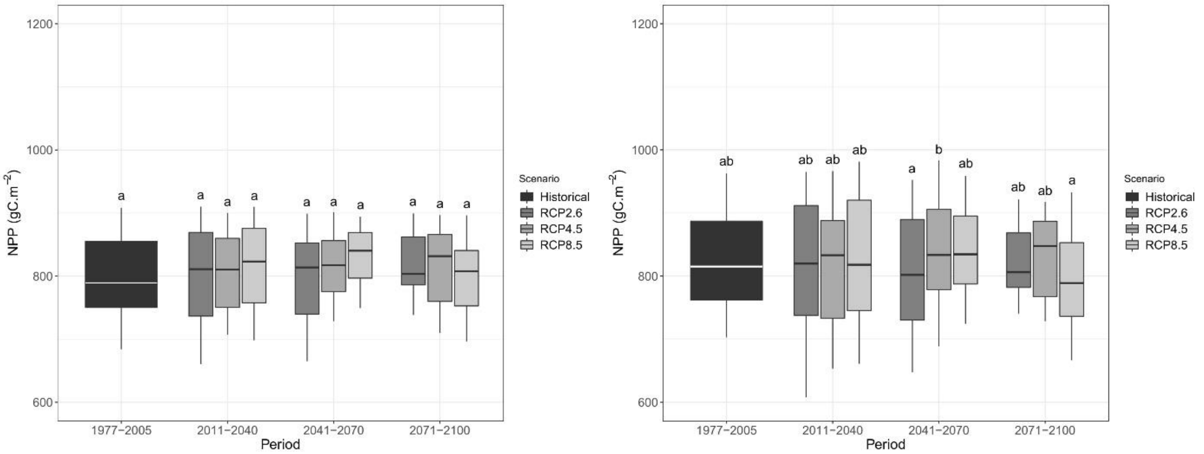

a. Baileux-beech

b. Baileux-mixed

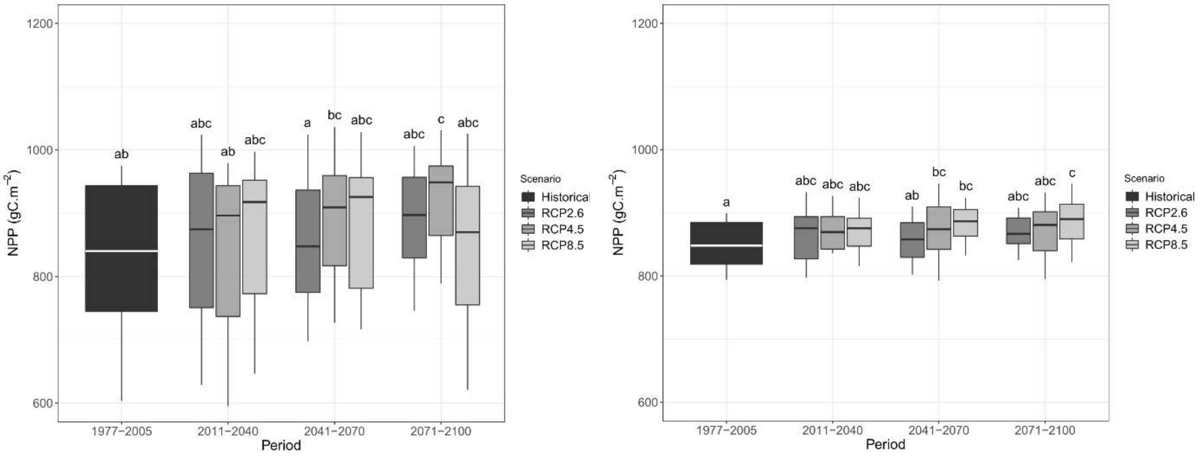

c. Baileux-oak

d. Chimay

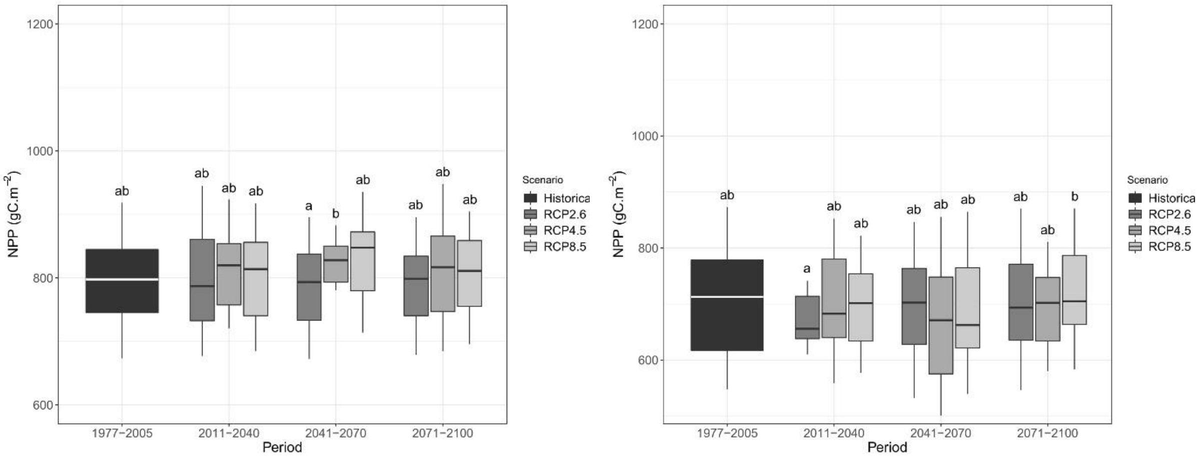

e. Louvain-la-Neuve

f. Virton

**Figure 4.S1: NPP comparisons among RCP scenarios and with the historical period (1976-2005) for three 30-year periods in the different study sites and with constant $CO_2$ atmospheric concentrations. The horizontal line corresponds to the median, the box ends indicate the upper and lower quartiles and the whiskers show the values above and below these quartiles within 1.5 interquartile. Common letters indicate that the distributions are non-significantly different according to a paired Wilcoxon signed-rank (between scenarios of the same period) or an unpaired Mann-Whitney (between scenarios of different periods) tests.**

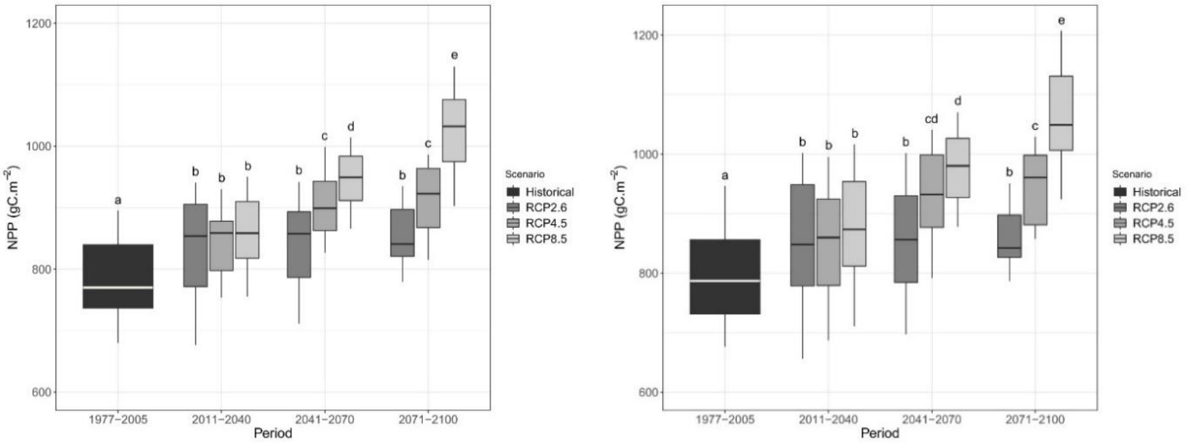
a. Baileux-beech

b. Baileux-mixed

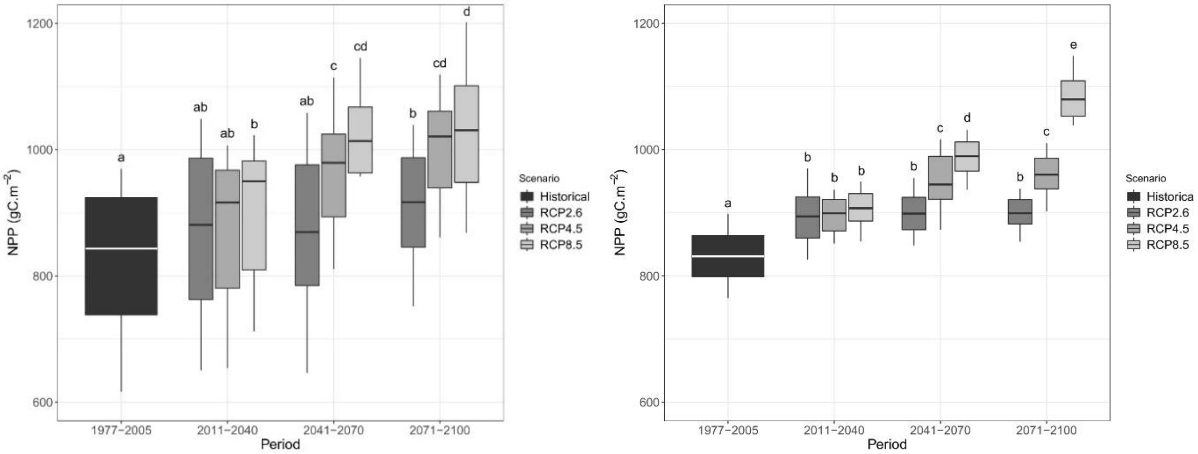
c. Baileux-oak

d. Chimay

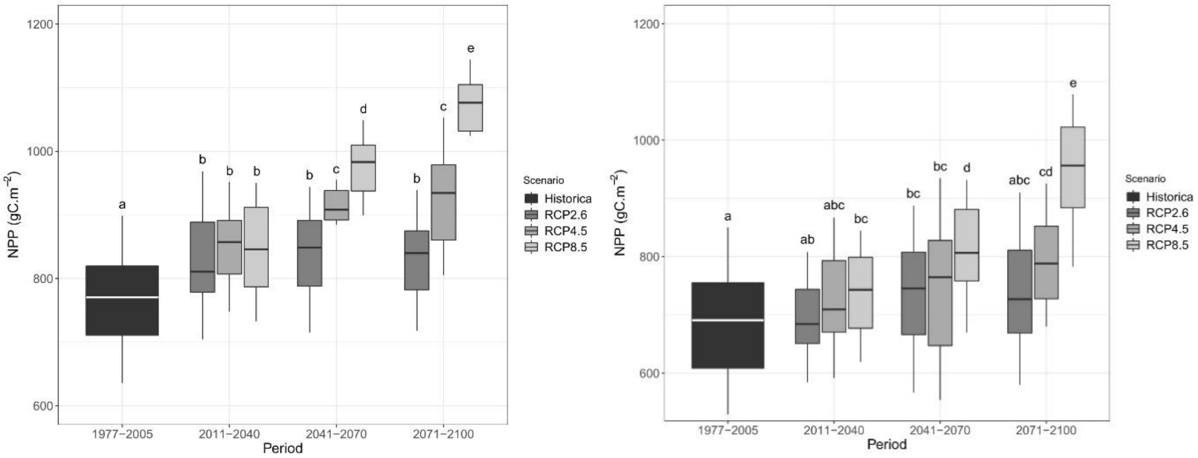
e. Louvain-la-Neuve

f. Virton

**Figure 4.S2: NPP comparisons among RCP scenarios and with the historical period (1976-2005) for three 30-year periods in the different study sites and with time-dependent $CO_2$ atmospheric concentrations. The horizontal line corresponds to the median, the box ends indicate the upper and lower quartiles and the whiskers show the values above and below these quartiles within 1.5 interquartile. Common letters indicate that the distributions are non-significantly different according to a paired Wilcoxon signed-rank (between scenarios of the same period) or an unpaired Mann-Whitney (between scenarios of different periods) tests.**

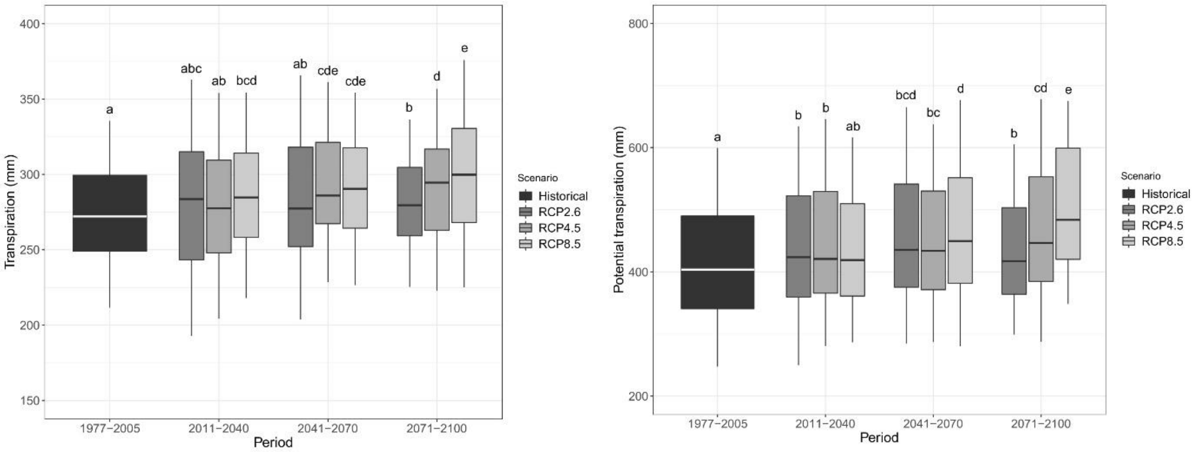

**Figure 4.S3: Actual transpiration (left) and potential transpiration (right) comparisons among RCP scenarios and with the historical period (1976-2005) for three 30-year periods in the different study sites and with constant $CO_2$ atmospheric concentrations. The horizontal line corresponds to the median, the box ends indicate the upper and lower quartiles and the whiskers show the values above and below these quartiles within 1.5 interquartile. Common letters indicate that the distributions are non-significantly different according to a paired Wilcoxon signed-rank (between scenarios of the same period) or an unpaired Mann-Whitney (between scenarios of different periods) tests.**

# Chapter 5

## SIMULATING TREE GROWTH RESPONSE TO CLIMATE CHANGE IN OAK AND BEECH STANDS THROUGHOUT EUROPE

## ABSTRACT

*This study aimed to simulate oak and beech forest growth under various scenarios of climate change and to evaluate how the forest response depends on site properties and particularly on stand characteristics using the individual process-based model HETEROFOR. First, this model was evaluated on a large diversity of stand structures and on a wide range of site conditions. We used the data from 36 long-term forest monitoring plots (ICP Forests and LTER) to initialize, calibrate, and evaluate HETEROFOR. This evaluation showed that HETEROFOR predicts individual tree radial growth and height increment reasonably well under different growing conditions when evaluated on independent sites.*

*In our simulations under constant atmospheric* $CO_2$ *concentration (*$[CO_2]_{cst}$*) for the 2071-2100 period, climate change induced a moderate net primary production (NPP) gain in continental and mountainous zones and no change in the oceanic climate zone. The NPP changes were negatively affected by air temperature during the vegetation period and by the annual rainfall decreases and the magnitude of the impact depended on the model used for the climate projections. To a lower extent, they were also influenced by soil extractable water reserve and stand characteristics. These NPP changes were positively affected by longer vegetation periods and negatively affected by drought for beech and larger autotrophic respiration costs for oak. For both species, the NPP gain was much larger when considering an increase in atmospheric* $CO_2$ *concentration (*$[CO_2]_{var}$*) mainly due to the* $CO_2$ *fertilization effect. Even if the species composition and structure had a limited influence on the forest response to climate change, both explained a large part of the NPP variability (44% and 34% for* $[CO_2]_{cst}$ *and* $[CO_2]_{var}$*, respectively) compared to the climate change scenario effect (5% and 29% for* $[CO_2]_{cst}$ *and* $[CO_2]_{var}$*, respectively) and to the inter-annual climate variability (20% and 16% for* $[CO_2]_{cst}$ *and* $[CO_2]_{var}$*, respectively). This gives the forester the possibility to act on the stand productivity of broadleaved forests and to prepare them for possible adverse effects of climate change by reinforcing their resilience.*

---

### 1. INTRODUCTION

In the future, European temperate broadleaved forests will experience warmer conditions, the magnitude of which will depend on the climate zone and the amount of anthropogenic greenhouse gas emissions. Higher temperature increases are likely to occur in mountainous (between 1.9 and 6.0°C depending on the climate scenario) and continental areas (between 1.6 and 5.2°C) than in the Atlantic area (between 1.4 and 3.6°C), the temperatures of which are buffered by the ocean proximity (Jacob *et al*., 2014 Coppola *et al.*, 2020). In addition, changes in rainfall regime are also expected with generally wetter winters, especially in the North of Europe but drier summers in the South (Spinoni *et al*., 2020; Coppola et al., 2020). Finally, heat waves, droughts and storms are likely to become more frequent and severe compared to the current observed climate (for more details, see Sillmann *et al*., 2013; Kovats *et al*., 2014; Spinoni *et al*., 2020).

European forests cover an area of 215 million ha, representing 33% of the continent. Temperate forest, roughly occupying Central-Western and Central-Eastern Europe, is the main forest type in Europe in terms of area and productivity and are dominated by broadleaved forests (FAO, 2020), mainly composed of European beech (*Fagus sylvatica* L.) and pedunculate or sessile oak (*Quercus robur* L. or *Quercus petraea* (Matt.) Liebl.) (De Rigo *et al*., 2016; Mauri *et al*., 2017; Buras and Menzel, 2018). Their distribution range is limited northward and eastward and in elevation due to their frost sensitivity (Lenz *et al*., 2016). The cold margin is approximately located where the average temperature of the coldest month is –3.5°C for European beech and sessile oak (Sykes *et al*., 1996). The xeric (dry) margin depends on both rainfall and temperature. For European beech, it corresponds to 500 mm when mean annual temperature (MAT) is 10°C and 650 mm for 12.5°C (Kölling, 2007). Oaks, which are more drought tolerant, can withstand lower mean annual precipitation (MAP: 450 mm) at sites with MAT up to 12°C (Kölling, 2007; Mette *et al*., 2016).

The combined effects of changes in atmospheric $CO_2$ concentration, air temperature, and rainfall will affect the growth of temperate broadleaved forests but the effects are expected to differ depending on whether the sites are located at the warm, cold or dry margin of their species distribution range (Jump *et al*., 2006; Goldblum, 2010; Santini *et al.*, 2014; Dulamsuren *et al*., 2017). Additionally, the stand (e.g. species composition, density, structure and development stage) and soil (e.g. water retention capacity, nutrient content) properties as well as atmospheric deposition will also modulate the climate change effect, which complicates the projections of the future state of the temperate forests (e.g. Boisvenue and Running, 2006; Reyer, 2015; Martin-Benito and Pederson, 2015; Noce et al., 2017; Anderegg *et al*., 2018).

Future response of European forests to climate change can be predicted using different modelling approaches, which are designed to answer specific questions at different spatial and temporal scales and using different initialization data (Ruiz-Benito *et al*., 2020; Reyer *et al*., 2020). With an approach based on plant functional types (PFTs) and a limited data requirement for model initialization, the dynamic global vegetation models (DGVMs) is a standard tool used to estimate the impact of climate change on the European or global forests (Cramer *et al.*, 2001; Poulter *et al*., 2011; Luyssaert *et al*., 2018). While essential to obtain continental or global estimates of carbon exchange, their predictions are however associated with considerable uncertainties, in particular at smaller scales (Schwalm *et al*., 2010; Huntzinger *et al*., 2017). At the regional scale, the forest landscape models (FLMs) provide information on how climate change affects long-term forest dynamics but have a simplified eco-physiological process description and coarse stand-level spatial representation due to their large-scale and long-term perspective (Reyer, 2015; Maréchaux *et al.*, 2021).

Process-based stand models were designed to account more in-depth for local environmental conditions (soil, climate, tree species) but generally without considering the within-stand heterogeneity and the tree-tree interactions (e.g. big leaf or average tree approaches; e.g. Collalti *et al.*, 2016). Given the detailed information needed to initialize and calibrate such models, they have generally been used on a restricted number of well-documented sites. During recent decades, the data collected in long-term forest monitoring networks (e.g. ICP Forests: International Co-operative Programme on Assessment and Monitoring of Air Pollution Effects on Forests, ICOS: Integrated Carbon Observation System in EU, eLTER; Long-Term Ecosystem Research in Europe) and in national forest inventories (NFIs) allowed extension of the application possibilities for such models.

Process-based stand models display good predictive ability for even-aged monocultures but the oversimplified spatial representation of the stand structure is problematic for studies in more complex stands. Yet, a large proportion of the European forest consists of more than two tree species (67%) and of uneven-aged stands (28%) (FAO, 2020). This shortcoming has partly been overcome by grouping the trees in cohorts of the same tree species and age while keeping a relatively simple spatial representation (cohort-based models). Still, the assumption of horizontal homogeneity in cohort-based models limits the possibility to fully account for the inter-tree variability and for the local environment conditions (Berger *et al*., 2008). To account for the spatial heterogeneity in structurally-complex stands, spatially explicit individual-based models are required but given the massive initial data requirement and the resulting computational time, the individual-based models (IBM) are used in a restricted number of case studies, which can limit their validity domains (Pretzsch *et al*., 2015). Despite their advantages and their complementarity with other models, very few studies have made use of these spatially explicit models to estimate the impact of future climate changes on forest growth. In addition, such projections with IBMs were achieved only on a limited number of sites (e.g. Rötzer et al., 2005; Rötzer et al., 2013; Simioni et al., 2016).

The HETEROFOR model has been specifically designed to simulate individual tree growth in structurally complex stands based on a resource-sharing approach and to test the ability of innovative silvicultural systems to improve forest resilience to climate change (de Wergifosse *et al*., 2020a; Jonard *et al*., 2020).

In this study, we assumed that calibrating a process-based model on a large range of ecological conditions will increase its generality and robustness for simulations under changing climatic conditions. Hence, we aimed to calibrate and evaluate the HETEROFOR model on contrasting site conditions benefiting from harmonised data collected in long-term monitoring networks (mainly ICP Forests level II plots and LTER sites). The calibrated and validated model was subsequently used:

(i) to simulate the response of sessile/pedunculate oak and European beech to climate change for a set of European sites covering a large range of environmental conditions (soil and climate) and stand characteristics;

(ii) to quantify the relative importance of the long-term climate change effects on tree growth compared to the inter-site and inter-annual variability;

(iii) to decompose the inter-site variability in its components (stand, soil and climate) and evaluate how it affects the response of tree growth to climate change.

## 2. MATERIAL AND METHODS

### 2.1. SITE DESCRIPTION

For the model evaluation, 36 forest monitoring plots distributed over Europe and covering a large range of ecological conditions were selected. The plot size ranges from 0.2 to 1.8 ha. Most of the plots (30) are part of the level II network of the ICP Forests programme (Ferretti and Fischer, 2013). This network aims to better understand the cause-effect relationships between forest condition and stress factors (e.g. air pollution) by means of intensive monitoring. The six remaining plots are located in Baileux (Wallonia/Belgium) and in Cansiglio (Italy). The three plots in Baileux were installed to study the impact of species mixture on forest ecosystem functioning. In Cansiglio, the three plots are part of the ManFor C.BD. project ("Managing forests for multiple purposes: carbon, biodiversity and socio-economic wellbeing"; LIFE09 ENV/IT/000078) which assesses how forest management affects carbon sequestration, biodiversity and socio-economic well-being.

All these plots were selected based on their species composition (broadleaved forests dominated by either sessile, pedunculate oak or European beech) and the data availability (for the model initialization) while seeking to maximize the diversity of stand types, soils and climates (Table 5.1 and 5.2). In the study, sessile and pedunculate oaks are not differentiated and will be called "oak" while European beech will be referred to as "beech" in the following.

The stands were classified according to their composition and structure. We considered a stand as pure when dominated by one species or when the main species represented at least 75% of the total basal area. The same threshold was used to distinguish even-aged (i.e. at least 75% of trees are in the same cohort) from uneven-aged stands. Among the 36 stands, 10 were classified as even-aged oak-dominated, 13 as even-aged beech-dominated, three as uneven-aged beech-dominated and 10 as uneven-aged mixed. In addition to the variability in species composition and stand structure, the stands were also very diverse in terms of mean trunk girth (42.4 to 176.6 cm), dominant height (16.9 to 36.8 m) and basal area (13.6 to 53.9 $m^2 ha^{-1}$) (Table 5.2).

Among the 12 classes of the soil textural triangle elaborated by the United States Department of Agriculture (Soil Science Division Staff, 2017), nine were represented in the study sites. This variability in soil texture explains some of the large range in maximum extractable water (154 to 594 mm) which is also due to variations in the coarse fraction (0 to 41%) and soil depths (1 to 1.6 m) (Table 5.1).

The 36 plots of the study are distributed to 32 sites with 10 in the continental, three in the mountainous and 19 in the oceanic temperate zones (see Simons *et al.* 2001 and FAO 2012; for climate zone definition). The climates covered by the study sites are representative of those encountered in the distribution range of oak and beech (Sykes *et al.*, 1996; Kölling, 2007), with MAT ranging from 4.8 to 12.9°C and MAP from 612 to 2153 mm (Table 5.1).

**Table 5.1: Climate and soil characteristics of the different study sites. Climate zones follow the FAO classification (FAO, 2012) while the soil texture is based on the textural triangle proposed by the USDA (Soil Science Division Staff, 2017). The function used to calculate the maximum extractable water is given in the equation 80 of de Wergifosse et al. (2020a). Mean annual air temperature (MAT) and rainfall (MAP) are provided for the period 1976-2005 and are the same for the two climate models, mean values for the vegetation period (fixed from the 1st of May to the 30th of September) are indicated between parentheses and are differentiated for the two climate models. The change in MAT and MAP for the period 2071-2099 considering the scenario RCP8.5 is similarly expressed annually and for the vegetation period (between parentheses) for the two climate models separately.**

|  | Site (country) | Plot ID (ICP) | Climate zone | Soil texture | Max extractable water over 1.6m (mm) | MAT (°C) (ALARO/RCA4) 1976-2005 | MAP (mm) (ALARO/RCA4) 1976-2005 | Δ MAT (°C) ALARO 2071-2099 | Δ MAP (mm) ALARO 2071-2099 | Δ MAT (°C) RCA4 2071-2099 | Δ MAP (mm) RCA4 2071-2099 |
|---|---|---|---|---|---|---|---|---|---|---|---|
| 1 | Baileux (BE) | - | Oceanic | Silt (clay) loam | 154-239 | 9.2 (15.2/14.5) | 950 (496/379) | 3.08 (2.81) | 176 (40) | 3.77 (4.28) | 161 (-103) |
| 2 | Chimay (BE) | 8 | Oceanic | Clay loam | 208 | 9.1 (15.2/14.4) | 911 (496/337) | 3.10 (2.83) | 178 (34) | 3.71 (4.20) | 246 (-72) |
| 3 | Eupen (BE) | 5 | Oceanic | Clay loam | 229 | 7.3 (13.4/12.8) | 965 (582/420) | 3.16 (2.85) | 165 (11) | 3.82 (4.21) | 152 (-63) |
| 4 | Gontrode (BE) | 16 | Oceanic | Loam | 309 | 10.3 (16.1/15.4) | 895 (509/404) | 2.90 (2.49) | 177 (46) | 3.31 (3.58) | 173 (-92) |
| 5 | Hoeilaart (BE) | 21 | Oceanic | Silt loam | 400 | 10.5 (16.4/15.7) | 779 (457/366) | 2.93 (2.54) | 168 (41) | 3.39 (3.69) | 110 (-94) |
| 6 | Louvain-la-Neuve(BE) | 9 | Oceanic | Silt loam | 427 | 10.4 (16.4/15.7) | 772 (451/356) | 3.00 (2.71) | 165 (39) | 3.54 (3.96) | 158 (-100) |
| 7 | Virton (BE) | 7 | Oceanic | Clay | 159 | 9.2 (15.6/14.9) | 1077 (544/407) | 3.16 (2.99) | 198 (25) | 3.97 (4.59) | 252 (-70) |
| 8 | Wellin (BE) | 6 | Oceanic | Loam | 406 | 9.2 (15.2/14.5) | 950 (496/379) | 3.08 (2.81) | 176 (40) | 3.76 (4.19) | 302 (-77) |
| 9 | Wijnendale (BE) | 11 | Oceanic | Sandy loam | 590 | 10.2 (15.9/15.2) | 770 (418/324) | 2.98 (2.63) | 173 (48) | 3.23 (3.51) | 180 (-46) |
| 10 | Bavaria-North (DE) | 921 | Oceanic | Silty clay | 165 | 8.7 (15.8/15.0) | 612 (341/338) | 3.19 (2.98) | 130 (38) | 4.32 (4.68) | 82 (-46) |
| 11 | Bavaria-South (DE) | 919 | Continental | Silt loam | 159 | 7.9 (15.3/14.6) | 851 (482/430) | 3.56 (3.50) | 114 (22) | 4.61 (4.92) | 134 (-15) |
| 12 | North Rhine-W. (DE) | 508 | Continental | Silty clay loam | 199 | 7.7 (14.4/13.7) | 1209 (646/621) | 3.10 (2.64) | 251 (78) | 4.08 (4.27) | 80 (-61) |
| 13 | Saarland (DE) | 1001 | Oceanic | Clay loam | 242 | 10.3 (17.0/16.3) | 912 (430/358) | 3.12 (2.95) | 159 (55) | 4.04 (4.60) | 145 (-69) |
| 14 | Saxony (DE) | 1406 | Continental | Silt loam | 217 | 8.8 (16.1/15.3) | 654 (372/335) | 3.18 (2.74) | 119 (21) | 4.36 (4.35) | 81 (-6) |
| 15 | Schleswig-H. (DE) | 101 | Oceanic | Loamy sand | 441 | 8.8 (15.3/14.7) | 692 (347/333) | 3.02 (2.58) | 158 (62) | 3.97 (4.06) | 167 (24) |
| 16 | Thuringia (DE) | 1606 | Continental | Silty clay loam | 242 | 7.4 (14.4/13.8) | 660 (398/387) | 3.17 (2.85) | 142 (60) | 4.37 (4.47) | 88 (-30) |
| 17 | Suserup (DK) | 74 | Oceanic | Sandy loam | 365 | 8.2 (14.5/14.0) | 633 (290/283) | 3.15 (2.86) | 102 (27) | 3.96 (4.00) | 127 (3) |
| 18 | Vestkoven (DK) | 85 | Oceanic | Sand clay loam | 428 | 8.6 (15.0/14.6) | 635 (297/318) | 3.26 (3.03) | 132 (71) | 4.04 (4.07) | 127 (10) |
| 19 | CHP40 (FR) | 3 | Oceanic | Loam | 290 | 12.0 (18.2/17.6) | 1127 (604/418) | 3.49 (3.71) | -44 (-39) | 4.02 (4.56) | -181 (-249) |
| 20 | CHP65 (FR) | 7 | Oceanic | Silty clay loam | 182 | 12.1 (17.9/17.0) | 1047 (582/322) | 3.39 (3.54) | 3 (-15) | 3.74 (4.24) | -323 (-207) |
| 21 | CHS72 (FR) | 25 | Oceanic | Silt loam | 252 | 11.0 (16.7/16.1) | 757 (391/274) | 3.28 (3.36) | 61 (-17) | 3.75 (4.62) | 91 (-121) |
| 22 | HET30 (FR) | 57 | Mountainous | Sandy loam | 156 | 6.5 (12.6/12.2) | 2153 (953/826) | 3.61 (2.85) | 68 (-156) | 4.42 (5.37) | -352 (-421) |
| 23 | HET64 (FR) | 63 | Oceanic | Silty clay | 162 | 12.9 (18.2/17.6) | 1384 (773/549) | 3.07 (3.23) | -17 (-28) | 3.61 (4.30) | -373 (-274) |
| 24 | Alice Holt (GB) | 512 | Oceanic | Clay | 247 | 9.9 (14.9/14.6) | 747 (323/268) | 2.93 (2.71) | 210 (105) | 3.09 (3.54) | 197 (-24) |
| 25 | Cansiglio (IT) | - | Mountainous | Silt loam | 172-178 | 5.5 (12.5/12.7) | 2012 (855/455) | 3.92 (4.11) | -31 (-104) | 4.47 (4.55) | -17 (-168) |
| 26 | Collelongo (IT) | 1 | Mountainous | Loam | 260 | 6.4 (13.1/12.6) | 1072 (573/270) | 3.59 (3.64) | 62 (11) | 4.88 (5.39) | -198 (-120) |
| 27 | Bircza (PO) | 804 | Continental | Clay loam | 311 | 7.2 (15.4/14.9) | 902 (602/607) | 3.50 (3.55) | 370 (223) | 5.26 (5.18) | 198 (12) |
| 28 | Gdansk (PO) | 116 | Continental | Loamy sand | 582 | 8.2 (15.6/15.1) | 938 (500/544) | 3.67 (3.56) | 294 (138) | 4.80 (4.70) | 286 (127) |
| 29 | Krotoszyn (PO) | 322 | Continental | Sandy loam | 402 | 8.2 (16.4/15.6) | 738 (447/474) | 3.53 (3.39) | 181 (69) | 4.81 (4.88) | 160 (32) |
| 30 | Lack (PO) | 326 | Continental | Loamy sand | 594 | 8.8 (17.1/16.4) | 716 (478/496) | 3.54 (3.38) | 221 (123) | 4.82 (4.65) | 209 (63) |
| 31 | Fundata (RO) | 11 | Continental | Sandy loam | 234 | 4.8 (12.5/12.5) | 977 (646/303) | 3.80 (4.00) | 179 (115) | 5.91 (5.45) | 67 (-74) |
| 32 | Mihaesti (RO) | 13 | Continental | Loam | 208 | 8.8 (17.2/17.0) | 675 (334/305) | 3.49 (3.75) | 87 (40) | 5.09 (5.15) | 23 (-18) |

**Table 5.2: Initial characteristics of the different study stands. Stand type is considered mixed (uneven-aged) when the main species (cohort) accounts for less than 75% of the total basal area. Girth was measured at 1.3 m and is characterized by its mean value and its standard deviation. Dominant height is the mean height of the 100 tallest trees per ha.**

| Plot name (country) | Plot ID (ICP) | Location | Altitude (m) | Assessment period | Area (ha) | Stand type | Tree density ($N.ha^{-1}$) | Basal area ($m^2.ha^{-1}$) | Girth (SD) (cm) | Dominant height (m) |
|---|---|---|---|---|---|---|---|---|---|---|
| Baileux-oak (BE) | - | 50.02N 4.40E | 309 | 2001-2011 | 0.9 | Oak even-aged | 468 | 21.6 | 63.7 (40.4) | 23.0 |
| Baileux-beech (BE) | - | 50.02N 4.40E | 309 | 2001-2011 | 1.4 | Mixed | 297 | 23.1 | 90.3 (38.5) | 25.6 |
| Baileux-mixed (BE) | - | 50.02N 4.40E | 309 | 2001-2011 | 1.8 | Mixed | 484 | 30.0 | 77.3 (42.0) | 27.0 |
| Chimay (BE) | 8 | 50.10N 4.27E | 260 | 1999-2014 | 1.3 | Mixed | 697 | 18.9 | 42.4 (40.1) | 19.7 |
| Eupen (BE) | 5 | 50.59N 6.10E | 440 | 1999-2018 | 0.81 | Beech even-aged | 279 | 21.4 | 88.8 (41.9) | 26.3 |
| Gontrode (BE) | 16 | 50.97N 3.80E | 20 | 1987-2009 | 0.28 | Mixed | 301 | 22.8 | 87.9 (42.8) | 25.1 |
| Hoeilaart (BE) | 21 | 50.74N 4.41E | 120 | 1990-2009 | 0.28 | Beech uneven-aged | 145 | 24.8 | 138.9 (47.8) | 36.8 |
| Louvain-la-Neuve (BE) | 9 | 50.68N 4.60E | 130 | 1999-2014 | 1.1 | Beech even-aged | 108 | 29.4 | 176.6 (49.6) | 33.4 |
| Virton (BE) | 7 | 49.52N 5.57E | 370 | 1999-2014 | 1.4 | Mixed | 425 | 23.3 | 73.6 (36.0) | 25.7 |
| Wellin (BE) | 6 | 50.05N 5.22E | 415 | 1999-2009 | 0.81 | Mixed | 419 | 27.4 | 73.7 (53.0) | 25.7 |
| Wijnendale (BE) | 11 | 51.07N 3.04E | 27 | 1987-2009 | 0.28 | Beech even-aged | 279 | 27.8 | 108.2 (28.3) | 25.1 |
| Bavaria-North (DE) | 921 | 49.73N 9.89E | 325 | 1995-2014 | 0.27 | Mixed | 1004 | 34.9 | 58.8 (30.2) | 27.1 |
| Bavaria-South (DE) | 919 | 48.41N 11.66E | 525 | 1995-2014 | 0.3 | Mixed | 412 | 34.2 | 87.4 (53.2) | 31.3 |
| North Rhine-W. (DE) | 508 | 51.71N 8.99E | 375 | 2001-2015 | 0.25 | Beech even-aged | 257 | 31.6 | 115.8 (45.2) | 30.6 |
| Saarland (DE) | 1001 | 49.32N 7.02E | 317 | 2010-2019 | 0.3 | Oak even-aged | 678 | 53.9 | 93.7 (35.0) | 33.3 |
| Saxony (DE) | 1406 | 51.18N 12.83E | 204 | 2000-2014 | 0.25 | Oak even-aged | 424 | 13.6 | 61.5 (16.3) | 20.9 |
| Schleswig-H. (DE) | 101 | 54.10N 10.24E | 25 | 2003-2012 | 0.38 | Beech even-aged | 196 | 38.1 | 154.3 (24.4) | 34.1 |
| Thuringia (DE) | 1606 | 51.34N 10.87E | 420 | 2000-2014 | 0.28 | Beech even-aged | 684 | 35.7 | 77.4 (24.1) | 27.0 |
| Suserup (DK) | 74 | 55.38N 11.56E | 30 | 2005-2015 | 0.21 | Mixed | 607 | 40.0 | 67.4 (61.2) | 32.9 |
| Vestkoven (DK) | 85 | 55.70N 12.35E | 20 | 2005-2015 | 0.21 | Oak even-aged | 1061 | 25.9 | 53.2 (15.7) | 16.9 |
| CHP40 (FR) | 3 | 43.74N 0.84W | 70 | 2000-2014 | 0.5 | Oak even-aged | 244 | 21.2 | 101.3 (25.7) | 27.6 |
| CHP65 (FR) | 7 | 43.20N 0.04W | 380 | 2000-2014 | 0.5 | Oak even-aged | 582 | 22.5 | 60.5 (34.6) | 28.0 |
| CHS72 (FR) | 25 | 47.80N 0.38E | 170 | 2000-2014 | 0.5 | Mixed | 878 | 26.3 | 52.5 (31.7) | 27.7 |
| HET 30 (FR) | 57 | 44.12N 3.54E | 1440 | 2000-2014 | 0.5 | Beech even-aged | 466 | 31.8 | 88.8 (26.4) | 19.8 |
| HET 64 (FR) | 63 | 43.15N 0.66W | 400 | 2000-2014 | 0.5 | Beech uneven-aged | 580 | 28.7 | 70.5 (35.2) | 30.2 |
| Alice Holt (GB) | 512 | 51.12N 0.86W | 80 | 2004-2015 | 0.3 | Oak even-aged | 497 | 25.2 | 78.6 (14.1) | 22.0 |
| Cansiglio-innov (IT) | - | 46.04N 12.37E | 1343 | 2011-2019 | 0.38 | Beech even-aged | 365 | 45.2 | 121.2 (29.3) | 28.5 |
| Cansiglio-trad (IT) | - | 46.04N 12.37E | 1343 | 2011-2019 | 0.38 | Beech even-aged | 341 | 45.5 | 127.6 (22.0) | 28.5 |
| Cansiglio-unman (IT) | - | 46.04N 12.37E | 1343 | 2011-2019 | 0.38 | Beech even-aged | 390 | 43.7 | 116.4 (22.8) | 28.0 |
| Collelongo (IT) | 1 | 41.85N 13.59E | 1560 | 1992-2017 | 0.2 | Beech even-aged | 760 | 32.7 | 68.3 (27.3) | 23.2 |
| Bircza (PL) | 804 | 49.66N 22.49E | 450 | 2005-2014 | 1.01 | Beech uneven-aged | 369 | 28.8 | 88.0 (45.4) | 26.7 |
| Gdansk (PL) | 116 | 54.56N 18.27E | 118 | 2005-2014 | 0.98 | Beech even-aged | 500 | 34.7 | 87.8 (31.6) | 30.0 |
| Krotoszyn (PL) | 322 | 51.77N 17.58E | 166 | 2005-2014 | 0.75 | Oak even-aged | 612 | 31.3 | 76.3 (24.6) | 24.6 |
| Lack (PL) | 326 | 52.48N 19.60E | 108 | 2005-2014 | 0.88 | Oak even-aged | 449 | 28.5 | 86.0 (24.2) | 27.4 |
| Fundata (RO) | 11 | 45.43N 25.27E | 1300 | 2014-2019 | 0.25 | Beech even-aged | 1125 | 32.8 | 57.2 (19.7) | 23.3 |
| Mihaesti (RO) | 13 | 45.05N 25.00E | 500 | 2014-2019 | 0.25 | Oak even-aged | 593 | 34.6 | 83.4 (19.4) | 28.7 |

## 2.2. MODELLING APPROACH

### 2.2.1 Model description

For the simulations, we used the individual tree, spatially explicit and process-based model HETEROFOR that has been implemented in the CAPSIS simulator (Dufour-Kowalski *et al.*, 2012) and is especially convenient for simulating the impact of climate change on structurally complex stands. In the following, we present a brief overview of the model functioning while for a more in-depth description, we refer the reader to Chap.2.

The model determines the key phenological phases (budburst, leaf yellowing and falling) from meteorological data. Then, the radiation intercepted by each tree is calculated with the SAMSARALIGHT library using a ray tracing approach (Courbaud *et al.*, 2003). From the radiation intercepted by the foliage and the soil water potential (calculated with the water balance routine), the gross primary production (GPP, in kgC tree$^{-1}$ h$^{-1}$) of each tree is estimated hourly with the biochemical photosynthesis model of the CASTANEA library (Dufrêne *et al.*, 2005). The net primary production (NPP, in kgC tree$^{-1}$ h$^{-1}$) is obtained empirically from the GPP through the Carbon Use Efficiency (CUE = NPP / GPP) approach. CUE varies with tree size and shape, competition for light and MAT. NPP is first allocated to foliage and fine roots (<2 mm) by ensuring a functional balance and then to structural components using allometric equations, which allows deriving tree dimensional growth. The water balance routine partitions rainfall into throughfall, stemflow and interception (André *et al.*, 2008a), calculates tree transpiration and evaporation from foliage, bark and soil using the Penman- Monteith equation (Monteith 1965) and estimates root water uptake (Couvreur *et al.*, 2012) and soil water movements based on the Darcy law.

In the model version 1.0 presented in Jonard *et al.* (2020) and de Wergifosse *et al.* (2020a), the water balance was calculated before photosynthesis, and the stomatal conductance for water did not depend on atmospheric $CO_2$ concentration. In the new model version used for this study, the two processes were coupled and the stomatal conductance was calculated in the same way for water and $CO_2$ using the formulation of Ball *et al.* (1987) adapted to the tree level by accounting for the influence of tree height (Schäfer *et al.*, 2000). This modification allows taking the effect of atmospheric $CO_2$ concentration on stomatal conductance for water transpiration into account.

### 2.2.2 Model initialisation

During the initialization phase, the model requires various data describing: (i) the soil horizons, (ii) the stand and (iii) the meteorological conditions at an hourly time step (see below for description). The data necessary for the model initialization were collected from the national focal centres regarding the ICP Forests level II plots and from the site managers for the Baileux (LTER site, Belgium) and Cansiglio (Italy) experimental sites.

*Soil data*

For each soil horizon, the soil input data include: thickness, volumetric coarse fraction, bulk density, sand, silt and clay contents, organic carbon content and fine root proportion. Soil water contents at saturation, field capacity and wilting point are estimated by the model using pedotransfer functions (Weynants *et al.*, 2009). The maximum soil depth was fixed to 1.6 m for the sake of comparability among sites. Indeed, 80 to 90% of fine roots are generally found within the top 60 cm of the soil and fine roots deeper than 2 m are scarce (Crow, 2005). When the soil depth was less than 1.6 m, the real soil depth was retained.

*Stand data*

The stand inventory data describe site and tree level characteristics. Among the site level information, the plot geographic coordinates, slope and orientation are required to simulate the radiation transfer with the ray tracing approach. Tree position and dimensions (diameter at breast height: dbh; tree height, height to crown base, height of largest crown extension, crown radii in the four cardinal directions) are necessary input variables for the simulations. However, only dbh is really essential as the other tree dimensions can be estimated based, if necessary, on empirical relationships during a pre-processing phase. Depending on the data availability for each tree species, the relationships used for the gap filling were either common for various sites or site-specific. For each tree dimension and each site, the parameters of the equations used to estimate them are provided in supplementary materials (Table 5.S1, 5.S2, 5.S3 and 5.S4). Finally, tree positions are required to run the model. Missing coordinates were either randomly generated taking tree size and the degree of crown overlap into account, either estimated based on the stump position and/or on the spatial pattern of tree numbering.

*Meteorological data*

Meteorological variables needed by HETEROFOR include air temperature, rainfall, incoming short-wave solar radiation, relative humidity, and wind speed at an hourly resolution. As far as possible, we selected sites for which these variables were monitored in open field stations in close proximity to the forest stand. In order to have continuous time series covering the period of the tree growth monitoring, we used ERA5 reanalysis data corrected based on meteorological observations. Consisting of a combination of past observations and model predictions, ERA5 is the new version of ERA reanalysis and provides hourly estimates of over 240 meteorological parameters with a spatial resolution of 31 km (Hersbach *et al.*, 2020). The biases in the ERA5 data (when compared to meteorological observations) were corrected using the quantile mapping method from the R package downscaleR (Bedia *et al.*, 2020), which allowed us to obtain continuous hourly data from 1979 to 2019. The quantile mapping consists in correcting the distribution of simulated time series using observations. Practically, quantile mapping creates cumulative distribution functions of the observed and predicted time series and adjusts the different quantiles individually (Maraun and Widmann, 2018). Compared to simpler bias correction methods modifying only the mean bias, quantile mapping better preserves extreme values and can, for example, suppress the bias in the number of wet days that is often overestimated in simulated climate time series (Gutowski *et al.*, 2003). For some sites, we had only daily meteorological observations. In this case, bias correction was applied at the daily time step and then, the daily cycle of ERA5 was added to obtain hourly values. The daily cycle was calculated for each hour of the day as the difference between the hourly value and the mean daily value for the air temperature (Eq. 1) or the ratio for the other climate variables (Eq. 2) as follows:

$$x_{ERA5\_COR\_h} = x_{ERA5\_COR\_d} + \left(x_{ERA5\_h} - x_{ERA5\_d}\right) \tag{1}$$

$$x_{ERA5\_COR\_h} = x_{ERA5\_COR\_d} * \frac{x_{ERA5\_h}}{x_{ERA5\_d}} \tag{2}$$

with $x_{ERA5\_COR\_h}$ and $x_{ERA5\_h}$, the corrected and original ERA5 hourly values

$x_{ERA5\_d}$ and $x_{ERA5\_d}$, the corrected and original ERA5 mean daily value

### 2.2.3 Model parameterization

The HETEROFOR model requires parameters most of which are species-specific. The parameters used for oak and beech in this study are valid at the European scale for a large range of ecological conditions and provided in supplementary materials (Table 5.S5). Some species parameters (e.g. specific leaf area, leaf size, leaf/needle turnover, leaf retranslocation, taper function, volume functions, drought sensitivity) were obtained directly from the literature on functional traits, tree ecophysiology or dendrometry. The parameters used for carbon allocation were obtained by fitting allometric relationships predicting, for example, leaf biomass or aboveground woody biomass from dbh and/or height. To make these adjustments, we benefited from biomass data gathered for meta-analyses (André and Ponette, 2003; André *et al.*, 2010; Falster *et al.*, 2015; Ung *et al.*, 2017; Schepaschenko *et al.*, 2017). Other parameters were associated with relationships predicting some tree dimensions (crown base height and crown radius) based on dbh and/or tree height. These relationships were fitted using the tree measurement data collected at the various study sites.

Budburst for oak and beech was estimated based on Duputié *et al.* (2015), who used phenological models already implemented in HETEROFOR (namely, the optimum model for oak and the sigmoid model for beech). Still, the optimum response function during chilling had to be slightly adapted to correspond to that given in Wang and Engel (1998):

$$R_c = \begin{cases} 0, & T < T_{min} \\ \frac{2(T-T_{min})^{\alpha}(T_{opt}-T_{min})^{\alpha}-(T-T_{min})^{2\alpha}}{(T_{opt}-T_{min})^{2\alpha}}, & T_{min} \leq T \leq T_{max} \\ 0, & T_{max} < T \end{cases} \qquad (3)$$

with $\alpha = \frac{\ln(2)}{ln\left(\frac{T_{max}-T_{min}}{T_{opt}-T_{min}}\right)}$

and *Tmin*, *Tmax* and *Topt*, species-specific parameters corresponding to the minimum, maximum and optimal temperatures for chilling (in ° C), respectively, and *T*, the daily average temperature (in °C).

Leaf yellowing and fall parameters were empirically fitted with the observations provided for 13 of the study sites located in Belgium, Germany, France and Romania.

Most parameters were derived directly from measurements or by fitting relationships. However, two very important aspects required to run the model for their calibration: (i) the CUE, and (ii) the tree height growth function. Because of uncertainty related to mechanistic computation of whole-plant respiration (see Collalti *et al.*, 2020b) three different methods were used here to estimate CUE (and indirectly plant respiration): (i) a constant value (e.g. Waring *et al.*, 1998), (ii) a function dependent on nine variables common for all sites or (iii) with a site-dependent intercept (parameter a in Eq. 4).

The function estimates empirically individual CUE from dbh (cm), total tree height (h in m), crown diameter (D in m), height of crown base (hcb in m), light competition index (LCI: the ratio between the absorbed radiation calculated with and without neighbouring trees), and MAT (in °C).

$$CUE = a + b\, dbh_{cm} + c\, {dbh_{cm}}^2 + d\, h + e\, h^2 + f\, \frac{h}{dbh_m} + g\, Dd_{index} + i\, \frac{h-hcb}{h} + j\, ln(LCI) + k\, MAT \qquad (4)$$

with $dbh$ and $h$ characterising the tree size,

$h/dbh$, $Dd_{index}$ (see Eq. 24 to 25 in sect. 1.3.5), $\frac{h-hcb}{h}$ describing the tree shape independently of its size (slenderness, crown horizontal and vertical extension),

$LCI$, the light competition index varying between 0 (no light reaching the tree) and 1 (no competition),

$MAT$, the mean annual air temperature,

$a$ to $k$, fitting parameters.

The constant CUE and Eq. 4 were fitted with CUE data obtained by dividing the reconstructed NPP (sect. 1.3.9 in Chap. 2) by the predicted GPP using the whole dataset and also using a subset of sites dedicated to the calibration. The principle of parsimony was applied, and non-significant effects were removed using a stepwise forward procedure based on BIC (Bayesian information criterion).

For beech, the mean CUE was 0.59. The final model (4) included tree height, the height to dbh ratio, the Dd index and the natural logarithm of LCI. CUE increased with tree height and decreased with the height to dbh ratio, Dd index, and LCI (Table 5.S5). The general function accounted for 43.5% of the CUE variability whereas the site-dependent function accounted for 61.7%.

For oak, the mean CUE was 0.67. In the final model, CUE increased with dbh and was negatively correlated with the natural logarithm of LCI, crown length fraction, Dd index, and MAT (Table 5.S5). The shift from the general to the site-dependent function increased the explained variability from 42.0 to 64.3%.

The height growth function estimates the annual height growth (m $\text{yr}^{-1}$) based on the light competition index ($LCI$), the potential height growth ($\Delta h_{pot}$ in m $\text{yr}^{-1}$), the height (in m), and/or the dbh (in cm) considering also an error term (standard error of the residuals).

$$\Delta h = a + b\ LCI + c\ \Delta h_{pot} + d\ \Delta {h_{pot}}^2 + e\ h + f\ h^2 + g\ dbh + error \tag{5}$$

with $\Delta h_{pot} = \frac{\Delta\, dbh^2 h}{\frac{dbh^2}{100}}$

$\Delta h_{pot}$ is the potential height increment if all the growth potential is allocated to the primary growth in height (and nothing is left for the secondary growth in dbh). This equation was fitted based on tree growth data and on the mean LCI estimated by HETEROFOR for the period during which height growth was monitored. The model explained 50.9% and 67.9% of the height increment variability for oak and beech, respectively.

### 2.2.4 Model performances

The model evaluation is focused on tree dimensional growth and on phenology. For tree growth, we evaluated the ability of the model to reproduce the individual increment in tree height, girth and basal area estimated on 5 to 10-year periods (n = 10108 trees in 36 stands). The tree growth evaluation was conducted for the three modalities of CUE calculation considering each tree separately or grouped in 10 cm girth classes in each plot. In a second time and to evaluate the robustness of our model, the general CUE function was recalibrated on half of the sites (calibration dataset, n = 4859 trees in 18 stands) and an independent evaluation was carried out on the remaining sites (evaluation dataset, n = 5249 trees in 18 stands). The partitioning of the sites between the calibration and evaluation datasets was achieved in order to cover the diversity of stands, soils, and climates in both sets.

Budburst, leaf yellowing and fall were observed only on a limited number of sites (13). The dates characterizing these phenological phases were those for which they were completed for 50% of the trees. For the budburst, the comparison of the observed and predicted dates provided an independent evaluation while it gave only an indication of the calibration quality for the leaf yellowing and fall since the same observations were used to adjust some parameters (the leaf yellowing parameter, $y$ and the falling rate, $R_{fall;}$ see Table 5.S5).

Multiple statistical indices were used to test the model predictive ability. First, we calculated the bias (average error, AE) or the relative bias (normalised average error, NAE). The NAE is the difference between the average values of the predictions and observations (i.e. AE), divided by the average of observations. The bias significance was assessed using a paired *t*-test. To check the absence of bias throughout the range of values (and not only on the average), regression tests were done using the Deming fitting procedure (mcreg function of the mcr package in R) since both observations and predictions were characterised by uncertainties. The error ratio was determined based on the variances of observations and predictions. Finally, we estimated the agreement between observations and predictions based on the Pearson's correlation (r) and on the root mean square error (RMSE), which provides information on the prediction accuracy. All the tests were carried out with R software (R core Team, 2020).

## 2.3. SIMULATION EXPERIMENT

### 2.3.1 Simulation set-up

The set of 36 plots available for this study is limited compared to the diversity of conditions in Europe's forests. Furthermore, the effects of the site components (soil, stand and climate) can be confounded. To disentangle the various components of the site effect and to assess how they impact the tree growth response to climate change, we not only ran the simulations for the 36 plots (namely '*real'* sites), but also for a large number of '*virtual'* plots, representing recombinations of the different soils, stands and climates from the 36 plots. As a full factorial experiment was not feasible given the number of possible combinations (36 soils x 36 stands x 32 climates = 41472), we selected subsets of stands, soils and climates representative of the diversity of oak and beech growth conditions in Europe. Twelve stands were chosen, three in each of the four stand categories (even-aged beech/oak, uneven-aged beech/mixed); six soils, three in each of the two soil types (low and high maximum extractable water, MEW), and nine climates, three in each of the three climate zones (continental, mountainous and oceanic). Nine *virtual* sites were created for each of the 24 combinations of site component categories (9 replicates x 4 stand types x 2 soil types x 3 climate zones = 216 *virtual* sites). For each combination, the first three *virtual* sites were constructed in order to have no common site components (soil, stand, and climate) while the remaining six sites were randomly selected (without replacement).

Two consecutive 15-year simulations were conducted for a historical period (1976-1990, 1991-2005) and for a period in the future (2071-2085, 2086-2100). A 15-year period was retained as it corresponds to the average monitoring period for which we know the cutting operations. For the simulations of future growth, two RCP (Radiative Concentration Pathway) scenarios (Meinshausen *et al.*, 2011; Van Vuuren *et al.*, 2011) were used:

RCP4.5 and RCP8.5. The scenario names depict the increase in radiative forcing in 2100 relative to preindustrial levels (+ 4.5 W $m^{-2}$, + 8.5 W $m^{-2}$). All the 15-year simulations started with the same initial conditions. For a given period (historical or future), the stand conditions were therefore reinitialized after 15 years to avoid that stand characteristics differ to much with time among RCP scenarios. Indeed, in this case, the direct climate change impact could be partly confounded with an indirect effect due to a divergence in stand evolution. During these 15-year periods, we applied the same thinning operations (or mortality rates) as those observed during the monitoring period in the stand selected for the creation of the *virtual* sites.

One of the main uncertainties when simulating long-term forest growth is whether or not the $CO_2$ so-called "fertilization effect" can persist or saturate to a certain level (Terrer *et al*., 2019; Wang *et al*., 2020). In order to highlight this effect, the simulations were run with a constant atmospheric $CO_2$ concentration ($[CO_2]_{cst}$=380 µmol $mol^{-1}$) or a $CO_2$ concentration changing over time ($[CO_2]_{var}$) and corresponding to their corresponding RCP scenarios (~530 µmol $mol^{-1}$ for RCP4.5 and ~930 µmol $mol^{-1}$ for RCP8.5 by 2100, respectively).

### 2.3.2 Climate projections

As important differences between climate model results can occur (Kjellström et al., 2018; Christensen and Kjellström, 2020) and in order to test the sensibility of the results to contrasted climate evolution, we used climate projections from two different models for the simulations (historical, RCP4.5 and RCP8.5 scenarios). These projections were produced by two regional climate models (RCM), ALARO-0 (Giot *et al*., 2016; Termonia *et al.*, 2018) and RCA4 (Samuelsson et al., 2011; Strandberg et al., 2015), within the framework of the European branch of the Coordinated Regional Downscaling Experiment (EURO-CORDEX; Giorgi *et al*., 2009; Jacob *et al*., 2020). Three-hourly time series with a spatial resolution of 12.5 km were used. The RCMs were driven at their boundarties by the results of two different global climate models (GCM): CNRM-CM5 (Voldoire *et al.*, 2013) for ALARO-0 and IPSL-CM5A (Dufresne et al., 2013) for RCA4. In the following, they will be called CNRM-ALARO and IPSL-RCA4. GCMs provide projections with a horizontal resolution too coarse (~150 km) to be used in local impact studies as sites are locally affected by meso-scale meteorological processes. However, even after this dynamic downscaling using the RCMs, climatological distributions can still substantially differ from those of *in situ* measurements due to model biases and representativity errors. For this reason, the projections were bias-corrected using the quantile mapping method earlier described and discretized (transformation from three to one-hour time step) as the model requires hourly data.

### 2.3.3 Model simulation analysis

Based on the results of the model runs for the *virtual* sites, we performed the following analyses: (i) significance of climate change effects on NPP, vegetation period length and transpiration deficit, (ii) magnitude of the change in NPP due to climate change compared to the inter-annual climate variability and relative importance of stand, soil and climate effects on NPP and on its response to climate change. The simulations achieved with both climate models were generally analysed together.

The impact of climate change on NPP and the other tree growth-related variables (vegetation period length and transpiration deficit) was assessed separately for the different categories of stand, soil and climate and for the two $CO_2$ modalities (constant and changing over time). The stand net primary production simply consists of the sum of individual tree NPP and then scaled per square meter per year. We define the vegetation period length as the number of days between the time the green leaf proportion reaches 50% during spring and when it drops below 50% during fall. The transpiration deficit (mm) is the difference between the potential transpiration (without soil water limitation) and the actual transpiration. These values were calculated for all trees annually and were then aggregated at the stand scale and divided by the stand area. In addition, we have evaluated the evolution of the lowest stand NPP values (7th percentile), which are representative for the years with the harshest conditions.

To investigate whether the climate scenarios generated significant differences in the response variables, an unpaired Mann-Whitney test was conducted between the historical period and the future projections, whereas a paired Wilcoxon signed-rank test was performed between the two RCP scenarios as they correspond to the same period (Wilcoxon, 1945). We chose those non-parametric tests due to their lower sensitivity to non-normal variables than parametric tests. Levene tests were used to assess whether the variance was equal between the different scenarios. Those tests were produced in R using the lme4 package (Bates *et al*., 2014).

To evaluate the relative importance of climate change effects on tree growth compared to the spatial (stand, soil and climate) and temporal variability, we used a linear mixed model, which considers the climate scenario (considering both the RCP scenario and the differences between the climate models) as a fixed effect and stand, soil and climate as random factors. In addition, the interactions between the three site components (soil, stand, and climate) and the climate scenario were also included in the model as random coefficients to account for the impact of the site components on the climate change effect as follows:

$$NPP \sim [scenario]_{fixed} + \ [stand + soil + climate + (stand + soil + climate).scenario]_{random} \qquad (6)$$

The partial R² of the fixed effect in the model was considered as the difference between the R² of the model when the effect was included (but without the interactions) and without the considered effect. The partial R² of the random effects was calculated as the ratio of the variance component for the effect to the total variance.

To identify the underlying factors at the origin of the stand, soil and climate effects on NPP and on its response to climate change, multivariate linear models were elaborated by selecting the main explanatory variables using a stepwise forward procedure based on BIC (Bayesian information criterion). The selection was achieved among a series of variables describing the stand, soil and climate characteristics. A first model explaining the NPP variability across *virtual* sites and climate scenarios was built to get a general overview. Then, the stand, soil and climate impacts on the forest response to climate change were assessed with a model explaining the change in NPP between the historical period (averaged over the entire period) and the 2071-2100 period under the RCP8.5 scenario. The selected variables related to the stand properties were the altitude (m), the beech and oak percentages (%), the stem number per unit area ($N.ha^{-1}$), basal area ($m^2.ha^{-1}$), mean and standard deviation of *dbh*, and the dominant height (height of 100 tallest trees per ha; in m) at the start of the simulation. Concerning soil, the soil depth, MEW, sand, silt and clay contents were chosen. Finally, the climate-related variables selected were the mean temperature (°C) and total precipitation (mm), both annually and for the vegetation period (May to September) and atmospheric $CO_2$ concentration, all five averaged over the historical period; as well as the change of these five variables for the two RCP scenarios. All the statistical analyses were carried out with R software (R core Team, 2020) except the linear mixed models, which were fitted with the JMP software (JMP®, Version 15).

# 3. RESULTS

## 3.1. MODEL EVALUATION

### 3.1.1 Individual height, girth and basal area increment

The model was evaluated on tree height, girth and basal area increments for each of the three CUE calculation modalities (i.e. constant value, general and site-dependent function).

For both tree species, the constant CUE displayed the lowest relative bias (NAE) for the three evaluated metrics (bias between 16 and 97% lower for the constant CUE, except for oak basal area). Except for tree height, the regression test showed a closer proximity to the identity line for the general and site-dependent functions than for the constant CUE. Similarly, these functions led to better performances evaluated from RMSE and Pearson's r (RMSE between 14 and 45% lower for general and site-dependent function compared to constant CUE and Pearson's r between 0.2 and 29% higher). Compared to the general function, better results were achieved with the site-dependent function regarding Pearson's r and RMSE, except for height concerning the latter (Table 5.3, Fig. 5.S1 and 5.S2).

**Table 5.3: Statistical evaluation of the predicted height, girth and basal area increments (vs. individual observations) over 5 to 10-year periods for the three calibration modalities of the CUE and the entire dataset using normalized average error (NAE), paired t test, Deming regression test, root mean square error (RMSE) or Pearson's correlation (Pearson's r). Standard deviation or confidence intervals are provided in parentheses.**

| Tree species | NAE | Paired *t* test | Deming regression | | RMSE | Pearson's r |
|---|---|---|---|---|---|---|
| NPP to GPP calculation | | *P* value | intercept | slope | | |
| Height | | | | | | |
| Oak | | | | | | |
| Constant ratio | 0.0081 | 0.81 | 0.42 (±0.80) | -1.00 (±3.15) | 0.21 | -0.025 |
| Overall function | -0.061 | 0.02 | -0.09 (±0.18) | 1.53 (±0.81) | 0.16 | 0.163 |
| Site-dep. function | -0.075 | 0.00 | -0.06 (±0.11) | 1.39 (±0.49) | 0.15 | 0.264 |
| Beech | | | | | | |
| Constant ratio | 0.0056 | 0.88 | -0.01 (±0.23) | 1.06 (±0.80) | 0.29 | 0.054 |
| Overall function | -0.18 | 0.00 | -0.03 (±0.15) | 1.39 (±0.67) | 0.25 | 0.106 |
| Site-dep. function | -0.19 | 0.00 | -0.02 (±0.07) | 1.38 (±0.33) | 0.24 | 0.201 |
| Girth | | | | | | |
| Oak | | | | | | |
| Constant ratio | -0.0037 | 0.84 | 0.39 (±0.09) | 0.64 (±0.07) | 0.84 | 0.446 |
| Overall function | -0.12 | 0.00 | 0.05 (±0.12) | 1.09 (±0.12) | 0.60 | 0.448 |
| Site-dep. function | -0.079 | 0.00 | 0.06 (±0.08) | 1.02 (±0.07) | 0.54 | 0.576 |
| Beech | | | | | | |
| Constant ratio | -0.044 | 0.00 | 0.22 (±0.04) | 0.77 (±0.04) | 0.70 | 0.548 |
| Overall function | -0.13 | 0.00 | 0.09 (±0.04) | 1.02 (±0.04) | 0.54 | 0.636 |
| Site-dep. function | -0.13 | 0.00 | 0.08 (±0.03) | 1.03 (±0.04) | 0.50 | 0.684 |
| Basal area | | | | | | |
| Oak | | | | | | |
| Constant ratio | 0.073 | 0.00 | 0.75 (±0.13) | 0.58 (±0.05) | 2.01 | 0.544 |
| Overall function | -0.087 | 0.00 | 0.26 (±0.14) | 0.95 (±0.07) | 1.28 | 0.597 |
| Site-dep. function | -0.064 | 0.00 | 0.12 (±0.12) | 1.00 (±0.06) | 1.10 | 0.680 |
| Beech | | | | | | |
| Constant ratio | -0.013 | 0.34 | 0.25 (±0.07) | 0.84 (±0.03) | 1.46 | 0.652 |
| Overall function | -0.093 | 0.00 | 0.15 (±0.06) | 0.99 (±0.03) | 1.13 | 0.748 |
| Site-dep. function | -0.097 | 0.00 | 0.10 (±0.05) | 1.04 (±0.03) | 1.02 | 0.786 |

Overall, tree height increment was better predicted for oak than for beech whatever the CUE calculation modalities while the opposite was found for the radial increments, especially when considering RMSE and Pearson’s r (Table 5.3, Fig. 5.S1 and 5.S2).

Basal area increment predictions displayed the lowest relative bias (values between 6.4 and 9.7%) and the highest Pearson’s r (between 0.544 and 0.786) compared to height or girth increment. Slightly lower performances were found for girth while the height increment performed significantly worse with relative bias values ranging from 0.8 to 19% and Pearson’s r never exceeding 0.264 (Table 5.3).

When evaluating model performances on sites not used for the calibration, we considered only one CUE calculation modality (the general function) and focused on the individual girth increment aggregated in 10 cm girth classes. Compared to the calibration sites, evaluation sites performed only slightly worse. Concerning beech, the Pearson’s r between predicted and observed girth increment decreased from 0.828 (calibration sites) to 0.775 (evaluation sites). The bias remained equivalent for the evaluation sites, being even slightly lower (from –12.06 to –11.17%). For oak, the negative bias significantly increased for the evaluation site (from –5.65 to –14.27%) while the Pearson’s r was a little higher for the evaluation sites (from 0.473 to 0.537) (Fig. 5.1). The same evaluation procedure was applied to the tree height increment. Compared to the prediction quality obtained using the calibration dataset, the model performed equally well for oak (except for the relative bias) but less good for beech (Fig. 5.S3).

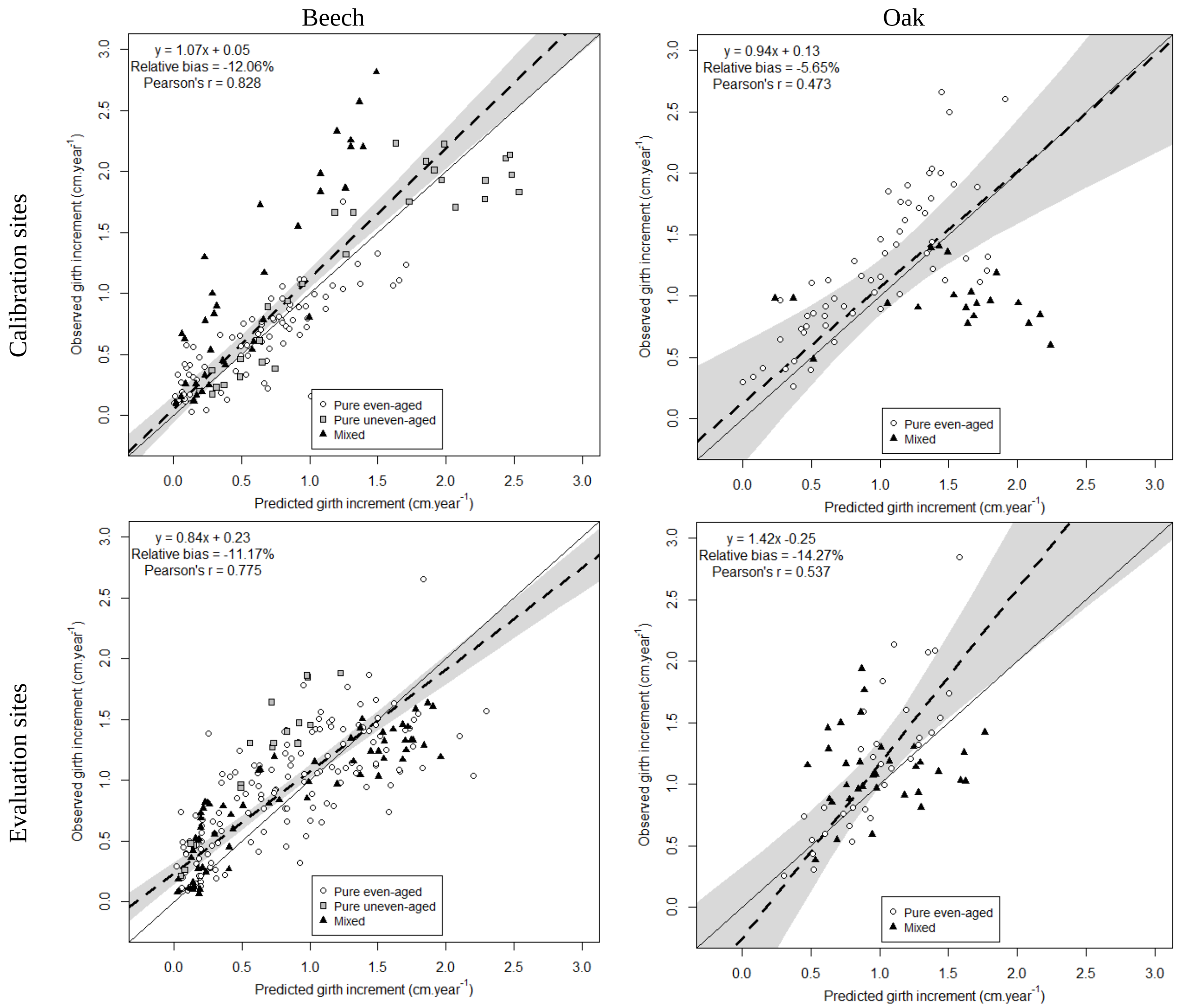

**Figure 5.1: Comparison of the observed and predicted girth increment based on the general CUE function, aggregated by 10 cm girth classes for beech (left) and oak (right) and for the calibration (top) and the evaluation (bottom) sites. The prediction quality is assessed based on the relative bias, the Pearson's r and the Deming regression test (position of the identity line (solid line) with respect to the confidence interval of the regression line (dashed line)).**

### 3.1.2 Budburst, yellowing and fall dates

The prediction of the budburst date suffered from a bias of only 0.4 day and the Pearson's r reached a high value of 0.833. Apart from a little delay in the prediction of oak budburst for the sites with an early leafing, the budburst was well reproduced (Fig. 5.2). The evaluation was performed on a large range of observed values, from the 29th of March to the 21st of May for beech and from the 15th of March to the 20th of May for oak. In turn, the model predicted a range of budburst dates ranging from the 4th of April and the 18th of May for beech and from the 29th of March to the 14th of May.  Leaf yellowing and leaf fall displayed limited biases of 1.7 and –0.5 day and Pearson's r of 0.527 and 0.491, respectively. Furthermore, the confidence interval of both Deming regression lines included the identity line. Finally, the model correctly reproduced the pattern of later leaf yellowing and fall in oak compared to beech (Fig. 5.2).

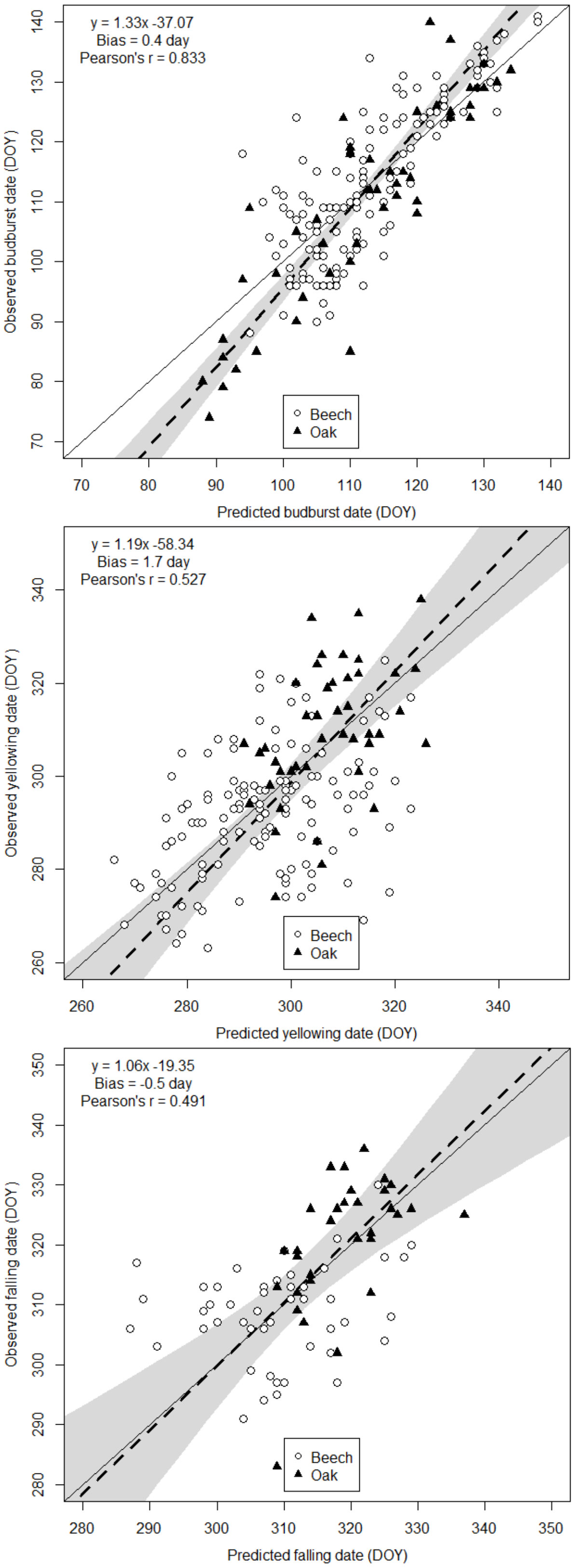

**Figure 5.2: Comparison of the observed and predicted mean stand budburst (top), yellowing (middle) and falling (bottom) dates, separated according to the tree species. The prediction quality is assessed based on the relative bias, the Pearson's r and the Deming regression test (position of the identity line (solid line) with respect to the confidence interval of the regression line (dashed line)).**

### 3.2. SIMULATIONS ON *REAL* SITES

In a first step, the changes in NPP induced by climate change were assessed for the *real* sites using to the site-dependent CUE function and the two types of climate projections (CNRM-ALARO and IPSL-RCA4).

For CNRM-ALARO and the $[CO_2]_{cst}$ runs, the NPP changes between the historical period and 2071-2100 were comprised between –106 gC $m^{-2}$ $yr^{-1}$ (-12.8%) and +100 gC $m^{-2}$ $yr^{-1}$ (+17.0%) for an average value of +43 gC $m^{-2}$ $yr^{-1}$ (+5.5%) for the scenario RCP4.5 and between –226 gC $m^{-2}$ $yr^{-1}$ (-27.2%) and +160 gC $m^{-2}$ $yr^{-1}$ (+23.1%) with a mean increase of 56 gC $m^{-2}$ $yr^{-1}$ (+7.4%) for RCP8.5.

The sites showing NPP decreases under RCP8.5 scenario were all mixed or oak-dominated stands. Compared to the other sites, they were characterized by a lower mean girth (71 vs. 92 cm) and were located at lower altitude (247 vs. 491 m). In addition, their climates were warmer and dryer both annually (9.9°C and 823 mm vs. 8.4°C and 1054 mm) and during the vegetation period (16.8°C and 459 mm vs. 14.9°C and 541 mm).

Under the $[CO_2]_{var}$, an important shift towards more positive NPP changes were highlighted. For the scenario RCP4.5, the sites displayed NPP values on average 197 gC $m^{-2}$ $yr^{-1}$ (+23.0%) superior to the historical period with values between +9 and +294 gC $m^{-2}$ $yr^{-1}$ (+1.1% and +39.0%). For the scenario RCP8.5, large NPP increases appeared with an average increase of 360gC $m^{-2}$ $yr^{-1}$ (41.9%) (Table 5.S6).

For IPSL-RCA4, NPP changes exhibited a higher variability and more negative values. For the $[CO_2]_{cst}$ runs, the NPP change under RCP4.5 and RCP8.5 was on average +23 (-190 to +136) and -27 (-357 to 149) gC $m^{-2}$ $yr^{-1}$, respectively. This correspond to mean relative increase of 2.9% (-25 to +16%) for RCP4.5 and a decrease of 2.4% (-46.2 to +20.0%) for RCP8.5 (Table 5.S6 and bottom of Fig. 5.3 for RCP8.5).

Around half the sites displayed a decrease in NPP under the scenario RCP8.5 (17 out of 36 sites). Compared to the sites with increasing NPP, they showed lower mean girth (77 vs. 97 cm), were located at lower altitude (302 vs. 557 m) and had a lower MEW (262 vs 300 mm). These sites were warmer (9.7 vs. 7.8 °C) but not significantly dryer. However, they displayed lower annual rainfall increases (+42 vs. +112 mm) and higher vegetation period rainfall decreases (-96 vs. -64 mm).

Under the $[CO_2]_{var}$, the differences with CNRM-ALARO were less marked. For RCP4.5, NPP was, on average, 210 gC $m^{-2}$ $yr^{-1}$ (25.4%) higher than during the historical period for a range from -37 to +340 gC $m^{-2}$ $yr^{-1}$ (-4.9 to +41.2 %). For RCP8.5, an average increase of 324 gC $m^{-2}$ $yr^{-1}$ (+39.8%) was observed (range comprised between -126 and +531 gC $m^{-2}$ $yr^{-1}$ or -16.9 and +85.8%) (Table 5.S6).

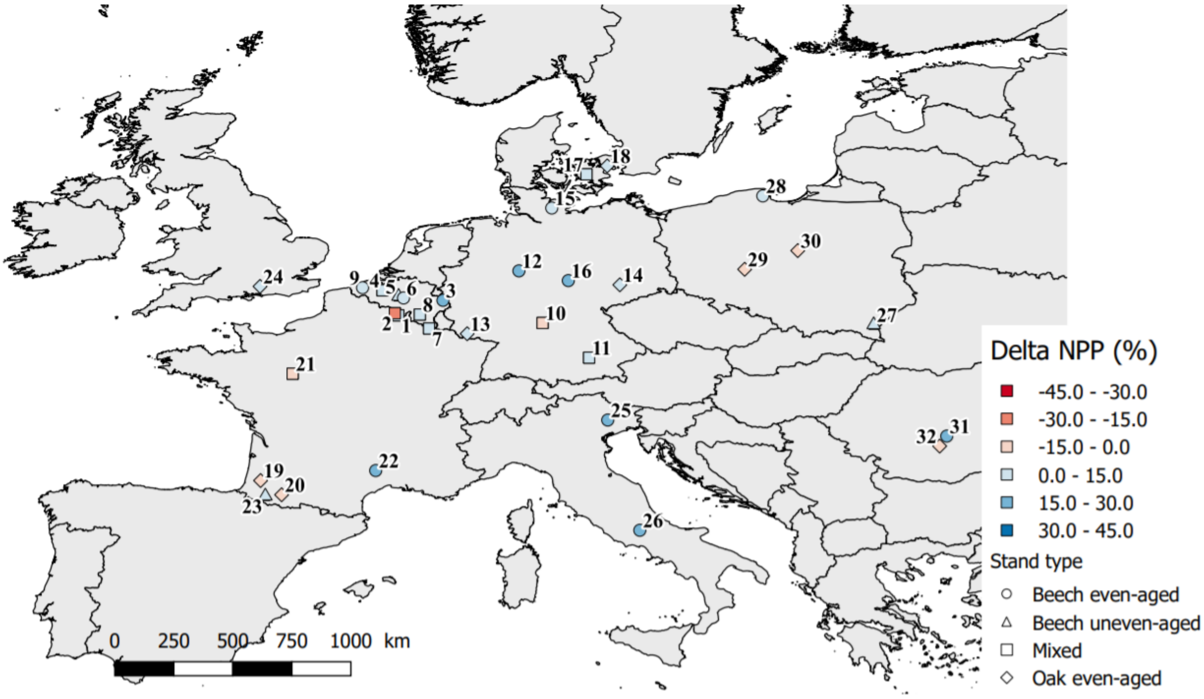

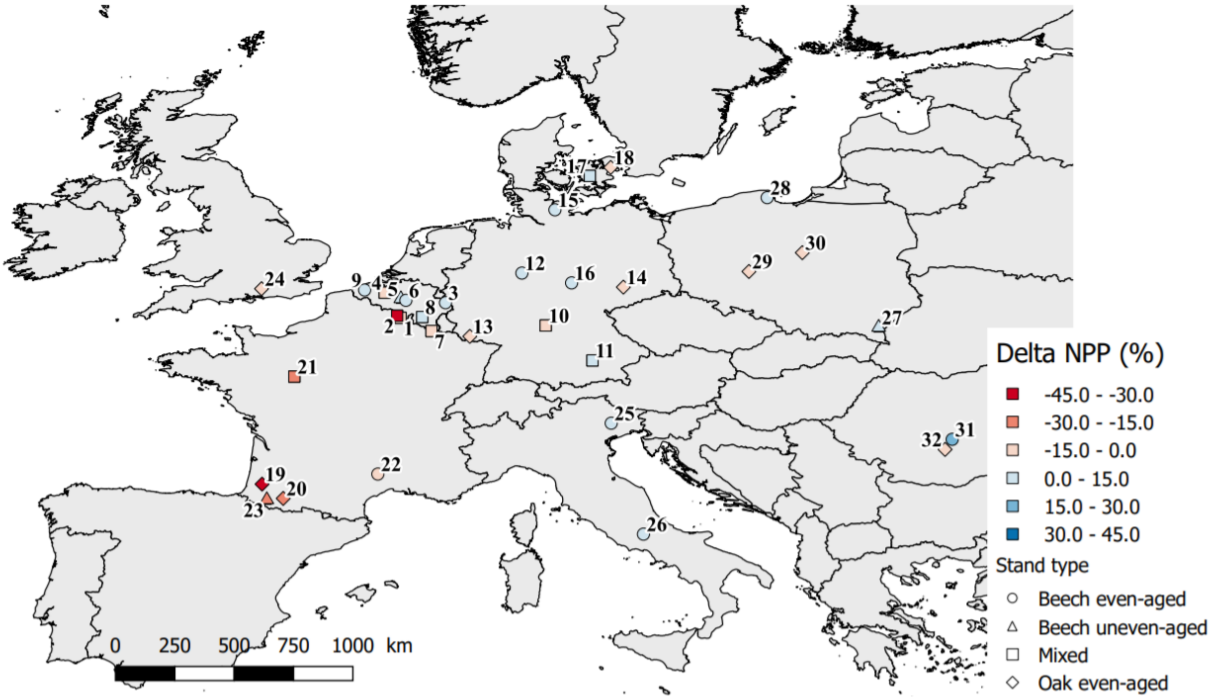

**Figure 5.3. Relative change in NPP between the historical period (1976-2005) and the scenario RCP8.5 (2071-2100) in the *real* sites used for the calibration and evaluation of the model under the constant $CO_2$ modality and the site-dependent CUE function for CNRM-ALARO (top) and IPSL-RCA4 (bottom). Based on the number, the site characteristics can be found in Table 5.1.**

### 3.3. SIMULATIONS ON *VIRTUAL* SITES

**Vegetation period**

Since phenology was not $CO_2$ dependent in the model, no distinction was made between the two $CO_2$ modalities. In addition, the simulations for the two types of climate projections were treated together. Overall, the vegetation period increased for the RCP scenarios compared to the historical period and this increase was always higher for RCP8.5 than RCP4.5 (Fig. 5.4). For beech, the vegetation period increased at the highest rate in the mountainous zone: +2.3 and +3.9 days per decade for the scenario RCP4.5 and 8.5, respectively. In the continental and oceanic zones, changes in beech vegetation period occurred at a lower rate (+2.1 and +1.8 day per decade for RCP4.5 and +3.5 and +2.9 days per decade for RCP8.5, respectively). For oak, the vegetation period extension was greater than for beech. It was similar in the continental zone (+2.6 and +4.3 days per decade for RCP4.5 and RCP8.5, respectively) and in mountainous climate (+2.5 and +4.4 days per decade for RCP4.5 and RCP8.5, respectively) and considerably higher than in the oceanic zone (+1.8 and +2.7 days per decade for RCP4.5 and RCP8.5, respectively).

For beech, the increase in vegetation period compared to the historical period was equally driven by an earlier budburst and a later yellowing, except for the oceanic climate where the delay in leaf yellowing was more marked (Fig. 5.S4). For oak in continental and mountainous zones, the increase in vegetation period mainly originated from earlier budburst while, in the oceanic zone, the earlier leafing and later yellowing were of similar magnitude.

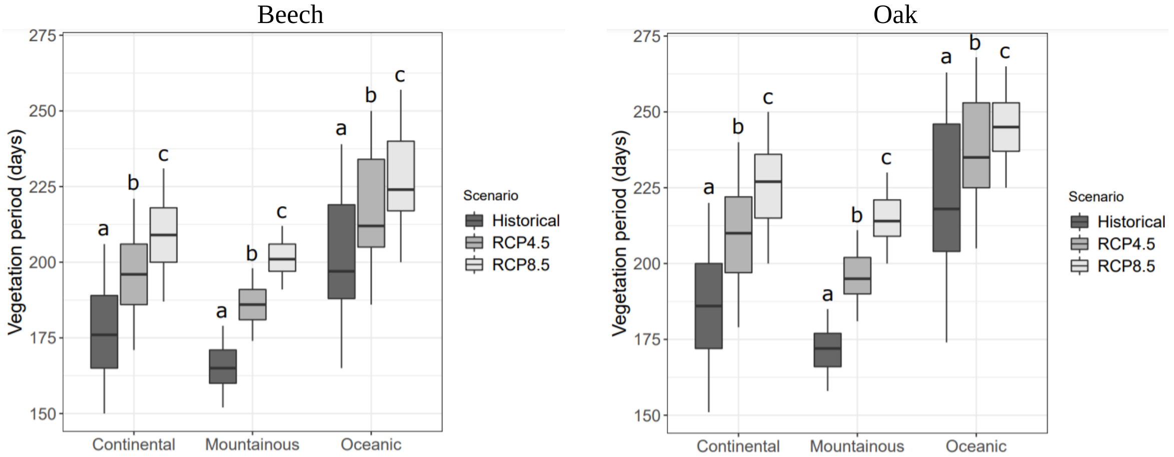

**Figure 5.4: Comparison of the vegetation period length in *virtual* sites simulated for the historical period (1976-2005) and for the future (2071-2099) according to two RCP scenarios; three climate types were considered as well as both tree species. For each box, the horizontal line corresponds to the median, the ends indicate the 25th and 75th percentiles and the whiskers show the values above and below these quartiles within 1.5 interquartile. For a same climate type, scenarios with common letters are not significantly different (paired Wilcoxon signed- rank between RCP4.5 and RCP8.5 and unpaired Mann-Whitney test between historical and RCP scenarios). The simulations made based on the two types of climate projections (CNRM-ALARO and IPSL-RCA4) were included in the analysis.**

**Transpiration deficit**

Transpiration deficit was strongly affected by the soil water reserve (MEW) and stand type and responded to the RCP scenarios in opposite ways for the two $CO_2$ modalities (Fig. 5.5). With $[CO_2]_{cst}$, transpiration deficit always significantly increased with the intensity of the radiative forcing. Whatever the RCP scenario used, soils with high MEW had a lower transpiration deficit than those with a low MEW (–19 mm in continental, –15 mm in mountainous and –27 mm in oceanic climates). Under $[CO_2]_{var}$, transpiration deficit decreased with the radiative forcing intensity for the continental and oceanic climates while an increase was detected for the mountainous climate (excepted RCP8.5 with high MEW). Stands in the oceanic zone benefited the most from the decrease in transpiration deficit but still exhibited the highest level of transpiration deficit. The soil water reserve effect was of the same magnitude for the $[CO_2]_{var}$ than for the $[CO_2]_{cst}$ modality (Fig. 5.5).

Stand type influenced transpiration deficit through a strong species composition effect (higher transpiration deficit for beech). However, the transpiration deficit response to climate change was not much affected by stand type (Fig. 5.5).

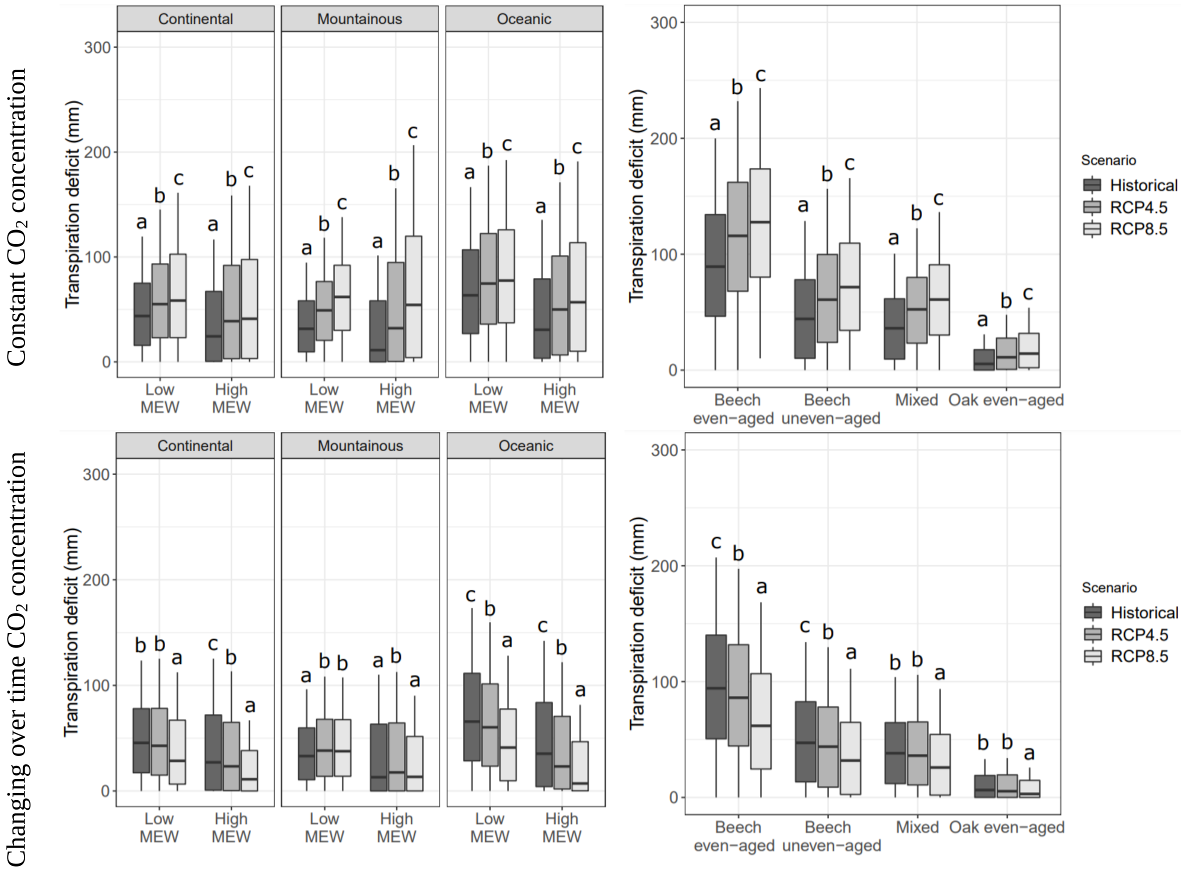

**Figure 5.5: Comparison of the simulated transpiration deficit in *virtual* sites among RCP scenarios (2071-2099) and the historical period (1976-2005) for the two atmospheric $CO_2$ modalities: highlighting of the climate zone, soil water reserve (MEW) and stand type effects. For each box, the horizontal line corresponds to the median, the ends indicate the 25th and 75th percentiles and the whiskers show the values above and below these quartiles within 1.5 interquartile. For a same stand, soil or climate type, scenarios with common letters are not significantly different (paired Wilcoxon signed- rank between RCP4.5 and RCP8.5 and unpaired Mann-Whitney test between historical and RCP scenarios). The simulations made based on the two types of climate projections (CNRM-ALARO and IPSL-RCA4) were included in the analysis.**

### NPP

Compared to the historical period and assuming a $[CO_2]_{cst}$, future NPP slightly increased under continental and mountainous climates and remained unchanged in the oceanic zone. The largest NPP increase occurred in the mountainous zone with high soil water reserve and amounted to 13.3% and 16.7% for RCP4.5 and RCP8.5, respectively (Fig. 5.S5).

The RCP scenario effect on NPP was much more pronounced with the $[CO_2]_{var}$ runs (NPP increase from 21.9% to 34.9% under RCP4.5 and from 35.7% to 63.1% under RCP8.5) but the modulation of this effect according to the soil water reserve (MEW) and the climate was less marked (Fig. 5.S5).

When looking at the lowest simulated NPP values (< 7th percentile) under the $[CO_2]_{cst}$ runs, no clear scenario effect appeared, except for an increase with radiative forcing intensity for the mountainous zone with high MEW and a decrease for the oceanic climate zone with low MEW and for even-aged oak stands. With $[CO_2]_{var}$, the lowest simulated NPP values substantially increased for the two RCP scenarios compared to the historical period (Fig. 5.S6).

Overall, the relative changes in NPP were similar between the lowest (< 7th percentile) and the whole NPP values under $[CO_2]_{var}$. However, under $[CO_2]_{cst}$, more negative changes were pointed out for the lowest NPP values. For the whole NPP values, mean changes were comprised between -0.6 and +16.7% while, for the lowest NPP values, mean changes ranged from -11.3 to 11.6% for RCP8.5 (Fig. 5.S6).

### Comparison of the long-term trend with the inter-annual and inter-site variability and decomposition of the site effect

In order to evaluate the relative importance of the climate change effect compared to the climate inter-annual and inter-site variations, a linear mixed model was built to decompose the various sources of NPP variability.

For the $[CO_2]_{cst}$, the climate scenario effect only explained 4.7% of the NPP variability, while the effects of the inter-annual climate variations (residual variability) accounted for 19.9%. The total site effect explained 66.3% of the NPP variability and was decomposed into three components: 43.7% for the stand effect, 14.1% for the soil and 8.5% for the climate effect. 9.0% of NPP variability was attributed to interactions between the site components and the climate change scenario effects. These interactions with the site were dominated by the climate component (explaining 6.3% out of the 9.0%) representing the effect of the historical climate on the NPP response to climate change while the stand and soil effects explained a similar fraction of the remaining 2.7% (Table 5.4a).

Under $[CO_2]_{var}$, the proportion of the NPP variability explained by the RCP scenario was considerably higher and amounted to 28.5%. The inter-annual climate variations explained a lower proportion of the total NPP variability (16.4%). However, this NPP variability was higher than for the $[CO_2]_{cst}$ runs (+79.9%). Similarly, the site effect diminished but remained the major explaining factor with a partial $R^2$ of 0.476, which can be further divided in its stand (0.340), soil (0.069) and climate (0.067) components. Finally, the modulation of the climate scenario effect by the site components slightly decreased to explain 7.5% of the NPP variability with a dominance of the climate component (4.1%), followed by the stand (2.1%) and finally the soil (1.3%) (Table 5.4b).

To identify more precisely the factors at play behind the climate, soil and stand effects on NPP, multivariate models were elaborated. For the $[CO_2]_{cst}$, the stand effect was first explained by the mean dbh (18% of the total N variability) and then by the beech proportion in basal area (5%), the basal area (2%) and the standard deviation of the dbh (2%). Regarding the soil effect, the mean extractable water (MEW) accounted for 12% of the NPP variability. For the climate, the main driver was the MAT calculated for each climate scenario (6%); the mean air temperature and the rainfall during vegetation period contributed both to explain about 3%. Under $[CO_2]_{var}$, the relative importance of the factors explaining the NPP variability was similar than for the $[CO_2]_{cst}$ (mean dbh: 14%, beech %: 4%, BA: 1%, dbh SD: 1%, MEW: 6% MAT: 4%, AT during VP%) except that the atmospheric $CO_2$ concentration was considered in addition (27%) and that the rainfall during the vegetation period was not anymore retained. Except the proportion of beech and the mean air temperature during vegetation period, all these factors had a positive effect on NPP for both $CO_2$ modalities (Table 5.S7). It is worth to note that the climate variables not only account for the climate component of the site effects but also for the climate scenario effects.

The same exercise was done on the NPP change to highlight the factors explaining the NPP response to climate change. For the $[CO_2]_{cst}$, the mean temperature during the vegetation period (for the historical period) was the main driver of the NPP change (17%), then the MAP change (10%) and the rainfall during the vegetation period for the historical period (5%). The beech proportion and the MEW both accounted for 2% of the variability in NPP change. Under $[CO_2]_{var}$, the mean temperature during the vegetation period was also the main driver (12%) but the stand variable played a more important role (mean dbh: 8% and BA: 3.5%). All effects were positive except the mean temperature during the vegetation period (Table 5.S7). This effect was represented in Fig. 5.6 for the two climate models separately. For both models, a significant decrease was observed with increasing temperature during vegetation period for all stand types and both $CO_2$ modalities but was more pronounced for the constant one. For the latter and the CNRM-ALARO model, the change in NPP was negative in the even-aged oak stands with a mean temperature during the vegetation period superior to 19°C (Fig. 5.6 top). For the IPSL-RCA4 model, all stand types displayed negative changes when the temperature during vegetation period exceeded 20°C, except in beech even-aged stands (Fig. 5.6 bottom).

**Table 5.4: Estimate, standard error, P value and partial $R^2$ of the linear mixed model parameters (Eq. 6) used to highlight the climate change effect and decompose the site effect in its climate, soil and stand components in order to explain the NPP (gC m$^{-2}$ yr$^{-1}$) variability for the *virtual* sites with constant (a) and changing over time (b) atmospheric $CO_2$ concentration. The scenario includes differences in climate projections due to both the RCP scenario (hist, 4.5 and 8.5) and to the climate models (CNRM-ALARO and IPSL-RCA4).**

| | Estimate | Standard error | *P* value | Partial $R^2$ |
|---|---|---|---|---|
| a. Constant atmospheric $CO_2$ concentration | | | | |
| *Fixed effects* | | | | |
| Scenario [AL_Hist., AL_4.5, AL_8.5, RC_Hist, RC_4.5, RC_8.5] | [874.3, 956.9, 982.5, 836.7, 872.2, 851.5] | 71.8 | < .0001 | 0.047 |
| *Random effects* | | | | |
| Stand | 0 | 12094.2 | / | 0.437 |
| Soil | 0 | 5855.5 | / | 0.141 |
| Climate | 0 | 3087.6 | / | 0.085 |
| Stand x Scenario | 0 | 165.8 | / | 0.013 |
| Soil x Scenario | 0 | 261.2 | / | 0.014 |
| Climate x Scenario | 0 | 917.7 | / | 0.063 |
| Residuals | 0 | 95.7 | / | 0.199 |
| b. Changing over time atmospheric $CO_2$ concentration | | | | |
| *Fixed effects* | | | | |
| Scenario [AL_Hist., AL_4.5, AL_8.5, RC_Hist, RC_4.5, RC_8.5] | [848.2, 1094.2, 1286.6, 805.6, 1041.7, 1217.3] | 79.1 | < .0001 | 0.285 |
| *Random effects* | | | | |
| Stand | 0 | 16443.3 | / | 0.340 |
| Soil | 0 | 5057.5 | / | 0.069 |
| Climate | 0 | 4143.3 | / | 0.067 |
| Stand x Scenario | 0 | 454.1 | / | 0.021 |
| Soil x Scenario | 0 | 425.7 | / | 0.013 |
| Climate x Scenario | 0 | 1033.2 | / | 0.041 |
| Residuals | 0 | 136.8 | / | 0.164 |

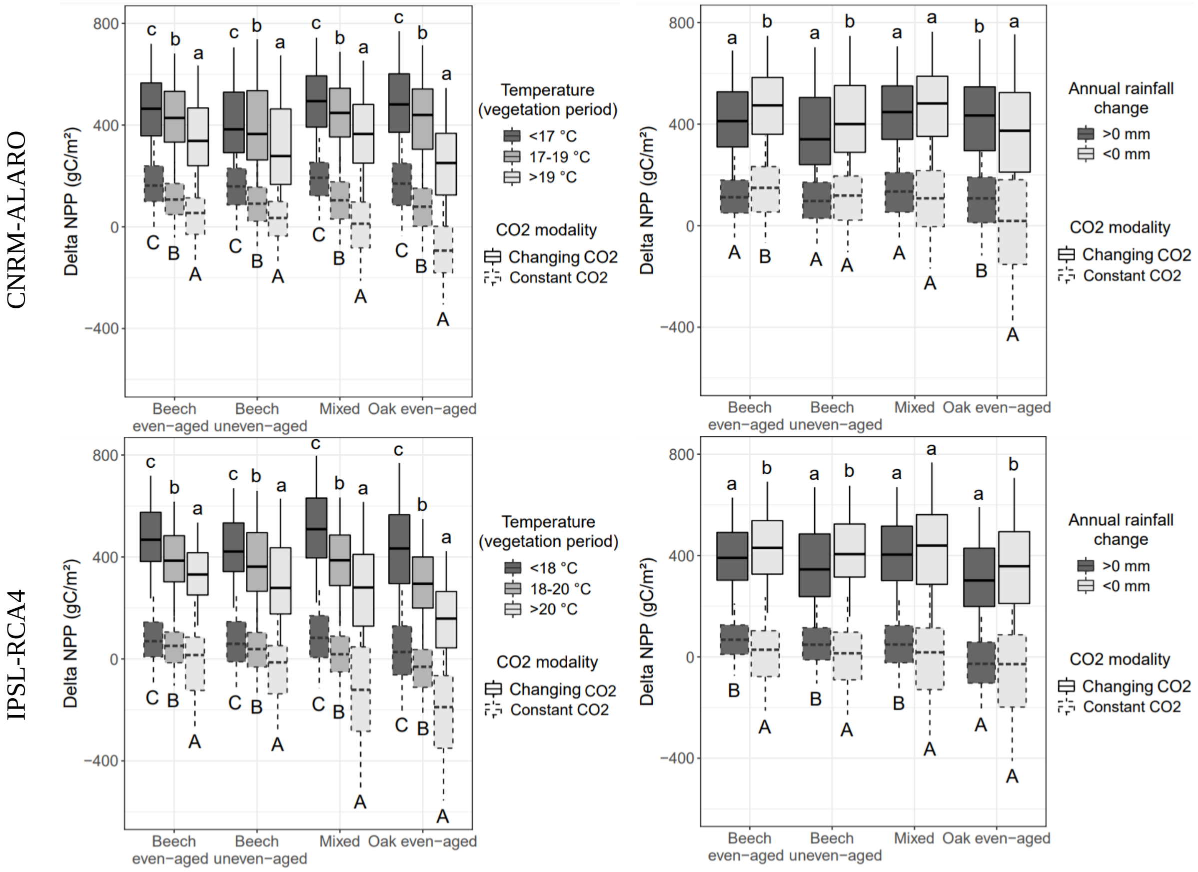

**Figure 5.6: Comparison of the simulated change in annual NPP in *virtual* sites between historical period (1976-2005) and RCP8.5 scenario (2071-2099) for the two atmospheric CO$_2$ modalities and the model CNRM-ALARO (top) and IPSL-RCA4 (bottom): highlighting of the stand type effect as well as the effects of the air temperature during the vegetation period (left) and the change in annual rainfall (right). For each box, the horizontal line corresponds to the median, the ends indicate the 25th and 75th percentiles and the whiskers show the values above and below these quartiles within 1.5 interquartile. For a same stand type, temperatures during vegetation period with common letters are not significantly different (paired Wilcoxon signed- rank).**

## 4. DISCUSSION

### 4.1. MODEL CALIBRATION AND PERFORMANCES

The model evaluation focused on the individual tree radial and height increment over periods ranging mostly from 10 to 15 years. Independent of the CUE calculation method used, the predictions were better for the radial growth (girth and basal area) than for the tree height (Table 5.3). This difference in prediction capacity was already highlighted in other studies (e.g. Schwalm and Ek, 2004; Vospernik and Eckmüllner, 2012) and can be attributed, to some extent, to the measurement errors that are considerably higher for tree height than for girth, which affects model parameterization, calibration and evaluation.

With the constant CUE, the model displayed already satisfying results for the radial growth (low bias and Pearson's r between 0.446 and 0.652) but was just able to provide unbiased mean height increment while it failed to capture its variability (Table 5.3). With this method, tree growth was slightly better predicted for beech than for oak, especially regarding tree height (Table 5.3). The constant CUE amounted to 0.67 for oak and to 0.59 for beech.

These values are a bit high compared to the 0.47 (±0.04 s.d.) value used by Waring *et al.* (1998) and implemented in many models (e.g. 3-PG, HyLand, 4C, BASFOR, early versions of 3D-CMCC-FEM). CUE has been estimated in various biomes for many tree species at different development stages. The observed range in CUE (0.22 to 0.79) reported by Collalti and Prentice (2019) and by Collalti *et al.* (2020a) is too large to be disregarded and questions the central value of Waring *et al.* (1998). Our values should rather be compared with the CUE obtained by DeLucia *et al.* (2007) for temperate broadleaved (0.58). This value is very close to the CUE obtained here for beech (0.59). Regarding oak, our value corresponds to the 75th percentile of the CUE distribution for temperate broadleaved forests (DeLucia *et al.*, 2007). This high value could partly be explained by an overestimated branch mortality rate (3%). Indeed, in HETEROFOR, carbon allocation to branches is in priority used to compensate for branch mortality.

When accounting for the influence of tree size, shape, local competition and MAT (only for oak) on CUE, the quality of the tree height predictions substantially increased, especially for oak. For the radial growth, improvements in the prediction quality were also observed (strong RMSE reduction and better regression test). The radial growth predictions were still a little bit better for beech than for oak, but the opposite was observed for tree height.

The CUE concept allows converting the GPP into NPP and therefore implicitly accounts for the growth and maintenance respiration. While the growth respiration (i.e. the metabolic cost of building new tissues) is proportional to NPP, the maintenance respiration depends on temperature and on the living biomass whose proportion changes with tree size and shape, and competition conditions (Collalti *et al.* 2020b). The living biomass proportion is higher in trees experiencing limited competition with well-developed crown. Indeed, such trees have a higher proportion of branches, leaves and fine roots and produce larger growth rings that increase their sapwood proportion (Canham *et al.*, 2004). This appears in our results as CUE decreased with the crown to stem diameter ratio, the crown length fraction and the light availability (in the CUE function). In addition, we observed a negative effect of MAT on CUE for oak (but not for beech), which can be explained by a strong temperature dependence of maintenance respiration (Yamori *et al.*, 2013; Zhang *et al.*, 2017; Collalti *et al.* 2020a). Although we used the CUE concept to convert GPP into NPP, an alternative option also exists in HETEROFOR to calculate explicitly maintenance respiration based on the N content of the living biomass of each tree compartment and accounting for the temperature dependence (sect. 1.3.5 in Chap. 2). We used this option to estimate the effect of the MAT on CUE and compared it with the one obtained by fitting the general CUE function. With this alternative method, we obtained a temperature effect ($-0.015\ °C^{-1}$) of the same order of magnitude as the one of the oak CUE function ($-0.020 °C^{-1}$). Such a negative temperature effect on CUE was also highlighted by Gifford (2003) and Piao *et al.* (2010) beyond a certain threshold even if the opposite was recently found by Collalti *et al.* (2020a). Regarding beech, the temperature effect was not considered in the CUE function as it was not significant, which is equivalent to assume that the autotrophic respiration and photosynthesis have a similar dependence on temperature. This temperature dependence could also be related to the effect of light availability (in the CUE function) since the trees with higher light availability experience greater temperatures and therefore could have a higher respiration rate.

Finally, accounting for the site effect in the CUE function allowed capturing more variability in radial growth for oak and in height increment for both species. The prediction quality was similar for both species regarding the radial growth and was still a little better for oak concerning tree height. Even if considering the site effect in the CUE function improved the prediction quality, this effect only moderately contributed to the explained variability, highlighting the generality of our function.

To assess the robustness of our modelling approach, the general CUE function was calibrated on a subset of sites and we compared the model performances on the calibration and evaluation sites (Fig. 5.1). The loss in prediction capacity was very limited between the two subsets of sites, which reinforced our confidence in the predictability of our model.

It is difficult to compare the evaluation results with other studies as the models applied on many sites across Europe are exclusively stand or cohort-based models, whose evaluation is done on observations averaged at the stand scale. Therefore, we compared our results to models that were locally and individually evaluated, which do not represent many studies as most individual-based models still make their evaluation at the stand-scale. Empirical models usually display the best results with relative biases most of the time below 13% and $R^2$ as high as 0.67 regarding girth increment (Schmid *et al*., 2005; Froese and Robinson 2007; Mette *et al*., 2009) while in process-based models, biases ranged between –30 and 30% and $R^2$ did not exceed 0.44 (Pretzsch 2002; Thürig 2005; Albrecht 2007; Schmidt and Hansen 2007; Kiernan 2008). Our prediction quality evaluation based on the independent dataset was similar to that of empirical models for beech (relative bias of –11.2 and $R^2$ of 0.60) and intermediate between empirical and process-based models for oak (relative bias of –14.3% and $R^2$ of 0.29). Tree height increment is much less evaluated and results differed considerably between the studies with relative biases covering a range from –70 to 61% and $R^2$ values from 0.04 to 0.48 (Sterba *et al*., 2001; Lacerte 2006; Vospernik 2007; Mette *et al*., 2009; Vospernik and Eckmüllner, 2012). With such a large span of statistical indices, our results easily fit in the range for bias but were at the lower margin regarding $R^2$.

### 4.2. SIMULATED CLIMATE CHANGE IMPACTS

We chose to validate the model on a large panel of contrasting climates in order to improve its extrapolation ability to simulate the climate change impact in the future. In a certain way, we applied the space-for-time substitution but not with the classical approach, which considers that tree growth at a given location in a warmer future will follow the current tree growth in warmer locations. One of the limits of this space-for-time approach is that spatial variations in tree growth are not only due to climate but also to soil conditions, stand type and forest management (Gugger *et al*., 2010; Collalti *et al*., 2018; Klesse *et al*., 2019). In our study, we overcome these limits by validating a process-based model in space and use it for temporal extrapolation. The reinforcement of the approach lies in the description of the eco-physiological processes, which is more likely to remain valid for the future conditions than statistical relationships built on present-day climate.

We decided to simulate future tree growth not only for *real* sites but also for *virtual* ones created by combining various stands, soils and climates from existing sites in order to encompass the diversity of conditions in Europe. The reason for using *virtual* in addition to *real* sites was to avoid correlations among the components of the site (soil, stand, climate) and to cover a large range of site conditions and stand types while limiting the simulation number and the computing time.

#### Impact on vegetation period

Our predicted rates of change in budburst and yellowing dates for 2071-2100 are in agreement with other modelling studies. For beech, we found that budburst could advance between 0.5 and 2.1 days/decade and yellowing delay between 1.2 and 1.9 days/decade. This is consistent with values found in literature: 0.6 to 1.9 day/decade for budburst and 1.4 to 2.3 days/decade for yellowing (Davi *et al.*, 2006; Menzel *et al.*, 2008; Delpierre *et al.*, 2009; Vitasse *et al.*, 2011; Collalti *et al.*, 2018; Zohner *et al.*, 2020a). For oak, the 0.9 to 3.3 days/decade earlier budburst and the 0.8 to 1.4 days/decade later yellowing are also in agreement with the ranges found in the literature, knowingly 1.1 to 2.3 days/decade for budburst and 0.7 to 1.7 days/decade for yellowing (Davi *et al.*, 2006; Menzel *et al.*, 2008; Delpierre *et al.*, 2009 Vitasse *et al.*, 2011; Collalti *et al.*, 2018; Nölte *et al.*, 2020; Zohner *et al.*, 2020a).

Interestingly, the greater advance in budburst for oak than for beech, compensated its initial delay during the historical period so that, in 2071-2100 under RCP8.5, budburst occurred more or less simultaneously for the two species (Fig. 5.S4). This stronger budburst sensitivity to temperature of oak compared to beech was highlighted in different studies (e.g. Vitasse et al., 2009; Cole and Sheldon, 2017). Regarding yellowing, the opposite trend was found, the greater delay in leaf senescence induced by climate warming for beech partly compensates for its earlier yellowing during historical period compared to oak. Finally, it is also interesting to note that, for oak, the photoperiod effect limited the yellowing delay induced by warmer temperature (Fig. 5.S4). These phenological changes and particularly budburst advances could be problematic as they increase the risk of late frost events during the tree leafing (Ma et al., 2019; Zohner et al., 2020b), for which oak and beech are particularly sensitive (San-Miguel-Ayanz et al., 2016; D'Andrea *et al.*, 2020a; D'Andrea *et al.*, 2020b).

**Impact on water cycling**

Under the assumption of $[CO_2]_{cst}$, a nearly generalised increase in transpiration deficit was observed. However, the level of transpiration deficit was strongly determined by the soil water reserve (MEW) and species composition. The soils with the highest MEW and the stands with the largest proportion of oak displayed the lowest deficits. These results are in agreement with our expectations since sites with large soil water reserve are less subject to transpiration deficit and oaks are known to be less sensitive to drought than beech (Jonard *et al.*, 2011; Scharnweber *et al.*, 2011; Scherrer *et al.*, 2011; Vanhellemont *et al.*, 2019).

Two processes can increase the transpiration deficit: a higher evapotranspiration due to warmer air temperatures or the reduction in rainfall amount especially during the vegetation period. In the simulations with *virtual* sites, we observed that evapotranspiration increased on average by 17.1 and 25.1% for oak-dominated stands and by 10.4 and 16.8% for beech dominated stands for the scenarios RCP4.5 and RCP8.5, respectively while the rainfall during the vegetation period was reduced by 4.8 and 5.7%. However, a considerable sensibility to the choice of the climate model is hidden behind these mean values. In CNRM-ALARO, the evapotranspiration increase corresponds to 19.9 and 34.3% for oak and to 13.6 and 24.4% for beech while evapotranspiration rises of 14.3 and 16.0% for oak and 7.2 and 9.2% for beech with IPSL-RCA4. In the CNRM-ALARO projections under RCP4.5 and RCP8.5, the rainfall during the vegetation period increased by 4.0 and 8.2% while vegetation period rainfall decreases by 13.5 and 19.6% in IPSL-RCA4 projections. Such differences between climate model results are a known issue (Kjellström et al., 2018; Christensen and Kjellström, 2020) and, in the case of European summer rainfall, the main source of variability is the choice of GCM (Christensen and Kjellström, 2020). In our case, the GCM CNRM-CM5 displays winter rainfall changes in line with most climate projections but for the summer they tend to be at the high end compared to the other CMIP5 models while IPSL-CMA5 presents rainfall changes in the middle of the range of the other models for all seasons (McSweeney et al., 2015). The large-scale changes to the pressure fields that drive summer-time storm track over Europe could induce these wet summers in CNRM-CM5 (see Dong et al., 2008). In addition, the RCM ALARO-0 associated to CNRM-CM5 also shows a tendency to produce wet summers as shown in Termonia et al. (2018). The two models considered here can be seen as illustrative of the sensitivity of our results to the uncertainty in the climate input. In the future, the use of climate projections from other climate global models would be interesting to verify the conclusions presented in this paper while being more representative of the climate model variability and, doing so, better account for the large uncertainty linked to the climate modelling of precipitation changes (Goberville *et al*., 2015; Dyderski *et al*., 2018; Nölte *et al*., 2020).

Under the $[CO_2]_{var}$ modality and RCP8.5 scenario, the transpiration deficit decreased in continental and oceanic zones and for all stand types (Fig. 5.5). This confirms that, under higher $CO_2$ levels, the stomatal conductance regulation allowed increasing photosynthesis and $CO_2$ fixation while limiting water loss. This decreases the pressure on soil water reserves, except in mountainous zones where a significant decrease in rainfall during the vegetation period was observed for both climate models (Table 5.1).

**Impact on NPP**

While NPP slightly increased for the $[CO_2]_{cst}$ runs in continental and mountainous climates and remained unchanged in the oceanic zone under the RCP8.5 scenario, NPP gains were observed everywhere and with greater magnitude with the $[CO_2]_{var}$ runs (Fig. 5.S5). Furthermore, it is interesting to note that NPP changes obtained with the $[CO_2]_{cst}$ runs are much more limited than those derived from the $[CO_2]_{var}$ runs (Fig. 5.6). The contrasting response of tree growth between the two $CO_2$ modalities can be ascribed to the enhanced photosynthesis and the lower stomatal conductance under elevated atmospheric $CO_2$ concentration, which induces higher water use efficiency (Ainsworth and Rogers, 2007; Norby and Zak, 2011). By comparing the two $CO_2$ modalities, we noticed that 60% to 100% of the NPP increase under the $[CO_2]_{var}$ scenario can be ascribed to the so called $CO_2$ fertilisation effect (Fig. 5.6). In other modelling studies comparing simulations with a constant and changing $CO_2$ modality for oak and beech, the contribution of the $CO_2$ fertilisation effect to the predicted productivity gain was pretty similar and amounted to 75% - 100% (Davi *et al*., 2006; Reyer *et al*., 2014; Collalti *et al.*, 2018; Nölte *et al*., 2020).

This $CO_2$ fertilization effect was highlighted in Free-Air Carbon dioxide Enrichment (FACE) experiments (Ainsworth and Long, 2005; Norby *et al*., 2005). However, its persistence in time remains quite uncertain. It will depend on the way the nutrient demand and the uptake capacity of the trees will evolve as well as on the soil ability to satisfy the increased nutrient demand (Oren *et al*., 2001; Wieder *et al*., 2015). Indeed, as the water use efficiency is expected to increase with rising $[CO_2]$, nutrient use efficiency could also increase and allow maintaining productivity gain with a limited increase in nutrient demand (Caldararu *et al*., 2020). However, even if an increase in nutrient use efficiency could temporarily delay the appearance of nutritional limitations, the nutrient availability will constrain the productivity gains sooner or later and the stands installed on nutrient-poor soils will be potentially the first to be affected (Norby *et al*., 2010; Warren *et al*., 2015). A decline of the $CO_2$ fertilisation effect is already observed at the global scale (Terrer *et al*., 2019; Wang *et al*., 2020). Consequently, the most likely scenario lies probably in between the two $CO_2$ modalities and will be closer to one or the other depending on the nutrient availability of the site, which is not considered here. Except in nitrogen-saturated forest ecosystems, high nitrogen (N) deposition could help maintain a persistent $CO_2$ fertilisation effect (Etzold *et al.*, 2020). With this regard, the current decline in N deposition in Europe will probably contribute to limit the increase in forest productivity (Waldner *et al.*, 2015; Craine *et al.*, 2018).

Under $[CO_2]_{cst}$ runs, the relative change in NPP (*virtual* sites and both RCP scenarios) amounted on average to +7% (–29 to 28%) while the changes reported in the literature for oak and beech in Europe are on average slightly negative (–2%) with decreases up to 15% and increases up to 10% (Lasch *et al.*, 2002; Davi *et al.*, 2006; Reyer *et al.*, 2014; Albert *et al.*, 2018; Collalti *et al.*, 2018; Nölte *et al.*, 2020; Sperlich et al., 2020). The mean NPP increase observed in our study is partly due to the fact that mountainous sites in colder climates are much more represented (one third of our *virtual* sites correspond to such climates) and because the NPP increase was much more marked in these mountainous sites, especially when the soil water reserve was large (Fig. 5.S5). The gain in NPP strongly decreased with the increase in temperature (mean annual and, particularly, during the vegetation period). This gain turned into NPP decreases under the warmest climates for even-aged oak stands with CNRM-ALARO climate projections and for most stand types with IPSL-RCA4 climate projections (Fig. 5.6 left). A decrease in annual rainfall compared to the historical period also had a statistically significant negative effect on NPP evolution but it mainly appeared under the $[CO_2]_{cst}$ modality and the IPSL-RAC4 climate projections (Fig. 5.6 right). In this case, the rainfall decreased significantly affected all stand types excepted oak. The absence of effect for CNRM-ALARO projections is not surprising as only a limited number of sites displayed a rainfall decrease.

When simulating the forest response to climate change on the *real* sites, we obtained overall a lower mean NPP change of +3.3% (-46.2 to 23.1%) under $[CO_2]_{cst}$ (Fig. 5.3 and Table 5.S6). Another reason explaining why our model simulated positive NPP change is linked to the climate projections we used for the simulations, one of which predicting particularly high summer precipitations compared to other climate models while the other displays average precipitation projections.

Under $[CO_2]_{cst}$ runs, the length of the vegetation period was the main driver of the NPP change as also mentioned by Keenan et al. (2014) and Park et al. (2016). As photosynthesis is a temperature-dependent process reaching an optimum for leaf temperature between 20 and 30°C and then declines (Yamori et al., 2013), the rise in air temperature favours GPP but up to some extent and is especially marked in colder climates. Among the processes acting negatively on NPP, the higher transpiration deficit observed for beech stands under the $[CO_2]_{cst}$ modality reduced the NPP while the transpiration deficit remained negligible regarding oak. Maintenance respiration is also influenced by temperature. This effect is accounted for in the CUE function (see in Eq. 5 term “k MAT”) for oak but not for beech as it was not significant.

For the sites in which the fertilizing $CO_2$ effect is not constrained ($[CO_2]_{var}$ runs), the long-term trend could account for 29% of NPP variability which would be nearly twice the inter-annual climate variations (Table 5.4). In this case, the expected change corresponds to an increase in productivity, which is favourable to forest growth and vitality. In sites more constrained, for example by nutrient availability, as represented by the $[CO_2]_{cst}$ runs, the long-term trend would explain a limited part of the NPP variability compared to the inter-site and inter-annual climate variations (Table 5.4).

A large part of the NPP variability is explained by the site effect which is dominated by its stand component (Table 5.4). The variables we used to characterized the stand were able to account for 60% of the variability due to the stand effect but the remaining 40% were not possible to capture and can be ascribed to more complex structure effects (Table 5.S7). In a more limited extend, the site also influenced the NPP response to climate change but, in this case, with a dominance of its climate component (Table 5.4). Some stand characteristics influenced however the NPP change which, under $[CO_2]_{cst}$, was more positive in stands with a higher beech proportion and, under $[CO_2]_{var}$, in stands with higher density and mean tree size (Table 5.S7). The positive effect of beech on NPP change is due to the fact that its CUE was not decreased with increasing MAT contrary to oak. A negative MAT effect on beech CUE was not considered as it was not significant based on the available observations. If a MAT effect similar to that on oak CUE had been included for beech, the tendency could have been reverse, with more positive effect of oak on NPP change, especially for the climate projections showing a decrease in rainfall during vegetation period (IPSL-RCA4) given the higher sensitivity of beech NPP to drought. Under $[CO_2]_{var}$, the stand characteristics favouring NPP change probably partly reflect the stand ability to intercept more solar radiation (the density and the mean tree size) and then to benefit more from the $CO_2$ fertilization effect. With other climate projections conducting, for example, to drier conditions during the vegetation period, the role played by the stand characteristics could change. The effects of the stand characteristics on NPP and on its response to climate change show that the forester has the possibility to act on the stand productivity and to prepare forests to possible adverse effects of climate change by reinforcing forest resilience.

Our results might sound optimistic, especially for beech for which drought-induced growth decline has been observed at the southern edge of their distribution area (Charru *et al*., 2010; Zimmerman *et al*. 2015; D'Andrea *et al*. 2020), raising concern about their persistence under warmer and drier conditions (Noce *et al*. 2017). However, other studies point out opposite results (Tegel *et al*., 2014) or emphasize the swift recovery ability of beech after drought episodes (Vanhellemont *et al*., 2019). At the European scale, a very slight crown defoliation increase of 2.4% and 2.2% in 20 years is observed for beech and oak in the level II plots of ICP Forests (Timmerman *et al*., 2020). In addition, a 5% increase in basal area increment was detected between 1980 and 2007 for European beech in France as well as a 4% increase for sessile oak and 3% decline for pedonculate oak (Charru et al. 2017). Forrester et al. (2021) reconstructing past growth with 3-PG obtained similar changes (12% increase in stem biomass between 1960 and 2010) for European beech in Switzerland. These rates of change in tree growth are intermediate between those we obtained with constant and changing $CO_2$ runs.

Even if the future climate is on average more favourable for tree growth, extreme events could occur occasionally and trigger a high rate of mortality. Currently, HETEROFOR does not account for vitality loss and mortality due to hydraulic failure, late frost, storms and biotic causes. We plan to describe the mortality by hydraulic failure and the damages due to late frost in the next versions of the model but accounting for pest attacks and diseases is less straightforward. More data and knowledge are required before all mortality causes can be adequately addressed in individual-based models (Hartmann *et al*., 2018).

## 5. CONCLUSION AND FUTURE PROSPECTS

Our simulation results showed that the climate change could have a positive effect on forest productivity in most sites, except those displaying particularly warm spring and summer temperatures and a strong reduction in rainfall. There is however a large uncertainty on the magnitude of this effect depending on the model used for the climate projections, the RCP scenarios and on whether the $CO_2$ fertilisation effect will persist or not. Apart from the $CO_2$ fertilisation, the main drivers of the positive changes are the increase in the vegetation period length and the improved water use efficiency. The negative NPP changes observed in some sites can be explained by higher transpiration deficit and maintenance respiration costs. While the site effect and mainly the stand characteristics explained the major part of the NPP variability, they showed only a limited influence on the forest response to climate change.

Given the strong influence of the choice of the climate model on our results, it would be interesting to repeat the simulations with climate projections from other models to still better apprehend the uncertainty associated with this aspect. With some climate projections, water stress could be more pronounced, especially in beech stands and lead to productivity losses in more sites. Now that a full methodology has been created and verified, the repetition of new simulations will be very straightforward and could be done each time new and more accurate climate projections are produced or when new model developments allow better capturing the effect of climate change on individual tree growth.

## 6. SUPPLEMENTARY MATERIALS

**Table 5.S1: Site-dependent parameters of the dendrometric relationship used to estimate missing values of total tree height in the inventory file of HETEROFOR. The equation of Dhôte and de Hercée (1994) was used**

$$\boldsymbol{h} = \frac{\mu_{11}+\mu_{12}*age-1.3+\mu_2.girth-\sqrt{(\mu_{11}+\mu_{12}*age-1.3+\mu_2.girth)^2-4\mu_2.\tanh(\lambda_4).(\mu_{11}+\mu_{12}*age-1.3).girth}}{2\tanh(\lambda_4)} + \mathbf{1.3}$$

| Site ID | $\mu_{11}$ | $\mu_{12}$ | $\mu_2$ | $\lambda_4$ |
|---|---|---|---|---|
| *Beech* | | | | |
| 1 (Baileux-oak) | -892.78 | 0.459 | 0.456 | 0.902 |
| 1 (Baileux-beech) | -102.65 | 0.0645 | 0.297 | 2.141 |
| 1 (Baileux-mixed) | -159.73 | 0.0942 | 0.348 | 1.663 |
| 3 | 14.59 | 0.187 | 0.383 | 1.813 |
| 4, 5, 9 | 2.128 | 0.3959 | 0.3027 | 2.616 |
| 6 | 38.01 | 0.0 | 0.280 | 1.588 |
| 7 | 2.505 | 0.583 | 0.529 | 0.496 |
| 8 | 20.77 | 0.0690 | 0.305 | 2.577 |
| 10, 13 | 23.012 | 0.111 | 0.468 | 1.053 |
| 11 | -4.743 | 0.358 | 0.361 | 1.21 |
| 12 | -4.743 | 0.358 | 0.361 | 1.21 |
| 15 | 17.812 | 0.167 | 0.372 | 2.422 |
| 16 | 17.812 | 0.167 | 0.372 | 2.422 |
| 17 | 45.75 | 0 | 0.545 | 0.05 |
| 21 | 6.791 | 0.187 | 0.401 | 2.19 |
| 22 | 21.276 | 0.0 | 0.295 | 1.5 |
| 23 | 32.383 | 0.061 | 0.42 | 1.029 |
| 25, 26 | 5.79 | 0.228 | 0.636 | 0.612 |
| 27 | -105.655 | 1.367 | 0.322 | 1.704 |
| 28 | 7.778 | 0.283 | 0.43 | 1.447 |
| 31, 32 | 5.391 | 0.344 | 0.352 | 2.641 |
| *Oak* | | | | |
| 1 (Baileux-oak) | -526.92 | 0.276 | 0.439 | 1.0 |
| 1 (Baileux-beech) | -134.35 | 0.0804 | 0.560 | 1.0 |
| 1 (Baileux-mixed) | -326.11 | 0.178 | 0.452 | 1.0 |
| 2 | 23.56 | 0.0 | 0.336 | 1.0 |
| 4 | -0.9318 | 0.4945 | 0.6102 | 0.2716 |
| 6 | 35.54 | 0.0 | 0.496 | 1.0 |
| 7 | 64.71 | 0.0 | 0.127 | 2.0 |
| 8 | 15.68 | 0.154 | 0.492 | 1.0 |
| 10, 13, 14 | 16.86 | 0.148 | 0.344 | 2.017 |
| 11 | 16.86 | 0.148 | 0.344 | 2.017 |
| 12 | 23.021 | 0.093 | 0.446 | 0.874 |
| 17, 18 | 10.51 | 0.216 | 0.356 | 1.648 |
| 19 | 18.068 | 0.268 | 0.444 | 1.0 |
| 20 | 6.375 | 0.414 | 0.467 | 1.003 |
| 21 | 21.425 | 0.171 | 0.414 | 1.0 |
| 23 | 31.165 | 0.055 | 0.379 | 1.0 |
| 24 | 24.7 | 0.234 | 0.841 | 0.1 |
| 28, 29 | -18.139 | 0.523 | 0.362 | 2.155 |
| 30 | 28.915 | 0 | 0.37 | 1.909 |
| 32 | 9.857 | 0.26 | 0.441 | 2.017 |

**Table 5.S2: Site-dependent parameters of the dendrometric relationship used to estimate missing values of crown base height. An equation predicting the fraction of the total height corresponding to the crown base height was used**

$$hcb\% = e^{a} * girth^{b} * age^{c}$$

| Site ID | a | b | c | conditions |
|---|---|---|---|---|
| *Beech* | | | | |
| 1 (Baileux-oak) | 154.65 | -0.187 | -20.31 | |
| 1 (Baileux-beech) | 0.464 | -0.191 | 0.0 | |
| 1 (Baileux-mixed) | 143.63 | 0.154 | -19.05 | |
| 3, 6, 7, 8 | -1.497 | 0.159 | 0.0 | |
| 4, 5 | 4.215 | -0.4995 | -0.8724 | tree height <22.5m |
| 4, 5 | 1.853 | -0.4031 | -0.153 | tree height >=22.5m |
| 9 | 1.569 | -0.3731 | -0.1526 | |
| 10, 16, 27, 28 | 8.39 | -0.127 | -1.909 | |
| 11 | -1.116 | -0.207 | 0.348 | |
| 12, 15 | -4.251 | -0.222 | 1.011 | |
| 17 | 0.00944 | -0.169 | 0.0 | |
| 21 | -1.603 | 0.182 | 0.0 | |
| 22 | -3.516 | -0.405 | 0.947 | |
| 23 | 1.698 | -0.524 | 0.0 | |
| 25, 26 | 0.05 | -0.118 | 0.0 | |
| 31 | 0.403 | -0.214 | 0.0 | |
| 32 | 0.153 | -0.193 | 0.0 | |
| *Oak* | | | | |
| 1 (Baileux-oak) | 122.36 | -0.278 | -15.98 | |
| 1 (Baileux-beech) | 0.467 | -0.166 | 0.0 | |
| 1 (Baileux-mixed) | 0.767 | -0.231 | | |
| 2, 6, 7, 19, 20 | 0.573 | -0.232 | 0.0 | |
| 3 | | | | |
| 4 | 0.7991 | -0.3095 | 0.0 | |
| 8 | | | | |
| 10, 14, 16, 28 ,29, 30 | 3.394 | -0.116 | -0.814 | |
| 11, 13 | -10.544 | -0.208 | 2.274 | |
| 12 | -0.3857 | 0.0 | 0.0 | |
| 17, 18 | -0.1 | -0.137 | 0.0 | tree girth < 200 cm |
| 17, 18 | -0.713 | 0.0 | 0.0 | tree girth >= 200 cm |
| 21 | -0.403 | 0.0 | 0.0 | |
| 23 | 0.918 | -0.29 | 0.0 | |
| 24 | -0.1453 | -0.1084 | 0.07169 | |
| 32 | 1.623 | -0.483 | 0.0 | |

**Table 5.S3: Site-dependent parameters of the dendrometric relationship used to estimate missing values of the height of largest crown extension. An equation predicting the fraction of the total height corresponding to the height of largest crown extension was used**

$$hlce\% = e^{a} * girth^{b} * age^{c}$$

| Site ID | a | b | c |
|---|---|---|---|
| *Beech* | | | |
| 1 (Baileux-oak) | -107.30 | 0.0 | 14.06 |
| 1 (Baileux-beech) | -85.53 | -0.0568 | 11.25 |
| 1 (Baileux-mixed) | -0.854 | 0.127 | 0.0 |
| 3 | -6.192 | 0.0 | 1.360 |
| 6 | -6.774 | 0.127 | 1.188 |
| 7 | -2.294 | 0.164 | 0.229 |
| 8 | -5.751 | 0.0 | 1.212 |
| others | -0.640 | 0.0790 | 0.0 |
| *Oak* | | | |
| 1 (Baileux-oak) | -125.26 | -0.199 | 16.56 |
| 1 (Baileux-beech) | 0.0660 | -0.0591 | 0.0 |
| 1 (Baileux-mixed) | -50.22 | -0.103 | 6.645 |
| 2 | -9.078 | -0.174 | 1.975 |
| 6 | -1.793 | -0.266 | 0.601 |
| 7 | 4.917 | -2.236 | 1.574 |
| 8 | -0.843 | -0.128 | 0.227 |
| others | 0.155 | -0.0788 | 0.0 |

**Table 5.S4: Site-dependent parameters of the dendrometric relationship used to estimate missing values of crown radius. An equation predicting the crown to stem diameter ratio (Dd in m $m^{-1}$) was used**

$$Dd = e^{a} * girth^{b} * age^{c}$$

| Site ID | a1 | b1 | c1 |
|---|---|---|---|
| *Beech* | | | |
| 10, 11, 13, 16 | 4.804 | -0.504 | 0.16 |
| 12 | 6.246 | -0.691 | 0.0 |
| 15 | 4.1 | -0.226 | 0.0 |
| 21, 22, 23 | 4.509 | -0.304 | 0.0 |
| others | 5.926 | -0.582 | 0.0 |
| *Oak* | | | |
| 10, 14 | 2.982 | 0.0 | 0.0 |
| 11, 13 | 2.477 | 0.0 | 0.0 |
| 12 | 2.833 | 0.0 | 0.0 |
| 19, 20, 21, 23 | 3.01 | 0.0 | 0.0 |
| 24 | 2.323 | 0.0 | 0.0 |
| others | 3.697 | -0.138 | 0.0 |

**Table 5.S5. Description of model parameters for Sessile/Pedunculate oak and European beech and origin of their value.**

| *Symbol* | *Description* | *Units* | *Value* | | **Origin** |
|---|---|---|---|---|---|
| | | | *Sessile/Pedunculate oak* | *European beech* | |
| ***Phenology*** | | | | | |
| $t_0$ | chilling starting date | day of year | 244 | | Duputié et al. (2015) |
| $R_c$ *(optimal)* | chilling rate function ($T_{min}$, $T_{max}$, $T_{opt}$ in Eq 3) | °C | -48.0, 30.2, 2.7 | | Duputié et al. (2015) |
| $R_c$ *(sigmoid)* | chilling rate function ($C_a$, $C_b$, $C_c$ in Eq 2 de Wergifosse et al., 2020) | °C | | 0.007, -0.347, -13.1 | Duputié et al. (2015) |
| $C*$ | chilling threshold | °C | 157.7 | 194.0 | Duputié et al. (2015) |
| $R_f$ | forcing rate function ($F_b$, $F_c$ in Eq 3 de Wergifosse et al., 2020) | °C | -0.4, 9.0 | -0.138, 17.3 | Duputié et al. (2015) |
| $T_{b\ for}$ | base temperature for forcing | °C | -20 | | fixed |
| $F*$ | forcing threshold | °C | 22.5 | 8.2 | Duputié et al. (2015) |
| $t_{2a\ shift}$ | budburst shift | days | -15 | | calibrated (Baileux plots) |
| $LD*$ | leaf development threshold | °C | 312 | | calibrated (Baileux plots) |
| $t_3$ | ageing starting date | day of year | 213 | | Dufrêne et al. (2005) |
| $T_{b\ age}$ | base temperature for ageing | °C | 20 | | Dufrêne et al. (2005) |
| $A*$ | ageing threshold | °C | 230 | | Dufrêne et al. (2005) |
| $y$ | leaf yellowing parameter | - | 0.07557 | 0.27 | calibrated (ICP forests plots) |
| $Y*$ | yellowing threshold | kgC.kgC$^{-1}$ | 0.01 | | fixed |
| $R_{fall}$ | falling rate | s.m$^{-1}$.day$^{-1}$ | 0.01 | 0.0075 | calibrated (ICP forests plots) |
| $F_{ampl}$ | frost amplifier coefficient | - | 2 | | calibrated (ICP forests plots) |
| ***Light interception*** | | | | | |
| $k$ | extinction coefficient | m$^{-1}$ | 0.322 | 0.463 | calibrated (André et al. submitted) |
| $SLA$ | specific leaf area (min, max) | m$^2$ kg$^{-1}$ | 5.9, 20.0 | 9.9, 30.0 | Forrester et al. (2017) |
| ***Water balance*** | | | | | |
| $c_{foliage}$ | foliage storage capacity | l.m$^{-2}$ leaf | 0.272 | 0.174 | André et al. (2008a) |
| $c_{bark\ ll}$ | leafless bark storage capacity function (c,d, $R_{min}$ in Eq 16 of de Wergifosse et al., 2020) | l | -9.08, 0.16, 6.0 | -9.53, 0.18, 1.5 | André et al. (2008b) |
| $c_{bark\ ld}$ | leaved bark storage capacity function (c,d, $R_{min}$ in Eq 16 of de Wergifosse et al., 2020) | l | -4.21, 0.08, 10.9 | -4.15, 0.09, 3.4 | André et al. (2008b) |
| $g_{s\ bark}$ | bark vapour conductance function ($g_{s\ min}$, $g_{s\ max}$) | m.s$^{-1}$ | 0.00775, 0.125 | | soil values x 100 |
| $g_{s\ soil}$ | soil vapour conductance function ($g_{s\ min}$, $g_{s\ max}$) | m.s$^{-1}$ | 7.75E-05, 0.00125 | | Dufrêne et al. (2005) |
| **Photosynthesis** | | | | | |
| $M_{height}{}^1$ | height effect on stomatal conductance function (a, b, $g_{s\ min}$) | - | 1.0, 0.0, 0.0 | 435.0, 0.1, 56.0 | Schäfer et al. (2000) |
| $M_{soil\ water}$ | soil water effect on stomatal conductance function ($p_1$, $p_2$ in Eq. 55 of de Wergifosse et al., 2020) | - | 0.127, 5.0 | 0.527, 3.0 | fitted (data from Jonard et al., 2011) |
| **Respiration** | | | | | |
| $r_{npp\ gpp}$ | npp to gpp ratio function (a, b, c, d, e, f, g, i, j, k in Eq. 4) | kgC.kgC$^{-1}$ | 0.98,0.017,-1.5E-04,0,0, 0,-0.54,-0.45,-0.39,-0.020 | 0.093,0,0,0.032,-2.5E-04, -0.0023,-0.24,0,-0.25,0 | calibrated (ICP forest plots) |
| $R_{gr}$ | growth respiration per unit biomass increment | kgC.kgC$^{-1}$ | 0.2 | | Dufrêne et al. (2005) |
| **Carbon allocation** | | | | | |
| $b_{leaf}$ | leaf biomass function (α, β, γ in Eq. 15 of Jonard et al., 2020) | gOM | 0.005, 1.96, 1.96 | 1.47, 2.0, 0.0 | fitted (data from Jonard et al., 2006) |
| $b_{stru\ abg}$ | aboveground structural biomass (α, β, γ in Eq. 26 of Jonard et al., 2020) | kgOM | 0.0, 321.6, 0.96 | 0.0, 273.6, 1.00 | fitted on biomass data[2] |
| $p_{fruit}$ | fruit production function (α, β, $dbh_{min}$ in Eq. 22 of Jonard et al., 2020) | kgC | 0.0016, 2.34, 25 | 4.5E-04, 2.68, 25 | fitted (Baileux plots) |
| $\rho$ | stem volumetric mass | kgOM.m$^{-3}$ | 587.7 | 560.5 | calculated from biomass and volume |
| $r_{root\ shoot}$ | root to shoot ratio | kgC.kgC$^{-1}$ | 0.18 | | Schepaschenko et al. (2017) |
| $r_{fr\ leaf}$ | fine root to leaf ratio | kgC.kgC$^{-1}$ | 1.0 | | fixed |
| $\delta_{leaf}$ | leaf relative loss rate | kgC.kgC$^{-1}$.yr$^{-1}$ | 1.0 | | |
| $\delta_{branch}$ | branch relative loss rate | kgC.kgC$^{-1}$.yr$^{-1}$ | 0.03 | 0.01 | fitted (Baileux plots) |
| $\delta_{root}$ | root relative loss rate | kgC.kgC$^{-1}$.yr$^{-1}$ | 0.03 | 0.01 | same as branch |
| $\delta_{fr}$ | fine root relative loss rate | kgC.kgC$^{-1}$.yr$^{-1}$ | 1.0 | | Leushner and Meier (2018) |
| $rt_{leaf}$ | leaf retranslocation rate | kgC.kgC$^{-1}$.yr$^{-1}$ | 0.216 | | Vergutz et al. (2012) |
| $rt_{root}$ | fine root retranslocation rate | kgC.kgC$^{-1}$.yr$^{-1}$ | 0.216 | | Vergutz et al. (2012) |
| **Tree dimension increment** | | | | | |
| $\Delta h$ | height growth function (a, b, c, d, e, f, g in Eq. 5) | m.yr$^{-1}$ | 0.0098, -0.13, 0.46, -0.090, 0.0, 0.0, 0.0 | -0.016, -0.29, 0.58, -0.096, -0.0014, -8.1E-05, 0.0022 | calibrated (ICP forests and Baileux plots) |
| $\Delta dbh$ | default dbh increment | cm.yr$^{-1}$ | 0.32 | 0.37 | estimated (ICP forests and Baileux plots) |
| $hcb\%^3$ | crown base height function (a, b, c, d) | m.m$^{-1}$ | 0.88, -0.0013, -0.29, 0.30 | 0.43, 6.0E-04,0.13, 0.0 | fitted (ICP forests and Baileux plots) |
| $lcpf\%$ | lower crown part fraction | m.m$^{-1}$ | 0.45 | 0.44 | estimated (ICP forests and Baileux plots) |
| $\Delta hlce_{max}$ | maximum annual change in the height of largest crown extension | m.yr$^{-1}$ | 0.7 | 1.0 | estimated (ICP forests and Baileux plots) |
| $\Delta hcb_{max}$ | maximum annual change in the crown base height | m.yr$^{-1}$ | 0.7 | 0.6 | estimated (ICP forests and Baileux plots) |
| $Dd$ | crown to stem diameter function (a, b, c, d, e) | m.m$^{-1}$ | 19.12, 0.0063, 0.0, 0.0, 0.0 | 12.22, 0.0, 1368.7, 0.0, -2.71 | fitted (ICP forests and Baileux plots) |
| $Sh$ | coefficient to shift the mean crown to stem diameter ratio to its maximum | - | 1.35 | 1.50 | estimated (ICP forests and Baileux plots) |
| $v_{stru\ abg}$ | tree total volume function (a, b, c in Eq. 5 in Deleuze et al. 2014a) | m$^3$ | 0.56, 0.66, -0.0024 | 0.54, 0.66, -0.0015 | Deleuze et al. (2014a) |
| $v_{stem}\%$ | stem fraction of tree total volume (d, e, f, g in Eq. 5 in Deleuze et al. 2014b) | m$^3$.m$^{-3}$ | 1.09, 0.11, -8.24, 0.0048 | 0.62, 0.11, 1.28, -0.0046 | fitted on biomass data[1] |

[1] $M_{height} = \frac{gs_{min}+(a-gs_{min})\cdot e^{-b\cdot h}}{a}$

[2] biomass data from André and Ponette (2003), André et al. (2010), Schepaschenko et al. (2017), Falster et al. (2015) and Ung et al. (2017)

[3] $\%hcb = a + b\ girth + c\ LCI + d\ LCI^2$

**Table 5.S6: Average NPP values in *real* sites during the historical period (1976-2005) and the scenarios RCP4.5 and RCP8.5 (2071-2100) in the different sites used for the calibration and evaluation of the model under the constant and changing CO2 modalities and the site-dependent CUE function. The results are presented separately for the simulations made with the two types of climate projections (CNRM-ALARO and IPSL-RCA4).**

| Site | NPP CNRM-ALARO (constant $CO_2$) | | | NPP CNRM-ALARO (changing $CO_2$) | | | NPP IPSL-RCA4 (constant $CO_2$) | | | NPP IPSL-RCA4 (changing $CO_2$) | | |
|---|---|---|---|---|---|---|---|---|---|---|---|---|
| | Hist | 4.5 | 8.5 | Hist | 4.5 | 8.5 | Hist | 4.5 | 8.5 | Hist | 4.5 | 8.5 |
| Baileux-oak (BE) | 990.0 | 999.1 | 1008.9 | 966.7 | 1108.7 | 1252.8 | 887.3 | 837.2 | 717.8 | 871.2 | 998.0 | 1069.3 |
| Baileux-beech (BE) | 909.6 | 965.9 | 1032.3 | 888.4 | 1065.6 | 1262.1 | 867.3 | 947.9 | 897.8 | 842.6 | 1090.9 | 1182.6 |
| Baileux-mixed (BE) | 1103.7 | 1164.9 | 1230.9 | 1077.4 | 1285.6 | 1504.4 | 1045.0 | 1115.4 | 1045.9 | 1017.1 | 1284.3 | 1393.4 |
| Chimay (BE) | 832.2 | 725.8 | 605.7 | 808.7 | 818.0 | 776.1 | 772.1 | 581.7 | 415.4 | 743.2 | 706.6 | 617.4 |
| Eupen (BE) | 714.9 | 786.1 | 874.5 | 697.8 | 868.1 | 1068.2 | 689.9 | 776.8 | 785.6 | 671.4 | 904.5 | 1037.9 |
| Gontrode (BE) | 1007.4 | 1031.4 | 1064.1 | 978.6 | 1163.4 | 1327.0 | 937.9 | 959.0 | 886.1 | 920.9 | 1140.5 | 1217.6 |
| Hoeilaart (BE) | 1253.4 | 1299.7 | 1355.9 | 1218.3 | 1471.7 | 1731.9 | 1178.7 | 1245.4 | 1202.9 | 1143.9 | 1448.8 | 1611.2 |
| Louvain-la-Neuve (BE) | 911.5 | 948.3 | 998.4 | 887.5 | 1062.0 | 1234.7 | 842.3 | 884.3 | 850.1 | 817.6 | 1026.8 | 1136.2 |
| Virton (BE) | 951.4 | 1013.0 | 1062.2 | 911.9 | 1205.9 | 1490.2 | 838.0 | 810.6 | 768.1 | 805.6 | 1015.5 | 1176.1 |
| Wellin (BE) | 903.9 | 961.9 | 1030.3 | 879.6 | 1071.3 | 1275.4 | 748.7 | 827.2 | 824.9 | 726.1 | 969.5 | 1102.0 |
| Wijnendale (BE) | 888.9 | 944.1 | 992.8 | 863.9 | 1068.4 | 1254.1 | 831.3 | 899.6 | 876.4 | 805.6 | 1044.1 | 1158.4 |
| Bavaria-North (DE) | 1061.8 | 1056.4 | 1020.3 | 1029.4 | 1220.0 | 1349.4 | 1125.4 | 1082.9 | 966.8 | 1089.3 | 1278.9 | 1349.8 |
| Bavaria-South (DE) | 1003.1 | 1085.6 | 1130.4 | 979.1 | 1201.0 | 1396.8 | 1009.4 | 1145.3 | 1158.7 | 982.1 | 1302.8 | 1486.0 |
| North Rhine-W. (DE) | 857.6 | 923.2 | 988.3 | 840.6 | 1003.7 | 1158.6 | 833.9 | 963.1 | 939.4 | 815.7 | 1069.5 | 1137.6 |
| Saarland (DE) | 930.3 | 965.2 | 963.9 | 903.8 | 1078.2 | 1208.0 | 895.9 | 900.6 | 821.4 | 866.7 | 1065.1 | 1152.9 |
| Saxony (DE) | 621.9 | 644.3 | 626.0 | 597.8 | 739.1 | 828.1 | 600.1 | 595.8 | 574.3 | 579.3 | 701.6 | 776.6 |
| Schleswig-H. (DE) | 1049.8 | 1096.0 | 1150.8 | 1021.8 | 1249.6 | 1466.4 | 1010.1 | 1101.7 | 1073.6 | 980.6 | 1267.3 | 1377.0 |
| Thuringia (DE) | 864.6 | 937.3 | 995.1 | 839.5 | 1072.1 | 1287.5 | 857.0 | 926.0 | 937.5 | 830.5 | 1086.3 | 1255.1 |
| Suserup (DK) | 1195.5 | 1290.3 | 1325.7 | 1160.0 | 1453.1 | 1700.3 | 1227.7 | 1330.8 | 1298.7 | 1190.7 | 1530.5 | 1656.5 |
| Vestkoven (DK) | 685.5 | 737.1 | 727.3 | 661.6 | 835.4 | 935.4 | 691.5 | 729.2 | 656.3 | 669.3 | 839.5 | 859.6 |
| CHP40 (FR) | 1073.4 | 1041.3 | 926.1 | 1037.8 | 1196.6 | 1245.0 | 933.7 | 808.8 | 646.5 | 899.7 | 983.6 | 1009.7 |
| CHP65 (FR) | 1257.7 | 1233.5 | 1125.8 | 1218.8 | 1431.1 | 1529.5 | 994.0 | 851.3 | 699.5 | 954.7 | 1040.2 | 1087.7 |
| CHS72 (FR) | 1435.6 | 1370.1 | 1305.4 | 1376.9 | 1662.9 | 1963.4 | 1268.8 | 1137.8 | 1005.7 | 1215.7 | 1419.2 | 1594.2 |
| HET 30 (FR) | 637.0 | 709.5 | 769.6 | 620.3 | 805.8 | 994.6 | 665.0 | 699.1 | 640.4 | 639.7 | 831.6 | 948.4 |
| HET 64 (FR) | 658.3 | 678.4 | 668.0 | 641.0 | 754.5 | 841.4 | 739.1 | 706.6 | 622.5 | 712.7 | 841.2 | 921.1 |
| Alice Holt (GB) | 677.8 | 716.6 | 737.2 | 649.7 | 847.3 | 1015.0 | 633.1 | 634.2 | 592.8 | 607.5 | 772.0 | 844.0 |
| Cansiglio-innov (IT) | 874.4 | 974.5 | 1030.1 | 853.3 | 1123.6 | 1366.1 | 837.0 | 856.1 | 858.2 | 803.8 | 1028.6 | 1284.6 |
| Cansiglio-trad (IT) | 592.2 | 686.9 | 728.8 | 575.5 | 800.2 | 976.4 | 577.5 | 600.0 | 600.6 | 557.6 | 735.6 | 906.2 |
| Cansiglio-unman (IT) | 576.6 | 674.7 | 703.8 | 564.3 | 757.7 | 896.1 | 594.3 | 616.3 | 615.7 | 574.6 | 748.9 | 905.5 |
| Collelongo (IT) | 741.8 | 841.1 | 871.3 | 720.0 | 968.5 | 1187.8 | 645.8 | 689.0 | 716.2 | 618.9 | 863.8 | 1150.1 |
| Bircza (PL) | 713.6 | 768.9 | 783.8 | 692.4 | 867.5 | 992.7 | 735.4 | 800.3 | 824.6 | 713.6 | 930.2 | 1102.5 |
| Gdansk (PL) | 912.8 | 978.4 | 983.7 | 887.7 | 1097.0 | 1228.8 | 905.8 | 1023.5 | 982.3 | 882.5 | 1153.1 | 1208.2 |
| Krotoszyn (PL) | 1210.1 | 1246.3 | 1193.7 | 1174.8 | 1405.5 | 1524.9 | 1186.4 | 1216.3 | 1116.9 | 1147.8 | 1408.0 | 1459.6 |
| Lack (PL) | 1031.2 | 1061.4 | 1008.0 | 1002.4 | 1190.5 | 1271.2 | 1011.8 | 1035.3 | 953.9 | 980.9 | 1184.0 | 1216.9 |
| Fundata (RO) | 614.3 | 713.3 | 747.1 | 603.6 | 773.9 | 885.3 | 668.7 | 777.2 | 802.5 | 645.2 | 911.1 | 1136.3 |
| Mihaesti (RO) | 1093.6 | 1110.1 | 1092.6 | 1059.1 | 1275.5 | 1429.5 | 1131.1 | 1126.5 | 1072.0 | 1088.0 | 1341.9 | 1544.6 |

**Table 5.S7: Estimate, P value and partial R² of the parameters of a multivariate linear model used to identify the stand, soil and climate characteristics that best explain the NPP (a) or NPP change (b) variability across *virtual* sites and climate scenarios with constant (left) and changing over time (right) atmospheric $CO_2$ concentration. The simulations made based on the two types of climate projections (CNRM-ALARO and IPSL-RCA4) were included in the analysis. BA corresponds to the stand basal area, % beech to the beech percentage regarding the basal area, *dbh* SD to the standard deviation of *dbh*, MT VP and Rain VP to the mean temperature and rainfall during the vegetation period averaged for the historical period and Delta Rain to the change in annual rainfall between the historical period and the RCP scenario considered.**

| | Constant CO2 | | | Changing CO2 | | |
|---|---|---|---|---|---|---|
| Effect | Estimate | P value | Partial R² | Estimate | P value | Partial R² |
| **a) NPP (gC $m^{-2}$ $yr^{-1}$)** | | | | | | |
| intercept | -354.60 | <.0001 | | -658.67 | <.0001 | |
| mean *dbh* | 6.22 | <.0001 | 0.177 | 7.34 | <.0001 | 0.139 |
| BA | 19.27 | <.0001 | 0.016 | 22.72 | <.0001 | 0.012 |
| % beech | -2.21 | <.0001 | 0.054 | -2.63 | <.0001 | 0.044 |
| *dbh* SD | 3.31 | <.0001 | 0.017 | 3.88 | <.0001 | 0.012 |
| MEW | 0.62 | <.0001 | 0.118 | 0.58 | <.0001 | 0.061 |
| $[CO2]_{atm}$ | | | | 0.80 | <.0001 | 0.267 |
| MAT | 58.77 | <.0001 | 0.057 | 65.66 | <.0001 | 0.041 |
| MT VP | -42.59 | <.0001 | 0.028 | -50.93 | <.0001 | 0.019 |
| Rain VP | 0.22 | <.0001 | 0.033 | | | |
| Total | | | 0.499 | | | 0.594 |
| **b) NPP change (gC $m^{-2}$ $yr^{-1}$)** | | | | | | |
| intercept | 380.88 | <.0001 | | 409.81 | <.0001 | |
| mean *dbh* | | | | 3.39 | <.0001 | 0.080 |
| BA | | | | 8.51 | <.0001 | 0.035 |
| % beech | 0.61 | <.0001 | 0.024 | | | |
| MEW | 0.16 | <.0001 | 0.021 | | | |
| MT VP | -34.98 | <.0001 | 0.174 | -37.04 | <.0001 | 0.119 |
| Rain VP | 0.16 | <.0001 | 0.046 | | | |
| Delta Rain | 0.33 | <.0001 | 0.102 | | | |
| Total | | | 0.367 | | | 0.234 |

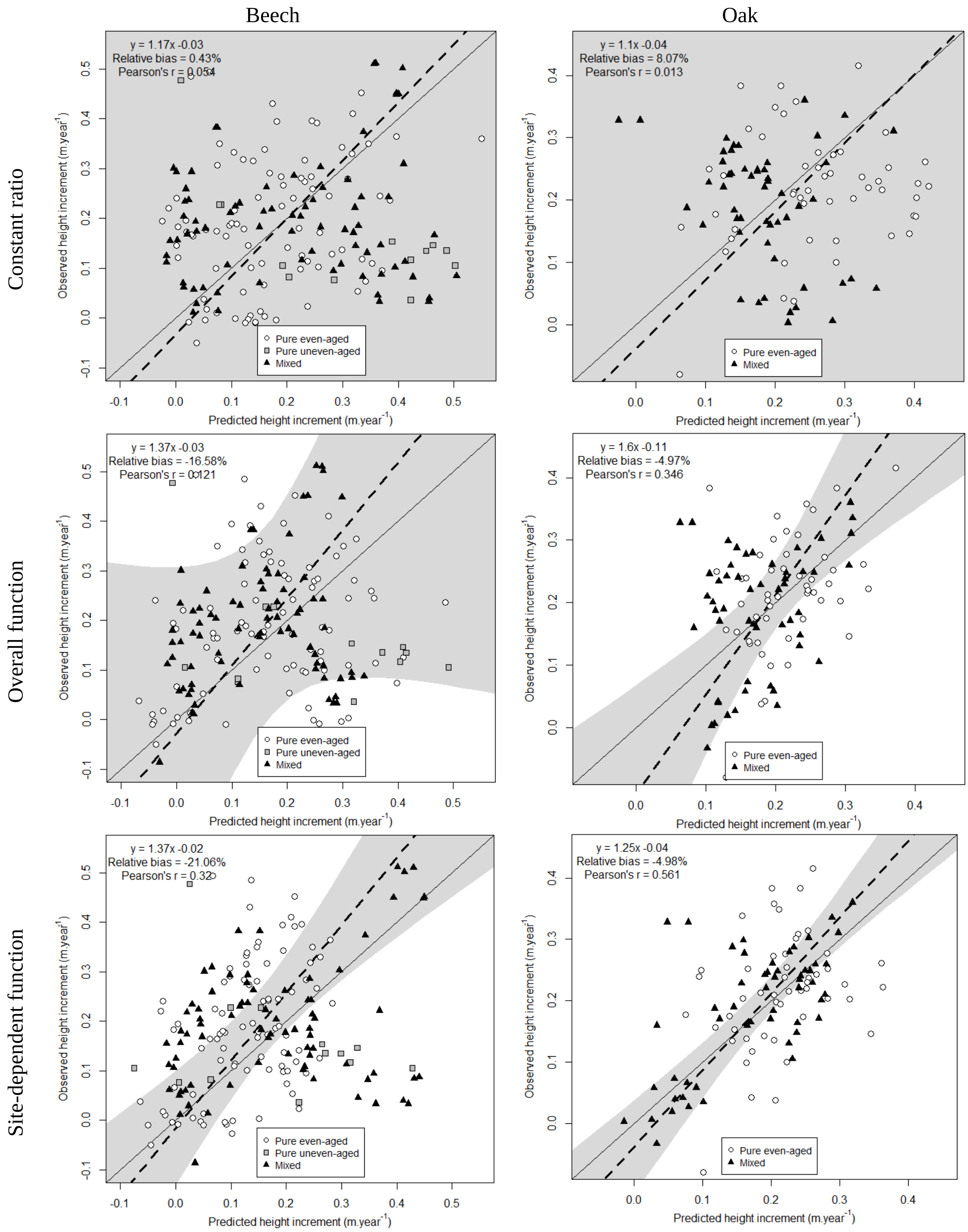

**Figure 5.S1: Comparison of the observed and predicted height increment aggregated by 10 cm girth classes for beech (left) and oak (right) and for the three CUE calculation modalities: constant ratio (top), general function (middle) and site-dependent function (bottom). The prediction quality is assessed based on the relative bias, the Pearson's r and the Deming regression test (position of the identity line (solid line) with respect to the confidence interval of the regression line (dashed line)).**

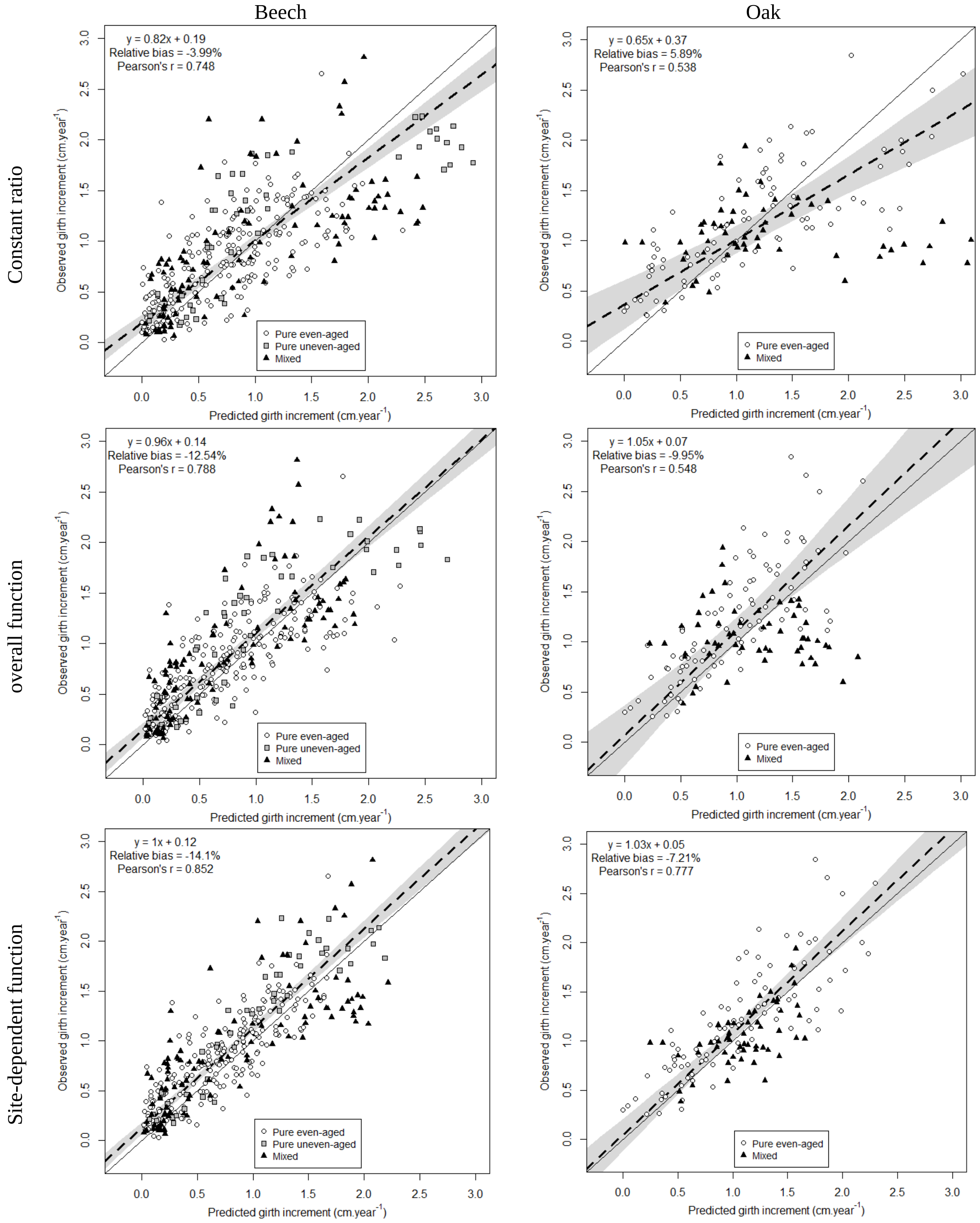

**Figure 5.S2: Comparison of the observed and predicted girth increment aggregated by 10 cm girth classes for beech (left) and oak (right) and for the three CUE calculation modalities: constant ratio (top), general function (middle) and site-dependent function (bottom). The prediction quality is assessed based on the relative bias, the Pearson's r and the Deming regression test (position of the identity line (solid line) with respect to the confidence interval of the regression line (dashed line)).**

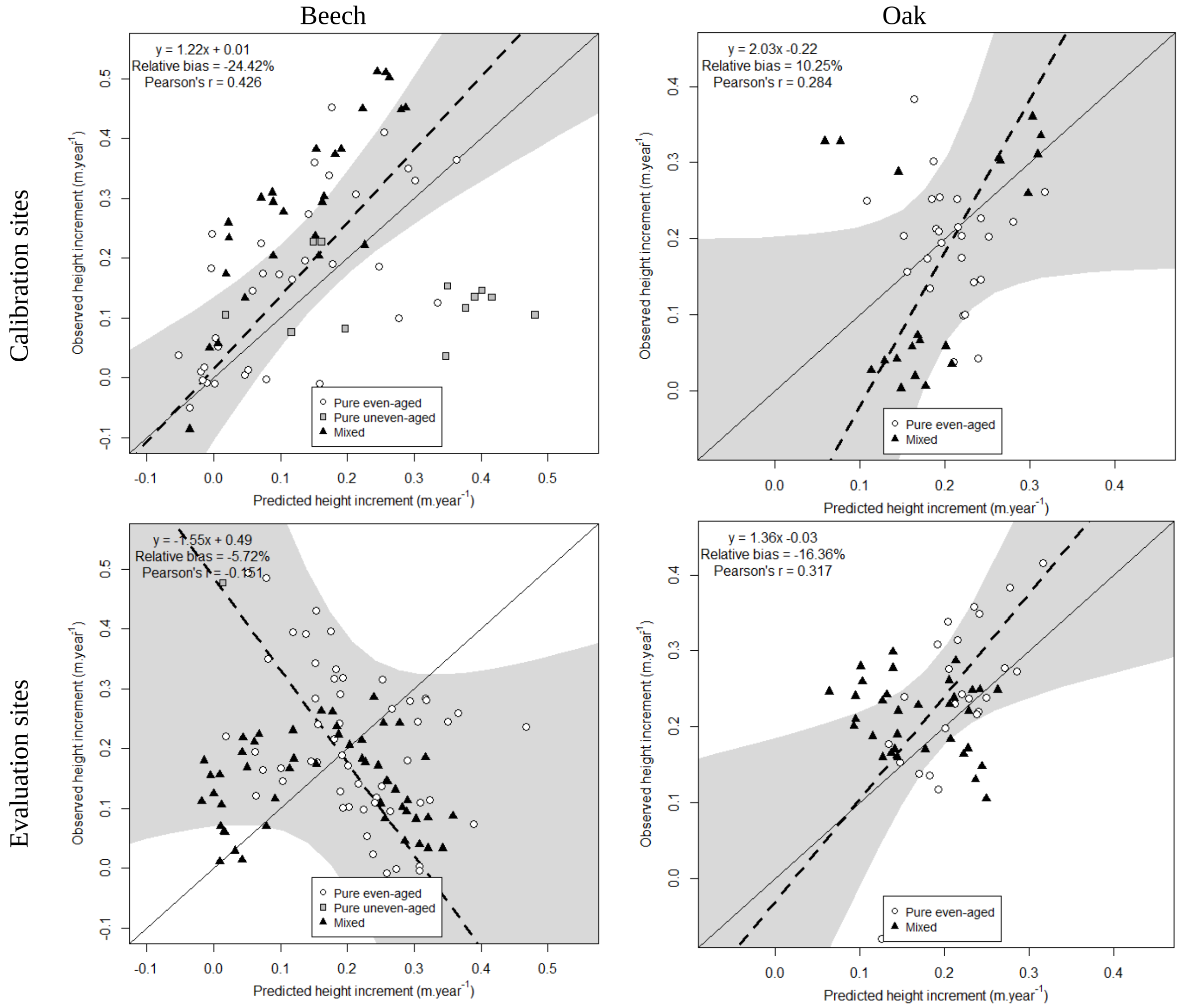

**Figure 5.S3: Comparison of the observed and predicted height increment based on the general CUE function, aggregated by 10 cm girth classes for beech (left) and oak trees (right) and for the calibration (top) and the evaluation (bottom) sites. The prediction quality is assessed based on the relative bias, the Pearson's r and the Deming regression test (position of the identity line (solid line) with respect to the confidence interval of the regression line (dashed line)).**

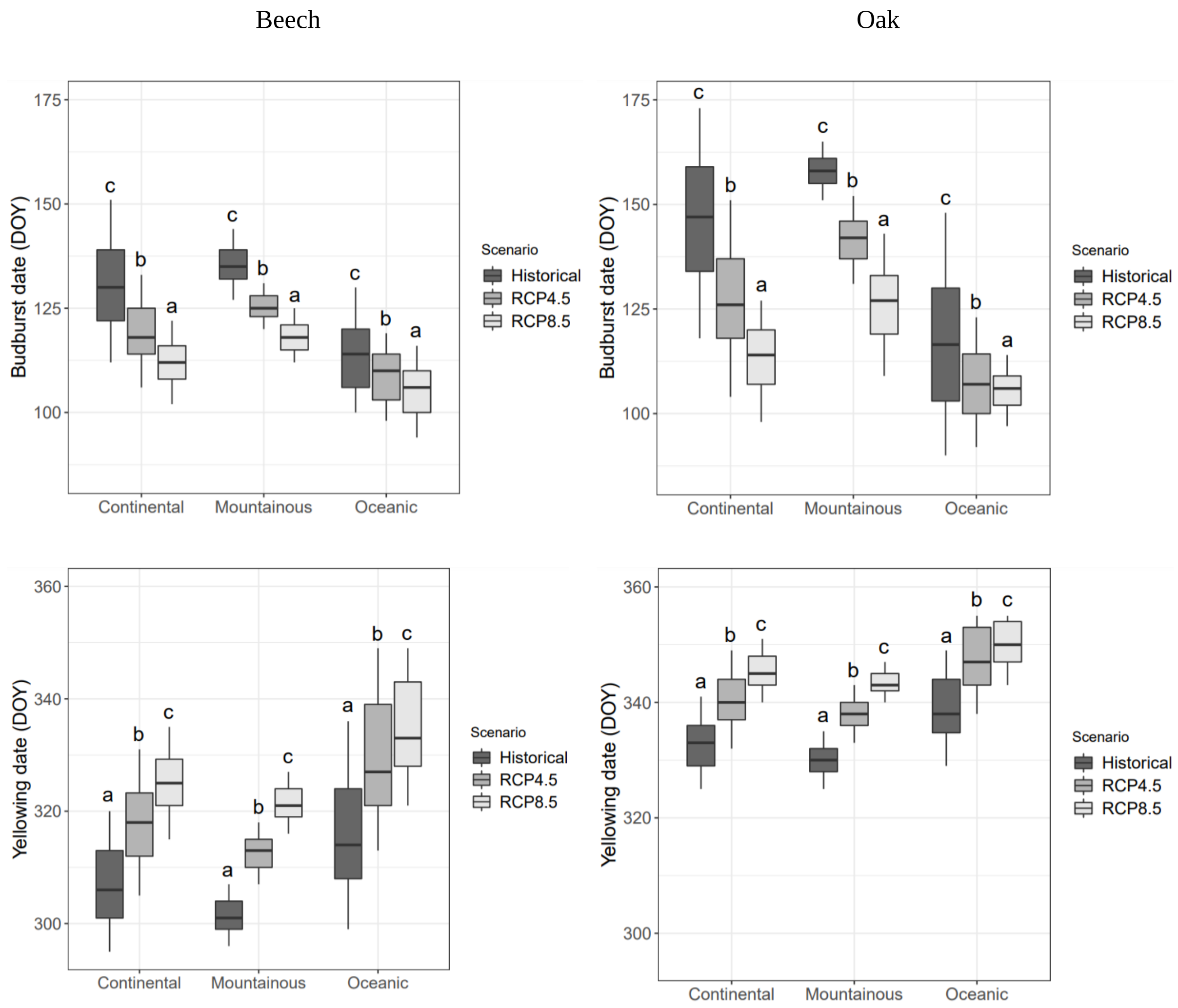
Beech

Oak

**Figure 5.S4: Comparison of the budburst (top) and yellowing (bottom) dates in *virtual* sites simulated for the historical period (1976-2005) and for the future (2071-2099) according to two RCP scenarios; three climate types were considered as well as both tree species. The horizontal line corresponds to the median, the box ends indicate the 25th and 75th percentiles and the whiskers show the values above and below these quartiles within 1.5 interquartile. For a same climate type, scenarios with common letters are not significantly different (paired Wilcoxon signed- rank between RCP4.5 and RCP8.5 and unpaired Mann-Whitney test between historical and RCP scenarios). The simulations made based on the two types of climate projections (CNRM-ALARO and IPSL-RCA4) were included in the analysis.**

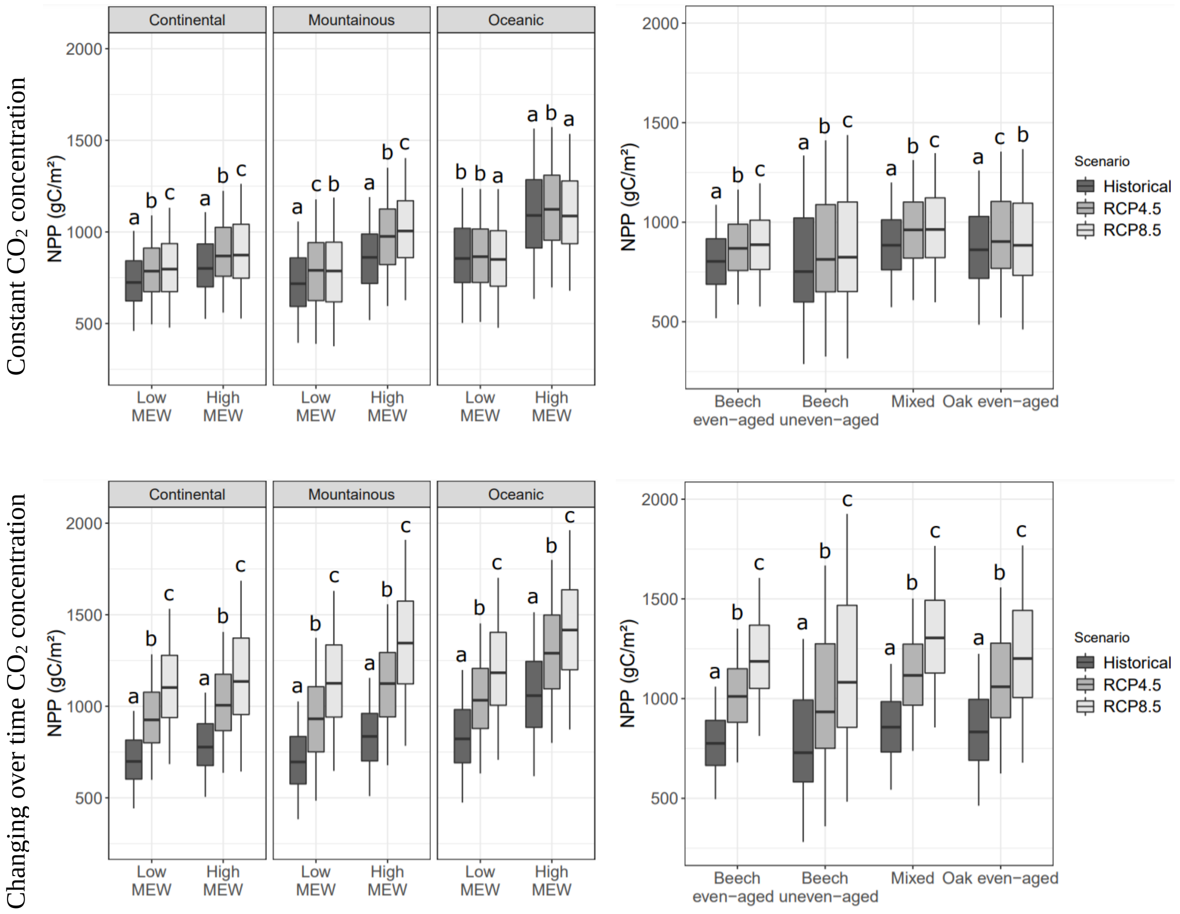

**Figure 5.S5: Comparison of the simulated annual NPP in *virtual* sites among RCP scenarios (2071-2099) and the historical period (1976-2005) for the two atmospheric $CO_2$ modalities: highlighting of the climate zone, soil water reserve (MEW) and stand type effects. For each box, the horizontal line corresponds to the median, the ends indicate the 25th and 75th percentiles and the whiskers show the values above and below these quartiles within 1.5 interquartile. For a same stand, soil or climate type, scenarios with common letters are not significantly different (paired Wilcoxon signed- rank between RCP4.5 and RCP8.5 and unpaired Mann-Whitney test between historical and RCP scenarios). The simulations made based on the two types of climate projections (CNRM-ALARO and IPSL-RCA4) were included in the analysis.**

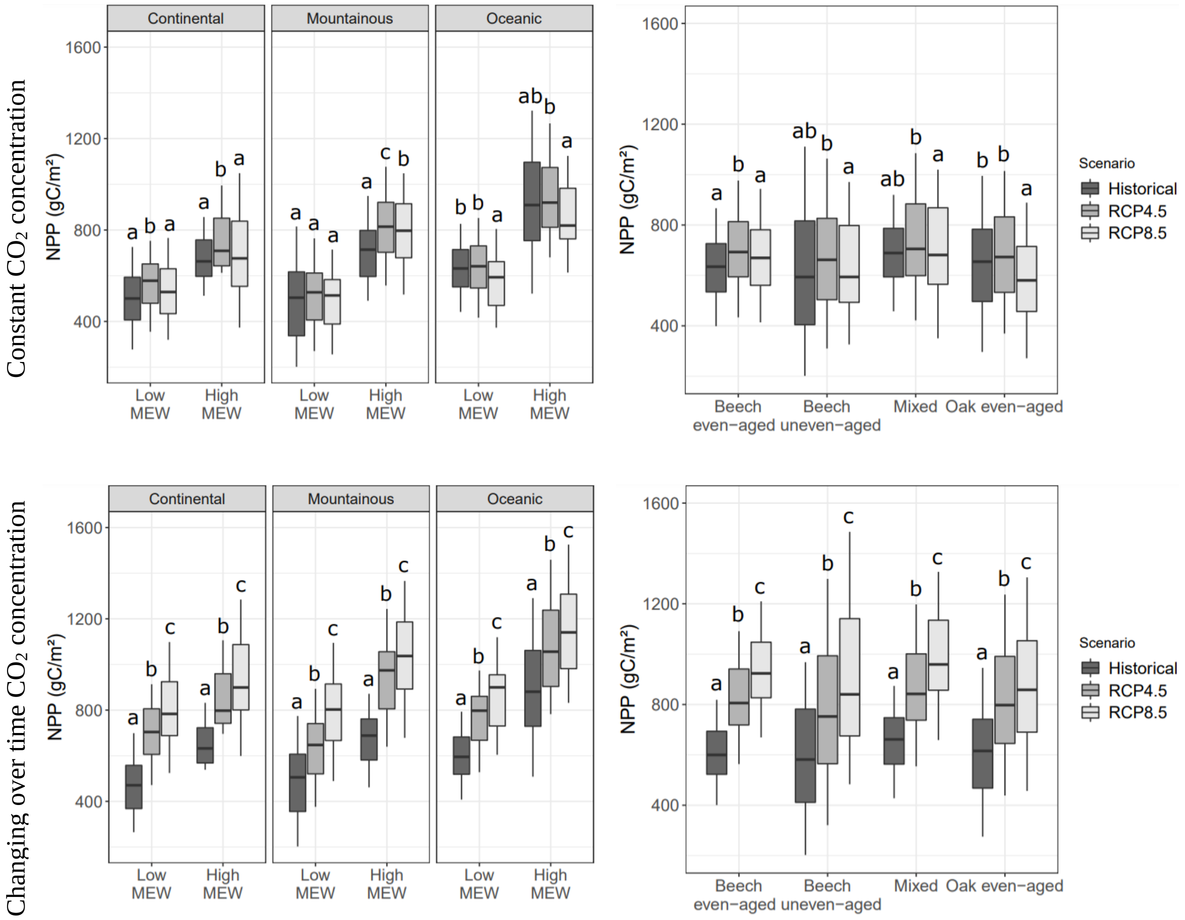

**Figure 5.S6: Comparison of the lowest simulated annual NPP values (< 7th percentile) in *virtual* sites among RCP scenarios (2071-2099) and the historical period (1976-2005) for the two atmospheric $CO_2$ modalities: highlighting of the climate zone, soil water reserve (MEW) and stand type effects. For each box, the horizontal line corresponds to the median, the ends indicate the 25th and 75th percentiles and the whiskers show the values above and below these quartiles within 1.5 interquartile. For a same stand, soil or climate type, scenarios with common letters are not significantly different (paired Wilcoxon signed-rank between RCP4.5 and RCP8.5 and unpaired Mann-Whitney test between historical and RCP scenarios). The simulations made based on the two types of climate projections (CNRM-ALARO and IPSL-RCA4) were included in the analysis.**

# Chapter 6

# DISCUSSION AND CONCLUSION: MAIN FINDINGS AND PERSPECTIVES

In the uncertain context of global changes, mixed and uneven-aged stands have received a lot of attention due to their supposed higher resilience to abiotic and biotic stressors. This has led, in temperate Europe, to a continuous increase in the proportion of monospecific even-aged forests turned into more complex stands. However, there is a lack of information on the way these structurally-complex stands will respond to climate change. Individual-based spatially explicit models are among the tools that exist to study the impact of climate change on forest while accounting for the stand structure complexity. Yet, they are usually calibrated on a restricted number of sites due to their important initialization data requirements.

To address some of the shortcomings highlighted, I pursued the following objectives in my thesis:

(i) Adapt an individual-based model to account for the climate sensitive processes and for the stand structure effect on the forest ecosystem functioning

(ii) Evaluate and calibrate the model over a large range of environmental conditions and stand structures across the temperate European region

(iii) Use the model to predict the response of oak and beech growth to climate change and assess how it is modulated by the different site components (climate, soil and stand) with a particular focus on the stand effect

I will discuss in this section the main progresses and findings related to each objective and suggest some further research perspectives.

## 1. OBJECTIVE I: ADAPTATION OF THE INDIVIDUAL-BASED MODEL HETEROFOR TO ACCOUNT FOR THE IMPACT OF CLIMATE CHANGE IN HETEROGENEOUS FORESTS

At the beginning of my thesis, a first version of HETEROFOR was already existing and was able to simulate individual tree growth based on local light conditions using the radiative transfer module SAMSARALIGHT and a PAR use efficiency approach coupled to a carbon allocation module. Then, the main processes through which climate influence tree growth were introduced in the model. I developed the phenological and water balance modules while the photosynthesis and the respiration routines were elaborated by other team members.

### Phenology

Phenology is a complex and multifactorial process, which functioning is still imperfectly understood in spite of the major progresses realised over the last decades, making its modelling particularly difficult (Piao et al., 2018). Most of the phenological models can be seen as hybrid models as they integrate the driving variables triggering the different phenological phases but using empirical response functions. For budburst, models are often classified into one and two-phase models whether they account or not for the chilling in addition to the forcing period.

As there is no consensus on whether one approach is better than the other (Fu et al., 2014; Basler, 2016; Melaas et al., 2016), we implemented the two options in the model. In addition, two different chilling temperature response functions were considered: a sigmoid function very modular but more difficult to calibrate and a more straightforward optimum function. The integration of several phenological models is interesting in order to assess the conceptual uncertainty related to this process. Moreover, it is assumed that the performance of one-phase models is better when chilling requirements are always fulfilled (Leinonen and Kramer, 2002; Fu et al., 2014a).

Another originality of HETEROFOR is the possibility to account for inter-individual variations in budburst, yellowing and falling dates. Within a same stand, the budburst and senescence periods vary a lot among the individuals of a same species. This variation range corresponds to 19 and 26 days, respectively, which is comparable to the differences observed along an altitudinal gradient of 560 and 1300m (Delpierre et al., 2017). These large inter-individual variations are generally not accounted for in individual-based models (IBMs) due to the lack of knowledge on the processes driving these differences and to the limited availability of individual phenological observations. Ontogeny is supposed to be one of the main factors explaining the inter-individual variability as demonstrated by Vitasse et al. (2009). This effect is however difficult to disentangle from the warmer temperatures found in spring in the understory due to the canopy buffering effect (Zellweger et al., 2019) since they produce the same effect, an earlier budburst of younger/smaller trees. However, the micro-climate seems to play a secondary role compared to ontogeny (Vitasse et al., 2009). Among individuals of the same development stage, the influence of other variables such as genetics and local water availability is confirmed by the high inter-annual repetition in phenological ranking between trees (Delpierre et al., 2017).

In HETEROFOR, we rely on the assumption that tree size (as proxy of tree age) is the only driver of the intra-species variability. This is a rough and simplistic assumption that is partly verified when considering trees of different development stages but it allows to evaluate the possible magnitude of the temporal niche partitioning (or avoidance strategy) between trees in the dominant canopy layer and in the understorey (Gill et al., 1998; Seiwa, 1999a; Augspurger and Bartlett, 2003; Schieber, 2006; Vitasse, 2013; Gressler et al., 2015). Considering this mechanism lengthens the vegetation period of smaller trees and, subsequently, enhances their productivity. To quantify this effect, I ran a couple of additional simulations. It appeared that, in its current form, compared to the stand-based approach, the individual phenology generates a NPP increase of the smallest trees that mostly ranges between 5 and 24% and a relatively steady NPP reduction of the tallest ones comprised between 1 and 7%. The use of the individual phenology option allowed to offset some of the slight underestimation (overestimation) of radial growth in smaller (taller) trees (Chap. 2).

To improve the modelling of the inter-individual variability, we could use a multifactorial model including other explanatory variables than the tree size and consider explicitly a random component to account for the unexplained variability that can be partly ascribed to the genetic differences among trees. Marchand et al. (2020) fitted a statistical model using phenological observations and explained 60% of budburst inter-individual variability when considering the site, species and tree size effects and 66% when considering in addition the onset of senescence and the cessation of wood formation of the previous year. In a perspective of using the model more as a tool for integrating monitoring data and understanding forest ecosystem functioning (rather than for predicting future forest growth), we could add the possibility to provide an input file with the ranking of trees for budburst and yellowing, taking advantage of the high repeatability of phenology inter-individual ranking. The model would only estimate the averaged budburst/yellowing date and the number of days between the first and last tree. All these model improvements should be calibrated and evaluated at the individual scale but such data are lacking since long-term monitoring usually only focus on a couple of representative trees.

An interesting experiment would be to combine individual phenological assessments with local meteorological measurements in forests with contrasted stand structures. This would allow to disentangle the ontogeny from the microclimate effect on individual phenology, to estimate the genetics differences and to evaluate the climate sensitivity of trees at different ages, which is still a big uncertainty source as warming experiments are essentially conducted on saplings (Piao et al., 2018). In addition, it would provide materials to integrate the buffering effect of canopy on air temperature and the vertical temperature profile in the model. Currently, air temperature is considered the same everywhere in the stand and usually corresponds to values taken from close meteorological stations. Yet, according to De Frenne et al. (2019) who compared temperature under the canopy and in the open, on average over the whole year, mean and maximum temperatures in the understory are lowered by 1.7 and 4.1°C, respectively and minimum temperatures are 1.1°C higher with important seasonal variations. The magnitude of this buffering effect is totally relevant compared to the expected climate warming. To include this effect, a radiative balance module could be implemented but while being relatively simple in dense and homogeneous forests, they are found to be particularly complex in heterogeneous forests (Bailey et al., 2016). Another option would be to use empirical models that consider different stand properties like canopy cover and openness, basal area, tree height, species shade-casting ability, shrub density or topographic position (Kovács et al., 2017; Zellweger et al., 2019).

With a refined description of inter-individual variations and of the vertical profile in air temperature, it would then be possible to take into account the effect of frost episodes on forests and particularly on young trees and saplings, which susceptibility and sensitivity are higher. Indeed, paradoxically, climate warming could increase the risk of such events due to earlier budburst (Vitasse et al., 2014; Hänninen et al., 2016; Ma et al., 2019; Liu et al., 2018).

Finally, further developments would also be interesting regarding the calculation of the different phenological states. Indeed, it is known that other variables than the single air temperature affect budburst such as water availability (Schmull and Thomas, 2000; Peñuelas et al., 2004; Fu et al., 2014b) or photoperiod (Basler and Körner, 2012; Vitasse and Basler, 2013; Laube et al., 2014). Similarly, leaf yellowing is not only affected by air temperature and photoperiod. A positive correlation between budburst and senescence was pointed out so that earlier leafing triggers earlier senescence and inversely (Fu et al., 2014c; Keenan and Richardson, 2015) and drought conditions can accelerate leaf yellowing occurrence (Xie et al., 2015; Liu et al., 2016; Massonnet et al., 2021). Still, fully empirical models accounting for numerous driving variables were found to improve only slightly modelling results or even decrease them while increasing the data requirements for calibration (Basler, 2016; Gauzere et al., 2017; Zohner et al., 2020). Therefore, a better knowledge of how these variables affect phenology and interact seems necessary before they can be efficiently introduced in models.

### Water balance module

Soil water availability is likely to be one of the main factors controlling future forest response to climate change. Different water pools and fluxes interact to fill or deplete the different soil horizons. In order to provide reliable simulations, a process-based approach with a fine level of spatial detail is crucial.

With respect to the other tree growth models, HETEROFOR displays some unique features. First, it separates the rainfall in two fluxes (throughfall and stemflow) and two interception pools (foliage and bark water storage), which are function of individual characteristics while rainfall partitioning is absent in most forest growth models (Table 3.5) and, when included, it only relies on general stand properties (Muzylo et al., 2009). Similarly, unlike most other models, tree transpiration is calculated individually based on tree characteristics (stomatal conductance depending on tree species and height) as well as of the micrometeorological conditions (local light availability and wind speed). A third element is the combination of Darcy equations with a procedure that ensure mass conservation to calculate soil water movements. This approach is not the state-of-the-art in soil flux calculation but its intermediate complexity level allows to calculate upward and downward water fluxes for all trees over several decades. This cannot be achieved by the numerous models using a bucket model approach, which fluxes are only downward, neither by models solving Richards equations that are too computationally expensive to be conducted on discretized soils and/or long term simulations. Finally, the possibility of conducting the water cycle calculation at the stand or individual scale is an additional specificity of HETEROFOR. The underlying assumption is whether soil water is horizontally redistributed or not. When the water cycle is calculated at the stand scale, an infinite soil horizontal conductance is considered whereas the individual option allocates a soil volume (pedon) to each tree, function of its leaf area, and no exchanges occur between the pedons of different trees.

The influence of the individual and stand approaches on soil water content and tree transpiration was demonstrated in Chap. 2. It appeared that transpiration was better predicted for beech and remained relatively unchanged for oak with the individual approach. It was assumed that the better results originated from the fact that the evaluation was conducted during the exceptionally dry year of 2003. Indeed, a dry soil has lower conductance and, subsequently, the assumption of no water exchange between pedons could be closer to the reality than a total horizontal water redistribution. The comparison of the two approaches also revealed significant differences in the soil water content between pedons, highlighting the interest of considering the two options. Finally, it is interesting to note that, for the three sites tested, the average of the individual soil water content under the individual approach was slightly lower than that obtained for the stand approach, probably due to higher water losses through deep drainage.

Some improvements could be brought to the description of the water cycle. Regarding the aboveground component, the estimation of individual evaporative demand would benefit from a vertical differentiation of air temperature inside the canopy as described for phenology. Furthermore, the representation of the soil-plant-atmosphere continuum would provide a good framework to implement mortality caused by hydraulic failure, leaf and branch fall and irreversible conductance loss due to vessel embolization or xylem shrinkage during severe drought episodes and would account for the higher drought sensitivity of tall trees (Bennett et al., 2015; Stovall et al., 2019). A soil-plant hydraulic model, SurEau, accounting for tree individual characteristics and providing mortality probability (Martin St-Paul et al., 2017) could be easily coupled to HETEROFOR as it is implemented in the same modelling platform CAPSIS.

For belowground processes, it is clear that the reality lies between the two assumptions of null or infinite horizontal conductance. An intermediate approach would be to calculate exchanges between pedons using, for example, Thiessen polygons but this would require some code optimisation as computation time is already very high with the individual option. A much more straightforward improvement would be to differentiate vertical root distribution at the species or individual-scale. It would allow to account for soil water facilitation (water from the deeper soil horizons transferred in the upper horizons by trees with deeper root systems to trees with shallower roots) (Grossiord, 2019) when the water balance is run at the stand scale. While the species-specific option seems relatively easy to achieve, calculating individual root distribution does not seem reasonable nor relevant. Indeed, in the study sites considered, the soil depth varies from 0.5 to 1.5 m. If one considers a vertical root development of 25 cm per year (Collet et al., 2006), the bottom of the soil profile would be reached after 2 to 6 years by seedling roots. Yet, in HETEROFOR, trees are recruited at a height of 12 m which correspond to 25-30 years old trees. So, when trees are recruited (individualized in HETEROFOR), they already have a vertical fine root development similar to that of the adult trees.  In addition, most of the fine roots are located within the upper soil horizon (Claus and George, 2005) and the vertical fine root profile appears only slightly affected by tree age (Bakker et al., 2008; Claus and George, 2005).

### Respiration

In the HETEROFOR model, two options can be used to account for maintenance respiration. Maintenance respiration is either considered as a proportion of the gross primary production (GPP) based on the concept of carbon use efficiency (CUE) or calculated hourly for each tree compartment by considering the nitrogen content of its living biomass and a Q10 function for the temperature dependency. These two options correspond to the two main approaches used in forest modelling.

The CUE approach was popularized by Waring et al. (1998) who published a paper showing that CUE was nearly constant (0.47 ± 0.04 SD). This result considerably simplified the modelling of tree respiration and was adopted in many models (e.g. 3-PG, HyLand, 4C, BASFOR, early versions of 3D-CMCC-FEM). Collalti and Prentice (2019), in a review, show that since the publication of Waring's paper, other measurement studies were conducted, some confirming the value of 0.47 (e.g., Gifford, 1995; Law et al., 1999; Litton et al., 2007; Peichl et al. 2010, Sun et al. 2014), others highlighting significant site variations (e.g. Medlyn and Dewar, 1999; Cannel and Thornley, 2000; Amthor, 2000) or the influence of height (Vaninen and Makela, 2005), stand age (Ryan et al., 2004; DeLucia et al., 2007; Thronley, 2011) or temperature (Gifford, 2003; Piao et al., 2010; Collalti et al., 2020). The main conclusion of this review was that variations in CUE are too important to be neglected even if 0.47 is a good average value (Collalti and Prentice, 2019).

The approach calculating respiration for each tree compartment and taking the temperature dependency into account was inspired by the work of Ryan et al. (1991). Theoretically, this approach is more appropriate to simulate the impact of climate change, but this is at the expense of much less accurate predictions at the tree level (Jonard et al., 2020). In addition, several studies showed that a thermal acclimation of the respiration process could occur

(Way and Oren, 2010; Way and Yamori, 2014). In this case, the temperature dependency should depend on the mean air temperature, such as is done in 3D-CMCC (Collalti et al., 2018). This thermal acclimation probably results in a more synchronized respiration and photosynthesis sensitivity to temperature than initially thought.

With the improvements they received with time, the two approaches seem to converge. I chose to make the simulations with the CUE approach since it provides much more accurate predictions at the individual level. In addition, the acclimation mechanism is not yet described in HETEROFOR. In the CUE approach, the effect of the mean air temperature was considered and its magnitude was in agreement with that generated by the temperature dependent approach. In addition, as many tree characteristics are taken into account to estimate CUE, this approach can be used to simulate long-term forest dynamics.

**Individual-based approach**

I have already demonstrated the interest of using an individual-based approach for modelling tree growth from a theoretical point of view and showed the differences generated when phenology and water cycle are considered at the individual or at the stand scale. However, HETEROFOR allows testing *a posteriori* the added-value of using an spatially explicit IBM compared to stand or cohort-based models. Indeed, cohort-based models account for the vertical heterogeneity but do not differentiate stands of the same species composition and tree-size distribution but displaying contrasted spatial aggregations of trees.

Therefore, I evaluated how changing tree spatial distribution and restricting the individual approach into a cohort approach affected simulation outputs. The results from this sensitivity analysis showed that differences in tree spatial distribution generated changes in LAI ranging from -35% to +23% and in annual transpiration between -25% and +9% depending on the year and on the cohort considered. In addition, the clustering in cohorts induced differences from -9% to +30% for the LAI and from -10% to +6% for the annual transpiration (Fig. 5.S2 and Fig. 5.S3). These effects were more pronounced at the cohort than at the stand scale as cohorts responded differently and partly offset each other at the stand level. These results indicate that HETEROFOR is sensitive to the tree spatial distribution and to the clustering in cohorts as expected. All the methodology, results and figures associated with this sensitivity analysis are presented in the supplementary materials.

Another element showing that HETEROFOR integrates complex structure effects is that, among the proportion of NPP variability explained by the stand effect (Table 5.4), only 60% was explained by stand-scale variables (Table 5.S7). The remaining variability (40%) is likely to come from structure effects more complex and more difficult to summarize with a few variables.

The influence of the modelling approach and spatial aggregation was highlighted in the sensitivity analysis presented here but this modelling exercise should be conducted on more sites and variables (NPP, basal area, mean tree height). In addition, other simulations could be conducted to highlight the structure effect (uneven-aged stands *vs* series of even-aged stands), the species composition effect (mixed stands *vs* corresponding pure stands), spatial resolution effect (stand *vs* cohort *vs* individual-based approach). Unfortunately, I was not able to conduct these sensitivity analyses myself by lack of time.

## 2. OBJECTIVE II: EVALUATION OF THE MODEL PREDICTIVE ABILITY

I focused the evaluation on the newly implemented phenology and water cycle modules as well as on tree growth, an integrative variable, for a large range of environmental conditions. This two-step evaluation is crucial to increase the reliability of tree growth projections under changing conditions. Indeed, a model must accurately reproduce the observed tree growth as well as the underlying processes of resource acquisition (Soares et al., 1995). A model based on a poor process description could provide accurate predictions for past conditions thanks to some compensations achieved during the calibration phase. This becomes however problematic when the model is used for projections in future unexperienced conditions.

The phenological evaluation was itself conducted in two steps. First, the three budburst models were calibrated using data from sites of the PEP725 network located in the Western part of Germany and evaluated against independent observations from 6 Walloon sites (Chap. 2). In a second step, an existing set of parameters corresponding to the two-phase budburst models (optimum model for oak and sigmoid model for beech) calibrated over Central Europe was used and evaluated against observations from different European sites in Belgium, Germany, France and Romania (Chap. 3).

The main findings linked to this evaluation were that the model accounting only for forcing (one phase sigmoid model) best accounted for the inter-annual variability at the Walloon scale when calibrated on nearby region (Chap. 2). However, the two-phase models calibrated over Central Europe displayed better statistical results at the European scale. They also outperformed the one-phase model when used on the Walloon sites only. Therefore, I recommend to use two-phase models when the calibration is based on a large range of conditions, especially warm sites so that the chilling requirements can be better estimated. One-phase model should be preferred when few or only very local observations are available.

The integration of different phenological models is interesting in order to assess the conceptual uncertainty related to this process but also to make multi-model comparison that can provide better estimations. In my case, for the Walloon sites, the budburst date averaged on the three models outperformed each of them taken individually.

The evaluation of the water balance module was applied on water fluxes and pools for which data were available. Predicted throughfall and transpiration fluxes were compared to individual-based observations while soil water content and deep drainage were evaluated at the stand scale (Chap. 2). An evaluation on so many water-related variables is rather unusual and the good results displayed for each of them deserve to be highlighted. Even more importantly, the fact that individual throughfall and transpiration prediction quality is consistent across the whole validation range (as shown by the Deming regression line) is a clear indication that a significant part of the stand heterogeneity effect is integrated in the model.

Tree growth was evaluated in 36 European sites at the tree level as well as at the stand scale. The evaluation at the tree level was based on two aspects: individual tree height and radial increments. A good match between observed and predicted radial increments was found with statistical results close to those from local and empirical IBMs. The model predictive ability was lower for the tree height increment mainly due to the higher measurement uncertainty but remained satisfying (Chap. 5). In addition to the evaluation at the individual level, I conducted a couple of additional evaluations at the stand scale on NPP, mean *dbh* and mean height increment using the same

36 European sites. The observed NPP was estimated using the HETEROFOR routine calculating a reconstructed NPP for each tree based on repeated inventory data (see sect. 1.3.9 in Chap. 2). The NPP predictions were unbiased and their correlation with observations amounted to 0.49, which shows that the process description at the individual level provide reliable predictions at the stand scale. The predicted mean *dbh* and height increments were also non-significantly biased (-2.7 and +1.4%, respectively) and their correlations with observations amounted to 0.73 and 0.37. When evaluated at the individual scale, Pearson's r ranged between 0.55 and 0.79 for the first and between and 0.12 and 0.35 for the second. The better results obtained at the stand scale shows that the errors on the different tree categories partly offset each other.

For his master thesis, Guillaume de Meue used eddy covariance data to assess how HETEROFOR predicted evapotranspiration and GPP in the mixed stand (beech and various conifers) of the Vielsalm ICOS site. For both variables, the model was able to reproduce the temporal dynamics, with however a slight overestimation regarding evapotranspiration (Fig. 6.S4 and 6.S5).

Individual-based models must also be able to represent stand-level process such as the density-induced mortality, also called self-thinning (Berger et al., 2008). During his master thesis aiming at the development of a regeneration module in HETEROFOR, Brieuc Reylandt conducted long-term simulations starting from beech and oak seedlings growing in full light conditions. The obtained results highlighted the model ability to reproduce the empirical self-thinning lines from Yoda (1963) and Charru et al. (2012) (Fig. 6.S6).

As tree growth was calibrated and evaluated on a large panel of environmental and stand conditions, the model genericity or, in other words, the probability to correctly reproduce the mechanisms in future projections is higher. In addition, the fact that the model performances were not deteriorated when evaluated on an independent dataset demonstrated its robustness (Fig. 5.1 and 5.S3). A generic and robust model is of primal importance for providing reliable projections in unexperienced conditions. It is also worth noting that, to my knowledge, HETEROFOR is the only IBM calibrated and evaluated on sites covering such a large range of environmental conditions in temperate Europe.

## 3. OBJECTIVE III: SIMULATION OF OAK AND BEECH INDIVIDUAL GROWTH RESPONSE TO CLIMATE CHANGE

The main purpose of the project was to study the response of structurally-complex oak and beech stands to climate change but this could only be achieved after the adaptation, calibration and evaluation of an existing spatially-explicit and individual-based model (HETEROFOR). I took advantage of the model properties to study specific objectives: the temporal changes in net primary production (NPP) according to various climate models and GHG emission scenarios and the identification of the main drivers of this evolution (i), the differentiation of the long-term trend in NPP from the inter-annual and inter-site variations (ii) and the quantification of the site component (stand, soil and climate) contributions to the NPP variability and to the variations of its response to climate change with a particular focus on the stand structure effect (iii). Linked to these objectives, different hypotheses were formulated about the impact of climate change on forest growth processes and the influence of site conditions on this impact. Hereafter, I discuss how the results were obtained, whether they confirm or not these hypotheses and possible options for further research.

**How climate change will affect oak and beech tree growth in European temperate forests?**

*Hypotheses: A longer vegetation period due to warmer spring and autumn conditions could increase forest productivity but this process could start to be limited by a slower coldness accumulation in winter and a growing photoperiod influence in autumn. Higher water stress levels and maintenance respiration costs generated by lower summer rainfall and warmer temperature could decrease forest productivity. Finally, rising atmospheric* $CO_2$ *concentration could have a double positive effect on forest growth by enhancing photosynthesis and reducing water loss by transpiration.*

To answer the question and test the hypotheses, a phenological and water cycling module were added to HETEROFOR in order to account for the influence of climate on forest growth. These modules were then evaluated for a large range of site conditions. The influence of temperature on maintenance respiration was calibrated based on a large tree growth dataset covering an important temperature spectrum. Finally, the simulations were run once with constant and once with changing CO2 concentrations to assess its effect on tree growth but also to account for the uncertainty concerning its persistence with time.

The vegetation period lengthening induced by climate change appeared clearly in the projections across Europe and the increase was similarly driven by budburst and senescence for beech while budburst had the main impact for oak (Chap. 4 and 5). In the oceanic zone displaying the warmest temperatures, the median budburst and yellowing dates also occurred respectively earlier and later but the date variability considerably decreased, sign of a buffering effect (Chap. 5). The role of the chilling period in this dampening can be pointed out as no buffering trend was observed for the Walloon sites when the one-phase budburst model was used (Chap. 4).

In the first simulation experiment on the six Walloon sites, when the $CO_2$ and water stomatal conductance were not coupled, climate change was found to increase the water stress levels (Chap. 4). However, in the simulation study at the European scale, with a unique value of stomatal conductance for water and $CO_2$, water stress increased when $CO_2$ was constant but decreased with the changing atmospheric $CO_2$ concentrations, except in mountainous areas where it remained constant (Chap. 5). For this process, the changing $CO_2$ scenario can be considered as more realistic because even if the fertilizing effect of $CO_2$ is constrained, the water use efficiency will increase in response to the elevated atmospheric $CO_2$ concentrations anyway.

Respiration costs were accounted based on a carbon use efficiency (CUE) approach (also called NPP to GPP ratio). For beech, as no temperature effect on CUE was detected based on the observations, I did not consider it in the CUE function meaning that respiration changed with temperature in the same proportion as photosynthesis. In contrast, as the negative temperature effect on oak CUE was significant, it was taken into account and induced a higher temperature impact on respiration than on photosynthesis (Chap. 5). This difference in respiration sensitivity to temperature explains why more negative changes in NPP were found in stands dominated by oak under warmer climates. However, this effect was partly cancelled out when rainfall decreases were observed due to the higher beech sensitivity to drought. This contrasted behaviour between oak and beech regarding respiration sensitivity to temperature should be confirmed by more observations and eventually by respiration measurements in warming experiments. In addition, it would be interesting to known if respiration response to temperature can be considered as relatively uniform across species and biomes or not (Mahecha et al., 2010; Heskel et al., 2016; Zhang et al., 2017).

For $[CO_2]_{cst}$ runs, the overall impact of climate change on the forest productivity was on average slightly positive with more positive changes under colder climates (such as in mountainous zone) and negative ones under warmer and drier climates and in case of substantially lower annual rainfall. The increase in productivity was considerably higher under the changing $CO_2$ modality, highlighting the influence of the fertilizing effect coupled to a better water use efficiency. Due to the partial compensation of the vegetation period lengthening and the increase in water stress and respiration under the constant $CO_2$ modality, the impact of climate change on forest productivity was considerably (more than 4 times) lower than the climate internal variability. Under the changing $CO_2$ modality, the climate change effect on forest productivity was approximately two times higher than the effect of internal variability.

According to a couple of simulation papers and six different models using RCP4.5 or RCP8.5 climate projections (4C, CASTANEA, WaldPlaner, 3D-CMCC-FEM, 3PG and GOTILWA+), the median NPP change under constant $CO_2$ concentration would be -2% (Lasch *et al.*, 2002; Davi *et al.*, 2006; Reyer *et al.*, 2014; Albert *et al.*, 2018; Collalti *et al.*, 2018; Nölte *et al.*, 2020) compared to the +7% found in my thesis (*virtual* sites and both RCP scenarios). However, behind this increase, both an important inter-site variability and an influence of the climate model choice coexist. For example, under the RCP8.5 scenario, for the simulations with the CNRM-ALARO projections on the *real* sites, NPP increased on average by 7.4% for a range between -27 and +23% whereas with IPSL-RCA4, the averaged NPP change amounted to -2.4% for an inter-site variability ranging from -46 to +20% (Chap. 5).

The differences between the NPP projections based on CNRM-ALARO and those from IPSL-RCA4 or other studies was caused by strong differences in the projected summer rainfall change. Regarding the global climate model (GCM) projections, an important variability exists among the 36 models of the CMIP-5 ensemble used for the 5th IPCC report (Coppola et al., 2020). The projections of IPSL-CM5A display a decrease in summer precipitation over nearly all the European temperate zone as obtained by the majority of CMIP-5 models. In contrast, the CNRM-CM5 projections show on average higher summer precipitations (Fig. 6.1). The origin of CNRM-CM5 particular behaviour is unfortunately largely unknown (A. Voldoire, personal communication 2021). Nevertheless, the simulated precipitation changes over Europe in summer might be related to modifications of the circulation in the model. Dong et al. (2013) showed that a summer southward shift of the storm tracks leads to enhanced precipitation over the UK and North-Western Europe. Yet, in Kjellström et al. (2018), in response to a 2°C warming (RCP8.5 scenario), ALADIN-CNRM projections display a dipole in sea-level atmospheric pressure that could give rise to such a southward shift of the storm tracks. This trend is however less clear when CNRM is associated with other regional climate models (RCMs).

Among the RCMs of EURO-CORDEX, ALARO-0 also tends to produce higher summer precipitation. For example, over Belgium, the end-of-the century change in summer precipitation is on average -30% for the GCMs

(CMIP5), on average -12% for RCMs (EURO-CORDEX) but +4% for the ALARO-0 RCM simulation (Termonia et al., 2018).

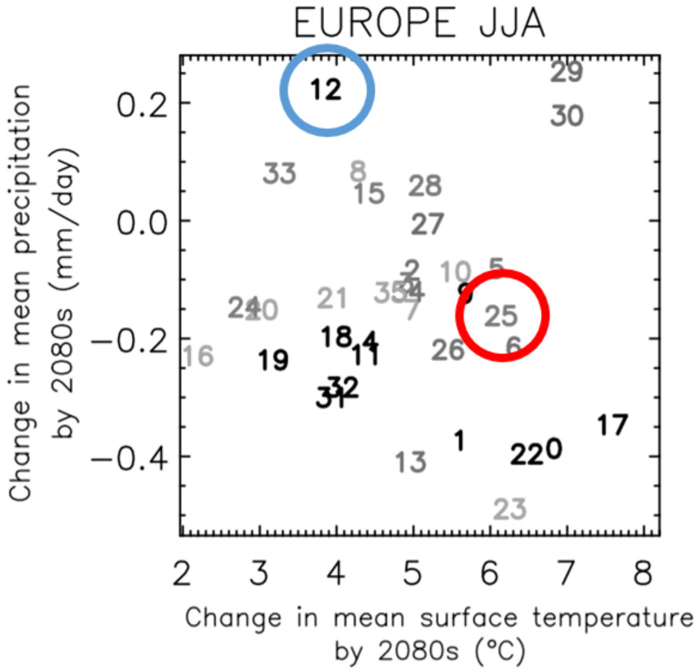

**Figure 6.1: Change in mean precipitation and surface temperature over Europe by 2080 projected by the CNRM-CM5 (blue circle) and the IPSL-CM5A model (red circle) under the scenario RCP8.5 among the other models of the CMIP-5 ensemble (adapted from McSweeney et al., 2015)**

Even if both CNRM-ALARO and IPSL-RCA4 projections are concerned by this downscaling effect, it is interesting to keep in mind that RCMs of the EURO-CORDEX predict considerably lower precipitation change in summer and smaller temperature increase compared to their forcing GCMs. On average over Europe, GCMs predict a 20% precipitation decrease compared to the 5% decline obtained by RCMs. The underlying mechanisms are not perfectly understood but the absence of decreasing anthropogenic aerosol concentration in RCMs is pointed out (Boé et al., 2020). Indeed, these aerosols scatter incident shortwave radiation and their decrease led to a brightening and surface warming over Europe (Nabat et al., 2015) that is expected to continue in the future (Bellucci et al., 2015). Then, as soil moisture becomes limiting, GCMs project a stronger decrease in relative humidity than RCMs, lowering the precipitation occurrence probability. This phenomenon is further enhanced as RCMs project higher evapotranspiration rates over Mediterranean sea, bringing moisture in Southern coastal areas (Boé et al., 2020). As a result, all the downscaled climate projections from EURO-CORDEX could suffer from a bias that make them colder and wetter.

Finally, the differences between the two climate models allows comparing the relative importance of the GHG emission (RCP) scenario and of the climate model in explaining the change in forest productivity. Under the constant $CO_2$ modality, the climate scenario had an insignificant effect compared to the model that accounted for 7% of the variability in productivity change. Inversely, under the changing $CO_2$ modality, the climate scenario explained a larger proportion of the variability than the model (23% vs 0.2%). The influence of the climate model could already be seen in the Fig. 5.6 where the delta NPP values are very close between the two models for the changing $CO_2$ concentration modality but differ significantly for the constant one. This highlights again the important role played by $CO_2$ effect when assessing the impact of climate change on forest productivity.

I have mainly discussed here the impact of climate change averaged over a period. However, many papers highlight the importance of extreme heat and drought waves on tree growth and mortality (Fuhrer et al., 2006; Lindner et al., 2010; Allen et al., 2010; Teskeley et al., 2015). These extreme events are important because tree functioning is a complex set of non-linear mechanisms where threshold exceedance can generate positive feedbacks and totally deregulate the system (Thompson, 2011; Reyer et al., 2015; D'Orangeville et al., 2018). In HETEROFOR, most of the leaf-level processes (photosynthesis, respiration, stomatal conductance and transpiration) (Teskeley et al., 2015) are temperature and/or water dependent and account for the impact of heat or drought waves. This could be seen in the simulation results as the impact of climate change on the lowest simulated annual NPP values (< 7th percentile) was more negative than on the whole NPP distribution (Fig. 5.S5 and 5.S6). However, this effect was limited. One of the reason is that, at the tree-level, while tree growth and phenology are temperature-dependent and can at least partially integrate the influence of intense drought and high temperature events, the influence of these extreme climate episodes on tree mortality and leaf shedding are not represented. Furthermore, pest and disease outbreaks that are critical mortality agents are often conditioned by a succession of previous drought and heat waves (Allen et al., 2010) and are not either included. The absence of these abrupt, non-linear mechanisms, which are mostly detrimental, should always be kept in mind when interpreting our simulation results.

**How the forest growth response to climate change will be modulated by the local soil, stand and climate conditions?**

*Hypotheses: In Southern warmer sites experiencing summer rainfall reduction and under constant atmospheric* $CO_2$*, we expected a dominance of the negative water stress and respiration effects that could be reinforced if the lengthening of the vegetation period became constrained. Inversely, in the cooler Northern and mountainous sites, we assumed that the positive effect of a longer vegetation period on forest productivity would be dominant. Regarding soil, the impact of water stress could be mitigated in deep soils able to accumulate large amounts of water during winter. Given their higher drought sensitivity and shallow root system, the water stress effect was supposed to be greater in beech- than oak-dominated stands. Then, stands with higher density where resource competition and growth potential are important, both negative and positive effects would be intensified. Similarly, negative and positive effects on forest growth would be enhanced in even-aged stands while more complex stands with separated niches would rather buffer these effects.*

To address the question of the influence of the different site components on the forest response to climate change with a modelling approach, some precautions must be taken. As soil, stand and climate conditions affect each other, an uncorrelation procedure is required. To this end, the creation of *virtual* sites according to a partial factorial design in the simulations at the European scale is an efficient approach. A full factorial design would have been better but was not feasible. In addition, the simulation period must be thought in accordance with the study purpose. Indeed, the climate of a site can only be determined on a sufficiently long period. Inversely, the stand properties evolve with time, which complexifies their interpretation when considered over a long period while a very short period gives an excessive weight to possible recent cutting operations or disturbances. The choice of a repetition of two 15-year simulation periods was the best compromise I found.

### Climate effect

For both $CO_2$ modalities, NPP changes were inversely correlated to the mean air temperature. Under constant $CO_2$ concentration, they were on average negative in the warmest sites for all stand types regarding the simulations with IPSL-RCA4 and for oak-dominated stands with CNRM-ALARO (Fig. 5.6). This mostly validates the emitted hypothesis. However, under changing $CO_2$, the overall effect of climate change was positive, even in sites displaying the warmest summer conditions. The complementary hypothesis of a dominant positive effect in the cooler sites was verified as the mountainous sites displayed the highest productivity gain whatever the climate scenario. Other modelling studies have shown that European mountainous forests would experience the highest productivity gain (e.g. Reyer et al., 2014; Gutsch et al., 2016) while the importance of the temperature during the vegetation period was stressed by different studies (Mérian et al., 2011; Fernandez-Martinez et al., 2014). A negative effect of reduced annual rainfall was also detected even if it played a secondary role compared to the mean air temperature (Table 5.S7). Under the constant (changing) $CO_2$ modality, the decomposition of the NPP variance showed that, at the continental scale, the climate explained 14.8% (10.8%) of the NPP variability and about half of these explained proportions concerned the interaction between the site and the climate scenario.

### Soil effect

The assumption that soils with an important water reserve could mitigate the negative effect of water stress was verified as levels of transpiration deficit decreased on average of 57% and 37% for the soils with the highest extractable water reserve under constant and changing $CO_2$ concentration, respectively. The soil explained a significant part of the inter-site productivity variability (14.1 and 6.9% of the NPP variability for the constant and time-dependent $CO_2$ modality, respectively), which was almost totally due to MEW (11.8 and 6.1%). However, it did not further affect the forest response to climate change. The marginal effect of the extractable water reserve on the response to climate change was also pointed out in observational (Härdtle, 2013) and other modelling studies (Gutsch et al., 2016).

### Stand effect

Simulations results pointed out that the species composition slightly affected the productivity response to climate change as the stands dominated by beech displayed more positive NPP changes. In spite of the difference in functional traits between the two species, this effect was rather limited, accounting only for 2.4% of the variability of NPP change. The two species were negatively affected by different processes: the oak higher respiration rate under warmer conditions and the higher water stress experienced by beech. The resulting effect advantaged slightly beech-dominated stands. The second hypothesis that the stand density would reinforce possible positive or negative effects was partly verified as the basal area were positively correlated with the change in NPP under changing $CO_2$ concentration. In addition, in the simulation experiment at the Walloon scale, I showed that the short-term effect of a thinning operation reducing the stand basal area of 25% was to reduce water stress by 32 to 40% (Fig. 4.3).

To further explore the influence of the stand structure on the forest response to climate change, the effect of the tree characteristics on individual NPP change were assessed separately for the two $CO_2$ modalities and the two species. To remove the tree size effect, the difference in NPP between the historical period (averaged over the entire period) and the RCP8.5 scenario was divided by the historical period value. The remaining influence of tree size was analyzed based on tree height and other variables, for which most tree size effect had been removed: the crown horizontal (*Ddindex*; see Eq. 24 to 25 in sect. 1.3.5) and vertical extension ($\frac{h-hcb}{h}$), the light competition index (*LCI*) and the tree slenderness (*h/dbh*). The results of this analysis reveal that NPP changes under constant atmospheric $CO_2$ were more pronounced on small dominated oak and beech trees with a limited crown extension. However, beech trees (contrary to oak ones) seem to better profit from the $CO_2$ fertilization effect when exposed to light (Table 6.S1). The difference between the $CO_2$ modalities could be the sign that dominant trees benefit more under favorable conditions while dominated trees would less suffer under more stressful conditions. The results are just preliminary ones and should be confirmed by more simulations carried out with different model options in order to identify exactly the processes at play.

These results highlight the influence of the stand structure and the local conditions on the tree response to climate change. At the stand scale, the influence of the stand structure would probably be more evident in longer simulations integrating disturbances. Indeed, the advantage of this type of stand is the better resilience it displays, allowing retrieving more quickly its initial productivity after a disturbance (Forrester and Bauhus, 2016; Brockerhoff et al., 2017; Zeller et al., 2018).

One may wonder if the stand impact on forest response to climate change would not be more pronounced with climate projections less favourable to tree growth (e.g. larger decrease in summer precipitations). Launching new simulations with climate projections obtained from other global and regional climate models would therefore be interesting. The limited stand effect on forest response to climate change could also be due to the fact that some processes are still not enough dependent on tree characteristics. Several model improvements allowing a better consideration of tree characteristics are mentioned in the discussion of the objective 1 and will be progressively integrated in the model. After these improvements, repeating the simulation experiments will allow identifying new key processes involved in the stand effect on forest response to climate change. Finally, one have

# GENERAL CONCLUSION

The new model developments presented in this thesis contributes to offer new domains of application to the individual-based model HETEROFOR and, in particular, to obtain a version that can be applied to study the impact of climate changes on structurally complex broadleaved stands in Europe. This new version was used to predict the forest growth in a large variety of European sites and for different climate scenarios.

The simulation results showed that climate change could have a slight positive effect on forest productivity under constant atmospheric $CO_2$, with, however, productivity losses observed in sites displaying particularly warm spring and summer temperatures and/or experiencing a decrease in annual rainfall. However, there is a large uncertainty on the magnitude of these changes depending on the climate model and the GHG emission scenario considered. For oak and beech, the productivity gain was much larger when considering an increase in atmospheric $CO_2$ concentration mainly due to the $CO_2$ fertilization effect.

Apart from the $CO_2$ fertilization, whose persistence is quite uncertain, the main drivers of the positive changes are the increase in the vegetation period length and the improved water use efficiency. The negative NPP changes observed in some sites can be explained by higher water stress levels and maintenance respiration costs.

Even if the species composition and the stand structure had a limited influence on the forest response to climate change, both explained a large part of the NPP variability (44% and 34% for $[CO_2]_{cst}$ and $[CO_2]_{var}$, respectively) compared to the climate change scenario effect (5% and 29% for $[CO_2]_{cst}$ and $[CO_2]_{var}$, respectively) and to the inter-annual climate variability (20% and 16% for $[CO_2]_{cst}$ and $[CO_2]_{var}$, respectively). This gives the forester the possibility to act on the stand productivity of broadleaved forests and to prepare them for possible adverse effects of climate change by reinforcing their resilience.

Now that a full methodology has been created and verified, the repetition of new simulations will be very straightforward and could be done each time new and more accurate climate projections are produced or when new developments allow better capturing the effect of climate change on individual tree growth. Regarding the latter, the priority will be given to the inclusion of mortality by hydraulic failure and late frost episodes in the model as well as a vertical differentiation of air temperature.

Since uncertainty will always remain in climate and forest modelling, this tool could also be used to quantify the total uncertainty and to decompose it in various sources (errors associated with the projections of the global climate models, the physical and statistical downscaling, the description of the eco-physiological processes and the model parameter distribution). As HETEROFOR is able to account for stand structure in a very detailed manner, the next step is to test various forest management strategies while considering climate change in long-term simulations. Such information is indeed needed by forest managers willing to reinforce the resilience of the forest.

# SUPPLEMENTARY MATERIALS

## 1. INDIVIDUAL VARIABILITY

**Table 6.S1: Estimate, P value and partial R² of the parameters of a multivariate model used to explain the mean relative individual NPP change (between the historical and RCP8.5 scenarios, gC $m^{-2}$ $yr^{-1}$) from mean individual tree characteristics for the *virtual* sites with constant (left) and changing over time (right) atmospheric $CO_2$ concentration and oak (top) and beech (bottom). The simulations made based on the two types of climate projections (CNRM-ALARO and IPSL-RCA4) were included in the analysis.**

| | Constant CO2 | | | Changing CO2 | | |
|---|---|---|---|---|---|---|
| | Estimate | P value | Partial R² | Estimate | P value | Partial R² |
| **a) Oak** | | | | | | |
| Intercept | 0.750 | <.0001 | | 0.498 | <.0001 | |
| h | -0.010 | <.0001 | 0.035 | -0.006 | <.0001 | 0.0425 |
| LCI | -0.482 | <.0001 | 0.198 | -0.061 | <.0001 | 0.0191 |
| DdIndex | -0.319 | <.0001 | 0.064 | -0.098 | <.0001 | 0.0281 |
| Total | | | 0.296 | | | 0.090 |
| **b) Beech** | | | | | | |
| Intercept | 0.328 | <.0001 | | 0.311 | <.0001 | |
| h | -0.005 | <.0001 | 0.094 | -0.008 | <.0001 | 0.054 |
| (h-hcb)/h | -0.176 | <.0001 | 0.025 | | | |
| LCI | -0.055 | <.0001 | 0.015 | 0.331 | <.0001 | 0.064 |
| DdIndex | | | | 0.075 | <.0001 | 0.015 |
| Total | | | 0.134 | | | 0.132 |

## 2. MODEL SENSITIVITY ANALYSIS FOR TREE SPATIAL DISTRIBUTION AND INTER-INDIVIDUAL VARIABILITY

In order to evaluate how changing tree spatial distribution and restricting our individual approach into a cohort approach affect the model results, different stands were created from an existing stand. The stand used was the site of ‘Baileux-mixed’ that is constituted from oak and beech trees in similar proportions and that was used for the evaluation of the model (Chap. 2). For testing the effect of the tree spatial distribution, two stands composed of exactly the same trees but with a contrasted spatial distribution were created: a patch-wise mixture in which the trees of a similar size and of the same species have a higher probability to be grouped and an intimate mixture where trees of different tree species and size are clumped together. To test the effect of restricting our approach to a cohort model, the trees of the intimate mixture were distributed in seven different cohorts (four beech and three oak cohorts) according to the girth-class distribution and the dimensions of the trees were replaced by those of the average tree of the cohort.

In the end, I obtained one stand where all the trees are represented with their own characteristics grouped in patches according to their size and species called patch-wise mixture (tree level approach), another where all the trees are represented according to their real dimensions but where trees of different size and species are mixed in an intimate way called intimate tree by tree mixture (tree level approach) and a last one with an intimate tree by tree mixture but where the trees of the same cohort have the same averaged dimensions. They are all represented in Fig. 6.S1.

The evolution of the three different stands was simulated between 2001 and 2011 and they were compared based on the LAI and on the annual transpiration (Figs. 5.S2 and 5.S3). The differences in LAI and in annual transpiration among stands were analysed for each cohorts and for all trees together. In addition, mixed linear models were fitted to highlight the effects of the tree spatial distribution and of the clustering in cohorts taking the tree and the year into account as random factors. The cohort clustering effect was tested by comparing the intimate mixtures at the tree and cohort level while the tree spatial distribution effect was assessed by comparing the patch-wise and intimate mixture.

The tree spatial distribution effect (patch-wise vs intimate mixture) generated differences in LAI ranging from -35% to +23% depending on the year and on the cohort considered (Fig. 6.S2). According to the linear mixed models, this effect was always significant, except for the beech > 140 cm cohort (Table 6.S2). Regarding annual transpiration, the relative differences between the patch-wise and the intimate mixture range between -25% to +9% and the corresponding effect was significant, except for the beech 106-140 cm cohort (Table 6.S3).

Compared to the individual approach, the clustering in cohorts induced differences from -9% to +30% for the LAI (Fig. 6.S2) and from -10% to +6% for the annual transpiration (Fig. 6.S3). The corresponding effect was significant, except for the oak 61-105 cm cohort concerning LAI and for the oak and beech 106-140 cm cohorts regarding annual transpiration (Table 6.S2 and 6.S3).

The effects of tree spatial distribution and of clustering in cohorts are less pronounced at the stand than at the cohort level since they vary from one cohort to the other and partly offset each other at the stand level.

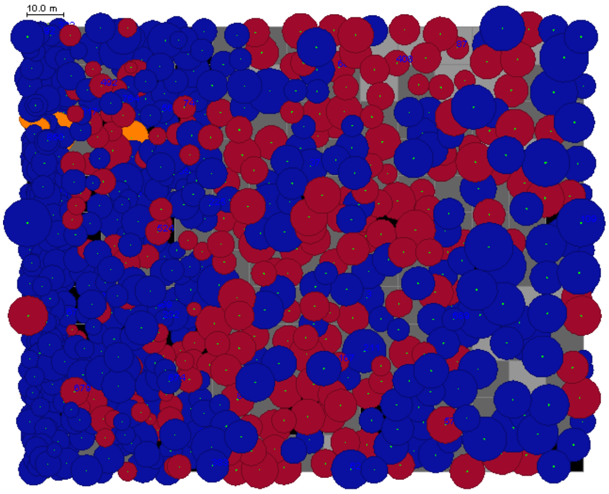

Patch-wise mixture (tree level approach)

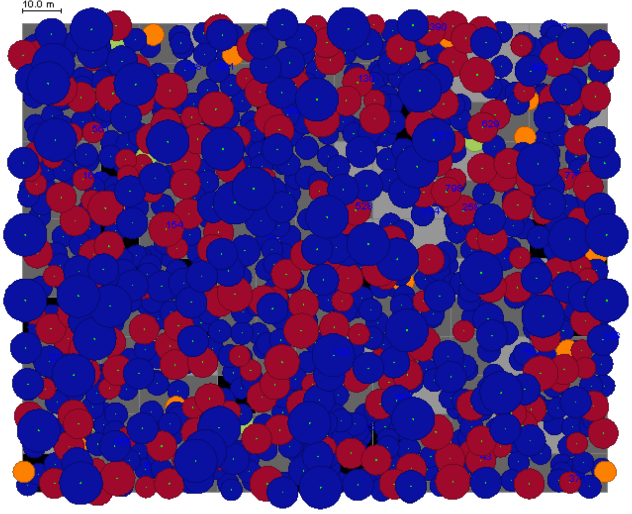

Intimate tree by tree mixture (cohort level approach)

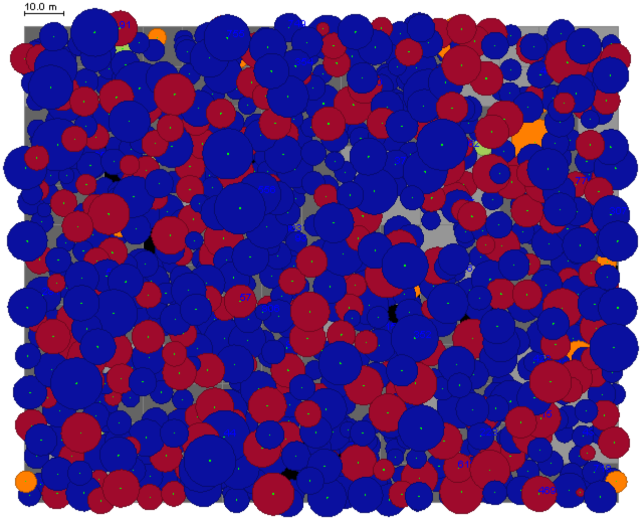

Intimate tree by tree mixture (tree level approach)

**Figure 6.S1: Visual representation of the three stands created for analysing the model sensitivity to the tree spatial distribution and the restriction of the individual approach into a cohort approach.**

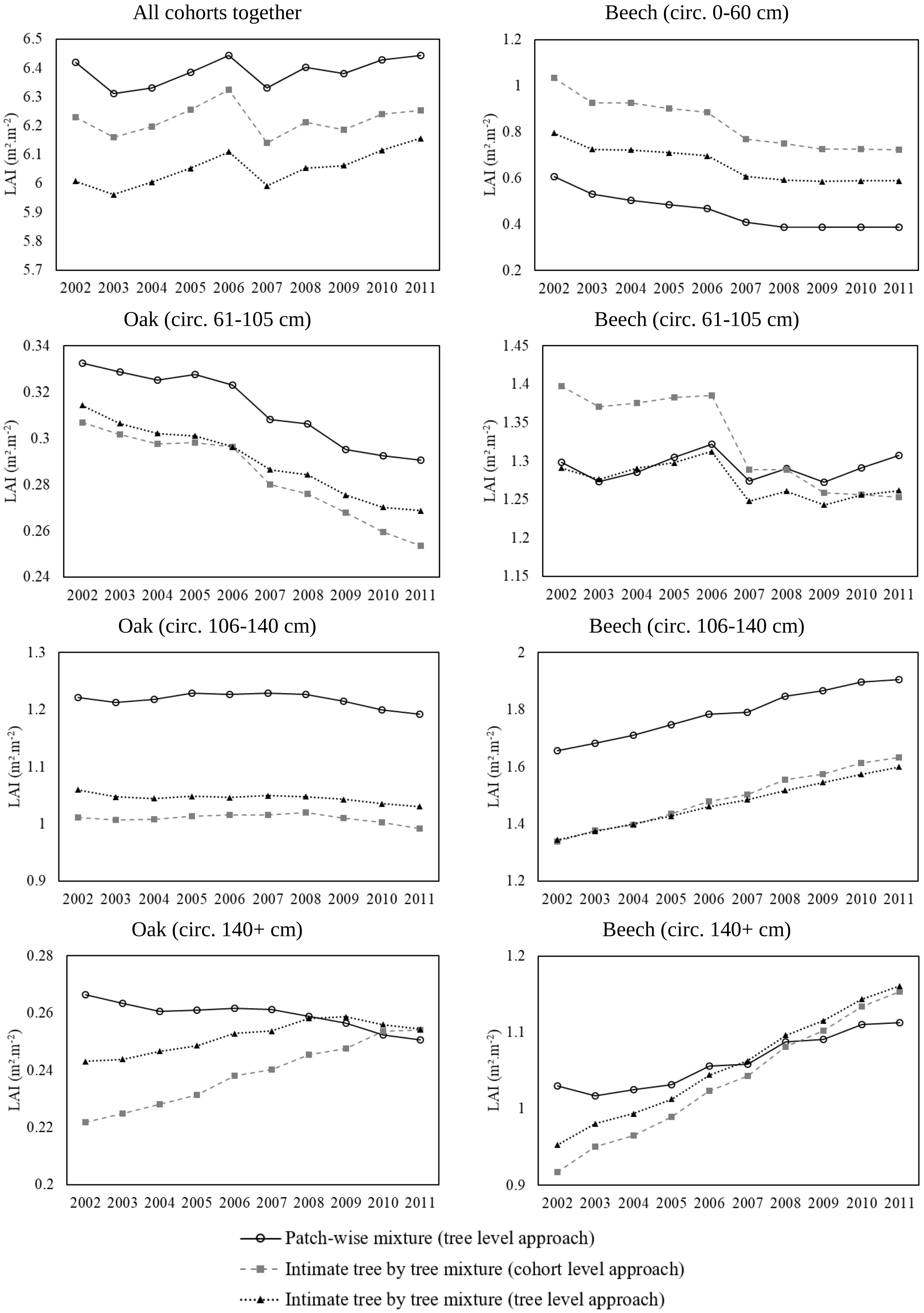

**Figure 6.S2: Temporal change in LAI (m²/m²) of the mixed stand in Baileux for all trees together and per cohort (four beech and three oak cohorts) according to three different stand configurations: a patch-wise mixture with a tree level approach and two intimate mixtures with a tree or a cohort level approach.**

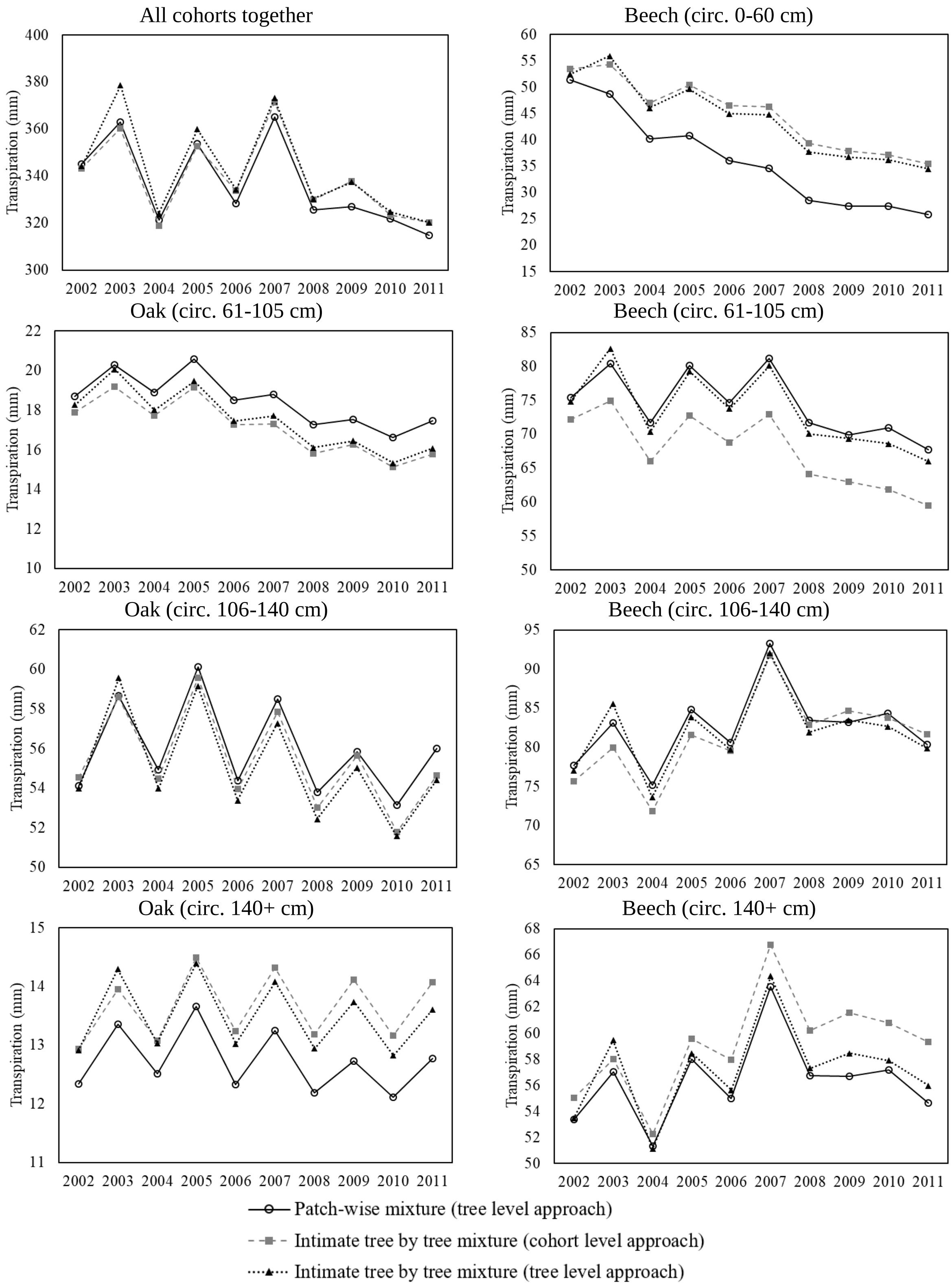

**Figure 6.S3: Temporal change in the annual transpiration (mm) of the mixed stand in Baileux for all trees together and per cohort (four beech and three oak cohorts) according to three different stand configurations: a patch-wise mixture with a tree level approach and two intimate mixtures with a tree or a cohort level approach.**

**Table 6.S2: Mixed linear model results for the different tree cohorts and for all trees to highlight the impact of tree spatial distribution (patch-wise vs intimate tree by tree mixture) and of cohort clustering (tree vs cohort approach) on LAI.**

| Effect | Cohort | Estimate (std dev) | p-value |
|---|---|---|---|
| Intimate *vs* patch mixture | Beech (circ. 0-60 cm) | -0.00032 (8.9 E$^{-6}$) | <.0001*** |
| | Beech (circ. 61-105 cm) | 5.8 E$^{-5}$ (2.7 E$^{-5}$) | 0.028* |
| | Oak (circ. 61-105 cm) | 0.00016 (2.7 E$^{-5}$) | <.0001*** |
| | Beech (circ. 106-140 cm) | 0.0018 (3.9 E$^{-5}$) | <.0001*** |
| | Oak (circ. 106-140 cm) | 0.00071 (3.6 E$^{-5}$) | <.0001*** |
| | Beech (circ. 140+ cm) | 7.6 E$^{-5}$ (0.00013) | 0.56 |
| | Oak (circ. 140+ cm) | 0.00019 (8.1 E$^{-5}$) | 0.018* |
| | All trees | 0.00021 (1.3 E$^{-5}$) | <.0001*** |
| Tree *vs* cohort approach | Beech (circ. 0-60 cm) | 0.00027 (1.0 E$^{-5}$) | <.0001*** |
| | Beech (circ. 61-105 cm) | 0.00017 (2.8 E$^{-5}$) | <.0001*** |
| | Oak (circ. 61-105 cm) | -4.9 E$^{-5}$ (3.3 E$^{-5}$) | 0.14 |
| | Beech (circ. 106-140 cm) | 9.7 E$^{-5}$ (4.0 E$^{-5}$) | 0.016* |
| | Oak (circ. 106-140 cm) | -0.00015 (3.4 E$^{-5}$) | <.0001*** |
| | Beech (circ. 140+ cm) | -0.00027 (9.9 E$^{-5}$) | 0.0070** |
| | Oak (circ. 140+ cm) | -0.00033 (8.0 E$^{-5}$) | <.0001*** |
| | All trees | 0.00010 (1.2 E$^{-5}$) | <.0001*** |

**Table 6.S3: Mixed linear model results for the different tree cohorts and for all trees to highlight the impact of tree spatial distribution (patch-wise vs intimate tree by tree mixture) and of cohort clustering (tree vs cohort approach) on annual transpiration.**

| Effect | Cohort | Estimate (std dev) | p-value |
|---|---|---|---|
| Intimate *vs* patch mixture | Beech (circ. 0-60 cm) | -0.012 (0.00043) | <.0001*** |
| | Beech (circ. 61-105 cm) | 0.0028 (0.00094) | 0.0028*** |
| | Oak (circ. 61-105 cm) | 0.0070 (0.00087) | <.0001*** |
| | Beech (circ. 106-140 cm) | 0.0034 (0.0014) | 0.016 |
| | Oak (circ. 106-140 cm) | 0.0036 (0.00089) | <.0001*** |
| | Beech (circ. 140+ cm) | -0.011 (0.0040) | 0.0049*** |
| | Oak (circ. 140+ cm) | -0.019 (0.0018) | <.0001*** |
| | All trees | -0.0037 (0.00043) | <.0001*** |
| Tree *vs* cohort approach | Beech (circ. 0-60 cm) | 0.0014 (0.00051) | 0.0082** |
| | Beech (circ. 61-105 cm) | -0.019 (0.0014) | <.0001*** |
| | Oak (circ. 61-105 cm) | -0.0025 (0.0011) | 0.026* |
| | Beech (circ. 106-140 cm) | -0.0036 (0.0022) | 0.11 |
| | Oak (circ. 106-140 cm) | 0.0014 (0.00092) | 0.14 |
| | Beech (circ. 140+ cm) | 0.025 (0.0060) | <.0001*** |
| | Oak (circ. 140+ cm) | 0.0042 (0.0018) | 0.019* |
| | All trees | -0.0022 (0.00057) | 0.0001*** |

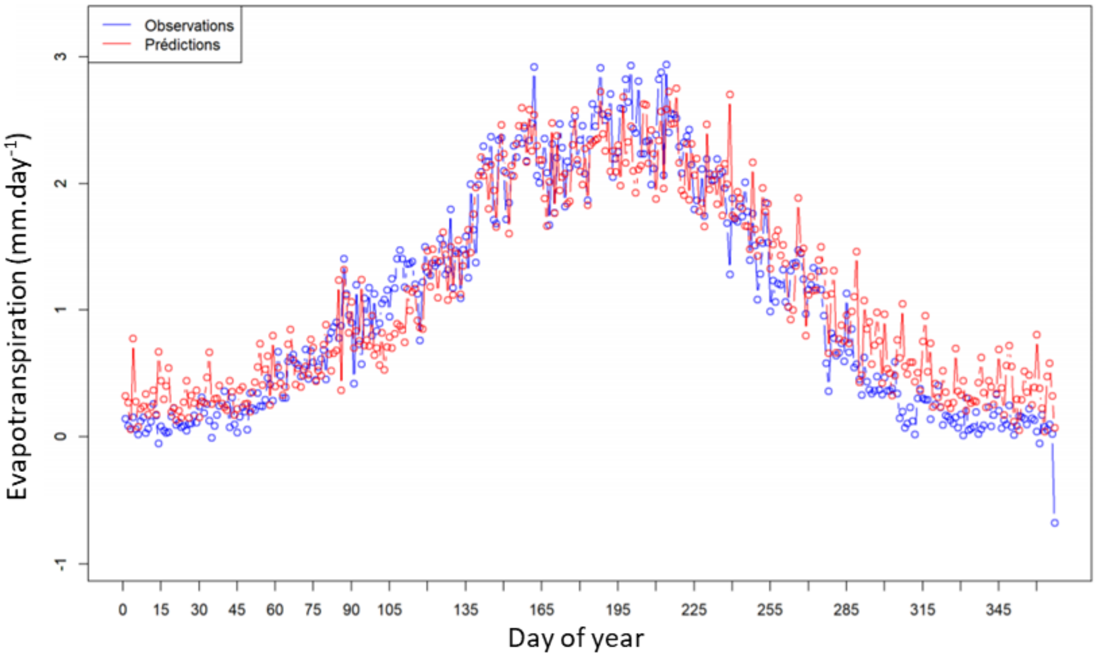

**Figure 6.S4: Daily evolution of the observed and predicted evapotranspiration (mm.day$^{-1}$) for an average year calculated on the 2010-2018 period. This figure comes from the master thesis of Guillaume de Meue (De Meue, 2020).**

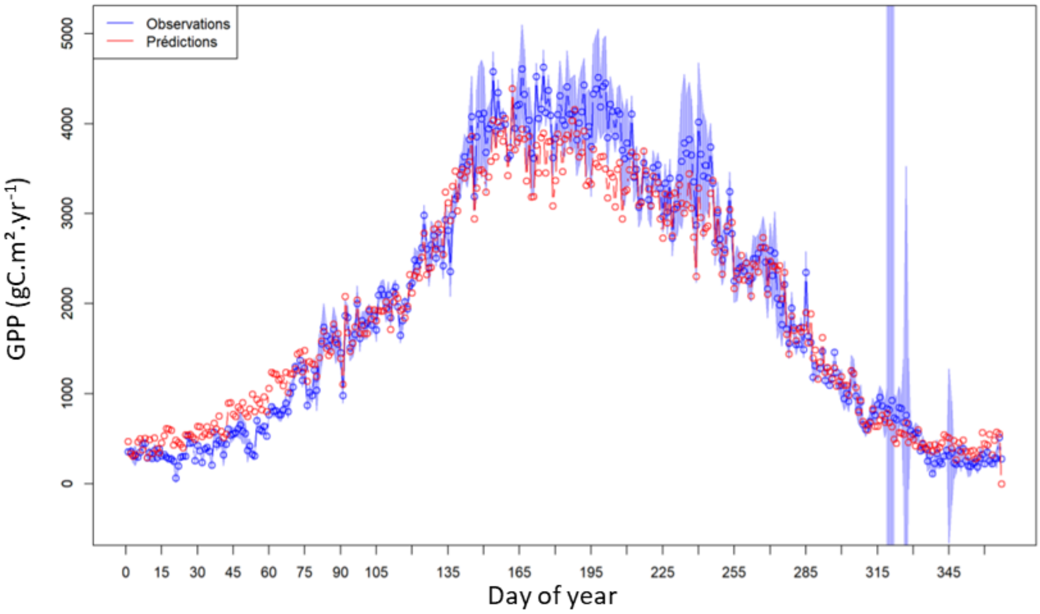

**Figure 6.S5: Daily evolution of the observed and predicted GPP (gC.m²$.yr^{-1}$) for an average year calculated on the 2010-2018 period. The shaded blue interval corresponds to the observation uncertainty. This figure comes from the master thesis of Guillaume de Meue (de Meue, 2020).**

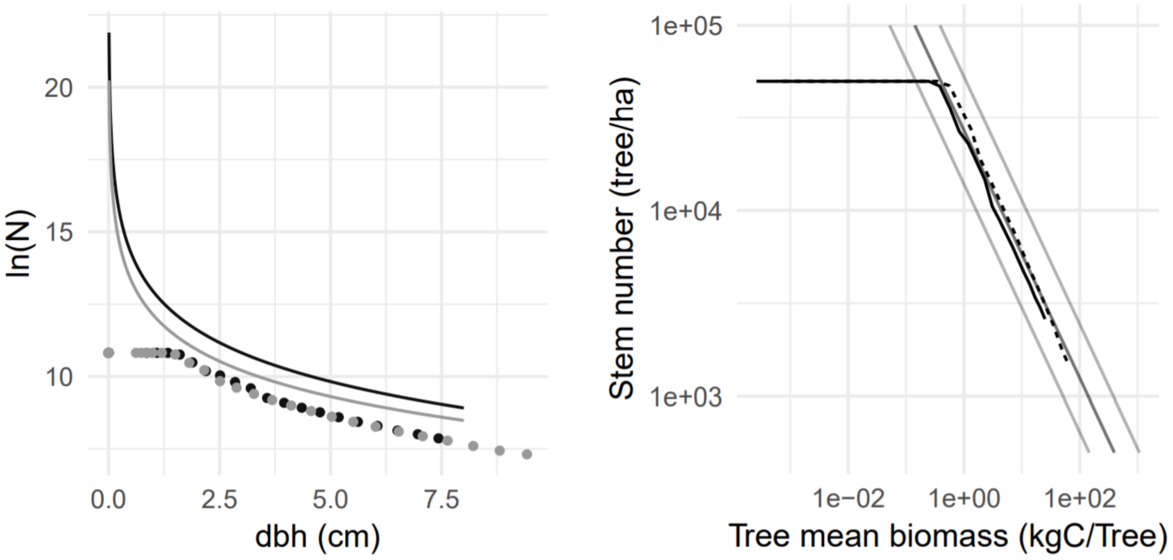

(a) Oak (gray) and beech (black)

(b) Oak (- - -) and beech (—)

**Figure 6.S6: Self-thinning process reproduced by simulations for two pure stands (one oak and one beech) compared with empirical equations. On the left, the self-thinning curve of oak (gray) and beech (black) are based on Charru et al. (2012). On the right, the gray lines correspond to self-thinning lines for three intercept parameters (k' = 15, 16, 17) based on Yoda (1963). These figures come from the master thesis of Brieuc Ryelandt (Ryelandt, 2019).**

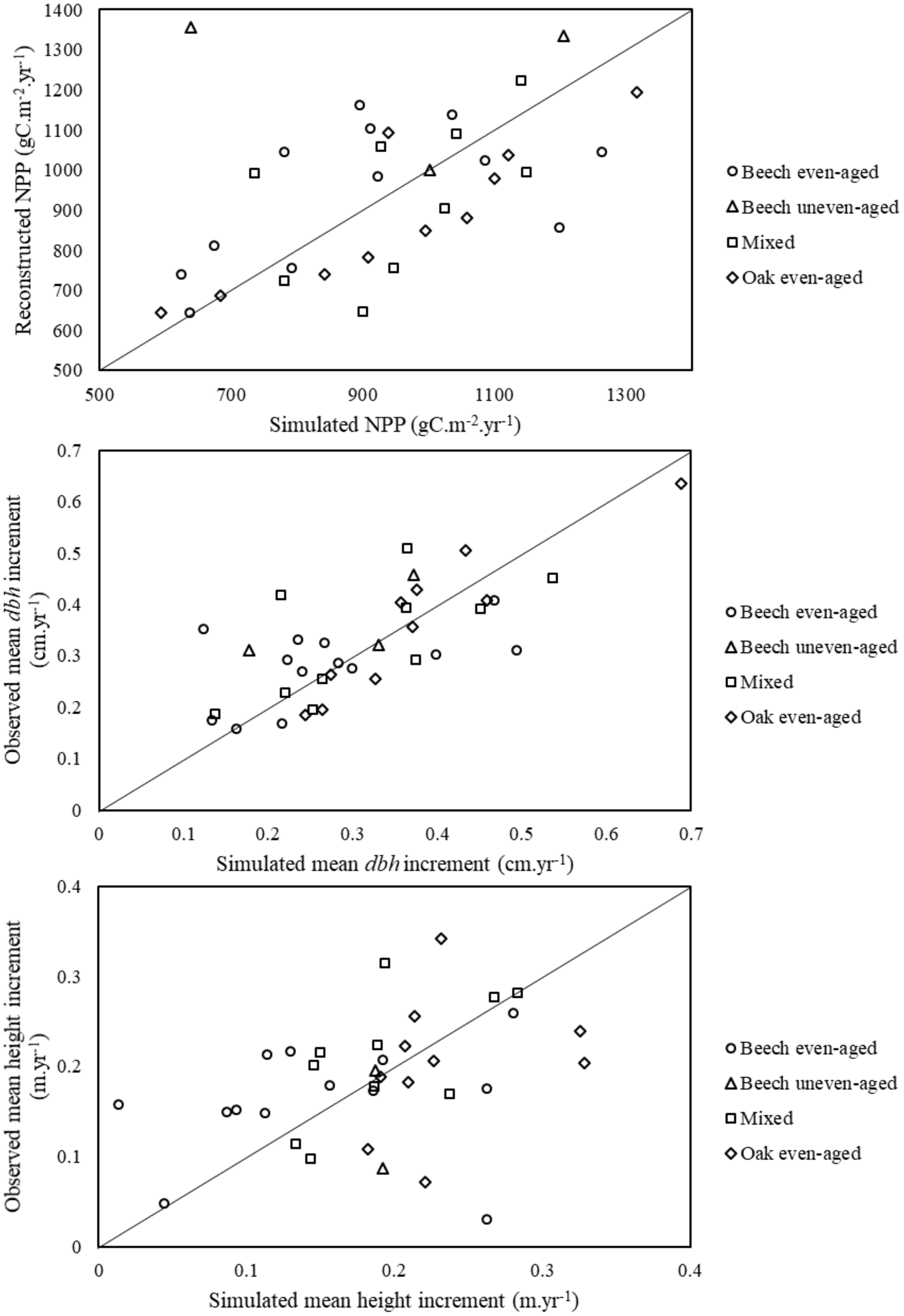

**Figure 6.S7: Comparison of the observed and predicted stand NPP (top), mean *dbh* increment (middle) and mean height increment (bottom) for the European sites of Chap. 5. Predictions were based on the general CUE function.**

# REFERENCES

Aalde H, Gonzalez P, Gytarsky M, Krug T, Kurz WA, Lasco RD, Verchot L (2006) Generic methodologies applicable to multiple land-use categories. IPCC guidelines for national greenhouse gas inventories 4: 1-59.

Adams HD, Zeppel MJ, Anderegg WR, et al. (59 more authors) (2017) A multi-species synthesis of physiological mechanisms in drought-induced tree mortality. Nat. Ecol. Evol. 1(9): 1285.

Ahmadi, M. T., Attarod, P., Mohadjer, M. R. M., Rahmani, R., and Fathi, J.: Partitioning rainfall into throughfall, stemflow, and interception loss in an oriental beech (Fagus orientalis Lipsky) forest during the growing season, Turk. J. Agric. For., 33(6), 557-568, 2009.

Ainsworth EA, Long SP (2005) What have we learned from 15 years of free-air CO2 enrichment (FACE)? A meta-analytic review of the responses of photosynthesis, canopy properties and plant production to rising CO2. New Phytol. 165(2): 351-372.

Ainsworth EA, Rogers A (2007) The response of photosynthesis and stomatal conductance to rising [CO2]: mechanisms and environmental interactions. Plant Cell Environ. 30(3): 258-270.

Aitken SN, Yeaman S, Holliday JA, Wang T, Curtis-McLane S (2008) Adaptation, migration or extirpation: climate change outcomes for tree populations. Evolutionary applications 1(1): 95-111.

Albert M, Nagel RV, Sutmöller J, Schmidt M (2018) Quantifying the effect of persistent dryer climates on forest productivity and implications for forest planning: a case study in northern Germany. For. Ecosyst. 5(1): 1-21.

Albrecht A (2007) Evaluierung des Waldwachstumssimulators Silva 2.2 anhand langfristiger ertragskundlicher Versuchsflächen in Baden-Württemberg. In: Nagel, J. (ed.): Sektion Ertragskunde Jahrestagung. Alsfeld-Eudorf 154-163.

Ali A (2019) Forest stand structure and functioning: Current knowledge and future challenges. Ecol. Indic. 98: 665-677.

Allen RG, Pereira LS, Raes D, Smith M (1998) Crop evapotranspiration-Guidelines for computing crop water requirements-FAO Irrigation and drainage paper 56. FAO, Rome.

Allen CD, Macalady AK, Chenchouni H, Bachelet D, McDowell N, Vennetier M, Kitzberger T, Rigling A, Breshears DD, Hogg EH, Gonzalez P, Fensham R, Zhang Z, Castro J, Demidova N, Lim JH, Allard G, Running SW, Semerci A, Cobb N (2010) A global overview of drought and heat-induced tree mortality reveals emerging climate change risks for forests. Forest Ecol. Manag. 259(4): 660-684.

Allen, C. D., Breshears, D. D., McDowell, N. G.: On underestimation of global vulnerability to tree mortality and forest die-off from hotter drought in the Anthropocene, Ecosphere, 6(8), 1-55, 2015.

Amthor JS (2000) The McCree–de Wit–Penning de Vries–Thornley respiration paradigms: 30 years later. Ann. Bot. 86(1): 1-20.

An, H., and Noh, S. J.: High-order averaging method of hydraulic conductivity for accurate soil moisture modelling, J. Hydrol., 516, 119-130, 2014.

Anderegg WR, Kane JM, Anderegg LD (2013) Consequences of widespread tree mortality triggered by drought and temperature stress. Nature Clim. Change 3(1): 30-36.

Anderegg WR, Konings AG, Trugman AT, Yu K, Bowling DR, Gabbitas R, Zenes N (2018) Hydraulic diversity of forests regulates ecosystem resilience during drought. Nature 561(7724): 538.

André F, Ponette Q (2003) Comparison of biomass and nutrient content between oak (Quercus petraea) and hornbeam (Carpinus betulus) trees in a coppice-with-standards stand in Chimay (Belgium). Ann. For. Sci. 60(6): 489-502.

André F, Jonard M, Ponette Q (2008a) Influence of species and rain event characteristics on stemflow volume in a temperate mixed oak–beech stand. Hydrol. Process. 22(22):4455–4466

André F, Jonard M, Ponette Q (2008b) Precipitation water storage capacity in a temperate mixed oak–beech canopy. Hydrol. Process. 22(20): 4130-4141.

André, F., Jonard, M., and Ponette, Q.: Effects of biological and meteorological factors on stemflow chemistry within a temperate mixed oak–beech stand, Sci. Total Environ., 393, 72-83, 2008c.

André F, Jonard M, Ponette Q (2010) Biomass and nutrient content of sessile oak (Quercus petraea (Matt.) Liebl.) and beech (Fagus sylvatica L.) stem and branches in a mixed stand in southern Belgium. Sci. Total Environ. 408(11): 2285-2294.

André F, Jonard M, Jonard F, Ponette Q (2011) Spatial and temporal patterns of throughfall volume in a deciduous mixed-species stand. J. Hydrol. 400(1-2): 244-254.

André F, de Wergifosse L, de Coligny F, Beudez N, Ligot G, Gauthray-Guyénet V, Courbaud B, Jonard M (2021) Radiative transfer modeling in structurally-complex stands: what aspects matter most?. Ann. For. Sci. (submitted)

Assouline, S., Or, D.: Anisotropy factor of saturated and unsaturated soils, Water Resour. Res., 42(12), 2006.

Aubertin, G. M.: Nature and extent of macropores in forest soils and their influence on subsurface water movement, USDA For. Serv. NE Res., 192, 1971.

Augspurger, C. K., Bartlett, E. A.: Differences in leaf phenology between juvenile and adult trees in a temperate deciduous forest, Tree Physiol., 23(8), 517-525, 2003.

Aussenac, G.: Interception des précipitations par le couvert forestier, Ann. Sci. Forest., 25(3), 135-156, 1968.

Aussenac, G.: Action du couvert forestier sur la distribution au sol des précipitations, Ann. Sci. Forest., 27(4), 383-399, 1970.

Aussenac, G., and Boulangeat, C.: Interception des précipitations et évapotranspiration réelle dans des peuplements de feuillu (Fagus silvatica L.) et de résineux (Pseudotsuga menziesii (Mirb) Franco), Ann. Sci. Forest., 37(2), 91-107, 1980.

Aussenac G, Granier A (1988) Effects of thinning on water stress and growth in Douglas-fir. Can. J. For. Res. 18(1): 100-105.

Bailey BN, Stoll R, Pardyjak ER, Miller NE (2016) A new three-dimensional energy balance model for complex plant canopy geometries: Model development and improved validation strategies. Agric. For. Meteorol. 218: 146-160.

Bakker MR, Turpault MP, Huet S, Nys C (2008) Root distribution of Fagus sylvatica in a chronosequence in western France. J. For. Res. 13(3): 176-184.

Baldocchi D (2008) 'Breathing'of the terrestrial biosphere: lessons learned from a global network of carbon dioxide flux measurement systems. Aust. J. Bot. 56(1): 1-26.

Ball JT, Woodrow IE, Berry JA. A model predicting stomatal conductance and its contribution to the control of photosynthetis under different environmental conditions, in: Progress in Photosynthesis Research, edited by: Biggins, J., vol. 4, 221–224, 1987.

Barbeito I, Montes F, Cañellas I (2009) Evaluating the behaviour of vertical structure indices in Scots pine forests. Ann. For. Sci. 66(710):1–10

Bargali SS (2018) Forest ecosystem: Structure and Functioning. Curr. Trends For. Res. 120.

Basist A, Bell GD, Meentemeyer V (1994) Statistical relationships between topography and precipitation patterns. J. Clim. 7(9): 1305-1315.

Basler D, Körner C (2012) Photoperiod sensitivity of bud burst in 14 temperate forest tree species. Agric. For. Meteorol. 165: 73-81.

Basler D (2016) Evaluating phenological models for the prediction of leaf-out dates in six temperate tree species across central Europe. Agricultural and Forest Meteorology, 217, 10-21.

Bastos A, Ciais P, Friedlingstein P, Sitch S, Pongratz J, Fan L, Zaehle S (2020) Direct and seasonal legacy effects of the 2018 heat wave and drought on European ecosystem productivity. Science advances 6(24): eaba2724.

Bastrup-Birk, A., and Gundersen, P.: Water quality improvements from afforestation in an agricultural catchment in Denmark illustrated with the INCA model, Hydrol. Earth Syst. Sci., 8(4), 764-777, 2004.

Bastrup-Birk A, Reker J, Zal N (2016) European Forest Ecosystems: State and Trends, EEA Report, Copenhagen, Denmark.

Batavia C, Nelson MP (2017) For goodness sake! What is intrinsic value and why should we care?. Biol. Conserv. 209: 366-376.

Bates D, Mächler M, Bolker B, Walker S (2014) Fitting linear mixed-effects models using lme4. arXiv:1406.5823.

Bauhus J, Puettmann KJ, Kühne C (2013) Close-to-nature forest management in Europe: does it support complexity and adaptability of forest ecosystems. In: Messier C, Puettmann KJ, Coates KD (eds) Managing forests as complex adaptive systems: building resilience to the challenge of global change, Oxford, pp. 187-213.

Bazuhair, A. S., and Wood, W. W.: Chloride mass-balance method for estimating ground water recharge in arid areas: examples from western Saudi Arabia, J. Hydrol., 186(1-4), 153-159, 1996.

Becker, M., Nieminen, T. M., & Gérémia, F. (1994). Short-term variations and long-term changes in oak productivity in northeastern France. The role of climate and atmospheric CO 2. In Annales des Sciences forestières (Vol. 51, No. 5, pp. 477-492). EDP Sciences.

Bedia J, Baño-Medina J, Legasa MN, Iturbide M, Manzanas R, Herrera S, Casanueva A, San-Martín D, Cofiño AS, Gutiérrez JM (2020) Statistical downscaling with the downscaleR package (v3. 1.0): contribution to the VALUE intercomparison experiment. Geosci. Model Dev. 13(3): 1711-1735.

Bellassen V, Viovy N, Luyssaert S, Le Maire G, Schelhaas MJ, Ciais P (2011) Reconstruction and attribution of the carbon sink of E uropean forests between 1950 and 2000. Glob. Change Biol. 17(11): 3274-3292.

Bello J, Hasselquist NJ, Vallet P, Kahmen A, Perot T, Korboulewsky N (2019a) Complementary water uptake depth of Quercus petraea and Pinus sylvestris in mixed stands during an extreme drought. Plant Soil 437(1-2): 93-115.

Bello J, Vallet P, Perot T, Balandier P, Seigner V, Perret S, Couteau C, Korboulewsky N (2019b). How do mixing tree species and stand density affect seasonal radial growth during drought events?. Forest Ecol. Manag. 432: 436-445.

Bellot, J., and Escarre, A.: Stemflow and throughfall determination in a resprouted Mediterranean holm-oak forest, in: Ann. Sci. Forest., 55(7), 847-865, 1998.

Bellucci A, Haarsma R, Bellouin N, Booth B, Cagnazzo C et al (2015) Advancements in decadal climate predictability: the role of nonoceanic drivers. Rev Geophys 53:165–202.

Bennett AC, McDowell NG, Allen CD, Anderson-Teixeira KJ (2015) Larger trees suffer most during drought in forests worldwide. Nat. Plants 1(10): 15139.

Bent, G. C.: Effects of forest-management activities on runoff components and ground-water recharge to Quabbin Reservoir, central Massachusetts, Forest Ecol. Manag., 143(1-3), 115-129, 2001.

Berger U, Piou C, Schiffers K, Grimm V (2008). Competition among plants: concepts, individual-based modelling approaches, and a proposal for a future research strategy. Perspectives in Plant Ecology, Evolution and Systematics 9(3-4): 121-135.

Bergès, L., Dupouey, J. L., & Franc, A. (2000). Long-term changes in wood density and radial growth of Quercus petraea Liebl. in northern France since the middle of the nineteenth century. Trees, 14(7), 398-408.

Beuker, E., Raspe, S., Bastrup-Birk, A., Preuhsler, T., and Fleck, S.: Part VI: Phenological Observations, in: UNECE ICP Forests Programme Co-ordinating Centre: Manual on methods and criteria for harmonized sampling, assessment, monitoring and analysis of the effects of air pollution on forests, Thünen Institute of Forest Ecosystems, 1-12, 2016.

Binkley, D., Campoe, O. C., Gspaltl, M., Forrester, D. I.: Light absorption and use efficiency in forests: Why patterns differ for trees and stands, Forest Ecol. Manag., 288, 5-13, 2013.

Boé J, Somot S, Corre L, Nabat P (2020) Large discrepancies in summer climate change over Europe as projected by global and regional climate models: causes and consequences. Clim. Dyn. 54(5): 2981-3002.

Bohn FJ, Huth A (2017) The importance of forest structure to biodiversity–productivity relationships. R. Soc. Open Sci. 4(1): 160521.

Boisvenue C, Running SW (2006) Impacts of climate change on natural forest productivity–evidence since the middle of the 20th century. Global Change Biology 12(5): 862-882.

Bolte A, Hilbrig L, Grundmann B, Kampf F, Brunet J, Roloff A (2010) Climate change impacts on stand structure and competitive interactions in a southern Swedish spruce–beech forest. Eur. J. For. Res. 129(3): 261-276.

Bolte A, Kampf F, Hilbrig L (2013) Space sequestration below ground in old-growth spruce-beech forests—signs for facilitation?. Front. Plant Sci. 4: 322.

Bonan GB (2008) Forests and climate change: forcings, feedbacks, and the climate benefits of forests. Science 320(5882): 1444-1449.

Bonhomme R (1993) The solar radiation: characterization and distribution in the canopy, INRA, Paris, pp 17–28. Crop Structure and Light Microclimate

Bontemps JD, Hervé JC, Leban JM, Dhôte JF (2011) Nitrogen footprint in a long-term observation of forest growth over the twentieth century. Trees 25: 237–251.

Bosc A (2000) EMILION, a tree functional-structural model: presentation and first application to the analysis of branch carbon balance. Ann. Forest Sci. 57: 555–569.

Bourdier T, Cordonnier T, Kunstler G, Piedallu C, Lagarrigues G, Courbaud B. 2016 Tree size inequality reduces forest productivity: an analysis combining inventory data for ten European species and a light competition model. PLoS ONE 11, e0151852.

Bradshaw, R. H., and Sykes, M. T., 2014, Ecosystem dynamics: From the past to the future, John Wiley and Sons.

Bravo, F., Fabrika, M., Ammer, C., Barreiro, S., Bielak, K., Coll, L., Fonseca, T., Kangur, A., Löf, M., Merganicova, K., Pach, M., Pretzsch, H., Stojanovic, D., Schuler, L., Peric, S., Rötzer, T., del Rio, M., Dodan, M., Bravo-Oviedo, A.: Modelling approaches for mixed forests dynamics prognosis. Research gaps and opportunities, Forest Syst., 28(1), eR002, 2019.

Bravo-Oviedo A, Pretzsch H, Ammer C, Andenmatten E, Barbati A, Barreiro S, Ponette Q, (…) Zlatanov T (2014). European mixed forests: definition and research perspectives. For. Sys. 23(3): 518-533.

Bréda N, Huc R, Granier A, Dreyer E (2006) Temperate forest trees and stands under severe drought: a review of ecophysiological responses adaptation processes and long-term consequences. Ann. For. Sci. 63(6): 625-644.

Brockerhoff EG, Barbaro L, Castagneyrol B, Forrester DI, Gardiner B, González-Olabarria JR, Jactel H (2017) Forest biodiversity, ecosystem functioning and the provision of ecosystem services. Biodiversity and Conservation 26: 3005–3035

Bücking, W., and Krebs, A.: Interzeption und Bestandesniederschläge von Buche und Fichte im Schönbuch, Das landschaftsökologische Forschungsprojekt Naturpark Schönbuch, 113-131, 1986.

Buckley, T. N.: Modeling stomatal conductance, Plant Physiol., 174(2), 572-582, 2017.

Buras, A., Menzel, A. (2019). Projecting tree species composition changes of European forests for 2061–2090 under RCP 4.5 and RCP 8.5 scenarios. Frontiers in Plant Science, 9, 1986.

Bussotti F, Pollastrini M, Holland V, Brueggemann W (2015) Functional traits and adaptive capacity of European forests to climate change. Environ. Exper. Bot. 111: 91-113.

Bussotti, F., Pollastrini, M.: Observing climate change impacts on European forests: what works and what does not in ongoing long-term monitoring networks. Front. Plant Sci., 8, 629, 2017.

Cailleret M, Jansen S, Robert EM, Desoto L, Aakala T, Antos JA, Martínez-Vilalta J (2017) A synthesis of radial growth patterns preceding tree mortality. Glob. Change Biol. 23(4): 1675-1690.

Caldararu S, Thum T, Yu L, Zaehle S (2020) Whole-plant optimality predicts changes in leaf nitrogen under variable CO 2 and nutrient availability. New Phytol. 225(6): 2331-2346.

Canham CD, LePage PT, Coates KD (2004) A neighborhood analysis of canopy tree competition: effects of shading versus crowding. Can. J. For. Res. 34(4): 778-787.

Cannell M, Thornley J (2000) Modelling the components of plant respiration: some guiding principles. Ann. Bot. 85: 45–54.

Carl C, Biber P, Veste M, Landgraf D, Pretzsch H (2018) Key drivers of competition and growth partitioning among Robinia pseudoacacia L. trees. Forest Ecol. Manag. 430: 86-93.

Carlyle-Moses, D. E., Laureano, J. F., and Price, A. G.: Throughfall and throughfall spatial variability in Madrean oak forest communities of northeastern Mexico, J. Hydrol., 297(1-4), 124-135, 2004.

Carnicer J, Coll M, Ninyerola M, Pons X, Sánchez G, Peñuelas J (2011) Widespread crown condition decline, food web disruption, and amplified tree mortality with increased climate change-type drought. Proceedings of the National Academy of Sciences 108(4): 1474-1478.

Carvalho A, Monteiro A, Flannigan M, Solman S, Miranda AI, Borrego C (2011) Forest fires in a changing climate and their impacts on air quality. Atmospheric Environment 45(31): 5545-5553.

Cepel, N. V.: Interzeption (= Niederschlagsverdunstung im Kronenraum) in einem Buchen-, einem Eichen-und einem Kiefernbestand des Belgrader Waldes bei Istanbul, Forstwiss. Centralbl., 86(5), 301-314, 1967.

Charru, M., Seynave, I., Morneau, F., Bontemps, J. D. (2010). Recent changes in forest productivity: an analysis of national forest inventory data for common beech (Fagus sylvatica L.) in north-eastern France. Forest Ecology and Management, 260(5), 864-874.

Charru M, Seynave I, Morneau F, Rivoire M, Bontemps JD (2012) Significant differences and curvilinearity in the self-thinning relationships of 11 temperate tree species assessed from forest inventory data. Ann. For. Sci. 69(2): 195-205.

Charru M, Seynave I, Hervé JC, Bertrand R, Bontemps JD (2017) Recent growth changes in Western European forests are driven by climate warming and structured across tree species climatic habitats. Annals of Forest Science 74(2): 33.

Chave J (2013) The problem of pattern and scale in ecology: what have we learned in 20 years?. Ecol. Lett. 16: 4-16.

Chiang, J. M., and Brown, K. J.: Improving the budburst phenology subroutine in the forest carbon model PnET, Ecol. Model., 205(3), 515-526, 2007.

Chmielewski FM, Rötzer T (2001) Response of tree phenology to climate change across Europe. Agric. For. Meteorol. 108: 101–112.

Choat, B., Brodribb, T. J., Brodersen, C. R., Duursma, R. A., Lopez, R., Medlyn, B. E.: Triggers of tree mortality under drought, Nature, 558(7711), 531-539, 2018.

Christiansen, J. R., Elberling, B., and Jansson, P. E.: Modelling water balance and nitrate leaching in temperate Norway spruce and beech forests located on the same soil type with the CoupModel, Forest Ecol. Manag., 237(1-3), 545-556, 2006.

Chuine I (2000) A united model for budburst of trees. J Theor Biol, 2007: 337-347.

Chuine I, Garcia de Cortazar Atauri I, Kramer K, Hänninen H (2013) Plant Development Models. In: Phenology: An Integrative Environmental Science (ed. Schwarz MD). Springer, Dordrecht, Netherlands, pp. 275-293.

Chuine I, Bonhomme M, Legave J, García de Cortázar-Atauri I, Charrier G, Lacointe A, Améglio T (2016) Can phenological models predict tree phenology accurately in the future? The unrevealed hurdle of endodormancy break. Glob. Change Biol. 22(10): 3444-3460.

Ciais P, Reichstein M, Viovy N, Granier A, Ogée J, Allard V, Aubinet M, Buchmann N, Bernhofer C, Carrara A, Chevallier F, De Noblet N, Friend AD, Friedlingstein P, Grünwald T, Heinesch B, Keronen P, Knohl A, Krinner G, Loustau D, Manca G, Matteucci G, Miglietta F, Ourcival JM, Papale D, Pilegaard K, Rambal S, Seufert G, Soussana JF, Sanz MJ, Schulze ED, Vesala T, Valentini R (2005) Europe-wide reduction in primary productivity caused by the heat and drought in 2003. Nature 437(7058): 529.

Clark J, Evans FC (1954) Distance to nearest neighbor as a measure of spatial relationships in populations. Ecology 35: 445–453.

Clark J, Salk C, Melillo J, Mohan J (2014) Tree phenology responses to winter chilling, spring warming, at north and south range limits. Funct. Ecol. 28(6): 1344-1355.

Claus A, George E (2005) Effect of stand age on fine-root biomass and biomass distribution in three European forest chronosequences. Can. J. For. Res. 35(7): 1617-1625.

Cole EF, Sheldon BC (2017) The shifting phenological landscape: Within-and between-species variation in leaf emergence in a mixed-deciduous woodland. Ecol. Evol. 7(4): 1135-1147.

Collalti, A., Perugini, L., Santini, M., Chiti, T., Nolè, A., Matteucci, G., Valentini, R.:. A process-based model to simulate growth in forests with complex structure: Evaluation and use of 3D-CMCC Forest Ecosystem Model in a deciduous forest in Central Italy, Ecol. Model., 272, 362-378, 2014.

Collalti, A., Marconi, S., Ibrom, A., Trotta, C., Anav, A., D'andrea, E., Matteuci, G., Montagnani, L., Gielen, B., Mammarella, I., Grünwald, T., Knohl, A., Berninger, F., Zhao, Y., Valentini, R., Santini, M.: Validation of 3D-CMCC Forest Ecosystem Model (v. 5.1) against eddy covariance data for 10 European forest sites, Geosci. Model Dev., 9(2), 479-504, 2016.

Collalti A, Prentice IC (2019) Is NPP proportional to GPP? Waring's hypothesis 20 years on. Tree Physiol. 39(8): 1473-1483.

Collet C, Löf M, Pagès L (2006) Root system development of oak seedlings analysed using an architectural model. Effects of competition with grass. Plant Soil 279(1-2): 367-383.

Cools N, De Vos B (2013) Forest soil: characterization, sampling, physical, and chemical analyses. In Developments in Environmental Science (Vol. 12, pp. 267-300). Elsevier.

Coppola E, Nogherotto R, Ciarlò JM, Giorgi F, van Meijgaard E, Kadygrov N, Wulfmeyer V (2020) Assessment of the European climate projections as simulated by the large EURO-CORDEX regional and global climate model ensemble. J. Geophys. Res. Atmos. e2019JD032356.

Cordonnier T, Kunstler G. 2015 The Gini index brings asymmetric competition to light. Perspect. Plant Ecol. Evol. Syst.17, 1–9.

Coşofreţ C, Bouriaud L (2019). Which silvicultural measures are recommended to adapt forests to climate change? A literature review. Bulletin of the Transilvania University of Brasov. Forestry, Wood Industry, Agricultural Food Engineering. Series II, 12(1), 13-34.

Courbaud B, de Coligny F, Cordonnier T (2003) Simulating radiation distribution in a heterogeneous Norway spruce forest on a slope. Agr. Forest Meteorol. 116:1–18

Couvreur V, Vanderborght J, Javaux M (2012) A simple three-dimensional macroscopic root water uptake model based on the hydraulic architecture approach. Hydrol. Earth Syst. Sci. 16: 2957–2971

Crabbe RA, Dash J, Rodriguez-Galiano VF, Janous D, Pavelka M, Marek MV (2016) Extreme warm temperatures alter forest phenology and productivity in Europe. Science of the Total Environment 563: 486-495.

Cramer W, Bondeau A, Woodward FI, Prentice IC, Betts RA, Brovkin V, Cox PM, Fisher V, Foley JA, Friend AD, Kucharik C, Lomas MR, Ramankutty N, Sitch S, Smith B, White A, Young-Molling C (2001). Global response of terrestrial ecosystem structure and function to CO2 and climate change: results from six dynamic global vegetation models. Glob. Change Biol. 7(4): 357-373.

Cristiano, E., Bogaard, T., Barontini, S.: Effects of Anisotropy of Preferential flow on the Hydrology and Stability of Landslides, Procedia Earth Planet. Sci., 16, 204-214, 2016.

Crow P (2005) The Influence of Soils and Species on Tree Root Depth: Information Note. Forestry Commission.

D'Orangeville L, Houle D, Duchesne L, Phillips RP, Bergeron Y, Kneeshaw D (2018) Beneficial effects of climate warming on boreal tree growth may be transitory. Nat. Commun. 9(1): 3213.

Dai, A.: Increasing drought under global warming in observations and models. Nat. Clim. Change, 3(1), 52, 2013.

D'Amato, A. W., Bradford, J. B., Fraver, S., & Palik, B. J. (2013). Effects of thinning on drought vulnerability and climate response in north temperate forest ecosystems. Ecological Applications, 23(8), 1735-1742.

Dănescu A, Albrecht AT, Bauhus J (2016) Structural diversity promotes productivity of mixed, uneven-aged forests in southwestern Germany. Oecologia 182: 319–333

Daniel TC, Muhar A, Arnberger A, Aznar O, Boyd JW, Chan KM, von der Dunk A (2012) Contributions of cultural services to the ecosystem services agenda. PNAS 109(23): 8812-8819.

Davi H, Dufrêne E, Francois C, Le Maire G, Loustau D, Bosc A, Sambal S, Granier A, Moors E (2006) Sensitivity of water and carbon fluxes to climate changes from 1960 to 2100 in European forest ecosystems. Agric. For. Meteorol. 141(1): 35-56.

De Beurs KM, Henebry GM (2005) Land surface phenology and temperature variation in the International Geosphere-Biosphere Program high-latitude transects. Glob. Change Biol. 11: 779–790.

De Frenne P, Zellweger F, Rodriguez-Sanchez F, Scheffers BR, Hylander K, Luoto M, Lenoir J (2019) Global buffering of temperatures under forest canopies. Nat. Ecol. Evol. 3(5): 744-749.

De Meue G (2020) Modélisation de la production primaire brute et de l'évapotranspiration dans une forêt de hêtre et de douglas et simulations selon différents scénarios climatiques. Université catholique de Louvain.

De Rigo D, Houston Durrant T, Caudullo G, Barredo JI (2016) European forests: an ecological overview. In: San-Miguel-Ayanz, J., de Rigo, D., Caudullo, G., Houston Durrant, T., Mauri, A. (Eds.), European Atlas of Forest Tree Species. Publ. Off. EU, Luxembourg, pp. e01e873+

de Wergifosse L, André F, Beudez N, de Coligny F, Goosse H, Jonard F, Ponette Q, Titeux H, Vincke C, Jonard M (2020a) HETEROFOR 1.0: a spatially explicit model for exploring the response of structurally complex forests to uncertain future conditions. II. Phenology and water cycle. Geosci. Model Dev. 13:1459–1498

de Wergifosse L, André F, Goosse H, Caluwaerts S, de Cruz L, de Troch R, van Schaeybroeck B and Jonard M (2020b) CO2 fertilization, transpiration deficit and vegetation period drive the response of mixed broadleaved forests to a changing climate in Wallonia. Ann. For. Sci. 77(3): 1-23.

Deckmyn, G., Verbeeck, H., De Beeck, M. O., Vansteenkiste, D., Steppe, K., and Ceulemans, R.: ANAFORE: a stand-scale process-based forest model that includes wood tissue development and labile carbon storage in trees, Ecol. Model., 215(4), 345-368, 2008.

Del Río M, Condés S, Pretzsch H (2014) Analyzing size-symmetric vs. size-asymmetric and intra-vs. inter-specific competition in beech (Fagus sylvatica L.) mixed stands. For. Ecol. Manag. 325: 90-98.

Del Río M, Pretzsch H, Alberdi I, Bielak K, Bravo F, Brunner A, Bravo-Oviedo A (2016) Characterization of the structure, dynamics, and productivity of mixed-species stands: review and perspectives. Eur. J. For. Res. 135(1): 23-49.

Deleuze C, Morneau F, Renaud JP, Vivien Y, Rivoire M, Santenoise P, Longuetaud F, Mothe F, Hervé JC, Vallet P (2014a) Estimer le volume total d'un arbre, quelles que soient l'essence, la taille, la sylviculture, la station. Rendez-vous techniques ONF 44: 22-32.

Deleuze C, Morneau F, Renaud JP, Vivien Y, Rivoire M, Santenoise P, Longuetaud F, Mothe F, Hervé JC, Vallet P (2014b) Estimation harmonisée du volume de tige à différentes découpes. Rendez-vous techniques ONF 44: 22-32.

Delpierre N, Dufrêne E, Soudani K, Ulrich E, Cecchini S, Boé J, François C (2009) Modelling interannual and spatial variability of leaf senescence for three deciduous tree species in France. Agric. For. Meteorol. 149(6-7): 938-948.

Delpierre N, Guillemot J, Dufrêne E, Cecchini S, Nicolas M (2017) Tree phenological ranks repeat from year to year and correlate with growth in temperate deciduous forests. Agric. For. Meteorol. 234: 1-10.

Del Río M, Pretzsch H, Alberdi I, Bielak K, Bravo F, Brunner A, Bravo-Oviedo A (2015) Characterization of the structure, dynamics, and productivity of mixed-species stands: review and perspectives. Eur. J. For. Res. 135(1): 23-49.

DeLucia EH, Drake JE, Thomas RB, Gonzalez-Meler M (2007) Forest carbon use efficiency: is respiration a constant fraction of gross primary production?. Glob. Chang. Biol. 13(6): 1157-1167.

Delzon S, Urli M, Samalens JC, Lamy JB, Lischke H, Sin F, Porté AJ (2013) Field evidence of colonisation by Holm oak, at the northern margin of its distribution range, during the Anthropocene period. PloS one 8(11): e80443.

DeRose RJ, Long JN (2014) Resistance and resilience: A conceptual framework for silviculture. For. Sci. 60(6): 1205-1212.

Dettmann, U., Bechtold, M., Frahm, E., and Tiemeyer, B.: On the applicability of unimodal and bimodal van Genuchten–Mualem based models to peat and other organic soils under evaporation conditions, J. Hydrol., 515, 103-115, 2014.

Dhôte JF, De Hercé E (1994) Un modèle hyperbolique pour l'ajustement de faisceaux de courbes hauteur–diamètre. Can. J. For. Res. 24(9): 1782-1790.

Didon-Lescot, J. F.: The Importance Of Throughfall in Evaluating Hydrological and Biogeochemical Fluxes: Example of a Catchment (Mont-Lozere, France), in: Proceedings of the International Conference on Catchment Hydrological and Biochemical Processes in Changing Environment (20-23), 1998.

Dobbertin M (2005) Tree growth as indicator of tree vitality and of tree reaction to environmental stress: a review. Eur. J. For. Res. 124(4): 319-333.

Dobrowski SZ, Abatzoglou J, Swanson AK, Greenberg JA, Mynsberge AR, Holden ZA, Schwartz MK (2013) The climate velocity of the contiguous United States during the 20th century. Glob. Change Biol. 19(1): 241-251.

Domec, J. C., King, J. S., Noormets, A., Treasure, E., Gavazzi, M. J., Sun, G., & McNulty, S. G. (2010). Hydraulic redistribution of soil water by roots affects whole-stand evapotranspiration and net ecosystem carbon exchange. New Phytologist, 187(1), 171-183.

Dong B, Sutton RT, Woollings T, Hodges K (2013) Variability of the North Atlantic summer storm track: Mechanisms and impacts on European climate. Environ. Res. Lett. 8(3): 034037.

Dragoni D, Schmid HP, Wayson CA, Potter H, Grimmond CSB, Randolph JC (2011) Evidence of increased net ecosystem productivity associated with a longer vegetated season in a deciduous forest in south-central Indiana, USA. Global Change Biol. 17(2): 886-897.

Dripps, W.R.: The spatial and temporal variability of groundwater recharge within the Trout Lake basin of northern Wisconsin, PhD Thesis, University of Wisconsin, 2003.

Dufour-Kowalski S, Courbaud B, Dreyfus P, Meredieu C, De Coligny F (2012) Capsis: an open software framework and community for forest growth modelling. Ann. For. Sci. 69:221–233

Dufrêne E, Davi H, François C, Le Maire G, Le Dantec V, Granier A (2005) Modelling carbon and water cycles in a beech forest: Part I: Model description and uncertainty analysis on modelled NEE, Ecol. Model. 185: 407–436.

Dulamsuren C, Hauck M, Kopp G, Ruff M, Leuschner C (2017) European beech responds to climate change with growth decline at lower, and growth increase at higher elevations in the center of its distribution range (SW Germany). Trees 31(2): 673-686.

Dupire S, Curt T, Bigot S (2017) Spatio-temporal trends in fire weather in the French Alps. Sci. Total Environ. 595: 801-817.

Duputié A, Rutschmann A, Ronce O, Chuine I (2015) Phenological plasticity will not help all species adapt to climate change. Global Change Biology 21(8): 3062-3073.

Duursma RA (2008) MAESPA: Development of a soil-plant-atmosphere model, Seminar at the UWS, available at: https://github.com/Maespa/maespa.github.io/blob/master/docs/MAESPAseminar.pdf (last access: 13 September 2018)

Duursma RA, Medlyn BE (2012) MAESPA: a model to study interactions between water limitation, environmental drivers and vegetation function at tree and stand levels, with an example application to [CO2] × drought interactions. Geosci. Model Dev. 5: 919–940.

Dyderski MK, Paź S, Frelich LE, Jagodziński AM (2018) How much does climate change threaten European forest tree species distributions?. Glob. Change Biol. 24(3): 1150-1163.

Edwards, K. J., Fyfe, R. M., and Jackson, S. T. (2017). The first 100 years of pollen analysis. Nature Plants, 3(2), 1-4.

Elkin C, Giuggiola A, Rigling A, Bugmann H (2015) Short-and long-term efficacy of forest thinning to mitigate drought impacts in mountain forests in the European Alps. Ecol. Applic. 25(4): 1083-1098.

Erbs DG, Klein SA, Duffie JA (1982) Estimation of the diffuse radiation fraction for hourly, daily and monthly-average global radiation. Solar Energy 28(4): 293–302

Ercanli İ (2018) Positive effect of forest structural diversity on aboveground stand carbon stocks for even-aged Scots pine (Pinus sylvestris L.) stands in the Sarıçiçek Forest, Northern Turkey. Scand. J. For. Res. 33(5): 455-463.

Etzold S, Ziemińska K, Rohner B, Bottero A, Bose AK, Ruehr NK, Rigling A (2019) One century of forest monitoring data in Switzerland reveals species-and site-specific trends of climate-induced tree mortality. Front. Plant Sci. 10: 307.

Europe, F., & Unece, F. A. O. (2015). State of Europe’s forests 2015.

Falster DS, Duursma RA, Ishihara MI, Barneche DR, FitzJohn RG, Vårhammar A, (89 more authors) York RA (2015) BAAD: a Biomass And Allometry Database for woody plants. Ecology 96(5): 1445.

FAO (2012a) Global ecological zones for FAO forest reporting: 2010 Update. FAO: Rome, Italy.

FAO (2012b) FRA 2015: Terms and Definitions.

FAO (2015) State of Europe’s forests 2015. FAO: Rome, Italy.

FAO (2020) State of Europe’s forests 2020. FAO: Rome, Italy.

Farquhar GD, von Caemmerer S, Berry JA (1980) A biochemical model of photosynthetic CO2 assimilation in leaves of C3 species. Planta 149: 78–80.

Fatichi, S., Pappas, C., and Ivanov, V. Y.: Modeling plant–water interactions: an ecohydrological overview from the cell to the global scale, Wires Water, 3(3), 327-368, 2016.

Fellner H, Dirnberger GF, Sterba H (2016) Specific leaf area of european larch (larix decidua mill.). Trees 30(4):1237–1244.

Fernandez-Carrillo, A., Patočka, Z., Dobrovolný, L., Franco-Nieto, A., & Revilla-Romero, B. (2020). Monitoring bark beetle forest damage in Central Europe. A remote sensing approach validated with field data. Remote Sensing, 12(21), 3634.

Fernandez-Martinez M, Vicca S, Janssens IA et al. (2014) Nutrient availability as the key regulator of global forest carbon balance. Nature Climate Change, 4, 471–476.

Fernández-Martínez M, Vicca S, Janssens IA, Luyssaert S, Campioli M, Sardans J, Estiarte M, Peñuelas J (2014). Spatial variability and controls over biomass stocks, carbon fluxes, and resource-use efficiencies across forest ecosystems. Trees 28(2): 597-611.

Fernández-Martínez M, Vicca S, Janssens IA, Ciais P, Obersteiner M, Bartrons M, Peñuelas J (2017) Atmospheric deposition, CO 2, and change in the land carbon sink. Sci. Reports 7(1): 1-13.

Ferretti M, Fischer R (2013) Forest monitoring: methods for terrestrial investigations in Europe with an overview of North America and Asia. Elsevier, Oxford, United Kingdom.

Flynn DFB, Wolkovich EM (2018) Temperature and photoperiod drive spring phenology across all species in a temperate forest community. New Phytol. 219(4): 1353-1362.

Forgeard, F., Gloaguen, J. C., and Touffet, J.: Interception des précipitations et apport au sol d'éléments minéraux par les eaux de pluie et les pluviolessivats dans une hêtraie atlantique et dans quelques peuplements résineux en Bretagne, Ann. Sci. Forest., 37(1), 53-71, 1980.

Forrester DI, Bauhus J (2016) A review of processes behind diversity—productivity relationships in forests. Current For. Rep. 2(1): 45-61.

Forrester DI, Tachauer IHH, Annighoefer P, Barbeito I, Pretzsch H, Ruiz-Peinado R, Stark H, Vacchiano G, Zlatanov T, Chakraborty T, Saha S, Sileshi GW (2017) Generalized biomass and leaf area allometric equations for European tree species incorporating stand structure, tree age and climate. For. Ecol. Manag. 396: 160-175.

FRA, F., Rome, I. (2010). global forest Resources assessment 2010. FAO forestry paper, 163.

Franklin JF, Shugart HH, Harmon ME (1987) Tree death as an ecological process. BioSci. 37(8): 550-556.

Franks, S. J., Weber, J. J., & Aitken, S. N. (2014). Evolutionary and plastic responses to climate change in terrestrial plant populations. Evolutionary Applications, 7(1), 123-139.

Friedlingstein P, O'Sullivan M, Jones MW, Andrew RM, Hauck J, Olsen A, Zaehle S (2020) Global carbon budget 2020. Earth System Science Data, 12(4), 3269-3340.

Friedman, S. P., Jones, S. B.: Measurement and approximate critical path analysis of the pore-scale-induced anisotropy factor of an unsaturated porous medium, Water Resour. Res., 37(12), 2929-2942, 2001.

Friend, A. D., Stevens, A. K., Knox, R. G., and Cannell, M. G. R.: A process-based, terrestrial biosphere model of ecosystem dynamics (Hybrid v3. 0), Ecol. Model., 95(2-3), 249-287, 1997.

Froese RE, Robinson AP (2007) A validation and evaluation of the Prognosis individual-tree basal area increment model. Can. J. For. Res. 37(8): 1438-1449.

Fu YS, Campioli M, Vitasse Y, De Boeck HJ, Van den Berge J, AbdElgawad H, Janssens IA (2014) Variation in leaf flushing date influences autumnal senescence and next year’s flushing date in two temperate tree species. PNAS 111(20): 7355-7360.

Fu YS, Zhang H, Dong W, Yuan W (2014a) Comparison of phenology models for predicting the onset of growing season over the Northern Hemisphere. PloS one 9(10): e109544.

Fu YS, Piao S, Zhao H, Jeong SJ, Wang X, Vitasse Y, Janssens IA (2014b) Unexpected role of winter precipitation in determining heat requirement for spring vegetation green-up at northern middle and high latitudes. Glob. Change Biol. 20(12): 3743-3755.

Fu Z, Stoy PC, Luo Y, Chen J, Sun J, Montagnani L, Wohlfahrt G, Rahman AF, Rambal S, Bernhofer C, Wang J, Shirkey G, Niu S (2017) Climate controls over the net carbon uptake period and amplitude of net ecosystem production in temperate and boreal ecosystems. Agr. Forest Meteorol. 243: 9-18.

Fuhrer J, Beniston M, Fischlin A, Frei C, Goyette S, Jasper K, Pfister C (2006) Climate risks and their impact on agriculture and forests in Switzerland. Clim. Change 79: 79-102.

Gauzere J, Delzon S, Davi H, Bonhomme M, de Cortazar-Atauri IG, Chuine I (2017) Integrating interactive effects of chilling and photoperiod in phenological process-based models. A case study with two European tree species: Fagus sylvatica and Quercus petraea. Agric. For. Meteorol. 244: 9-20.

Gazol A, Ibáñez R (2010) Scale-specific determinants of a mixed beech and oak seedling–sapling bank under different environmental and biotic conditions. Plant Ecol. 211(1): 37-48.

Gebauer, T., Horna, V., and Leuschner, C.: Canopy transpiration of pure and mixed forest stands with variable abundance of European beech, J. Hydrol., 442, 2-14, 2012.

Gehrig-Fasel J, Guisan A, Zimmermann NE (2007) Tree line shifts in the Swiss Alps: climate change or land abandonment?. J. Veg. Sci. 18(4): 571-582.

Genet A, Wernsdörfer H, Jonard M, Pretzsch H, Rauch M, Ponette Q, Nys C, Legout A, Ranger J, Vallet P, Saint-André L (2011) Ontogeny partly explains the apparent heterogeneity of published biomass equations for Fagus sylvatica in central Europe. For. Ecol. Manag. 261: 1188-1202.

Gerke, H.: Untersuchungen zum Wasserhaushalt eines Kalkbuchenwald-Ökosystems und zur Wasserbewegung in flachgründigen Böden und im durchwurzelten Kalkgestein als Grundlage zur Modellentwicklung, Forschungszentrum Waldökosysteme, Waldsterben, 1987.

Giacomin, A., and Trucchi, P.: Rainfall interception in a beech coppice (Acquerino, Italy), J. Hydrol., 137(1-4), 141-147, 1992.

Gifford RM (1995) Whole plant respiration and photosynthesis of wheat under increased CO2 concentration and temperature: longterm vs. short-term distinctions for modelling. Glob. Chang. Biol. 1: 385–396.

Gifford RM (2003) Plant respiration in productivity models: conceptualisation, representation and issues for global terrestrial carbon-cycle research. Functi. Plant Biol. 30(2): 171-186.

Gill, D. S., Amthor, J. S., Bormann, F. H.: Leaf phenology, photosynthesis, and the persistence of saplings and shrubs in a mature northern hardwood forest, Tree Physiol., 18(5), 281-289, 1998.

Giorgi F, Jones C, Asrar GR (2009) Addressing climate information needs at the regional level: the CORDEX framework. World Meteorological Organization Bulletin 58(3): 175.

Giot O, Termonia P, Degrauwe D, De Troch R, Caluwaerts S, Smet G, Berckmans J, Deckmyn A, De Cruz L, De Meutter P, Duerinckx A, Gerard L, Hamdi R, Van den Bergh J, Van Ginderachter M, Van Schaeybroeck B (2016) Validation of the ALARO-0 model within the EURO-CORDEX framework. Geosci. Model Dev. 9(3):1143–1152

Goberville E, Beaugrand G, Hautekèete NC, Piquot Y, Luczak C (2015) Uncertainties in the projection of species distributions related to general circulation models. Ecol. Evol. 5(5): 1100-1116.

Goldblum D (2010) The geography of white oak's (Quercus alba L.) response to climatic variables in North America and speculation on its sensitivity to climate change across its range. Dendrochronologia 28(2): 73-83.

Granier A (1985) A new method of sap flow measurement in tree stems. Ann. Sci.For. 42 (2): 193–200.

Granier, A., and Bréda, N.: Modelling canopy conductance and stand transpiration of an oak forest from sap flow measurements, in: Ann. Sci. Forest., 53(1-2), 537-546, 1996.

Granier, A., Biron, P., and Lemoine, D.: Water balance, transpiration and canopy conductance in two beech stands, Agric. For. Meteorol., 100(4), 291-308, 2000.

Granier A, Reichstein M, Bréda N, Janssens IA, Falge E, Ciais P, Grünwald T, Aubinet M, Berbigier P, Bernhofer C, Buchmann N, Facini O, Grassi G, Heinesch B, Ilvesniemi H, Keronen P, Knohl A, Köstner B, Lagergren F, Lindroth A, Longdoz B, Loustau D, Mateus J, Montagnani L, Nys C, Moors E, Papale D, Peiffer M, Pilegaard K, Pita G, Pumpanen P, Rambal S, Rebmann C, Rodrigues A, Seufert G, Tenhunen J, Vesala T, Wang Q (2007) Evidence for soil water control on carbon and water dynamics in European forests during the extremely dry year: 2003. Agr. Forest Meteorol. 143(1-2): 123-145.

Greenwood S, Ruiz-Benito P, Martínez-Vilalta J, Lloret F, Kitzberger T, Allen CD, Jump AS (2017) Tree mortality across biomes is promoted by drought intensity, lower wood density and higher specific leaf area. Ecology Letters 20(4): 539-553.

Gregow H, Laaksonen A, Alper ME (2017) Increasing large scale windstorm damage in Western, Central and Northern European forests, 1951-2010. Sci. Reports 7.

Gressler, E., Jochner, S., Capdevielle-Vargas, R. M., Morellato, L. P. C., Menzel, A.: Vertical variation in autumn leaf phenology of Fagus sylvatica L. in southern Germany, Agr. Forest Meteorol., 201, 176-186, 2015.

Grismer, M. E., Bachman, S., and Powers, T.: A comparison of groundwater recharge estimation methods in a semi-arid, coastal avocado and citrus orchard (Ventura County, California), Hydrol. Process., 14(14), 2527-2543, 2000.

Grossiord, C., Granier, A., Ratcliffe, S., Bouriaud, O., Bruelheide, H., Chećko, E., Forrester, D. I., Muhie Dawud S., Finer, L., Pollastrini, M., Scherer-Lorenzen, M., Valladares, F., Bonal, D., Gessler, A.: Tree diversity does not always improve resistance of forest ecosystems to drought, Proc. Natl. Acad. Sci., 111(41), 14812-14815, 2014.

Grossiord, C.: Having the right neighbors: how tree species diversity modulates drought impacts on forests, New Phytol., 2018.

Grossiord C (2019) Having the right neighbors: how tree species diversity modulates drought impacts on forests. New Phytol. doi.org/10.1111/nph.15667.

Grote R, Pretzsch H (2002) A model for individual tree development based on physiological processes. Plant Biol. 4: 167–180.

Grote, R., Korhonen, J., Mammarella, I.: Challenges for evaluating process-based models of gas exchange at forest sites with fetches of various species. Forest Syst., 20(3), 389-406, 2011.

Grote R, Gessler A, Hommel R, Poschenrieder W, Priesack E (2016) Importance of tree height and social position for drought-related stress on tree growth and mortality. Trees 30(5): 1467-1482.

Gugger PF, Sugita S, Cavender-Bares J (2010) Phylogeography of Douglas-fir based on mitochondrial and chloroplast DNA sequences: testing hypotheses from the fossil record. Mol. Ecol. 19(9): 1877-1897.

Guillemot J, Klein EK, Davi H, Courbet F (2015) The effects of thinning intensity and tree size on the growth response to annual climate in Cedrus atlantica: a linear mixed modeling approach. Ann. For. Sci. 72(5): 651-663.

Gutowski WJ, Decker SG, Donavon RA, Pan Z, Arritt RW, Takle ES (2003) Temporal–spatial scales of observed and simulated precipitation in central US climate. J. Clim. 16(22): 3841-3847.

Gutsch, M., Lasch-Born, P., Suckow, F., and Reyer, C.: Modeling of two different water uptake approaches for mono-and mixed-species forest stands, Forests, 6(6), 2125-2147, 2015.

Gutsch M, Lasch-Born P, Suckow F, Reyer CP (2016) Evaluating the productivity of four main tree species in Germany under climate change with static reduced models. Ann. For. Sci. 73(2): 401-410.

Haines-Young, R., and Potschin, M. B. (2018). Common international classification of ecosystem services (CICES) V5. 1 and guidance on the application of the revised structure. Nottingham, UK: Fabis Consulting Ltd.[Google Scholar].

Hänninen, H.: Modelling bud dormancy release in trees from cool and temperate regions. Acta For. Fenn., 213, 1-47, 1990.

Hänninen H (2016) The Annual Cycle Under Changing Climatic Conditions. In Boreal and Temperate Trees in a Changing Climate (pp. 263-335). Springer, Dordrecht.

Hanson, P. J., Amthor, J. S., Wullschleger, S. D., Wilson, K. B., Grant, R. F., Hartley, A., Hui, D., Hunt, R., Johnson, D., and Kimball, J.: Oak forest carbon and water simulations: model intercomparisons and evaluations against independent data, Ecol. Monogr., 74(3), 443-489, 2004.

Hardie, M. A., Cotching, W. E., Doyle, R. B., Holz, G., Lisson, S., and Mattern, K.: Effect of antecedent soil moisture on preferential flow in a texture-contrast soil, J. Hydrol., 398(3-4), 191-201, 2011.

Härdtle W, Niemeyer T, Assmann T, Aulinger A, Fichtner A, Lang A, von Oheimb G (2013) Climatic responses of tree-ring width and δ 13 C signatures of sessile oak (Quercus petraea Liebl.) on soils with contrasting water supply. Plant Ecol. 214(9): 1147-1156.

Hartmann H, Moura CF, Anderegg WR, Ruehr NK, Salmon Y, Allen CD, Arndt SK, Breshears DD, Davi H, Galbraith D, Ruthrof KX, Wunder J, Adams HD, Bloemen J, Cailleret M, Cobb R, Gessler A, Grams T, Jansen S, Kautz M, Lloret F, O'Brien M (2018). Research frontiers for improving our understanding of drought-induced tree and forest mortality. New Phytol. 218(1): 15-28.

Hassan, R., Scholes, R., and Ash, N. (2005). Ecosystems and human well-being: current state and trends.

Hastings WK (1970) Monte Carlo sampling methods using Markov chains and their applications.

Haylock MR, Hofstra N, Klein Tank AMG, Klok EJ, Jones PD, New M (2008) A European daily high-resolution gridded data set of surface temperature and precipitation for 1950–2006. J. Geophys. Res. Atmospheres 113(D20).

Heil, K.: Wasserhaushalt und Stoffumsatz in Fichten-(Picea abies (L.) Karst.) und Buchenökosystemen (Fagus sylvatica L.) der höheren Lagen des Bayer, Waldes, 1996.

Herbst, M., Eschenbach, C., and Kappen, L.: Water use in neighbouring stands of beech (Fagus sylvatica L.) and black alder (Alnus glutinosa (L.) Gaertn.), Ann. For. Sci., 56(2), 107-120, 1999.

Herbst, M., Rosier, P. T., Morecroft, M. D., and Gowing, D. J.: Comparative measurements of transpiration and canopy conductance in two mixed deciduous woodlands differing in structure and species composition, Tree Physiol., 28(6), 959-970, 2008.

Herr, A., Dambacher, J. M., Pinkard, E., Glen, M., Mohammed, C., and Wardlaw, T.: The uncertain impact of climate change on forest ecosystems–How qualitative modelling can guide future research for quantitative model development, Environ. Model. Softw., 76, 95-107, 2016.

Hersbach H, Bell B, Berrisford P, Hirahara S, Horányi A, Muñoz-Sabater J, Nicolas J, Peubey C, Radu R, Schepers D, Simmons A, Soci C, Abdalla S, Abellan X, Balsamo G, Bechtold P, Biavati G, Bidlot J, Bonavita M, De Chiara G, Dahlgren P, Dee D, Diamantakis M, Dragani R, Flemming J, Forbes R, Fuentes M, Geer A, Haimberger L, Healy S, Hogan RJ, Hólm E, Janisková M, Keeley S, Laloyaux P, Lopez P, Lupu C, Radnoti G, de Rosnay P, Rozum I, Vamborg F, Villaume S, Thépaut J-N (2020) The ERA5 global reanalysis. Q. J. R. Meteorol. Soc. 146(730): 1999-2049.

Heskel MA, O'Sullivan OS, Reich PB, Tjoelker MG, Weerasinghe LK, Penillard A, Atkin OK (2016) Convergence in the temperature response of leaf respiration across biomes and plant functional types. PNAS 113(14): 3832-3837.

Holdridge LR (1967) Life zone ecology. Tropical Science Center, San Jose, Costa Rica.

Hörmann, G., Branding, A., Clemen, T., Herbst, M., Hinrichs, A., and Thamm, F.: Calculation and simulation of wind controlled canopy interception of a beech forest in Northern Germany, Agric. For. Meteorol., 79(3), 131-148, 1996.

Hounzandji AP, Jonard M, Nys C, Saint-André L, Ponette Q (2015) Improving the robustness of biomass functions: from empirical to functional approaches. Ann. For. Sci. 72: 795-810.

Huntzinger DN, Michalak AM, Schwalm C, Ciais P, King AW, Fang Y, Schaefer K, Wei Y, Cook RB, Fisher JB, Hayes D, Huang M, Ito A, Jain AK, Lei H, Lu C, Maignan F, Mao J, Parazoo N, Peng S, Poulter B, Ricciuto D, Shi X, Tian H, Wang W, Zeng N, Zhao F (2017). Uncertainty in the response of terrestrial carbon sink to environmental drivers undermines carbon-climate feedback predictions. Sci. Rep. 7(1): 1-8.

IPCC (2013) Summary for Policymakers. In: Stocker TF, Qin D, Plattner GK, Tignor M, Allen SK, Boschung J, Nauels A, Xia Y, Bex V, Midgley PM (eds) Climate Change 2013: The Physical Science Basis. Contribution of Working Group I to the Fifth Assessment Report of the Intergovernmental Panel on Climate Change, Cambridge University Press, Cambridge, pp. 3-29.

Jacob D, Petersen J, Eggert B, et al. (36 more authors) (2014). EURO-CORDEX: new high-resolution climate change projections for European impact research. Reg. Environ. Change 14(2): 563-578.

Jacob D, Kotova L, Teichmann C, Sobolowski SP, Vautard R, Donnelly C, Koutroulis AG, Grillakis MG, Tsanis IK, Damm A, Sakalli A, van Vliet M (2018) Climate impacts in Europe under +1.5°C global warming. Earths Future 6(2):264–285

Jacovides CP, Boland J, Asimakopoulos DN, Kaltsounides NA (2010) Comparing diffuse radiation models with one predictor for partitioning incident par radiation into its dif- fuse component in the eastern mediterranean basin. Renewable Energy 35(8): 1820–1827

Jactel H, Bauhus J, Boberg J, Bonal D, Castagneyrol B, Gardiner B, Brockerhoff EG (2017) Tree diversity drives forest stand resistance to natural disturbances. Cur. For. Rep. 3(3): 223-243.

Jactel H, Moreira X, Castagneyrol B (2021) Tree Diversity and Forest Resistance to Insect Pests: Patterns, Mechanisms, and Prospects. Ann. Review Entomol. 66: 277-296.

Jeong SJ, HO CH, GIM HJ, Brown ME (2011) Phenology shifts at start vs. end of growing season in temperate vegetation over the Northern Hemisphere for the period 1982–2008. Global Change Biol. 17(7): 2385-2399.

Jetten, V. G.: Interception of tropical rain forest: performance of a canopy water balance model, Hydrol. Process., 10(5), 671-685, 1996.

JMP®, Version 15. SAS Institute Inc., Cary, NC, 1989-2019.

Johnson WC, Webb III T (1989) The role of blue jays (Cyanocitta cristata L.) in the postglacial dispersal of fagaceous trees in eastern North America. J. Biogeogr. 561-571.

Johnson GL, Hanson CL (1995) Topographic and atmospheric influences on precipitation variability over a mountainous watershed. J. Appl. Meteorol. 34(1): 68-87.

Jolly, W. M., Nemani, R., Running, S. W.: Enhancement of understory productivity by asynchronous phenology with overstory competitors in a temperate deciduous forest, Tree Physiol., 24(9), 1069-1071, 2004.

Jonard M, Andre F, Ponette Q (2006) Modeling leaf dispersal in mixed hardwood forests using a ballistic approach. Ecology 87(9): 2306-2318.

Jonard M, André F, Jonard F, Mouton N, Procès P, Ponette Q (2007) Soil carbon dioxide efflux in pure and mixed stands of oak and beech. Ann. For. Sci. 64(2): 141-150.

Jonard M, André F, Ponette Q (2008) Tree species mediated effects on leaf litter dynamics in pure and mixed stands of oak and beech. Can. J. For. Res. 38(3): 528-538.

Jonard F, André F, Ponette Q, Vincke C, Jonard M (2011) Sap flux density and stomatal conductance of European beech and common oak trees in pure and mixed stands during the summer drought of 2003. J. Hydrol. 409(1-2): 371-381.

Jonard M, Fürst A, Verstraeten A, Thimonier A, Timmermann V, Potočić N, Waldner P, Benham S, Hansen K, Merilä P, Ponette Q, de la Cruz AC, Roskams P, Nicolas M, Croisé L, Ingerslev M, Matteucci G, Decinti B, Bascietto M, Rautio P (2015) Tree mineral nutrition is deteriorating in Europe. Global Change Biol. 21(1): 418-430.

Jonard M, André F, de Coligny F, de Wergifosse L, Beudez N, Davi H, Ligot G, Ponette Q, Vincke C (2020) HETEROFOR 1.0: a spatially explicit model for exploring the response of structurally complex forests to uncertain future conditions. I. Carbon fluxes and tree dimensional growth. Geosci. Model Dev 13:905–935

Jump AS, Hunt JM, Penuelas J (2006) Rapid climate change-related growth decline at the southern range edge of Fagus sylvatica. Glob. Change Biol. 12(11): 2163-2174.

Kaplan JO, Krumhardt KM, Zimmermann NE (2009). The prehistoric and preindustrial deforestation of Europe. Quaternary Science Reviews, 28(27-28), 3016-3034.

Kaplan JO, Krumhardt KM, Zimmermann NE (2012) The effects of land use and climate change on the carbon cycle of Europe over the past 500 years. Glob. Change Biol. 18: 902–914,

Karl TR, Arguez A, Huang B, Lawrimore JH, McMahon JR, Menne MJ, Zhang HM (2015) Possible artifacts of data biases in the recent global surface warming hiatus. Science 348(6242): 1469-1472.

Keenan TF, Gray J, Friedl MA, Toomey M, Bohrer G, Hollinger DY, Richardson AD (2014) Net carbon uptake has increased through warming-induced changes in temperate forest phenology. Nat. Clim. Change 4(7): 598-604.

Keenan TF, Richardson AD (2015) The timing of autumn senescence is affected by the timing of spring phenology: implications for predictive models. Glob. Change Biol. 21(7): 2634-2641.

Kiernan DH, Bevilacqua E, Nyland R (2008) Individual tree diameter growth model for sugar maple trees in uneven-aged northern hardwood stands under selection system. For. Ecol. Manag. 256(9): 1579-1586.

Kint V, Aertsen W, Campioli M, Vansteenkiste D, Delcloo A, Muys B (2012) Radial growth change of temperate tree species in response to altered regional climate and air quality in the period 1901–2008. Clim. Change, 115(2): 343-363.

Kjellström E, Nikulin G, Strandberg G, Christensen OB, Jacob D, Keuler K, Vautard R (2018) European climate change at global mean temperature increases of 1.5 and 2 C above pre-industrial conditions as simulated by the EURO-CORDEX regional climate models. Earth Sys. Dyn. 9(2): 459-478.

Klein T (2014) The variability of stomatal sensitivity to leaf water potential across tree species indicates a continuum between isohydric and anisohydric behaviours. Funct. Ecol. 28(6): 1313-1320.

Klesse S, DeRose RJ, Babst F, Black BA, Anderegg LD, Axelson J, Ettinger A, Griesbauer H, Guiterman CH, Harley G, Harvey JE, Lo YH, Lynch AM, O'Connor C, Restaino C, Sauchyn D, Shaw JD, Smith DJ, Wood L, Villanueva-Díaz J, Evans ME (2020) Continental-scale tree-ring-based projection of Douglas-fir growth: Testing the limits of space-for-time substitution. Glob. Change Biol. 26(9): 5146-5163.

Knoche, D., Embacher, A., and Katzur, J.: Water and element fluxes of red oak ecosystems during stand development on post-mining sites (Lusatian Lignite District), Water Air Soil Poll., 141(1-4), 219-231, 2002.

Köhl M, Dominguez Torres G, Marchetti M, Tomé M, Martinez de Arano, Corona P, Jellesmark Thorsen B, Lasserre B, Pettenella D, Zasada M, Zingg A, Weiss G (2015). Maintenance and encouragement of productive functions of forests (wood and non-wood). State of Europe's forests 2015.

Kolář T, Giagli K, Trnka M, Bednářová E, Vavrčík H, Rybníček M (2016) Response of the leaf phenology and tree-ring width of European beech to climate variability. Silva Fennica 50(2): 1520.

Kölling C (2007) Klimahüllen von 27 Waldbaumarten. AFZ Wald 23: 1242–1244

Koontz MJ, Latimer AM, Mortenson LA, Fettig CJ, North MP (2021) Cross-scale interaction of host tree size and climatic water deficit governs bark beetle-induced tree mortality. Nature communications 12(1): 1-13.

Korhonen K, Stahl G, Freudenschuss A, Brändli UB, Fridman J, Cienciala A, Linser S (2020). Maintenance and appropriate enhancement of forest resources and their contribution to global carbon cycles. State of Europe's forests 2020.

Körner C (2006) Plant CO2 responses: an issue of definition, time and resource supply. New Phytol. 172(3): 393-411.

Kornhuber, K., Osprey, S., Coumou, D., Petri, S., Petoukhov, V., Rahmstorf, S., Gray, L.: Extreme weather events in early summer 2018 connected by a recurrent hemispheric wave-7 pattern, Environ. Res. Lett., 14(5), 054002, 2019.

Kostić S, Kesić L, Matović B, Orlović S, Stojnić S, Stojanović DB (2021) Soil properties are significant modifiers of pedunculate oak (Quercus robur L.) radial increment variations and their sensitivity to drought. Dendrochronologia 67, 125838.

Kovács B, Tinya F, Ódor P (2017) Stand structural drivers of microclimate in mature temperate mixed forests. Agric. For. Meteorol. 234: 11-21.

Kovats R, Valentini RS, Bouwer M, Georgopoulou E, Jacob D, Martin E, Rounsevell M, Soussana JF (2014) Chapter 23 - Europe In: Barros VR, Field CB, Dokken DJ, Mastrandrea MD, Mach KJ, Bilir TE, Chatterjee M, Ebi KL, Estrada YO, Genova RC, Girma B, Kissel ES, Levy AN, MacCracken S, Mastrandrea PR, White LL (eds) Climate Change 2014: Impacts Adaptation and Vulnerability Part B: Regional Aspects, Cambridge University Press, Cambridge, pp 1267-1326.

Kovats, R.S., Valentini, R., Bouwer, L.M., Georgopoulou, E., Jacob, D., Martin, E., Rounsevell, M., and Soussana, J.-F.: Europe. In: Climate Change 2014: Impacts, Adaptation, and Vulnerability. Part B: Regional Aspects. Contribution of Working Group II to the Fifth Assessment Report of the Intergovernmental Panel on Climate Change, Cambridge University Press, 1267-1326, 2014.

Kramer K (1994a) A modelling analysis of the effects of climatic warming on the probability of spring frost damage to tree species in The Netherlands and Germany. Plant, Cell, Environ. 17(4): 367-377.

Kramer K (1994b) Selecting a model to predict the onset of growth of Fagus sylvatica. J. Appl. Ecol. 172-181.

Lacerte V, Laroque GR, Woods M, Parton WJ, Penner M (2006) Calibration of the forest vegetation simulator (FVS) model to the main forest species in Ontario, Canada. Ecol. Mod. 199: 336-349.

Ladekarl, U. L., Rasmussen, K. R., Christensen, S., Jensen, K. H., and Hansen, B.: Groundwater recharge and evapotranspiration for two natural ecosystems covered with oak and heather, J. Hydrol., 300(1-4), 76-99, 2005.

Lanz A, Marchetti M, Bosela M, Lasserre B, Pettenella D, Adame P, Nunes L, Linser S (2020). Maintenance and encouragement of productive functions of forests (wood and non-wood). State of Europe's forests 2020.

Lasch P, Badeck FW, Lindner M, Suckow F (2002) Sensitivity of simulated forest growth to changes in climate and atmospheric CO2. Forstwissenschaftlisches Centralblatt 121: 155-171.

Laube J, Sparks TH, Estrella N, Höfler J, Ankerst DP, Menzel A (2014) Chilling outweighs photoperiod in preventing precocious spring development. Glob. Change Biol. 20(1): 170-182.

Law B, Ryan M, Anthony P (1999) Seasonal and annual respiration of a ponderosa pine ecosystem. Glob. Chang. Biol. 5: 169–182.

Le Quéré C, Andrew RM, Friedlingstein P, Sitch S, Hauck J, Pongratz J, Arneth A (2018) Global carbon budget 2018. Earth Syst. Sci. Data 10: 2141-2194.

Lefcheck JS, Byrnes JE, Isbell F, Gamfeldt L, Griffin JN, Eisenhauer N, Duffy JE (2015) Biodiversity enhances ecosystem multifunctionality across trophic levels and habitats. Nature communications 6(1): 1-7.

Leinonen I, Kramer K (2002) Applications of phenological models to predict the future carbon sequestration potential of boreal forests. Clim. Change 55(1): 99-113.

Lemée, G.: Recherches sur les ecosystemes des reserves biologiques de la foret de Fontainebleau. IV. Entrees d'elements mineraux par les precipitations et transfert au sol par le pluviolessivage, Oecolog. Plantar., 1974.

Lenssen NJ, Schmidt GA, Hansen JE, Menne MJ, Persin A, Ruedy R, Zyss D (2019) Improvements in the GISTEMP uncertainty model. J. Geophys. Res. Atmospheres 124(12): 6307-6326.

Lenz A, Hoch G, Vitasse Y (2016) Fast acclimation of freezing resistance suggests no influence of winter minimum temperature on the range limit of European beech. Tree Physiol. 36(4): 490-501.

Leuschner, C.: Walddynamik in der Lüneburger Heide: Ursachen, Mechanismen und die Rolle der Ressourcen, 1994.

Leuschner C, Meier IC (2018) The ecology of Central European tree species: Trait spectra, functional trade-offs, and ecological classification of adult trees. Perspect. Plant Ecol. Evol. Syst. 33: 89-103.

Leuzinger S, Zotz G, Asshoff R, Körner C (2005) Responses of deciduous forest trees to severe drought in Central Europe. Tree Physiol. 25(6): 641-650.

Levia Jr, D. F., and Herwitz, S. R.: Physical properties of water in relation to stemflow leachate dynamics: implications for nutrient cycling, Can. J. Forest Res., 30(4), 662-666, 2000.

Levin SA (1992) The problem of pattern and scale in ecology: the Robert H. MacArthur award lecture. Ecology 73(6): 1943-1967.

Liang, J., Crowther, T. W., Picard, N., Wiser, S., Zhou, M., Alberti, G., ... & Reich, P. B. (2016). Positive biodiversity-productivity relationship predominant in global forests. Science, 354(6309).

Lier M, Schuck A, Van Brusselen J, Bastrup-Birk A, Gasparini P, Bozzano M, Oggioni S, Rasi R, Vogt P, Biala K, Köhl M, Konczal A, de Koning J, Alberdi I, Vorisek P, Schwarz M, Linser S (2020). Maintenace, conservation and appropriate enhancement of biological diversity in forest ecosystems. State of Europe's forests 2020.

Ligot G, Balandier P, Courbaud B, Jonard M, Kneeshaw D, Claessens H (2014) Managing understory light to maintain a mixture of species with different shade tolerance. For. Ecol. Manag. 327: 189–200.

Lim PO, Kim HJ, Gil Nam H (2007) Leaf senescence. Annu. Rev. Plant Biol. 58: 115-136.

Lindner M, Maroschek M, Netherer S, Kremer A, Barbati A, Garcia-Gonzalo J, Seidl R, Delzon S, Corona P, Kolström M, Lexer MJ, Marchetti M (2010) Climate change impacts, adaptive capacity, and vulnerability of European forest ecosystems. Forest Ecol. Manag. 259(4): 698-709.

Lindner M, Fitzgerald JB, Zimmermann NE, Reyer C, Delzon S, van der Maaten E, Schelhaas MJ, Lasch P, Eggers J, van der Maaten-Theunissen M, Suckow F, Psomas A, Poulter B, Hanewinkel M (2014) Climate change and European forests: what do we know, what are the uncertainties, and what are the implications for forest management?. J. Environ. Manage. 146: 69-83.

Lisar SY, Motafakkerazad R, Hossain MM, Rahman IM (2012) Water stress in plants: causes effects and responses. In: Rahman I, Hasegawa H (eds) Water stress, InTech, Rijeka, Croatia, pp. 15-42.

Litton C, Raich J, Ryan M (2007) Carbon allocation in forest ecosystems. Glob. Chang. Biol. 13: 2089–2109.

Liu Q, Fu YH, Zhu Z, Liu Y, Liu Z, Huang M, Piao S (2016) Delayed autumn phenology in the Northern Hemisphere is related to change in both climate and spring phenology. Glob. Change Biol. 22: 3702–3711.

Liu Q, Fu YH, Liu Y, Janssens IA, Piao S (2018) Simulating the onset of spring vegetation growth across the Northern Hemisphere. Glob. Change Biol. 24: 1342–1356.

Liu, Q., Piao, S., Janssens, I. A., Fu, Y., Peng, S., Lian, X., Ciais, P., Myneni, R. B., Peñuelas, J., Wang, T.: Extension of the growing season increases vegetation exposure to frost, Nat. Commun., 9(1), 426, 2018.

Liu G, Chuine I, Denéchère R, Jean F, Dufrêne E, Vincent G, Berveiller D, Delpierre N (2021) Higher sample sizes and observer inter-calibration are needed for reliable scoring of leaf phenology in trees. J. Ecol.

Lopez, O. R., Farris-Lopez, K., Montgomery, R. A., Givnish, T. J.: Leaf phenology in relation to canopy closure in southern Appalachian trees, Am. J. Bot., 95(11), 1395-1407, 2008.

Lorenz EN (1963) Deterministic nonperiodic flow. J. Atmos. Sci. 20(2), 130-141.

Losseau J, Jonard M, Vincke C (2020) Pedunculate oak decline in southern Belgium: a long-term process highlighting the complex interplay among drought, winter frost, biotic attacks, and masting. Can. J. For. Res. 50(4): 380-389.

Luu TC, Binkley D, Stape JL (2013) Neighborhood uniformity increases growth of individual Eucalyptus trees. For. Ecol. Manag. 289: 90-97.

Luyssaert S, Marie G, Valade A, Chen YY, Djomo SN, Ryder J, Otto J, Naudts K, Lanso AS, Ghattas J, McGrath MJ (2018). Trade-offs in using European forests to meet climate objectives. Nature 562(7726): 259-262.

Ma Q, Huang JG, Hänninen H, Berninger F (2019) Divergent trends in the risk of spring frost damage to trees in Europe with recent warming. Glob. Change Biol. 25(1): 351-360.

Mahecha MD, Reichstein M, Carvalhais N, Lasslop G, Lange H, Seneviratne SI, Richardson AD (2010) Global convergence in the temperature sensitivity of respiration at ecosystem level. Science 329(5993): 838-840.

Mäkelä A (1986) Implications of the pipe model theory on dry matter partitioning and height growth in trees. J. Theor. Biol. 123: 103-120.

Mäkelä A, Valentine HT (2001) The ratio of NPP to GPP: evidence of change over the course of stand development. Tree Physiol. 21: 1015-1030.

Manion PD (1981) Tree Disease Concepts. Prentice-Hall, Englewood Cliffs, NJ, 402 pp.

Maraun D, Widmann M (2018) Statistical downscaling and bias correction for climate research. Cambridge University Press, Cambridge, United Kingdom

Marchand LJ, Dox I, Gričar J, Prislan P, Leys S, Van den Bulcke J, Campioli M (2020) Inter-individual variability in spring phenology of temperate deciduous trees depends on species, tree size and previous year autumn phenology. Agr. For. Meteorol. 290: 108031.

Martin-Benito D, Pederson N (2015) Convergence in drought stress, but a divergence of climatic drivers across a latitudinal gradient in a temperate broadleaf forest. J. Biogeogr. 42(5): 925-937.

Martínez-Vilalta, J., Lloret, F.: Drought-induced vegetation shifts in terrestrial ecosystems: the key role of regeneration dynamics, Glob. Planet. Change, 144, 94-108, 2016.

Martin-StPaul, N., Delzon, S., Cochard, H.: Plant resistance to drought depends on timely stomatal closure, Ecol. Lett., 20(11), 1437-1447, 2017.

Massonnet C, Chuste PA, Levillain J, Gérémia F, Silva DE, Maillard P, Bréda N (2021) Leafy season length is reduced by a prolonged soil water deficit but not by repeated defoliation in beech trees (Fagus sylvatica L.): comparison of response among regional populations grown in a common garden. Agric. For. Meteorol. 297: 108228.

Masson-Delmotte V (2018) Global Warming of 1.5°C: An IPCC Special Report on the Impacts of Global Warming of 1.5° C Above Pre-industrial Levels and Related Global Greenhouse Gas Emission Pathways, in the Context of Strengthening the Global Response to the Threat of Climate Change, Sustainable Development, and Efforts to Eradicate Poverty. Cambridge University Press, Cambridge, United Kingdom.

Mather, A. S. (1992). The forest transition. Area, 367-379.

Matte D, Larsen MAD, Christensen OB, Christensen JH (2019) Robustness and scalability of regional climate projections over Europe. Front. Environ. Sci. 6: 163.

Matzner, E., and Ulrich, B.: Bilanzierung jährlicher Elementflüsse in Waldökosystemen im Solling. Zeitschrift für Pflanzenernährung und Bodenkunde, 144(6), 660-681, 1981.

Mauri A, Strona G, San-Miguel-Ayanz J (2017) EU-Forest, a high-resolution tree occurrence dataset for Europe. Sci. Data 4(1): 1-8.

McDowell NG, Pockman WT, Allen CD, Breshears DD, Cobb N, Kolb T, Yepez EA (2008) Mechanisms of plant survival and mortality during drought: why do some plants survive while others succumb to drought?. New Phytol. 178(4): 719-739.

McDowell NG, Allen (2015) Darcy's law predicts widespread forest mortality under climate warming. Nat. Clim. Change 5(7): 669.

McGrath, M. J., Luyssaert, S., Meyfroidt, P., Kaplan, J. O., Bürgi, M., Chen, Y., Erb, K., Gimmi, U., McInerney, D., Naudts, K., Otto, J., Pasztor, F., Ryder, J., Schelhaas, M.J., and Valade, A. (2015). Reconstructing European forest management from 1600 to 2010. Biogeosciences, 12(14), 4291-4316.

McSweeney CF, Jones RG, Lee RW, Rowell DP (2015) Selecting CMIP5 GCMs for downscaling over multiple regions. Clim. Dyn. 44(11): 3237-3260.

MEA. 2005 Millennium Ecosystem Assessment, Ecosystems and Human Well-Being: Current State and Trends. Island Press

Medlyn B, Dewar R (1999) Comment on the article by R. H. Waring, J. J. Landsberg and M. Williams relating net primary production to gross primary production. Tree Physiol. 19: 137–138.

Medlyn BE, Barton CVM, Broadmeadow MSJ, Ceulemans R, De Angelis P, Forstreuter M, Rey A (2001) Stomatal conductance of forest species after long-term exposure to elevated CO2 concentration: a synthesis. New Phytol. 149(2): 247-264.

Meir, P., Wood, T. E., Galbraith, D. R., Brando, P. M., Da Costa, A. C., Rowland, L., Ferreira, L. V.: Threshold responses to soil moisture deficit by trees and soil in tropical rain forests: insights from field experiments, BioScience, 65(9), 882-892, 2015.

Melaas EK, Friedl MA, Richardson AD (2016) Multiscale modeling of spring phenology across Deciduous Forests in the Eastern United States. Glob. Change Biol. 22(2): 792-805.

Mellert KH, Göttlein A (2012) Comparison of new foliar nutrient thresholds derived from van den Burg's literature compilation with established central European references. Eur. J. For. Res. 131: 1461-1472.

Menzel A, Sparks TH, Estrella N, Koch E, Aasa A, Ahas R, Zust ANA (2006) European phenological response to climate change matches the warming pattern. Global change biology 12(10): 1969-1976.

Menzel A, Estrella N, Heitland W, Susnik A, Schleip C, Dose V (2008) Bayesian analysis of the species-specific lengthening of the growing season in two European countries and the influence of an insect pest. Int. J. Biometeorol. 52(3): 209-218.

Mérian P, Bontemps JD, Bergès L, Lebourgeois F (2011) Spatial variation and temporal instability in climate-growth relationships of sessile oak (Quercus petraea [Matt.] Liebl.) under temperate conditions. Plant Ecol. 212(11): 1855-1871.

Messier, C., Puettmann, K., Chazdon, R., Andersson, K. P., Angers, V. A., Brotons, L., Filotas, E., Tittler, R., Parrot, L. and Levin, S. A.: From management to stewardship: viewing forests as complex adaptive systems in an uncertain world, Conserv. Lett., 8(5), 368-377, 2015.

Metropolis, N., Rosenbluth, A. W., Rosenbluth, M. N., Teller, A. H., and Teller, E.: Equation of state calculations by fast computing machines, J. Chem. Phys., 21(6), 1087-1092, 1953.

Mette T, Albrecht A, Ammer C, Biber P, Kohnle U, Pretzsch H (2009) Evaluation of the forest growth simulator SILVA on dominant trees in mature mixed Silver fir–Norway spruce stands in South-West Germany. Ecol. Model. 220(13-14): 1670-1680.

Mette T, Dolos K, Meinardus C, Bräuning A, Reineking B, Blaschke M, Pretzsch H, Beierkuhnlein C, Gohlke A, Wellstein C (2013) Climatic turning point for beech and oak under climate change in Central Europe. Ecosphere 4(12): 1-19.

Meyfroidt, P., and Lambin, E. F. (2011). Global forest transition: prospects for an end to deforestation. Annual review of environment and resources, 36, 343-371.

Michopoulos, P., Baloutsos, G., Nakos, G., and Economou, A.: Effects of bulk precipitation pH and growth period on cation enrichment in precipitation beneath the canopy of a beech (Fagus moesiaca) forest stand, Sci. Total Environ., 281(1-3), 79-85, 2001.

Millar CI, Stephenson NL (2015) Temperate forest health in an era of emerging megadisturbance. Science 349(6250): 823-826.

Mina M, Bugmann H, Cordonnier T, Irauschek F, Klopcic M, Pardos M, Cailleret M (2017) Future ecosystem services from European mountain forests under climate change. J. Appl. Ecol. 54(2): 389-401.

Monteith JL (1965) Evaporation and environment. Symposia of the Society for Experimental Biology 19:205–234

Monteith JL (1977) Climate and the efficiency of crop production in Britain. Philos. Trans. Royal Soc. B. 281: 277–294.

Moon P, Spencer D (1942) Illumination from a non-uniform sky. Illumination Engineering 37(10): 707–426

Morice CP, Kennedy JJ, Rayner NA, Jones PD (2012) Quantifying uncertainties in global and regional temperature change using an ensemble of observational estimates: The HadCRUT4 data set. J. Geophys. Res. Atmospheres 117(D8).

Morin X, Chuine I (2014) Will tree species experience increased frost damage due to climate change because of changes in leaf phenology?. Can. J. For. Res. 44(12): 1555-1565.

Mosello, R., Brizzio, M. C., Kotzias, D., Marchetto, A., Rembges, D., and Tartari, G.: The chemistry of atmospheric deposition in Italy in the framework of the National Programme for Forest Ecosystems Control (CONECOFOR), J. Limnol., 61(1s), 77-92, 2002.

Müller, J., and Bolte, A.: The use of lysimeters in forest hydrology research in north-east Germany, Agric. For. Res., 59, 1-10, 2009.

Murphy, E. M., Ginn, T. R., and Phillips, J. L.: Geochemical estimates of paleorecharge in the Pasco Basin: Evaluation of the chloride mass balance technique, Water Resour. Res., 32(9), 2853-2868, 1996.

Muzylo A, Llorens P, Valente F, Keizer JJ, Domingo F, Gash JHC (2009) A review of rainfall interception modelling. J. Hydrol. 370(1-4): 191-206.

Myhre G, Shindell D, Breon FM, Collins W, Fuglestvedt J, Huang J, Koch D, Lamarque JF, Lee D, Mendoza B, Nakajima T, Robock A, Stephens G, Takemura T, Zhang H (2013) Anthropogenic and Natural Radiative Forcing In: Stocker TF, Qin D, Plattner GK, Tignor M, Allen SK, Boschung J, Nauels A, Xia Y, Bex V, Migley PM (eds) Climate Change 2013: The Physical Science Basis, Cambridge University Press, Cambridge, United Kingdom, pp. 659-740.

Nabat P, Somot S, Mallet M et al (2015) Direct and semi-direct aerosol radiative effect on the Mediterranean climate variability using a coupled regional climate system model. Clim Dyn 44:1127–1155.

Nagy, L.: Data to the precipitation interception of a Galatello-Quercetum roboris (forest steppe-forest) at Ujszentmargita, Acta Bot., 1974.

Naudts K, Chen Y, McGrath MJ, Ryder J, Valade A, Otto J, Luyssaert S (2016) Europe's forest management did not mitigate climate warming. Science 351(6273): 597-600.

Neal, C., Robson, A. J., Bhardwaj, C. L., Conway, T., Jeffery, H. A., Neal, M., Ryland, G.P., Smith, C.J. and Walls, J.: Relationships between precipitation, stemflow and throughfall for a lowland beech plantation, Black Wood, Hampshire, southern England: findings on interception at a forest edge and the effects of storm damage, J. Hydrol., 146, 221-233, 1993.

Neumann M, Mues V, Moreno A, Hasenauer H, Seidl R (2017) Climate variability drives recent tree mortality in Europe. Glob. Change Biol. 23(11): 4788-4797.

Nizinski, G., and Saugier, B.: Mesures et modélisation de l'interception nette dans une futaie de chênes, Oecolog. Plantar., 9(3), 311-329, 1988.

Nkotagu, H.: Application of environmental isotopes to groundwater recharge studies in a semi-arid fractured crystalline basement area of Dodoma, Tanzania, J. Afr.Earth Sci., 22(4), 443-457, 1996.

Nölte A, Yousefpour R, Hanewinkel M (2020) Changes in sessile oak (Quercus petraea) productivity under climate change by improved leaf phenology in the 3-PG model. Ecol. Model. 438: 109285.

Norby RJ, DeLucia EH, Gielen B, Calfapietra C, Giardina CP, King JS, Ledford J, McCarthy HR, Moore DJ, Ceulemans R, De Angelis P, Finzi AC, Karnosky DF, Kubiske ME, Lukac M, Pregitzer KS, Scarascia-Mugnozza GE, Schlesinger WH, Oren R (2005) Forest response to elevated CO2 is conserved across a broad range of productivity. PNAS 102(50): 18052-18056.

Norby RJ, Warren JM, Iversen CM, Medlyn BE, McMurtrie RE (2010) CO2 enhancement of forest productivity constrained by limited nitrogen availability. Proc. Natl. Acad. Sci.107(45): 19368-19373.

Norby RJ, Zak DR (2011) Ecological lessons from free-air CO2 enrichment (FACE) experiments. Annu. Rev. Ecol. Evol. Syst. 42.

Norton BG (2012) Valuing Ecosystems. Nature Education Knowledge 3(10):2

Öberg, G. M.: The biogeochemistry of chlorine in soil, in: Natural production of organohalogen compounds, 43-62, 2003.

Obiefuna, G. I., and Orazulike, D. M.: Application and comparison of groundwater recharge estimation methods for the semiarid Yola area, northeast, Nigeria, Global Journal of Geological Sciences, 9(2), 177, 2011.

Ogaya R, Peñuelas J (2007) Tree growth mortality and above-ground biomass accumulation in a holm oak forest under a five-year experimental field drought. Plant Ecol. 189(2): 291-299.

Oliver TH, Heard MS, Isaac NJB, Roy DB, Procter D, Eigenbrod F, Freckleton R, Hector A, Orme CDL, Petchey OL, Proença V, Raffaelli D, Suttle KB, Mace GM, Martín López B, Woodcock BA, Bullock JM (2015) Biodiversity and resilience of ecosystem functions. Trends Ecol. Evol. 30: 673–684.

Oren R, Ellsworth DS, Johnsen KH, Phillips N, Ewers BE, Maier C, Schäfer K, McCarthy H, Hendrey G, McNutty SG, Katul GG (2001). Soil fertility limits carbon sequestration by forest ecosystems in a CO 2-enriched atmosphere. Nature 411(6836): 469-472.

Osakabe Y, Osakabe K, Shinozaki K, Tran LSP (2014) Response of plants to water stress. Front. Plant Sci. 5: 86.

Pacala, S. W., Deutschman, D. H.: Details that matter: the spatial distribution of individual trees maintains forest ecosystem function, Oikos, 357-365, 1995.

Pach M, Sansone D, Ponette Q, Barreiro S, Mason B, Bravo-Oviedo A, Corona P (2018) Silviculture of mixed forests: a European overview of current practices and challenges. In Dynamics, silviculture and management of mixed forests (pp. 185-253). Springer.

Päivänen, J.: Hydraulic conductivity and water retention in peat soils, Suomen metsätieteellinen seura, 1973.

Pan Y, Birdsey RA, Fang J, Houghton R, Kauppi PE, Kurz WA, Hayes D (2011) A large and persistent carbon sink in the world's forests. Science 333(6045): 988-993.

Park T, Ganguly S, Tømmervik H, Euskirchen ES, Høgda KA, Karlsen SR, Brovkin V, Nemani RR, Myneni RB (2016) Changes in growing season duration and productivity of northern vegetation inferred from long-term remote sensing data. Environ. Res. 11(8): 084001.

Parmesan C, Yohe G (2003) A globally coherent fingerprint of climate change impacts across natural systems. Nature 421(6918): 37.

Pasho, E., Camarero, J. J., de Luis, M., & Vicente-Serrano, S. M. (2011). Impacts of drought at different time scales on forest growth across a wide climatic gradient in north-eastern Spain. Agricultural and Forest Meteorology, 151(12), 1800-1811.

Pedro, M. S., Rammer, W., & Seidl, R.: Tree species diversity mitigates disturbance impacts on the forest carbon cycle, Oecologia, 177(3), 619-630, 2015.

Peichl M, Brodeur J et al. (2010) Biometric and eddy-covariance based estimates of carbon fluxes in an age-sequence of temperate pine forests. Agric. For. Meteorol. 150: 952–965.

Penning de Vries FWT (1975) The cost of maintenance processes in plant cells. Ann. Bot. 39: 77-92.

Penuelas J, Boada M (2003) A global change-induced biome shift in the Montseny mountains (NE Spain). Glob. Change Biol. 9(2): 131-140.

Peñuelas J, Filella I, Zhang X, Llorens L, Ogaya R, Lloret F, Terradas J (2004) Complex spatiotemporal phenological shifts as a response to rainfall changes. New Phytol. 161(3): 837-846.

Penuelas J, Ogaya R, Boada M, Jump A (2007) Migration, invasion and decline: changes in recruitment and forest structure in a warming-linked shift of European beech forest in Catalonia (NE Spain). Ecography 30(6): 829-837.

Peñuelas J, Ciais P, Canadell JG, Janssens IA, Fernández-Martínez M, Carnicer J, Sardans J (2017) Shifting from a fertilization-dominated to a warming-dominated period. Nature Ecol. Evol. 1(10): 1438-1445.

Petit S, Claessens H, Vincke C, Ponette Q, Marchal D (2017) Le Fichier écologique des essences, version 2.0. Forêt.Nature (143): 12-19.

Petriţan, A. M., von Lüpke, B., Petriţan, I. C.: Influence of light availability on growth, leaf morphology and plant architecture of beech (Fagus sylvatica L.), maple (Acer pseudoplatanus L.) and ash (Fraxinus excelsior L.) saplings, Eur. J. For. Res., 128(1), 61-74, 2009.

Petritan AM, Bouriaud O, Frank DC, Petritan IC (2017) Dendroecological reconstruction of disturbance history of an old-growth mixed sessile oak–beech forest. J. Veg. Sci. 28(1): 117-127.

Phillips RP, Ibáñez I, D'Orangeville L, Hanson PJ, Ryan MG, McDowell NG (2016) A belowground perspective on the drought sensitivity of forests: Towards improved understanding and simulation. Forest Ecol. Manag. 380: 309-320.

Piao S, Luyssaert S, Ciais P, Janssens IA, Chen A, Cao C, Fang J, Friedlingstein P, Luo Y, Wang S (2010) Forest annual carbon cost: A global-scale analysis of autotrophic respiration. Ecology 91(3): 652-661.

Piao S, Liu Q, Chen A, Janssens IA, Fu Y, Dai J, Liu L, Shen M, Zhu X (2019) Plant phenology and global climate change: Current progresses and challenges. Glob. Change Biol. 25(6): 1922-1940.

Pielou EC (1959) The use of point to plant distances in the study of the pattern of plant populations. J. Ecol. 47: 607–613.

Ping, J., Nichol, C., and Wei, X.: Quantification of groundwater recharge using the chloride mass balance method in a semi-arid mountain terrain, South Interior British Columbia, Canada, J. Chem. Pharm. Res., 6(1), 383-388, 2014.

Pletsers A, Caffarra A, Kelleher CT, Donnelly A (2015) Chilling temperature and photoperiod influence the timing of bud burst in juvenile Betula pubescens Ehrh. and Populus tremulaL.trees. Ann. For. Sci. 72: 941–953.

Poncelet L (1956) Climat de la Belgique, Planches 12, 13, 14 et commentaires, Atlas de Belgique. Institut Géographique Militaire La Cambre, Brussel, Belgium.

Popkin G (2019) The forest question. Nature 565(7739): 280-282.

Poulter B, Frank DC, Hodson EL, Zimmermann NE (2011) Impacts of land cover and climate data selection on understanding terrestrial carbon dynamics and the CO2 airborne fraction. Biogeosciences 8: 2027-2026.

Pretzsch H (2002) Application and evaluation of the growth simulator SILVA 2.2 for forest stands, forest estates and large regions. Forstwissenschaftlisches Centralblatt 121: 28-51.

Pretzsch, H., Grote, R., Reineking, B., Rötzer, T. H., and Seifert, S. T.: Models for forest ecosystem management: a European perspective, Ann. Bot-London, 101(8), 1065-1087, 2007.

Pretzsch H, Schütze G, Uhl E (2013) Resistance of European tree species to drought stress in mixed versus pure forests: evidence of stress release by inter-specific facilitation. Plant Biol. 15(3): 483-495.

Pretzsch H, Forrester DI, Rötzer T (2015) Representation of species mixing in forest growth models. A review and perspective. Ecol. Model. 313: 276-292.

Pretzsch H, Biber P (2016) Tree species mixing can increase maximum stand density. Can. J. For. Res. 46(10): 1179-1193.

Primack RB, Ibáñez I, Higuchi H, Lee SD, Miller-Rushing AJ, Wilson AM, Silander Jr JA (2009) Spatial and interspecific variability in phenological responses to warming temperatures. Biol. Conserv. 142(11): 2569-2577.

R Core Team (2020). R: A language and environment for statistical computing. R Foundation for Statistical Computing, Vienna, Austria. https://www.R-project.org/.

Raftoyannis Y, Radoglou K (2002) Physiological responses of beech and sessile oak in a natural mixed stand during a dry summer. Ann. Bot. 89(6): 723-730.

Rasche, L., Fahse, L., Bugmann, H.: Key factors affecting the future provision of tree-based forest ecosystem goods and services, Clim. Change, 118(3-4), 579-593, 2013.

Reyer C, Lasch-Born P, Suckow F, Gutsch M, Murawski A, Pilz T (2014) Projections of regional changes in forest net primary productivity for different tree species in Europe driven by climate change and carbon dioxide. Ann. For. Sci. 71(2): 211-225.

Reyer C (2015) Forest productivity under environmental change—a review of stand-scale modelling studies. Curr. For. Rep. 1(2): 53–68

Reyer CP, Brouwers N, Rammig A, Brook BW, Epila J, Grant RF, Holmgren M, Langerswich F, Leuzinger S, Lucht W, Medlyn B, Pfeifer M, Steinkamp J, Vanderwel MC, Verbeeck H, Villela DM (2015) Forest resilience and tipping points at different spatio-temporal scales: approaches and challenges. J. Ecol. 103(1): 5-15.

Richardson AD, Keenan TF, Migliavacca M, Ryu Y, Sonnentag O, Toomey M (2013) Climate change, phenology, and phenological control of vegetation feedbacks to the climate system. Agr. Forest Meteorol. 169: 156-173.

Rigling A, Bigler C, Eilmann B, Feldmeyer-Christe E, Gimmi U, Ginzler C, Dobbertin M (2013) Driving factors of a vegetation shift from Scots pine to pubescent oak in dry Alpine forests. Global Change Biology 19(1): 229-240.

Risser, D. W., Gburek, W. J., and Folmar, G. J.: Comparison of recharge estimates at a small watershed in east-central Pennsylvania, USA, Hydrogeol. J., 17(2), 287-298, 2009.

Roberts, J., and Rosier, P.: The effect of broadleaved woodland on Chalk groundwater resources, Q. J. Eng. Geol. Hydrogeo., 39(2), 197-207, 2006.

Roberts, A. M., Tansey, C., Smithers, R. J., and Phillimore, A. B.: Predicting a change in the order of spring phenology in temperate forests, Glob. Change Biol., 21(7), 2603-2611, 2015.

Rötzer, T., Grote, R., and Pretzsch, H.: Effects of environmental changes on the vitality of forest stands, Eur. J. For. Res., 124(4), 349-362, 2005.

Rötzer T, Leuchner M, Nunn AJ (2010) Simulating stand climate, phenology, and photosynthesis of a forest stand with a process-based growth model. Int. J. Biometeorol. 54: 449–464.

Rötzer, T., Biber, P., Moser, A., Schäfer, C., Pretzsch, H.: Stem and root diameter growth of European beech and Norway spruce under extreme drought, Forest Ecol. Manag., 406, 184-195, 2017.

Rowe, L. K.: Rainfall interception by an evergreen beech forest, Nelson, New Zealand, J. Hydrol., 66(1-4), 143-158, 1983.

RStudio Team (2015) RStudio: Integrated Development for R. RStudio. Boston, MA (Computer Software v0.98.1074).

Rubio-Cuadrado Á, Camarero JJ, Del Rio M, Sánchez-González M, Ruiz-Peinado R, Bravo-Oviedo A, Montes F (2018) Drought modifies tree competitiveness in an oak-beech temperate forest. Forest Ecol. Manag. 429: 7-17.

Ruiz-Benito P, Madrigal-Gonzalez J, Ratcliffe S, Coomes DA, Kändler G, Lehtonen A, Zavala MA (2014) Stand structure and recent climate change constrain stand basal area change in European forests: a comparison across boreal, temperate, and Mediterranean biomes. Ecosystems 17(8): 1439-1454.

Ruiz-Benito P, Vacchiano G, Lines ER, Reyer CP, Ratcliffe S, Morin X, Hartig F, Mäkelä A, Yousefpour R, Chaves JE, Palacios-Orueta A, Benito-Garzón M, Morales-Molino C, Camarero JJ, Jump AS, Kattge J, Lehtonen A, Ibrom A, Owen HJF, Zavala MA (2020). Available and missing data to model impact of climate change on European forests. Ecol. Model. 416: 108870.

Rummukainen M (2010) State-of-the-art with regional climate models. WIRES Clim. Change 1(1): 82-96.

Ryan, M. G., and Yoder, B. J.: Hydraulic limits to tree height and tree growth, Bioscience, 47(4), 235-242, 1997.

Ryan M, Binkley D, Fownes J, Giardina C, Senock R (2004) An experimental test of the causes of forest growth decline with stand age. Ecol. Monogr. 74: 393–414.

Ryelandt B (2019) Modeling oak and beech regeneration in mixed and uneven-aged forests : a process-based approach for changing environments. Université catholique de Louvain.

Saltré F, Saint-Amant R, Gritti ES, Brewer S, Gaucherel C, Davis BA, Chuine I (2013) Climate or migration: what limited E uropean beech post-glacial colonization?. Glob. Ecol. Biogeogr. 22(11): 1217-1227.

Sammis, T. W., Evans, D. D., and Warrick, A. W.: Comparison of methods to estimate deep percolation rates 1, JAWRA J. Am. Water Resour. As., 18(3), 465-470, 1982.

San-Miguel-Ayanz J, Stahl G, Vidal C (2011). Maintenance and appropriate enhancement of forest resources and their contribution to global carbon cycles. State of Europe's forests 2011.

San-Miguel-Ayanz J, de Rigo D, Caudullo G, Houston Durrant T, Mauri A (Eds.) 2016 European Atlas of Forest Tree Species. Publ. Off. EU, Luxembourg, pp. e01e873+

Sanz-Perez V, Castro-Diez P (2010) Summer water stress and shade alter bud size and budburst date in three mediterranean Quercus species. Trees 24: 89-97

Sarris, D., Christodoulakis, D., & Koerner, C. (2007). Recent decline in precipitation and tree growth in the eastern Mediterranean. Global Change Biology, 13(6), 1187-1200.

Savolainen O, Pyhäjärvi T, Knürr T (2007) Gene flow and local adaptation in trees. Annu. Rev. Ecol. Evol. Syst. 38: 595-619.

Scanlon, B. R., Healy, R. W., and Cook, P. G.: Choosing appropriate techniques for quantifying groundwater recharge, Hydrogeol. J., 10(1), 18-39, 2002.

Schaber, J., and Badeck, F. W.: Physiology-based phenology models for forest tree species in Germany, Int. J. Biometeorol., 47(4), 193-201, 2003.

Schäfer KVR, Oren R, Tenhunen JD (2000) The effect of tree height on crown level stomatal conductance. Plant Cell. Environ. 23: 365–375.

Schäfer, C., Thurm, E. A., Rötzer, T., Kallenbach, C., Pretzsch, H.: Daily stem water deficit of Norway spruce and European beech in intra-and interspecific neighborhood under heavy drought, Scand. J. For. Res., 33(6), 568-582, 2018.

Scharnweber T, Manthey M, Criegee C, Bauwe A, Schröder C, Wilmking M (2011) Drought matters–Declining precipitation influences growth of Fagus sylvatica L. and Quercus robur L. in north-eastern Germany. For. Ecol. Manag. 262(6): 947-961.

Scharnweber, T., Manthey, M., & Wilmking, M. (2013). Differential radial growth patterns between beech (Fagus sylvatica L.) and oak (Quercus robur L.) on periodically waterlogged soils. Tree physiology, 33(4), 425-437.

Schelhaas MJ, Nabuurs GJ, Schuck A (2003) Natural disturbances in the European forests in the 19th and 20th centuries. Glob. Change Biol. 9(11): 1620-1633.

Schepaschenko D, Shvidenko A, Usoltsev V, Lakyda P, Luo Y, Vasylyshyn R, Myklush Y, See L, McCallum I, Fritz S, Kraxner F, Obersteiner M (2017). A dataset of forest biomass structure for Eurasia. Scientific data, 4(1): 1-11.

Scherrer D, Bader MK, Körner C (2011) Drought-sensitivity ranking of deciduous tree species based on thermal imaging of forest canopies. Agr. Forest Meteorol. 151(12): 1632-1640.

Schieber, B.: Spring phenology of European beech (Fagus sylvatica L.) in a submountain beech stand with different stocking in 1995–2004, J. For. Sci., 52(5), 208-216, 2006.

Schipka, F., Heimann, J., and Leuschner, C.: Regional variation in canopy transpiration of Central European beech forests, Oecolog., 143(2), 260-270, 2005.

Schmid S, Zingg A, Biber P, Bugmann H (2006) Evaluation of the forest growth model SILVA along an elevational gradient in Switzerland. Eur. J. For. Res. 125(1): 43-55.

Schmidt M, Hansen J (2007) Validierung der Durchmesserzuwachsprognosen des Wachstumssimulators BWINPro 7.0 für Fichte und Buche für den Bereich der alten Bundesländer. In: Nagel, J. (ed.): Sektion Ertragskunde Jahrestagung. Alsfeld-Eudorf 164-179.

Schmidt, M., Nagel, J., and Skovsgaard, J. P.: Evaluating individual tree growth models, in: Sustainable Forest Management, 151-163, Springer, Berlin, Heidelberg, 2006.

Schmidt, M.: Canopy transpiration of beech forests in Northern Bavaria–Structure and function in pure and mixed stands with oak at colline and montane sites (Doctoral dissertation), 2007.

Schmull M, Thomas FM (2000) Morphological and physiological reactions of young deciduous trees (Quercus robur L., Q. petraea [Matt.] Liebl., Fagus sylvatica L.) to waterlogging. Plant and Soil 225(1): 227-242.

Schuldt B, Buras A, Arend M, Vitasse Y, Beierkuhnlein C, Damm A, Kahmen A (2020) A first assessment of the impact of the extreme 2018 summer drought on Central European forests. Basic and Applied Ecology 45: 86-103.

Schwalm CR, Ek AR (2004) A process-based model of forest ecosystems driven by meteorology. Ecol. Model. 179(3): 317-348.

Schwalm CR, Williams CA, Schaefer K, Anderson R, Arain MA, Baker I, (40 more authors) Verma SB (2010). A model-data intercomparison of CO2 exchange across North America: Results from the North American Carbon Program site synthesis. Journal of Geophysical Research: Biogeosciences, 115(G3).

Schwendenmann, L., Pendall, E., Sanchez-Bragado, R., Kunert, N., Hölscher, D.: Tree water uptake in a tropical plantation varying in tree diversity: interspecific differences, seasonal shifts and complementarity, Ecohydrology, 8(1), 1-12, 2015.

Sedmáková, D., Sedmák, R., Bosela, M., Ležík, M., Blaženec, M., Hlásny, T., & Marušák, R. (2019). Growth-climate responses indicate shifts in the competitive ability of European beech and Norway spruce under recent climate warming in East-Central Europe. Dendrochronologia, 54, 37-48.

Seidl R, Lexer MJ, Jäger D, Hönninger K (2005) Evaluating the accuracy and generality of a hybrid patch model. Tree Physiol. 25(7): 939-951.

Seidl R, Schelhaas MJ, Lexer MJ (2011) Unraveling the drivers of intensifying forest disturbance regimes in Europe. Global Change Biology 17(9): 2842-2852.

Seidl, R., Rammer, W., Scheller, R.M., Spies, T.A.: An individual-based process model to simulate landscape-scale forest ecosystem dynamics, Ecol. Model., 231, 87-100, 2012.

Seidl R, Schelhaas MJ, Rammer W, Verkerk PJ (2014) Increasing forest disturbances in Europe and their impact on carbon storage. Nat. Clim. Change 4(9): 806.

Seidl R, Spies TA, Peterson DL, Stephens SL, Hicke JA (2016) Searching for resilience: addressing the impacts of changing disturbance regimes on forest ecosystem services. J. Appl. Ecol. 53(1): 120-129.

Seiwa, K.: Changes in leaf phenology are dependent on tree height in Acer mono, a deciduous broad-leaved tree, Ann. Bot., 83(4), 355-361, 1999a.

Seiwa, K.: Ontogenetic changes in leaf phenology of Ulmus davidiana var. japonica, a deciduous broad-leaved tree, Tree Physiol., 19(12), 793-797, 1999b.

Senf, C., & Seidl, R. (2018). Natural disturbances are spatially diverse but temporally synchronized across temperate forest landscapes in Europe. Global change biology, 24(3), 1201-1211.

Shifley SR, He HS, Lischke H, Wang WJ, Jin W, Gustafson EJ, Yang J (2017) The past and future of modeling forest dynamics: from growth and yield curves to forest landscape models. Landscape Ecology 32(7): 1307-1325.

Shvidenko A, Barber CV, Persson R. Forest and woodland systems. In Hassan, R., Scholes, R., and Ash, N. (Eds) (2005). Ecosystems and human well-being: current state and trends.

Silva Pedro M, Rammer W, Seidl R (2015) Tree species diversity mitigates disturbance impacts on the forest carbon cycle. Oecologia 177(3): 619-630.

Simioni G, Le Roux X, Gignoux J, Sinoquet H (2000) Treegrass: a 3D, process-based model for simulating plant interactions in tree–grass ecosystems. Ecol. Model. 131(1): 47-63.

Simioni G, Marie G, Huc R (2016) Influence of vegetation spatial structure on growth and water fluxes of a mixed forest: Results from the NOTG 3D model. Ecol. Model. 328: 119–135.

Simons H, Soto X, Zhu Z, Singh KD, Bellan MF, Iremonger S, Hirvonen S, Smith B, Watson B, Tosi J, Morales L, Shvidenko A, Bohn U, Hettwer C, Barkoudah Y, Du Z, Tickle P (2001). Global Ecological Zoning for the Global Forest Resources Assessment 2000-Final Report.

Skovsgaard JP, Vanclay JK (2008) Forest site productivity: a review of the evolution of dendrometric concepts for even-aged stands. Int. J. For. Res. 81(1): 13-31.

Skovsgaard JP, Vanclay JK (2013) Forest site productivity: a review of spatial and temporal variability in natural site conditions. Forestry 86(3): 305-315.

Soares P, Tomé M, Skovsgaard JP, Vanclay JK (1995) Evaluating a growth model for forest management using continuous forest inventory data. Forest Ecology and Management 71(3): 251-265.

Soares A, Leite HG, Souza AL, Silva SR, Lourenço HM, Forrester DI (2016) Increasing stand structural heterogeneity reduces productivity in Brazilian Eucalyptus monoclonal stands. For. Ecol. Manag. 373: 26-32.

Sohn JA, Saha S, Bauhus J (2016) Potential of forest thinning to mitigate drought stress: A meta-analysis. Forest Ecol. Manag. 380: 261-273.

Soil Survey Staff (2014) Keys to Soil Taxonomy, 12th edition. U.S. Department of Agriculture, Natural Resources Conservation Service, Washington, DC

Soil Science Division Staff (2017) Soil survey manual. Ditzler C, Scheffe K, Monger HC (eds.). USDA Handbook 18. Government Printing Office, Washington, D.C.

Sperlich D, Nadal-Sala D, Gracia C, Kreuzwieser J, Hanewinkel M, Yousefpour R (2020) Gains or Losses in Forest Productivity under Climate Change? The Uncertainty of CO2 Fertilization and Climate Effects. Climate 8(12): 141.

Spiecker, H., Mielikäinen, K., Köhl, M., & Skovsgaard, J. P. (Eds.). (2012). Growth trends in European forests: studies from 12 countries. Springer Science & Business Media.

Spinoni J, Naumann G, Vogt JV (2017) Pan-European seasonal trends and recent changes of drought frequency and severity. Glob. Planet. Change 148: 113-130.

Staelens, J., De Schrijver, A., Verheyen, K., and Verhoest, N. E.: Rainfall partitioning into throughfall, stemflow, and interception within a single beech (Fagus sylvatica L.) canopy: influence of foliation, rain event characteristics, and meteorology, Hydrol. Process., 22(1), 33-45, 2008.

Steckel M, del Río M, Heym M, Aldea J, Bielak K, Brazaitis G, Pretzsch H (2020) Species mixing reduces drought susceptibility of Scots pine (Pinus sylvestris L.) and oak (Quercus robur L., Quercus petraea (Matt.) Liebl.)– Site water supply and fertility modify the mixing effect. For. Ecol. Manag. 461: 117908.

Steenberg JW, Millward AA, Duinker PN, Nowak DJ, Robinson PJ (2015) Neighbourhood-scale urban forest ecosystem classification. J. Environ. Manage. 163: 134-145.

Sterba H, Korol N, Rössler G (2001) Ein Ansatz zur Evaluierung eines Einzelbaumwachstumssimulators für Fichtenreinbestände. Fw. Cbl. 120: 406-421.

Sterba H, Dirnberger G, Ritter T (2018) The Contribution of Forest Structure to Complementarity in Mixed Stands of Norway Spruce (Picea abies L. Karst) and European Larch (Larix decidua Mill.). Forests 9(7): 410.

Stocker TF, Qin D, Plattner GK, Tignor M, Allen SK, Boschung J, Midgley PM (2013) Climate change 2013: The physical science basis, Cambridge Univ Press, Cambridge, United Kingdom.

Stockli R, Vidale PL (2004) European plant phenology and climate as seen in a 20-year AVHRR land-surface parameter dataset. Intern. J. Remote Sens. 25: 3303–3330

Stovall AE, Shugart H, Yang X (2019) Tree height explains mortality risk during an intense drought. Nature communications 10(1): 1-6.

Sun Y, Gu L et al. (2014) Impact of mesophyll diffusion on estimated global land CO2 fertilization. PNAS 111: 15774–15779.

Sykes MT, Prentice IC, Cramer W (1996) A bioclimatic model for the potential distributions of north European tree species under present and future climates. J. Biogeogr. 203-233.

Szabo, M.: Net precipitation in a Hungarian oak forest ecosystem, Acta Bot., 1975.

Tarazona, T., Santa Regina, I., and Calvo, R.: Interception, throughfall and stemflow in two forests of the" Sierra de la Demanda" in the Province of Burgos, Pirineos, 147, 27-40, 1996.

Tegel W, Seim A, Hakelberg D, Hoffmann D, Panev M, Westphal T, Büntgen U (2014) A recent growth increase of European beech (Fagus sylvaticaL.) at its Mediterranean distribution limit contradicts drought stress. Eur J For Res 133:61–71

Teh, C.: Introduction to mathematical modeling of crop growth. How the equations are derived and assembled into a computer program, Brown Walker Press, Boca Raton, Florida, USA, 2006.

Temperli C, Bugmann H, Elkin C (2012) Adaptive management for competing forest goods and services under climate change. Ecol. Appl. 22(8): 2065-2077.

Termonia P, Van Schaeybroeck B, De Cruz L, De Troch R, Caluwaerts S, Giot O, Hamdi R, Vannitsem S, Duchêne F, Willems P, Tabari H, Van Uytven E, Hosseinzadehtalaei P, Van Lipzig N, Wouters H, Vanden Broucke S, van Ypersele JP, Marbaix P, Villanueva-Birriel C, Fettweis X, Wyard C, Scholzen C, Doutreloup S, De Ridder K, Gobbin A, Lauwaet D, Stavrakou T, Bauwens M, Müller JF, Luyten P, Ponsar S, Van den Eynde D, Pottiaux E (2018) The CORDEX. Be initiative as a foundation for climate services in Belgium. Clim. Serv. 11:49–61

Terrer C, Jackson RB, Prentice IC, Keenan TF, Kaiser C, Vicca S, ... Franklin O (2019) Nitrogen and phosphorus constrain the CO 2 fertilization of global plant biomass. Nat. Clim. Change 9(9): 684-689.

Teskey R, Wertin T, Bauweraerts I, Ameye M, McGuire MA, Steppe K (2015) Responses of tree species to heat waves and extreme heat events. Plant Cell Environ. 38(9): 1699-1712.

Thom D, Rammer W, Seidl R (2017) The impact of future forest dynamics on climate: interactive effects of changing vegetation and disturbance regimes. Ecol. Monogr. 87(4): 665-684.

Thompson I, Mackey B, McNulty S, Mosseler A (2009) Forest resilience, biodiversity, and climate change. A synthesis of the biodiversity/resilience/stability relationship in forest ecosystems. Secretariat of the Convention on Biological Diversity 43.

Thompson I (2011) Biodiversity, ecosystem thresholds, resilience and forest degradation. Unasylva 238(62): 25-30.

Thompson M, Gamage D, Hirotsu N, Martin A, Seneweera S (2017) Effects of elevated carbon dioxide on photosynthesis and carbon partitioning: a perspective on root sugar sensing and hormonal crosstalk. Front. Physiol. 8: 578.

Thornley J (2011) Plant growth and respiration re-visited: maintenance respiration defined it is an emergent property of, not a separate process within, the system and why the respiration: photosynthesis ratio is conservative. Ann. Bot. 108: 1365–1380.

Thürig E, Kaufmann E, Frisullo R, Bugmann H (2005) Evaluation of the growth function of an empirical forest scenario model. For. Ecol. Manag. 204: 51-66.

Timmerman V, Potocic N, Ognjenovic M, Kirchner T (2020). Tree crown conditions in 2019. In Forest Condition in Europe: 2016 Technical Report of ICP Forests: Report under the UNECE Convention on Long-Range Transboundary Air Pollution (CLRTAP)

Ting, C. S., Kerh, T., and Liao, C. J.: Estimation of groundwater recharge using the chloride mass-balance method, Pingtung Plain, Taiwan, Hydrogeol. J., 6(2), 282-292, 1998.

Titeux H, Jonard M, Elodie B, Christian L, Patrick M, Ponette Q (2018) L'évolution de la santé des forêts wallonnes. Principaux enseignements des réseaux de monitoring"ICP-forests". Forêt.Nature 147: 48-60.

Todd, D. K., Mays, L. W.: Groundwater hydrology edition, John Willey Sons, New York, USA, 2005

Topp, G. C., Davis, J. L., and Annan, A. P.: Electromagnetic determination of soil water content: Measurements in coaxial transmission lines, Water Resour. Res., 16(3), 574-582, 1980.

Torralba M, Lovrić M, Roux JL, Budniok MA, Mulier AS, Winkel G, Plieninger T (2020) Examining the relevance of cultural ecosystem services in forest management in Europe. Ecol. Soc. 25(3):2

Tucker C, Randolph J, Evans T, Andersson K, Persha L, Green G (2008) An approach to assess relative degradation in dissimilar forests: toward a comparative assessment of institutional outcomes. Ecol. Soc. 13(1) : 4.

Tuzet, A., Perrier, A., Leuning, R.: A coupled model of stomatal conductance, photosynthesis and transpiration. Plant Cell Envir., 26(7), 1097-1116, 2003.

Tyler, S. W., and Walker, G. R.: Root zone effects on tracer migration in arid zones, Soil Sci. Soc. Am. J., 58(1), 25-31, 1994.

Ulrich, E., Lelong, N., Lanier, M., and Schneider, A.: Interception des pluies en forêt: facteurs déterminants, Bulletin technique, (30), 33-45, 1995.

UNECE (2020). Forest Products Annual Market Review 2019-2020. United Nations Publications.

Ung CH, Lambert MC, Raulier F, Guo XJ, Bernier PY (2017) Biomass of trees sampled across Canada as part of the Energy from the Forest Biomass (ENFOR) Program.

Van der Perre R, Bythell S, Bogaert P, Claessens H, Ridremont F, Tricot C, Vincke C, Ponette Q (2015) La carte bioclimatique de Wallonie: un nouveau découpage écologique du territoire pour le choix des essences forestières. Forêt-Nature 135: 47-58.

Van Der Salm, C., Reinds, G. J., and De Vries, W.: Assessment of the water balance of European forests: a model study, In Biogeochemical Investigations of Terrestrial, Freshwater, and Wetland Ecosystems across the Globe, 175-190, Springer, Dordrecht, 2004.

Van Stan, J. T., and Gordon, D. A.: Mini-Review: Stemflow as a Resource Limitation to Near-Stem Soils, Front Plant Sci., 9, 248, 2018.

Vanclay, J. K., and Skovsgaard, J. P.: Evaluating forest growth models, Ecol. Model., 98(1), 1-12, 1997.

Vanhellemont M, Sousa-Silva R, Maes SL, Van den Bulcke J, Hertzog L, De Groote SR, Verheyen K (2019) Distinct growth responses to drought for oak and beech in temperate mixed forests. Sci. Total Environ. 650: 3017-3026.

Vanninen P, Mäkelä A (2005) Carbon budget for scots pine trees: effects of size, competition and site fertility on growth allocation and production. Tree Physiol. 25: 17–30.

Venäläinen A, Lehtonen I, Laapas M, Ruosteenoja K, Tikkanen OP, Viiri H, Peltola H (2020) Climate change induces multiple risks to boreal forests and forestry in Finland: A literature review. Glob. Chane Biol. 26(8): 4178-4196.

Vergutz L, Manzoni S, Porporato A, Novais RF, Jackson RB (2012) Global resorption efficiencies and concentrations of carbon and nutrients in leaves of terrestrial plants. Ecol. Monogr. 82(2): 205-220.

Villar R, Held AA, Merino J (1995) Dark leaf respiration in light and darkness of an evergreen and a deciduous plant species. Plant Physiol. 107: 421–427.

Vincke, C., Granier, A., Breda, N., and Devillez, F.: Evapotranspiration of a declining Quercus robur (L.) stand from 1999 to 2001. II. Daily actual evapotranspiration and soil water reserve, Ann. For. Sci., 62(7), 615-623, 2005.

Vitasse Y, Porté AJ, Kremer A, Michalet R, Delzon S (2009) Responses of canopy duration to temperature changes in four temperate tree species: relative contributions of spring and autumn leaf phenology. Oecologia 161(1): 187-198.

Vitasse Y, Delzon S, Dufrêne E, Pontailler JY, Louvet JM, Kremer A, Michalet R (2009) Leaf phenology sensitivity to temperature in European trees: do within-species populations exhibit similar responses?. Agr. Forest Meteorol. 149(5): 735-744.

Vitasse Y, François C, Delpierre N, Dufrêne E, Kremer A, Chuine I, Delzon S (2011) Assessing the effects of climate change on the phenology of European temperate trees. Agric. For. Meteorol. 151(7): 969-980.

Vitasse Y (2013) Ontogenic changes rather than difference in temperature cause understory trees to leaf out earlier. New Phytol. 198(1): 149-155.

Vitasse Y, Basler D (2013) What role for photoperiod in the bud burst phenology of European beech. European Journal of Forest Research, 132(1), 1-8.

Vitasse Y, Lenz A, Körner C (2014) The interaction between freezing tolerance and phenology in temperate deciduous trees. Front. Plant Sci. 5: 541.

Vospernik S, Bokalo M, Reimoser F, Sterba H (2007) Evaluation of a vegetation simulator for roe deer habitat predictions. Ecol. Mod. 202: 265-280.

Vospernik S, Eckmüllner O (2012) Evaluation of the individual tree growth model Prognaus. Austrian J. For. Sci. 129: 22-55.

Walker, J. P., Willgoose, G. R., and Kalma, J. D.: In situ measurement of soil moisture: a comparison of techniques, J. Hydrol., 293(1-4), 85-99, 2004.

Wang E, Engel T (1998) Simulation of phenological development of wheat crops. Agric. Syst. 58(1): 1-24.

Wang X, Piao S, Xu X, Ciais P, Macbean N, Myneni RB, Li L (2015) Has the advancing onset of spring vegetation green-up slowed down or changed abruptly over the last three decades? Glob. Ecol. Biogeogr. 24: 621–631.

Wang S, Zhang Y, Ju W, Chen JM, Ciais P, Cescatti A, Peñuelas J (2020) Recent global decline of CO2 fertilization effects on vegetation photosynthesis. Science 370(6522): 1295-1300.

Wardle DA (2001) Experimental demonstration that plant diversity reduces invasibility–evidence of a biological mechanism or a consequence of sampling effect?. Oikos 95(1): 161-170.

Waring RH, Landsberg JJ, Williams M (1998) Net primary production of forests: a constant fraction of gross primary production?. Tree Physiol. 18(2): 129-134.

Warren JM, Jensen AM, Medlyn BE, Norby RJ, Tissue DT (2015) Carbon dioxide stimulation of photosynthesis in Liquidambar styraciflua is not sustained during a 12-year field experiment. AoB Plants 7.

Way DA, Oren R (2010) Differential responses to changes in growth temperature between trees from different functional groups and biomes: a review and synthesis of data. Tree Physiol. 30(6): 669-688.

Way DA, Yamori W (2014) Thermal acclimation of photosynthesis: on the importance of adjusting our definitions and accounting for thermal acclimation of respiration. Photosynth. Res. 119(1): 89-100.

Weynants M, Vereecken H, Javaux M (2009) Revisiting Vereecken pedotransfer functions: Introducing a closed-form hydraulic model. Vadose Zone J. 8(1): 86-95.

Wieder WR, Cleveland CC, Smith WK, Todd-Brown K (2015) Future productivity and carbon storage limited by terrestrial nutrient availability. Nature Geosci. 8(6): 441-444.

Wilcoxon F (1945) Individual comparisons by ranking methods. Biometrics bulletin 1(6): 80–83

Williams AP, Allen CD, Macalady AK, Griffin D, Woodhouse CA, Meko DM, McDowell NG (2013) Temperature as a potent driver of regional forest drought stress and tree mortality. Nature Clim. Change 3(3): 292-297.

Willis, T. M., Black, A. S., Meyer, W. S.: Estimates of deep percolation beneath cotton in the Macquarie Valley, Irrig. Sci., 17(4), 141-150, 1997.

Wolkovich, E. M., Cook, B. I., Allen, J. M., Crimmins, T. M., Betancourt, J. L., Travers, S. E., Pau, S., Regetz, J., Davies T. J., Kraft N. J., Ault, T. R., Bolmgren, K., Mazer, S. J., McCabe, G. J., McGill, B. J., Parmesan, C., Salamin, N., Schwartz, M. D., Cleland, E. E.: Warming experiments underpredict plant phenological responses to climate change, Nature, 485(7399), 494, 2012.

Xie Y, Wang X, Wilson AM, Silander Jr JA (2018) Predicting autumn phenology: how deciduous tree species respond to weather stressors. Agr. Forest Meteorol. 250: 127–137.

Yamori W, Hikosaka K, Way DA (2013) Temperature response of photosynthesis in C3, C4, and CAM plants: temperature acclimation and temperature adaptation. Photosynth. Res. 119: 101–117.

Yoda K (1963) Self-thinning in overcrowded pure stands under cultivated and natural conditions. J. Inst. Polytech. Osaka City Univ. 14 : 107–129.

Yousefpour R, Temperli C, Jacobsen JB, Thorsen BJ, Meilby H, Lexer MJ, Hanewinkel M (2017) A framework for modeling adaptive forest management and decision making under climate change. Ecol. Soc. 22(4).

Yuang, Z., Tao, Y., Wenbao, M., Cheng, T., Zhipeng, S., Junqing, L.: Morphological and physiological response of Acer catalpifolium Rehd. Seedlings to water and light stresses, Glob. Ecol. Conserv., e00660, 2019.

Zang, C., Hartl-Meier, C., Dittmar, C., Rothe, A., & Menzel, A. (2014). Patterns of drought tolerance in major European temperate forest trees: climatic drivers and levels of variability. Global change biology, 20(12), 3767-3779.

Zanon, M., Davis, B. A., Marquer, L., Brewer, S., and Kaplan, J. O. (2018). European forest cover during the past 12,000 years: a palynological reconstruction based on modern analogs and remote sensing. Frontiers in plant science, 9, 253.

Zapater M, Hossann C, Bréda N, Bréchet C, Bonal D, Granier A (2011) Evidence of hydraulic lift in a young beech and oak mixed forest using 18 O soil water labelling. Trees 25(5): 885-894.

Zeller L, Liang J, Pretzsch H (2018) Tree species richness enhances stand productivity while stand structure can have opposite effects, based on forest inventory data from Germany and the United States of America. For. Ecosys. 5(1): 1-17.

Zeller L, Pretzsch H (2019) Effect of forest structure on stand productivity in Central European forests depends on developmental stage and tree species diversity. For. Ecol. Manag. 434: 193-204.

Zeller L, Caicoya AT, Pretzsch H (2021) Analyzing the effect of silvicultural management on the trade-off between stand structural heterogeneity and productivity over time. Eur. J. For. Res. 1-20.

Zellweger F, Coomes D, Lenoir J, Depauw L, Maes SL, Wulf M, De Frenne P (2019) Seasonal drivers of understorey temperature buffering in temperate deciduous forests across Europe. Glob. Ecol. Biogeogr. 28(12): 1774-1786.

Zhang Y, Chen HY (2015) Individual size inequality links forest diversity and above-ground biomass. J. Ecol. 103(5): 1245-1252.

Zhang Z, Zhang R, Cescatti A, Wohlfahrt G, Buchmann N, Zhu J, Chen G, Moyano F, Pumpanen J, Hirano T, Takagi K, Merbold L (2017) Effect of climate warming on the annual terrestrial net ecosystem CO2 exchange globally in the boreal and temperate regions. Sci. Reports 7(1), 1-11.

Zhou L, Tucker CJ, Kaufmann RK, Slayback D, Shabanov NV, Myneni RB (2001) Variations in northern vegetation activity inferred from satellite data of vegetation index during 1981 to 1999. J. Geophys. Res. Atmos. 1984–2012(106): 20069–20083.

Zhu Z, Piao S, Myneni RB, Huang M, Zeng Z, Canadell JG, Zeng N (2016) Greening of the Earth and its drivers. Nature Clim. Change 6(8): 791-795.

Zimmermann NE, Normand S, Pearman PB, Psomas A (2013) Chapter III: Future ranges in European tree species. In: Fitzergald J, Lindner M (eds) Adapting to climate change in European forests–Results of the MOTIVE project, Pensoft Publishers, Sofia, Bulgaria, pp.15-21 Bailey BN, Stoll R, Pardyjak ER, Miller NE (2016) A new three-dimensional energy balance model for complex plant canopy geometries: Model development and improved validation strategies. Agric. For. Meteorol. 218: 146-160.

Zimmermann J, Hauck M, Dulamsuren Ch, Leuschner C (2015) Climate warming-related growth decline affects Fagus sylvatica, but not other broad-leaved tree species in Central European mixed forests. Ecosystems 18:560–572.

Zohner CM, Mo L, Pugh TA, Bastin FJ, Crowther TW (2020) Interactive climate factors restrict future increases in spring productivity of temperate and boreal trees. Glob. Change Biol. 26(7): 4042-4055.

Zohner CM, Mo L, Renner SS, Svenning JC, Vitasse Y, Benito BM, Crowther TW (2020) Late-spring frost risk between 1959 and 2017 decreased in North America but increased in Europe and Asia. PNAS 117(22): 12192-12200.

# LIST OF TABLES

# LIST OF FIGURES